The Responses of the Respiratory System when Exposed to Volcanic Ash

CARDIFF UNIVERSITY

PRIFYSGOL CAERDYD

by

Sang Hee Lee

A thesis presented for the degree of Doctor in Philosophy at

the University of Wales College of Cardiff

July 2004

UMI Number: U200873

UMI U200873

ProQuest LLC
789 East Eisenhower Parkway
P.O. Box 1346
Ann Arbor, MI 48106-1346

Acknowledgements

Scientific Publications

Sang Hee Lee, Roy J Richards "Montserrat volcanic ash induces lymph node granuloma and delayed lung inflammation", Toxicology, 193 (2-3). *155-165* (2004)

Abstracts

Sang Hee Lee and Roy Richards: Montserrat ash and damaged lymph nodes: is there any health significance? July 2003. Cities on Volcanoes 3, Hilo, Hawaii.

Roy Richards, **Sang Hee Lee** and Kelly BeruBe: Toxicological studies with volcanic ash: methods, outcomes and critique. Cities on Volcanoes 3, July 2003. Hilo, Hawaii.

S. H. Lee and Roy J Richards The fibrogenic potential of Montserrat volcanic ash containing cristobalite. BALR summer meeting, September, 2002, Dublin, Ireland

S. H. Lee and Roy J Richards Montserrat Volcanic Ash is Weakly Bioreactive - 1-Year Instillation Study. 99 th ATS International meeting, May 16-22, 2002, Atlanta, GA, USA, *Am. J. Respir. Crit. Care. Med.* 165 (8) pB17

S. H. Lee, Bérubé and RJ Richards (2002). How bioreactive is the cristobalite component of Montserrat volcanic ash? *Exp. Lung Res.* 28, 141-179.

Summary

The Soufriere Hills volcano on Montserrat erupted in 1995 and the intermittent seismic activities continue to the present time. More vigorous activities were reported in 1997 and 2003 with earthquakes, eruptions, pyroclastic flow and surge generating massive amount of ash. Moreover, it was reported that Montserrat volcanic ash (MA) includes a relatively high content of toxic crystalline silica; cristobalite (CRS, up to 23 %). Such levels of crystalline silica content raised the concern for the health of residents in the vicinity of the volcano.

The toxicities of respirable fraction of the MA and its two major components, CRS and anorthite (ANR) were studied using a rat model and a non-invasive intratracheal instillation technique with three different doses (1.0, 2.5 and 5.0 mg). The changes in the lung were investigated at four different times (6, 13, 25 and 49 weeks post-exposure). Firstly, the respirable fraction of each dust specimen was characterised physicochemically using a environmental scanning electron microscopy and image analysis in order to utilise these particulate for toxicological studies. Secondly, the bioreactivity of the MA, CRS and ANR were investigated by four different approaches; quantitative biochemical and cellular assays, semi-quantitative histopathology and molecular biological analysis.

The size distributions of the MA, CRS and ANR demonstrated that more than 95 % of the instilled samples were respirable (<2.5 μm). Furthermore, the respirable fraction of the MA generated from dome collapse pyroclastic flow in 1997, contains approximately 21 % (w/w) crystalline silica.

The toxicological investigations demonstrated quite clearly the different toxicological properties of the MA, CRS and ANR. The CRS proved to be fibrogenic in rat lung with a 5.0 mg single instillation dose after long-term (1 year) exposure whereas ANR was minimally bioreactive. The MA did not cause inflammation in the lung until 49 weeks post-instillation even though size augmentation with granuloma formation in thoracic lymph nodes were recognised at 13 weeks. These findings suggested that the size and granuloma formation of thoracic lymph nodes were good early markers to assess the toxicity of crystalline silica containing volcanic ash. Histopathological and physicochemical investigations confirmed that the particles drained from the lung were deposited in mainly the granulomatous areas in the nodes. Furthermore, the crystalline silica content of the MA in the nodes was greater than that noted in the MA in the lung tissue and the original instillate. The macroarray technology has provided additional information on MA and CRS induced inflammation. A number of candidate inflammatory markers were identified including microsomal glutathione S-transferase 1, placenta growth factor and thioredoxin peroxidase although more minor changes were detected with a further 15 genes.

In summary, the MA did produce a delayed inflammatory effect in the lung but the earliest changes noted were granulomatous formation in thoracic lymph nodes, the site of clearance, The inflammatory actions noted were due to the high crystalline silica (CRS) component but unlike CRS, the MA did not prove to be fibrogenic.

Contents

Dedication

Declaration

Acknowledgements

Scientific publications

Summary

Table of contents

List of abbreviations

List of tables

List of figures

Abbreviation

abs	absolute
ANR	Anorthite
BSE	Back scattered electron
cDNA	Complementary deoxyribonucleic acid
COX4	Cytochrome c oxidase subunit IV
CRS	Cristobalite
cpm	Count per minute
DNase	Deoxyribnuclease
EDTA	Ethylenediaminetetraacetic acid
EDX	Electron dispersive x-ray
ELF	Epithelial lining fluid
ESD	Equivalent spherical diameter
E-SEM	Environmental scanning electron microscopy
FEV	Forced expiratory volume
γGT	Gamma-glutamyl transpeptidase
LDH	Lactate dehydrogenase
LRT	Lower respiratory tract
MA	Montserrat volcanic ash
MACs	Macrophages
mRNA	Messenger ribonucleic acid
NOS3	Nitric oxide synthase 3
PCR	Polymerase chain reaction
PMNs	Polymorphonuclear leukocytes
PM10	Particulate matter less than 10 micron
Q	Quartz
Q-PCR	Quantitative polymerase chain reaction
RBC	Red blood cell
RE	Respiratory epithelia
RNA	Ribonucleic acid
RNase	Ribonuclease

RT	Respiratory tract
ROS	Reactive oxygen species
RT-PCR	Reverse transcriptase polymerase chain reaction
SE	Secondary ele2tron
SEM	Scanning electron microscopy
SP-A	Surfactant protein A
SP-C	Surfactant protein C
SP-D	Surfactant protein D
TE	Tris-ethylendiaminetetracetic acid
TEM	Transition electron microscopy
TIF2	Transcriptional intermediary factor 2
TNF	Tumour necrosis factor
TSP	Total suspended particulates
URT	Upper respiratory tract
UV	Ultra violet

List of tables

List of Figures

1 General introduction

1. 1 Montserrat volcanic ash

1. 1. 1 Soufriere Hills volcano on Montserrat

In 1995 the Soufriere Hills volcano on Montserrat, a stratovolcano started to erupt and there have still been intermittent eruptions through to the present time, including the largest explosion and dome collapse in 1997 (Figure 1.1) (Robertson, 2000). Approximately 60 % of the Earth volcanoes are stratovolcanoes. In general the volcanoes have andesitic or dacitic magma, which have lower melting points, and higher silica contents than basaltic magma. (Press and Siever, 1982; http://volcano. und. nodak. edu). Therefore the lava is more viscous and can pile up at the vent forming a dome. The dome on Montserrat was growing at a rate of 6-7m^3/sec in late September 1997, and being a high unstable dome was prone to collapse (http://www.volcanoworld.com). Therefore the Montserrat volcano shows phreatic (inter-action with groundwater) explosive eruption, dome collapse or rockfall activity. Other stratovolcanoes include Mt. St. Helens, Mt. Rainier, Pinatubo, and Mt. Fuji (http://volcano. und. nodak. edu). The regional tectonic setting of Montserrat is responsible for the formation of this particular form of volcanism, with oceanic crust subduction creating an oceanic arc chain of volcanoes in the Caribbean. Similar regional settings exist in New Zealand, Japan and the Philippines, with similar volcanoes.
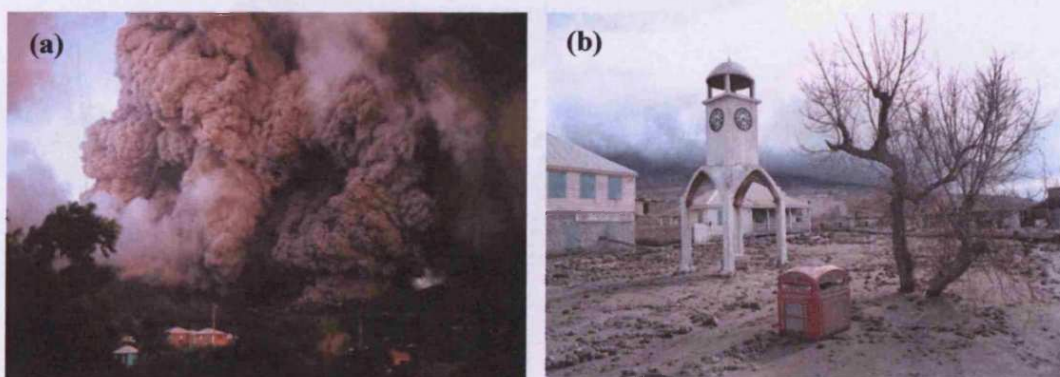
Figure 1. 1 The second major eruption of the Montserrat in August, 1997 (a) and volcanic ash and mud cover the whole city after the first eruption (b, Plymouth, capital city (http://www.discovery.com).

1. 1. 2 Montserrat volcanic ash and its components

Volcanic ash can contain potentially biohazardous crystalline silica, which could cause lung diseases, for example, chronic inflammation, fibrosis, and silicosis. The Montserrat volcanic ash (MA) is no exception. It is reported that the ash contains approximately 3 % weight cristobalite (CRS, toxic crystalline silica) in the explosive eruption ash and 10 to 24 % weight CRS in the dome-collapse pyroclastic flow ash (Nicholson *et al.* 2000; Baxter *et al.* 1999). In addition to the CRS, the main component of the MA is anorthite feldspar (ANR, about 70 weight %), which has a low bioreactivity in the rat lung (Housley *et. al.*, 2002). The difference in CRS content between the ash from the explosive eruption and that from the dome-collapse pyroclastic flow results from different volcanic processes. The explosion ash comes from the interaction of phreatic (ground) water and hot magma, resulting in an explosive event discharging ash into the atmosphere. With dome formation, magma is extruded from the volcanic vent at 600-800 °C. The rock contains small holes or 'vugs' from gas expansion. Within these vugs, CRS crystals grow from the magma glass matrix (amorphous silicon dioxide, SiO_2). When the dome collapses, the resulting violent pyroclastic flow smashes the rock to pieces, releasing the crystals of CRS from the vugs. These processes are illustrated in Figure 1. 2.
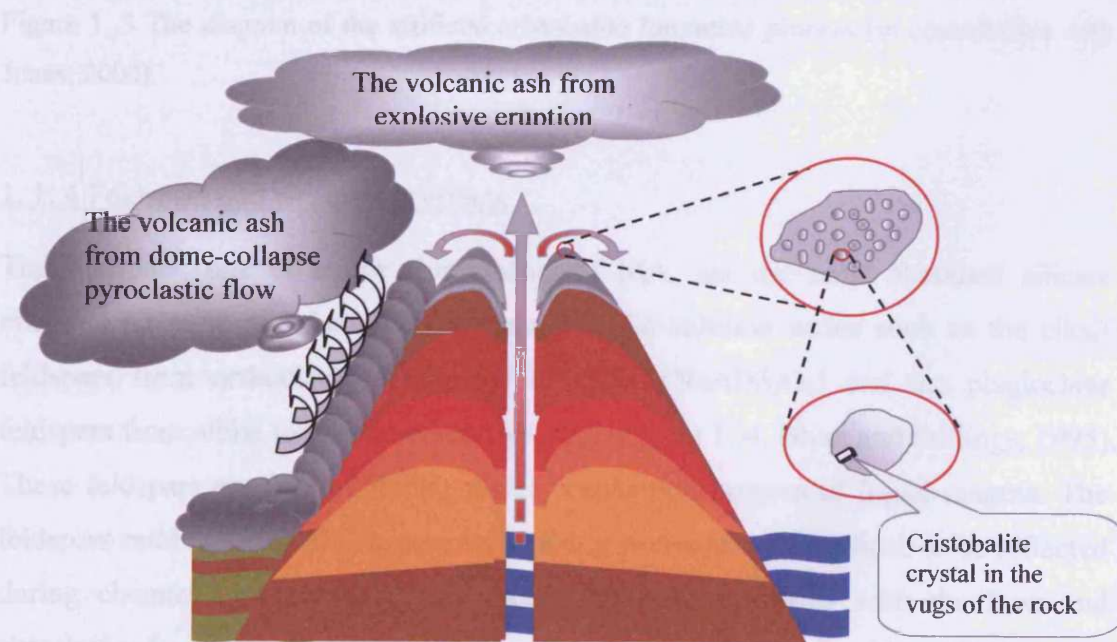
Figure 1. 2 The formation processes of the ash from the pyroclastic flow and volcanic cristobalite (in consultation with Jones, 2000).

1. 1. 3 The formation of artificial cristobalite (CRS)

Artificial CRS is generated during glass manufacture under similar condition to those seen in volcanic domes. Around a glass furnace rim, the temperature varies between 600 to 800 °C, and the moisture level is low. Artificial CRS is produced when drops of the molten silica glass land on the peripheral area of the pot, and they are maintained at 600-800 °C from some time, allowing crystal growth (Fig. 1. 3). Artificial CRS can be identified by components such as boron (B) which are used in glass manufacture (Williamson, 2000).

SiO$_2$ (molten)
~ 1200 °C

Artificial
Cristobalite
(600-800 °C)
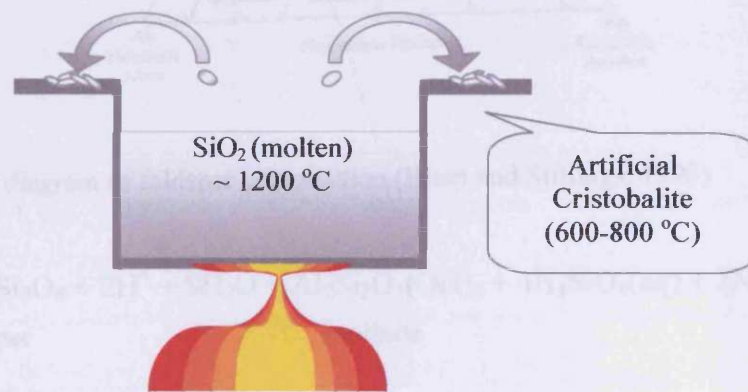
Figure 1. 3 The diagram of the artificial cristobalite formation process (in consultation with Jones, 2000).

1. 1. 4 Feldspars and weathering effects

The feldspars, one of major components of MA, are the most abundant silicate minerals on earth and form two continuous solid-solution series such as the alkali feldspars from orthoclase (KAlSi$_3$O$_8$) to albite (NaAlSi$_3$O$_8$) and the plagioclase feldspars from albite to anorthite (CaAl$_2$Si$_2$O$_8$) (Figure 1. 4, Blum and Stillings, 1995). These feldspars are formed during the crystallisation process of liquid magma. The feldspars established at high temperature and/or pressures and continue to be reflected during chemical weathering (dissolution reactions) associated with the flow and chemistry of water at the surface of the earth (eqn 1; White and Brantley, 1995).

Microcline
Orthoclase
Sanidine
KAlSi₃O₈
Or

Alkali Feldspars

Oligoclase | Andesine | Labradorite | Bytownite

Ab
NaAlSi₃O₈
Albite

Plagioclase Feldspars

An
CaAl₂Si₂O₈
Anorthite
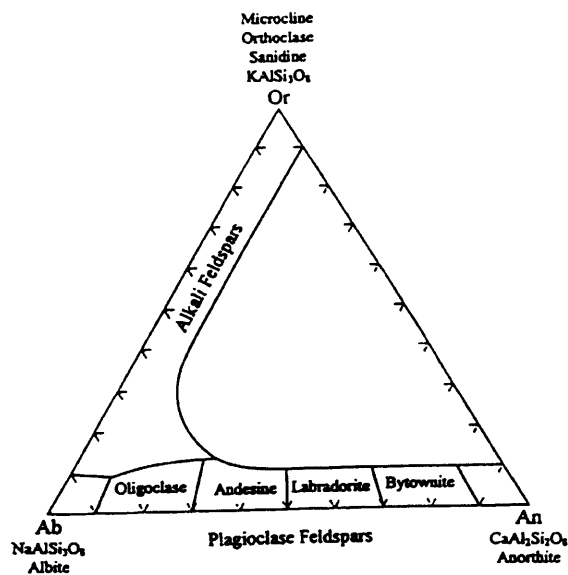
Figure 1. 4 A diagram of feldspar composition (Blum and Stillings, 1995)

$$2NaAlSi_3O_8 + 2H^+ + 9H_2O = Al_2Si_2O_5(OH)_4 + 4H_4SiO_4(aq) + 2Na^+ \quad (eqn\ 1)$$

feldspar   kaolinite
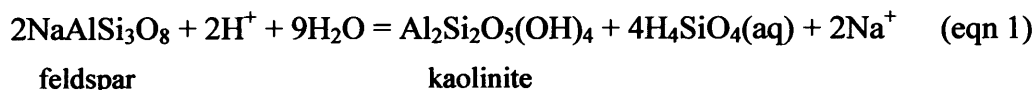
The feldspar is dissolved into solution initially and then kaolinite and other secondary phases from solution would be precipitated subsequently. Sometimes compositionally distinct regions of the crystal such as impurities or erosion lamellae could be dissolved resulting in elemental release. Aluminium could be leached from feldspar or kaolinite at lower pH during those reactions via preferential removal of one component from the structure. Protonation and/or deprotonation is involved in those reactions and thus solubility of silicate polymorphs and dissolution rate are increased under an acidic or basic condition. Therefore, the weathering rate is positively dependent on the acidity of the water.

This characteristic of feldspars implied that the feldspar component of the MA could be dissolved during phagocytosis since the pH in lysosomes of macrophages is approximately 3-5. This process could produce a fresh site of crystalline silica component of the MA resulting from demasking the feldspar component from crystalline silica. Interestingly, it was reported that the freshly ground albite powder

absorbs two or three times more proton (H^+) than albite which is annealed for 80 hours at 1,000 °C (Blums and Stillings, 1995) as freshly fractured crystalline silica is more bioreactive than aged samples (Fubini et. al., 1995; Fubini et. al., 1999).

1. 1. 5 Toxic potential of volcanic ash and cristobalite

Volcanic ash includes abrasive fine particles that can become airborne, and travel far from the volcano, contributing to respiratory problems or dermatological irritation. The toxicity of ash containing crystalline silica generated from volcanoes has been examined previously and results are summarised in Tables 1. 1, 2, 3, 4.

In vitro studies take a much shorter time to investigate the toxicity of the particles than in vivo or epidemiological studies. However, there are shortfalls. In vitro methods can only investigate the effects of the volcanic ash on the cells rather than organ or organism excluding defensive mechanisms, which normally active in any organisms. The results from in vitro studies of the toxicity of ash generated from volcanoes other than Montserrat, including Mount St Helens, El Chichon and Galunggung are shown in Table 1. 1. Samples from the last 3 volcanoes have a lower concentration of crystalline silica than that found in Montserrat volcanic ash. Most of the studies implied that volcanic ash has a low bioreactivity. Vallyathan et. al., (1984) and Wilson et. al., (2000) reported that the haemolytic activity of the volcanic ashes from Mt St. Helens and MA required high doses (12.5 mg/mL and 30 mg/mL). Haemolysis was not dependent on the crystalline silica content. Furthermore, it is difficult to make a link between the results gained from the use of extremely high does and the effects of the ash on the humans who were exposed to much lower concentration of particles in ambient air.

Because of the difficulties in extrapolation from in vitro data to humans, animal models have been employed to study the bioreactivity of volcanic ashes. There are two ways to expose animals to ashes namely by inhalation or instillation. The results from studies using an inhalation technique are shown in Table 1. 2. Most inhalation studies also showed the low bioreactive potential of volcanic ashes except those carried out by Wehner et. al., (1983). Wehner reported focal alveolar proteinosis at 8 months with a high dose (50 mg/m^3, 6 hours/day and 5 days/week) of the ash

collected from Mt. St. Helens. In spite of the high dose employed, any fibrogenic potential of volcanic ash was not detected. Such an extreme experimental exposure condition does raise concerns as to whether this study could reflect the real exposure conditions experienced by human subjects.

An alternative to inhalation is instillation whereby large numbers of animals may be treated in a short time period with exact doses of ash and other minerals. Instillation has been used to investigate the toxicity of volcanic ash (mostly Mt. St. Helens) (Table 1. 3). Most studies, even those using doses of 50 mg, report only minor or transient effects on the lungs. However, one study (Green et. al., 1981) utilising a high dose (10 mg, containing 7.2 % crystalline silica) reports focal inflammation and excess collagen deposition, suggesting fibrosis, at 6 months post-exposure. In the one previous study carried out with Montserrat ash (1 mg instillate containing 20.1% cristobalite (CRS), Housley et. al., 2002), no evidence was found for any inflammatory reaction up to 3 months post-treatment (Table 1. 3).

Epidemiological studies (Table 1. 4) would seem to confirm the toxicological investigations suggesting that volcanic ash is of low bioreactivity. However, again the one recent study undertaken on Montserratian children (Forbes et. al., 2003) raises concerns that health effects may be attributable to the volcanic ash.

Thus, in reviewing the literature regarding the toxicity and potential health effects of volcanic ashes it would seem that they correlate best with so called "nuisance dusts" and can be regarded as low bioreactivity materials. However, material generated during pyroclastic flows in Montserrat volcanic ash has 20.1 % CRS, a mineral known to be highly toxic and with potential long-term health concerns. It is possible therefore that the earlier toxicological studies of Montserrat ash carried out by Housley et. al., 2002 were insufficient in that they were short-term and utilised a single low dose of ash. More detailed studies are required to include histopathology, extended time periods and a range of instilled doses.

Table 1.1 *In vitro studies*

Origin	Composition dose and exposure period	Results	References
Mt St Helens	Crystalline silica 0.1-0.5 mg 20-24 h	Rabbit alveolar MACs/trypan blue exclusion; Same activity as TiO_2 and greater than feldspar Quartz (Q) is most toxic	Robinson & Schneider, 1982
Mt St Helens	99% particles> 10 µm Q (3%) & CRS (4.2%) 1.3-5 mg/mL 1 h	No effect on rabbit type 2 cell O_2 consumption; no effect on alveolar MACs integrity/ O_2 release consumption; small effect on superoxide in zymogen stimulated cells	Castranova et. al., 1982
Mt St Helens	ESD=0.11-11.5 µm Silica (Q & CRS) 1.5-7.2 % 12.5 mg/mL 50 mins	Sheep red blood cell (RBC) haemolysis Haemolytic activity: crystalline silica > volcanic ash ≈ chrysotile and talc > coal, bentonite, amosite or gypsum	Valiyathan et. al., 1983
Mt St Helens Galunggung El Chichon	Low Q:1.3-2.0% Variable 50 mins	Haemolysis and enzyme release studies from alveolar MACs; no real link to silica content	Valiyathan & Robinson 1983
Mt St Helens	1-10 mg/mL	Alveolar MACs & A549 cells:ash<<Q	Martin et. al., 1984
Mt Sakurajima	Mean dia.=3.6 µm α Q< 5% (w/w) 50-400 mg/mL 1 h – 6 days	V79-4 cell, human neutrophils, p338D, alveolar MACs cell line; Activity: volcanic ash<TiO_2<<CRS	Yano et. al., 1985
Mt St Helens	CRS (3-7%)+plagioclase 4 mg/mL	Sheep RBC haemolysis: Na feldspar not active Ash<CRS (4 times more)	Craighead et. al., 1983
Montserrat	CRS (3 %, explosive eruption) CRS (11% dome collapse) Particles< 3 µm 50 µg/mL (cell), 300 µg/mL (haemolysis)	Induced 40% haemolysis at high dose (30 mg/mL)	Wilson et. al., 2000

Key: Q: quartz, CRS: cristobalite, RBC: red blood cells, MACs: macrophages, TiO_2: titanium dioxide, ESD: equivalent spherical diameter

Table 1. 2 *In vivo* studies (inhalation)

Origin	Composition dose and exposure period	Results	References
Mt St Helens	60 kg collection May 1980 undistributed location 2 weeks after eruption. 95% particles< 5.4 μm crystalline silica (3%). 100 mg/m³, 6h/d for 10 days. 3days, 2 weeks, 1, 3, 6, 9 months	180 rats for exposure to ash,min-u-sil or air. 6 time points, 7 rat/group. ash damages type 1 cell at 3 days, interstitial thickening and collagen at 6 & 9 months. Min-u-sil more damaging. Ash causes no increase in lung dry weight , lung protein or phospholipids but min-u-sil does	Martin et. al., 1983
Mt St Helens	Composite from 3 sites: Sieved & heat steirilised, details in Task Force. Crystalline silica (3.5%). 5-50 mg/m³ 6h/d, 5d/wk up to 12 months. sacrifice 4 months intervals	5 mg/m³ ash: little pathology (focal alveolar MACs accumulation, limited hyperplasia, grossly enlarged lymph nodes 12 months post exposure). 50 mg/m³ ash: alveolar proteinosis by 8 months effects not as great as 50 mg/m³ Q	Wehner et. al., 1983
Mt St Helens	9.4 mg/m3 2h/d, 5d/wk; 850mg/rat recovery 9 months	No effects (histological/biochemical) in normal rats or those with elastase induce emphysema	Raub et. al., 1985
Non-volcanic ash Mixed dust (Q+coal mine dust)	Coal:16 or 4 % silica as artificial mixture compared with natural mine dust 100g/m³ 4-6h/d, 5d/wk for 12 months lung burden 40-60mg/rat 12, 18, 24 months	Artificial dusts much more damaging (increase lung weight and collagen) than natural mine dusts (with/without Q)	Le Bouffant et, al, 1982

Key as Table 1. 1

Table 1.3 *In vivo* studies (instillation)

Origin	Composition dose and exposure period	Results	References
Mt St Helens	Q and Min-u-sil; Mean dia=1.3 μm; Al_2O_3 (inert dust): respirable 1.3 μm; 0.15-3.75 mg/ 24 h	Hamsters: all 3 dusts cause PMN influx at 24 h but highest with Q; Lysosomal enzyme release highest with Q; LDH significantly higher with all dusts even non-toxic dusts; Q> Al_2O_3 ≈ volcanic ash	Beck et. al., 1981
Sand, modified sand or extracted Q from mine dusts (Q and feldspar); similar to volcanic ash	>3 μm; 30 mg instillation; 3, 6, 12 months post-instillation	No fibrogenesis with sands; tracheo bronchial nodes show retinoculohistocytic reaction with areas of reticulin fibrosis at 3 months; 6-12 months effects as bad as Q; sand resident in lung for 1 yr extracted and given by instillation immediately damaging	Le Bouffant et. al., 1982
Mt St Helens	Min-u-sil<5μm (+ control); 300 μg (low),50 mg (high); 6 months post-instillation	Crystalline silica has no effect at 300 μg instillation; At 50 mg doses effects of volcanic ash are slight compared with silica;	Raub et. al., 1985
Mt St Helens	Crystalline silica 7.2%; 99 % (dia<10 μm); 10 mg; 1, 7 days/ 1, 3, 6 months	Acute focal inflammation at 1 and 7 days; Granuloma at 1 and 3 months; Collagen accumulation at 6 months	Green et. al., 1981
Montserrat; CRS; anorthite	3% CRS (explosive eruption); 20.1% CRS (dome collapse); 1 mg/ 1, 3, 12 weeks	No time dependent changes; Bioreactivity: Q>> volcanic ash or anorthite; No evidence of inflammatory potential of ash	Housley et. al., 2002

Key as Table 1.1, LDH: lactate dehydrogenase

10

Table 1.4 Epidemiological studies

Origin	Composition dose and exposure period	Results	References
Mt St Helens	80% volcanic glass; most of crystalline silica coarse 96%<10 μm and 58%< 2μm TSP range: 100 μg/m³ to 1000-11,000 μg/m³ lung function tests during urban pollution episode and after volcanic eruption	No change in pulmonary function tests due to huge (10-fold) increases in TSP following volcanic eruption; noticeable effects when urban air polution increased 3-fold	Johnson et. al., 1982
Mt St Helens	Crystalline silica (3-7%) in respirable fraction Studied just after eruption	Loggers (exposed and non-exposed compared); C3 and C4 significantly decreased with ash exposure no effects on immunoglobulins compliment effects due to early alveolar MAC changes	Olenchock et. al., 1983
Mt St Helens	Q (2%) and CRS (4%) 450 mg/m³ (high), 270 mg/m³ (low) final value in 1981: both start at 560 mg/m³) 1 month after eruption and up to 4 yrs later	Transient drop in FEV (4% in first yr) Increase in cough and phlegm	Buist et. al., 1986
Mt Sakurajima	Daily TSP: 105 mg/m3	No direct link with repiratory disease and distance from crater Highest disease levels found close to crater	Yano et. al., 1986
Montserrat	School children (80 % of 443 children) Age 12 – 13 yr old 12 months period	Higher wheeze ratios were shown in the children exposed to ash heavily than the children who never lived in those areas.	Forbes et. al., 2003

Key as Table 1.1, TSP:total suspended particulates, FEV: forced expiratory volume

1. 2 Respiratory system

1. 2. 1 The responses between the respiratory system and xenobiotics

The respiratory system (upper and lower; Figure 1.5) is one of the first lines of defence (e.g. biotransformation), following exposure to airborne xenobiotic agents. The lung is sensitive to changes in atmospheric composition due to air pollution or natural disaster, i.e. volcanic eruption, and the defence mechanisms are therefore well developed. In order to protect the lungs from air pollution particles, there are several particle-removing systems. For example, in the upper respiratory tract (URT), hairs in the nasal cavity, mucus lining the respiratory epithelia (RE) and ciliated cells within the RE. All of these mechanisms trap particles and prevent their movement into the lower respiratory tract (LRT). The trapped particles are then cleared by the mucociliary escalator, which transports particles deposited on the surface of the respiratory tract (RT) upwards to the mouth, and then the particles are swallowed or removed by sneezing or expectorated. In the LRT, alveolar macrophages (MACs) remove those particles which have by-passed the URT defence mechanisms. The alveolar MACs phagocytose the particles and then join the mucociliary escalator and are removed as described above. Any particles, which are capable of further penetration into the distal airways of the lung, i.e. alveoli, despite these mechanisms, will be either removed via lymphatic drainage within alveolar MACs or become imbedded in the interstitium of the lung parenchyma (Richards *et. al.,* 1999; Adamson and Hedgecock, 1995).
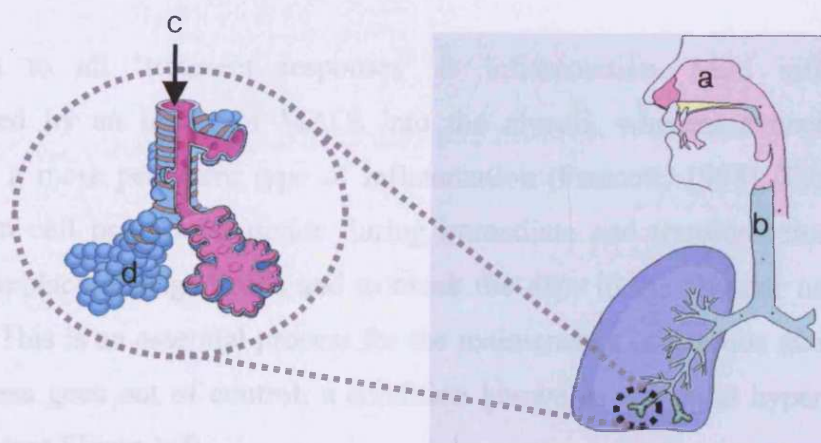
Figure 1. 5 A diagram of the respiratory system: (a) nasal cavity, (b) trachea, (c)

bronchioles, (d) alveoli (B. Young and J. W. Heath, 2000).

If the natural clearing actions of the respiratory system have failed, inflammatory processes may result. The various biological endpoints in the lung following inhalation of a biologically reactive material are shown in Table 1. 5. The responses are classified as being 'immediate', which refers to the very first reaction, and 'transient', which tells us that the reactions are short-lived and that the cells will recover back to a normal state, and finally, 'progressive', where recovery from cell damage is less likely. The response endpoints are also time and dose dependent.

If a biologically reactive particle is able to reach the alveoli, the first 'immediate' effect is the interaction with the epithelial lining fluid (ELF; Table 1.5). The particles can then penetrate the ELF and damage the underlying type 1 and type 2 cells to cause the alveolar unit (Figure 1.6) to leak protein onto the surface of the epithelium, or what is commonly referred to as 'pulmonary oedema'. Type 1 and type 2 are epithelial cells. Type 1 cells cover most of the alveolar surface and are therefore vulnerable to xenobiotic attack. Damage to these cells can result in the production of gaps in the alveolar unit leading to pulmonary oedema. Type 2 cells are less in number and injury resistant due to biotransformation capabilities. They also manufacture and secrete pulmonary surfactant, a lipoprotein complex important in preventing lung collapse and as a protective component of lung lining fluid. During type 1 cell damage, type 2 cells will differentiate into type 1 cells and fill the gaps in the alveolar surface.

Common to all 'transient responses' is inflammation. Mild inflammation is hallmarked by an influx of MACs into the alveoli, whereas a neutrophil influx indicates a more persistent type of inflammation (Prescott, 1998). Type 2 cells, or their stem cell precursors, divide during immediate and transient disease states in order to replace damaged cells and to block the gaps in the alveolar unit formed by oedema. This is an essential process for the maintenance of gaseous exchange. When this process goes out of control, a condition known as epithelial hyperplasia comes into play (see Figure 1.7).

DEPENDENT ON DOSE & TIME		
EPITHELIAL LINING FLUID INTERACTION	FLUID ON SURFACE OF LUNG	IMMEDIATE
EPITHELIAL CELL DAMAGE	CELL DEBRIS ON LUNG SURFACE	
PERMEABILITY CHANGES	PROTEIN LEAKED ONTO LUNG SURFACE	TRANSIENT
MILD INFLAMMATION	MACROPHAGE INFLUX	
SEVERE INFLAMMATION	NEUTROPHIL INFLUX	
EPITHELIAL HYPERPLASIA (LIPOPROTEINOSIS)	UNCONTROLLED CELL DIVISION	
EPITHELIAL METAPLASIA	ABNORMAL TRANSFORMATION OF TISSUE	MORE PROGRESSIVE
INTERSTITIAL FIBROGENESIS	DEPOSITION OF COLLAGEN	

Table 1.5 The response endpoints of the respiratory system following xenobiotic challenge (In consultation with Richards R. J.).
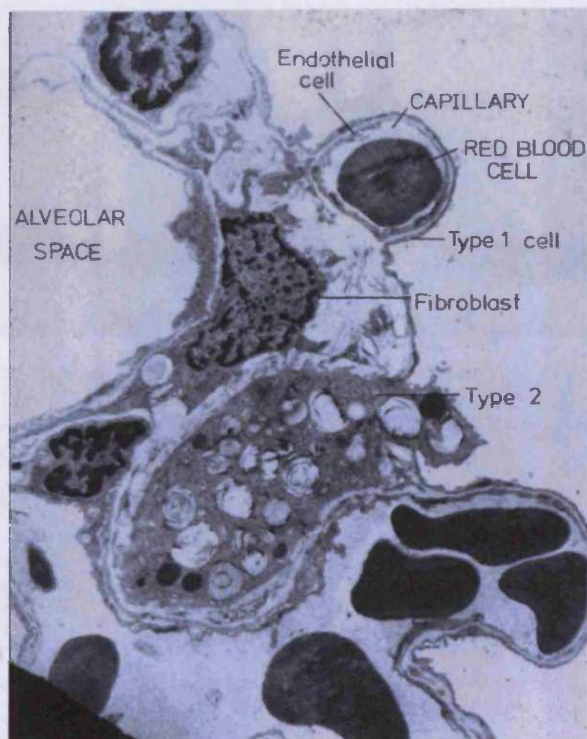
Figure 1.6 Transmission electron microscopy of the alveolar unit showing components (Richards *et. al*, 1999).

In this situation, type 2 cells proliferate and consequently, over secrete surfactant, and along with the oedema products already on the surface of the alveoli, a condition is produced which is called lipoproteinosis (excess accumulation of surfactant on the lung surface; Richards and Curtis, 1984). Hyperplastic cells can also differentiate and divide into cells that do not resemble the type 2 cell phenotype, and the resultant disease state is epithelial metaplasia. The problem with metaplasia is that it reduces the type 2 cell population and damaged type 1 cells cannot be replaced. Finally, underneath the metaplastic cells, the fibroblasts in the interstitium can divide out of control as well, with increased deposition of collagen leading to a condition known as fibrosis (Richards *et. al.*, 1991).
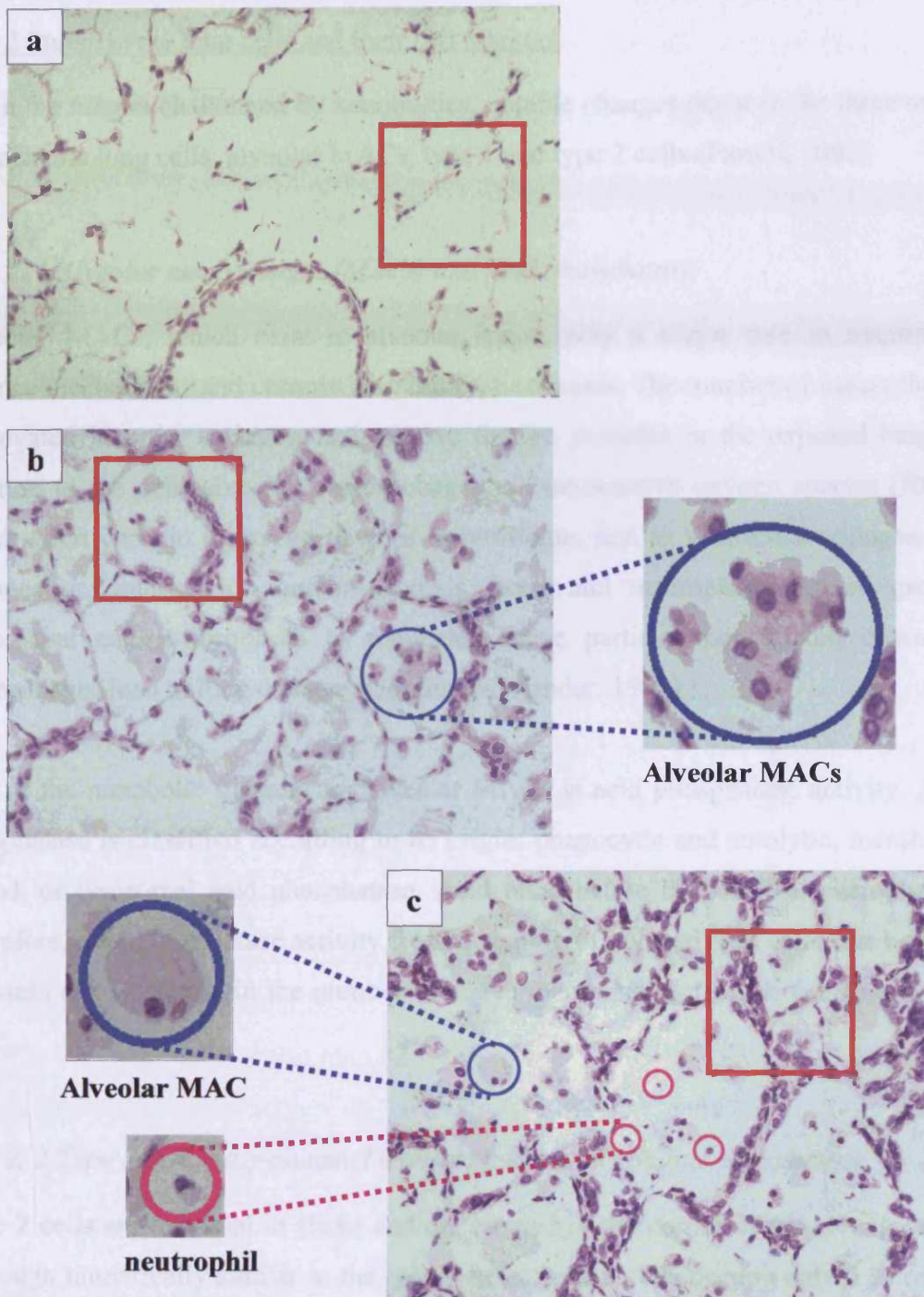
Figure 1. 7 These light micrographs represent (a) healthy lung, (b) mild inflammation and (c) severe inflammation in lung tissue exposed to silica.

Note: In untreated/healthy lung tissue, the empty air spaces and thin alveolar walls are observed (☐ in (a)). In mildly inflamed tissue, an influx of alveolar MACs is noticeable in the air spaces and the alveolar walls are thickened (☐ in (b)). With severe inflammation, the air spaces are now filled with alveolar MACs and neutrophils and further thickening of the alveolar walls (☐ in (c). 'hyperplasia'; adapted from Richards et. al, 1999).

1. 2. 2 Parenchyma lung cells and their cell markers

When the lung is challenged by xenobiotics, notable changes occur in the three major parenchyma lung cells: alveolar MACs, type 1 and type 2 cells (Farrell, 1982).

1. 2. 2. 1 Alveolar macrophages (MACs) and acid phosphatase

Alveolar MACs, which exist in alveolar space, play a major role in respiratory defence mechanisms and chronic lung injury, or fibrosis. The number of macrophages is elevated in order to ingest and remove foreign particles in the exposed lung. In addition to the defensive role, macrophages release reactive oxygen species (ROS), which elicit chronic injury via factors to proliferate and to synthesise collagen-like fibronectins, interleukin, tumour necrosis factor and macrophage-derived growth factor that cause fibroblasts to replicate. Those particles not broken down by macrophages lead to lung damage (Gordon and Amdur, 1991).

One of the metabolic markers for alveolar MACs is acid phosphatase activity. Acid phosphatase is classified according to its origin; phagocytic and autolytic, membrane bound, or lysosomal acid phosphatase. Acid phosphatase is found in macrophages. Therefore, acid phosphatase activity from a sample of lavaged free cells can be used to assess any alteration in the number of active macrophages (Kwok-wai Lam *et al.*, 1982).

1. 2. 2. 2 Type 2 cell and γ-glutamyl transpeptidase and alkaline phosphatase.

Type 2 cells are cuboidal in shape and are located in the corner of the alveolar unit. Although numerically similar to the type 1 cells, type 2 cells occupy only 5 % of the surface area. The type 2 cell has a relatively small surface area and being metabolically active contributes to the injury resistant character of the alveolar unit. One of the main roles of the type 2 cell in damage or repair processes is to maintain normal lung architecture by compensating for type 1 cell damage via proliferation and differentiation into type 1 cells. However, in lungs exposed to highly toxic material, the mechanism cannot keep up with the level of damage or leads to an abnormal alveolar structure formation like cuboidal epithelium. Unlike type 1 cells, type 2 cells

have high metabolic potential. For example, type 2 cells synthesise and secrete surfactant to maintain alveolar structure and hold several enzymes including γ-glutamyl transpeptidase (γGT), or several kinds of hydrolases such as alkaline phosphatase (Dinsdale *et. al.*, 1992). Therefore the proliferation or depression of the type 2 cell can be assessed using these enzyme activity assays following excess secretion by the cells or their damage and release of their contents into the epithelial lining fluid.

γGT, a membrane bound enzyme plays a key role in a transpeptidation reaction. It involves a group translocation in the γ-glutamyl cycle leading to the formation of isopeptides of glutamate and amino acids and releasing cysteinyl glycine, which is converted to free amino acid from glutathione (Figure 1. 8) (Davelin 1993). L-γ-glutamyl-L-cysteinyl-glycine, or glutathione is responsible for removal of hydrogen peroxide (H_2O_2) and protecting normal cells against radiation, free radicals and other oxidant injury (Forman and Skelton, 1990; Devlin, 1993). Typically γGT is found in pulmonary type 2 cells, Clara cells and in lower activity in alveolar MACs. Therefore, γGT activity can be a cell marker for type 2 cells and Clara cells when readily released into lavage fluid following epithelial cell damage.

Generally phosphatase has a function to switch on or off reactions in cells. In the type 2 cells, phosphatase is associated with surfactant synthesis. Alkaline phosphatase stored in the lamellar bodies in the type 2 cell is used as an epithelial cell marker since macrophages have little or none of this enzyme activity (Cohen 1978; Reasor *et. al.* 1978; Edelson *et. al.*, 1988).

1. 2. 3. Pulmonary surfactant.

Pulmonary surfactant, a lipoprotein-rich material, stored in the lamellar bodies in alveolar type 2 cells, is secreted constantly (Figure 1. 9). The surfactant is a thin film of biochemically heterogeneous and lipid-rich material covering the epithelial surface of the lung (Crouch *et. al.*, 1991). Two main roles of surfactant are to release lung surface tension in order to maintain normal alveolar structure (Mason, 1977; Devlin, 1993) and to contribute to the defence of the lung against xenobiotics. The main components of surfactant are phospholipid (~80%) mostly in the form of

dipalmitoylphosphatidylcholine with cholesterol (~10%) and proteins (~10%) (Khubchandani & Snyder, 2001).
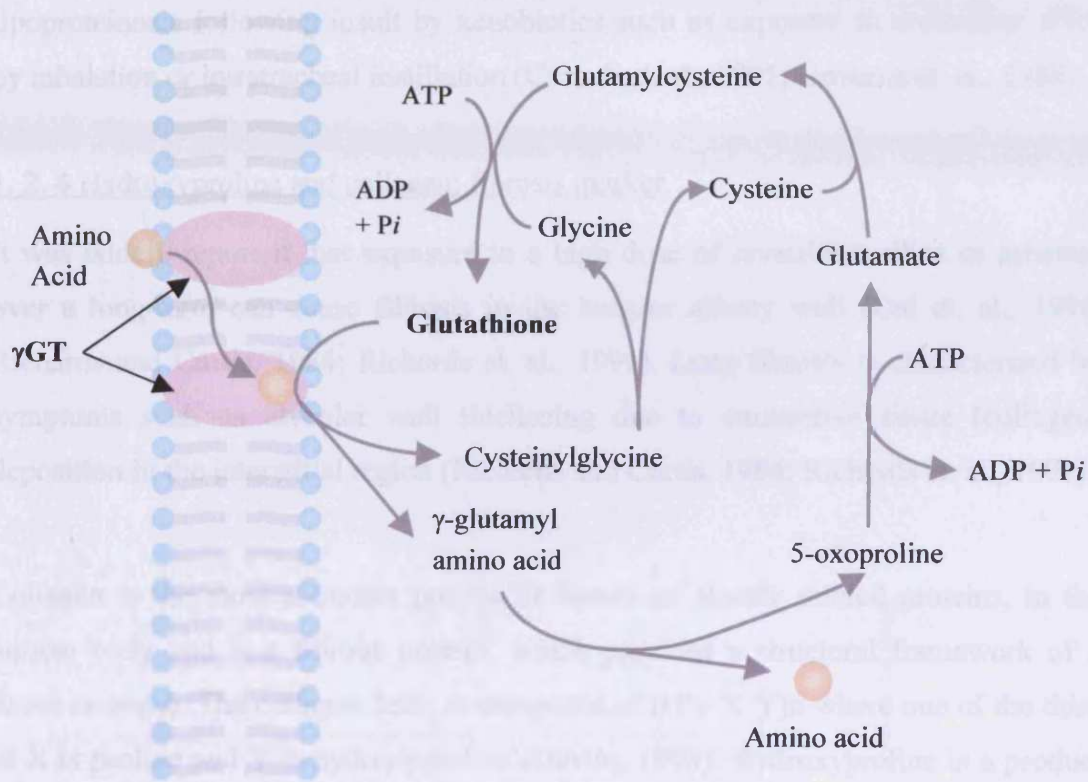
Figure 1. 8 The diagram represents the glutamyl cycle and the function of the γGT in the cycle. (modified from Devlin, 1993)

Figure. 1. 9 The swirl-like components (arrow) inside the type 2 cell are lamellar bodies, which contain surfactant (Young and Heath, 2000).

The surfactant secretion depends on the number of type 2 cells and their activity. Therefore, excessive secretion of surfactant material in alveolar spaces due to hyperactivity or hyperplasia of type 2 alveolar epithelial cells could cause alveolar lipoproteinosis following insult by xenobiotics such as exposure to crystalline silica by inhalation or intratracheal instillation (Crouch et. al., 1991; Governa et. al., 1986).

1. 2. 4 Hydroxyproline and collagen; fibrosis marker

It was widely reported that exposure to a high dose of crystalline silica or asbestos over a long-term can cause fibrosis in the lung or airway wall (Dai et. al., 1998; Richards and Curtis, 1984; Richards et. al., 1991). Lung fibrosis is characterised by symptoms such as alveolar wall thickening due to connective tissue (collagen) deposition in the interstitial region (Richards and Curtis, 1984; Richards et. al., 1991).

Collagen is the most abundant protein or family of closely related proteins, in the human body and is a fibrous protein, which provides a structural framework of a tissue or organ. The collagen helix is composed of (Gly-X-Y)n where one of the third of X is proline and Y is hydroxyproline (Devlin, 1993). Hydroxyproline is a product of hydroxylation of proline by prolyl 4-hydroxylase or prolyl 3-hydroxylase. Therefore, hydroxyproline is a good marker of collagen or, when this is deposited in excess, of fibrosis.

There are three particular ways to investigate the fibrotic potential of deposited mineral particles in the lung. Firstly, the hydroxyproline level in the lung can be studied using a colorimetric method or liquid chromatography. Secondly, quantitative histology is available to detect excessive collagen deposition in the interstitial region and to provide a visual image using a collagen-specific stain such as Masson's trichrome. Thirdly, mRNA expressional changes in connective tissue proliferation or growth factor or hydroxylation related genes can be studied using macro/micro array technology or reverse transcriptase polymerase chain reaction (RT-PCR).

1. 3 Lymph nodes and particle clearance

1. 3. 1 Lymph nodes

The lymphatic system is a part of the circulatory system and is composed of lymphatic vessels connected with lymph nodes, which are an aggregation of lymphoid tissue and circulating lymphocytes (Figure 1. 10, Kapit et. al, 2000; Thibodeau and Patton, 1993). The tracheobronchial lymph node is the organ where xenobiotics instilled or inhaled into the lung would be drained via lymph (Adamson I. Y. R. and Prieditis, 1998; Friedetzky *et. al.,* 1998; Muhle *et. al.,* 1995) and also filtered and phagocytosed (Kapit et. al, 2000; Thibodeu and Patton, 1993). It has also been reported that thoracic lymph nodes become frequently enlarged when there is silicosis in the lung (Reiser et. al., 1983; Adamson and Prieditis 1998; Friedetzky *et. al.,* 1998; Seaton and Cherrie 1998; Davis *et. al.,* 2001).
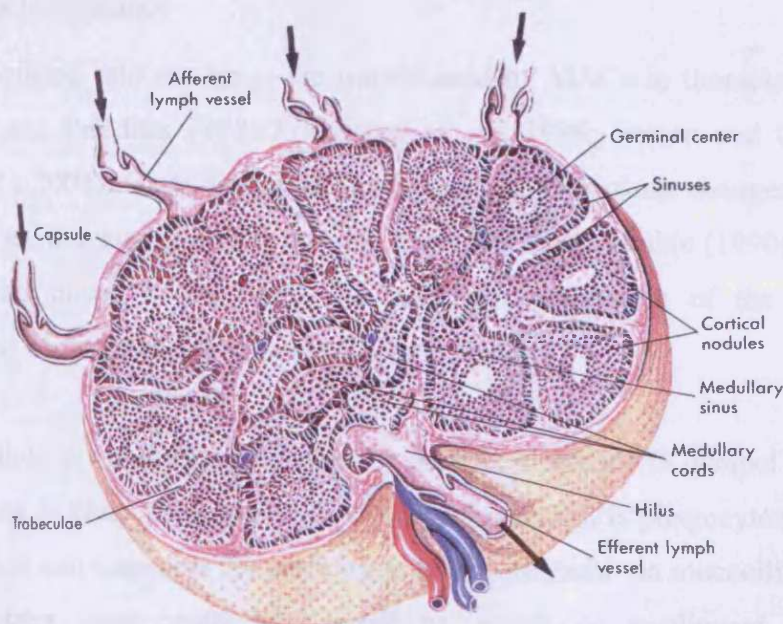
Figure 1. 10 Structure of a lymph node (Thibodeau and Patton, 1993)

The general structure of the lymph nodes is shown in Figure 1. 10 (Thibodeu and Patton, 1993). Generally, the lymph nodes are bean-shaped in structure. Each node is enveloped by a fibrous capsule and a trabercule extends from this capsule toward the centre of the lymph node. The trabercule is the border between sinuses and the

21

periphery or outer region of the central nodule, which is composed of packed lymphocytes in the nodes. Both central and medullar sinuses contain specialised reticuloendothelial cells capable of phagocytosis.

The two main functions of lymph nodes are defence and haematopoiesis (Thibodeu and Patton, 1993). Defensively, reticuloendothelial cells in the sinuses remove xenobiotics such as microorganisms or particles from lymph (filtration) and phagocytose them. Sometimes however, those cells fail to phagocytose injurious xenobiotics and the lymph node can become inflammed. Moreover, a local infection could cause regional lymph nodes to be inflammed as a result of the deposition of the toxins or microorganisms carried to the nodes by lymph (Kapit et. al, 2000). During haematopoiesis, lymphocytes and monocytes, which migrate from the bone marrow, mature in the lymphatic tissue of lymph nodes.

1. 3. 2 Particle clearance

Particles instilled into the lungs are translocated by MACs to thoracic lymph nodes (Adamson and Prieditis 1998; Friedetzky et. al., 1998; Seaton and Cherrie, 1998; Davis et. al., 2001). Once deposited bioreactive particles cause changes in the lymph nodes such as size augmentation or granuloma formation. Muhle (1990) also reported that overload doses in the lungs increase interstitialisation of the particles and translocation of the particles to thoracic lymph nodes.

There are three proposed mechanisms for particle clearance (Kuempel et. al., 2001). The first step to clear the particles in the alveolar region is phagocytosis by alveolar MACs, which can transport the particles to tracheobronchi via mucociliary clearance. These particles then could be cleared by cough or swallowed to enter the gastrointestinal tract. Secondly, some of the particles in the alveolar region can enter the interstitium of the lung through the epithelial region. Thirdly, the particles in the interstitium can be drained to thoracic lymph nodes by pulmonary lymphatic endothelial cells via the lymphatic vessels or alveolar/interstitial MACs during phagocytosis and translocation. The particles, which escape from all of the clearance mechanisms, could be involved in development of inflammation or fibrosis in the lung.

1. 4 In vivo studies using an intratracheal instillation technique

1. 4. 1 Intratracheal instillation and inhalation

There continues to be serious debate as to the advantages of inhalation versus instillation when investigating the effects of pulmonary toxins. The inhalation method is relatively natural and mild since anaesthesia is not included in the procedure. However, special equipment and expertise are required in order to perform the technique effectively, resulting in elevation of the cost. Moreover, a larger amount of particles is required to treat the animals than that needed for the instillation technique. Furthermore, the animals need to be exposed to particles for a longer duration in order to detect any change caused by the particles. This longer duration of treatment can cause high levels of stress in the animals, which may or may not affect results. Even with such a complicated procedure, it is still difficult to expose each animal in an identical manner, ensure that each receives an identical lung loading and thus identify links between the dose and any detrimental changes.

An alternative method is required in order to treat large number of animals with various doses under controlled conditions that minimise both duration of treatment and the stress incurred. Consequently, the non-invasive (no surgery involved) instillation technique is often employed. This simple and inexpensive approach allows the direct deposition of an exact dose, without any unnecessary exposure such as to the skin, eyes, or fur of the animal resulting in low level of stress. The characteristics of instillation and inhalation techniques are compared in Table 1. 6 (Driscoll et. al., 2000; Henderson et. al., 1995; Morrow et. al., 1996).

1. 4. 2 Doses chosen for a single instillation

The widely used dose for an instillation study in rats is 1.0 mg (single instillation) to investigate the toxicity of a respirable bioreactive mineral dust such as crystalline silica. If the particles were bioreactive then changes in the lung would be detected in 1-12 weeks post-instillation due to inflammatory reactions. However, higher doses and longer exposure periods are often employed to study further biological endpoints such as lipoproteinosis or fibrosis (Green *et. al.,* 1981; Richards, and Curtis, 1984; Richards, *et. al.,* 1991).

Table 1. 6 The strong and weak points of instillation and inhalation

	Instillation	Inhalation
Strong points	An exact dose is instilled	A natural route of entry in the host
	The technique is simpler than inhalation	Mild treatments possible
	Suitable for experiments required to treat a range of doses for short times	
	Avoids unnecessary exposure e.g. skin, eyes, fur, etc.	
	Makes it possible to evaluate not readily respirable materials to laboratory animals	
Weak points	Nonphysiological introduction	Expensive
	Invasive for a short period (minutes)	Special equipment is critical
	Higher dose or dose rate used	Special expertise is required
	Potentially different material distribution	Requires large amount of starting material
	Upper respiratory tract is bypassed	Safety considerations/ enclosure required
	Vehicle itself can cause effects	Most animals are obligate nasal breathers (unlike humans)
	Anaesthesia can give side effects	

1. 5 Macroarrays and data analysis

The exposure to particles would be expected to cause changes in pulmonary genes which reflect defence mechanisms or the development of disease states of the lung. The changes in the cDNA gene profiling in the lung can be studied using reverse transcriptase and mRNA extracted from the lung. Comparisons of gene expression between sham and treated lungs from animals can be made using conventional molecular techniques such as polymerase chain reaction (PCR) or northern blotting. However, at the outset of the present investigation in 2000, a new, if relatively untried, technology of macroarrays became available. Within our laboratory Reynolds and Richards (2001) reported the successful use of a commercially available macroarray system to examine changes in gene profiles in rat lungs treated with diesel exhaust particles, a dust of low bioreactivity. This system, described as a rat toxicology array permitted the investigation of 207 genes simultaneously. Since this time, more complicated arrays (with 1,200 genes) have been used within the group to study the effects of ambient pollution particles (Wise, PhD, 2004) and pulmonary oedema (Balharry, 2004).

Thus, the macroarray offers a powerful and informative technique to study gene profiling in the lungs under stress from a potential toxicant such as MA together with the opportunity to identify specific biomarkers of disease endpoints (Table 1. 5). The advantage of the technique is its high specificity and sensitivity with the potential to identify individual genes or clusters associated with conventional biochemical or histopathological changes in the lung. As with all new techniques there are a number of difficulties, which have been identified. Individual animal heterogeneity in gene expression can be important, as is the quality of the mRNA that is extracted from the lung. Extraction of mRNA can vary in a single lung lobe from one animal dependent on the focal distribution of an inflammatory response. Care has to be taken to prevent non-specific cross hybridisation of probe, account for differences in array membranes, primers and radioactive P^{32} samples. Finally, macroarrays generate enormous amounts of data and as yet there are no absolute guidelines (except Minimum Information about Microarray Experiment (MIAME), Brazma et. al., 2001) for the consideration of these data. The stringent analyses of these data sets may involve

several stages in order to minimise these variations. The first step is scaling which helps to minimise the variations among the arrays by matching overall mean intensities among arrays by calculating simple multiplicative factors. The second step is normalisation/standardisation in order to emphasise relative differences in mRNA expressional level. The third step is statistical analysis with a set stringency of fold changes and the fourth step is higher-level analysis such as clustering or prediction.

1. 6 The aims of this project

The overall aim of my studies was to investigate the toxicity of MA and its major component ANR alongside its minor component CRS.

Before starting toxicological or histopathological approaches, it is necessary to prepare the respirable fraction of MA and the two major components in order to utilise the particles for intratracheal instillation. The fractionated particles were then physicochemically characterised using an environmental scanning electron microscopy (E-SEM) and image analysis (Chapter 2). Characterised particles were instilled in varying dose (1.0 to 5.0 mg) into rats and changes at the lung surface/ tissue investigated at variable time point (6-49 weeks post-exposure) utilising conventional biochemical and cellular technique. The outcomes of these studies are reported in Chapter 3. To compliment the above studies, histopathology of lung tissue and thoracic lymph nodes, the site of particle clearance was undertaken (Chapter 4). Because early inflammatory reactions were detected in lymph nodes and delayed inflammation was observed in lung tissue treated with MA further physicochemical characterisation of deposited/ cleared particles were undertaken (Chapter 5).

Finally, a more mechanistic approach to understanding any potential damage caused by MA or its crystalline silica component was attempted utilising gene profiling (Chapter 6). It was anticipated that this multi-gene analytical approach could provide better markers of the inflammatory effects of MA.

2. Physicochemical characterisation

of Montserrat volcanic ash

and its major components; anorthite and cristobalite

2. 1 Introduction

Volcanic ash is defined as 'fine particles of pulverized rock blown from an explosion vent. Measuring less than 1/10 inch in diameter, ash may be either solid or molten when first erupted' (www.whfreeman.com). The size of volcanic ash is one of the important factors to decide its toxicity since only a respirable fraction (equivalent spherical diameter (ESD)<2.5 µm) can reach alveolar units. Therefore, respirable fractions of the Montserrat volcanic ash (MA) and its two major components such as anorthite (ANR) and cristobalite (CRS) were employed for toxicological investigations (see Chapter 3). All the physicochemical analyses were carried out for these respirable fractions of the mineral dust samples. Generally, volcanic ash contains various types of silicon compounds since silicon is the most abundant material in rock, soil or sediments (Krauskopf, 1995; White, 1995). These compounds can be categorised as a form of a crystalline silica/silicate or amorphous silica. The amorphous silica such as alkali/plagioclase feldspars (orthoclase, albite and anorthite) is known to be weakly bioreactive (Craighead et. al., 1983). In contrast, crystalline silica is known to be toxic. Therefore, the content of a crystalline silica such as cristobalite (CRS), α-quartz or β-quartz, tridymite, etc. may be one of the key factors contributing to the toxicity of mixed mineral dusts such as coalmine dust, diatomaceous clay or volcanic ash. The composition of volcanic ash varies depending on the date of collection, location, the type of volcanic activity such as explosive eruption or pyroclastic flow/surge etc. even though the ash was produced from the same volcano (Table 2. 1). Therefore, it is important to determine the physicochemical properties of each volcanic ash sample employed for toxicological studies.

Prof. Pooley (Cardiff University, UK) had previously analysed the compositions of MA using X-ray diffraction (XRD) and reported that MA contained 20.1% CRS and 78% feldspar, mainly anorthite. Dr. Berube (Cardiff University, UK) then measured the sizes of the MA, CRS and ANR particles to obtain the size distributions of these particles using transmission electron microscopy (TEM; Phillips) and an image analysis system. It was reported that some of smaller particles were attached to the

Table 2. 1 The crystalline silica content of volcanic ash used for different toxicological studies

Name of volcano	Type of crystalline silica	Amount	References
	Quartz and cristobalite	1.2 - 10.2 % in respirable fraction	Dollberg et al., 1986
	Quartz and cristobalite	3.8-4.3 % (w/w)	Graham et. al., 1985
	Free silica	2.8 %	Martin et.al., 1984
	Crystalline silica	1.5 %	Vallyathan and Robinson 1984
	Crystalline silica	2.73±0.22 %	Martin et. al., 1983
Mt St. Helens	Crystalline silica	3.7 % (<10 μm fraction)	Craighead et. al., 1983
	Crystalline silica	1.5-7.2 %	Vallyathan et. al., 1983
	Crystalline silica	3-4 %	Wehner et. al., 1983
	Crystalline silica	7.2 %	Castranova et. al., 1982
	(Quartz (Q) and cristobalite (C))	(Q: 3.0 % and C: 4.2 %)	
	Crystalline silica	1-3 %	Fruchter et. al., 1980
Mt Sakurajima	Crystalline silica	< 5.0 % (w/w)	Yano et. al., 1986
Mt Galunggung	Crystalline silica	1.36-1.95 %	Vallyathan and Robinson 1984
Mt El Chichon	Crystalline silica	1.72 %	Vallyathan and Robinson 1984
Soufrierie Hills	Crystalline silica	15-20 % (w/w)	Searl et. al., 2002
In Montserrat		13-20 % (w/w in respirable fraction)	Baxter et. al, 1999
	Cristobalite	3 % (explosion)	Wilson et. al., 2000
		11 % (dome collapse)	

larger particles. Nevertheless, TEM micrographs present these aggregation as one large particle and thus the measurement of some smaller particles could been excluded from the sizing.

The aims of the present study were to determine (a) the composition of the respirable fractions of MA, CRS, and ANR and the content of crystalline silica in the MA and (b) size distributions of all the particles including particle combinations (small particles attached to the larger ones). An environmental scanning electron microscopy (E-SEM 300, Phillips) was employed to obtain images of the particles for this study since these images showed three-dimensional morphology of the particles. Moreover, E-SEM images allowed identification/sizing of small particles found in aggregations whereas TEM images did not. An electron dispersive X-ray analysis (EDS; Oxford Isis 300, UK) combined with E-SEM was used for physicochemical analysis of the MA, the CRS and the ANR including atomic compositions of the particles.

2. 2 Materials and methods

2. 2. 1 Preparation of respirable particles

A bulk sample of MA was kindly provided by Prof. R. Maynard, CBE, (DoH, UK). The ash was collected on the 21st, September 1997 and originated from a dome-collapse pyroclastic flow. The respirable fraction of MA was prepared via wet centrifugal sedimentation by Prof. Pooley (Cardiff University, UK, Housley *et. al.,* 20 02). The pure artificial CRS was kindly provided by Dr. B. Williamson (The Natural History Museum, London, UK). A further control mineral was a sample of a natural mineral ANR [$CaAl_2Si_2O_8$], in the form of the igneous rock anorthosite (which consists of more than 90 % anorthite, Northern Minerals, Norway). A respirable fraction of this material was produced by Dr. T Jones (Cardiff University, UK, Housley *et. al.,* 2002).

2. 2. 2 Preparation of specimen for E-SEM analysis

The particles were spread on carbon tabs (12 mm dia, Agar Scientific Ltd. UK) attached to an aluminium stub (13 mm dia, Agar Scientific Ltd. UK) (Figure 2. 1). The specimen was then coated with carbon (K450, Emitech) or gold in a sputter coater (SC-500, BIO-RAD). This prevents charging and provides a better image under a high vacuum condition ($< 1.0 \times 10^{-5}$ atm) (Krinsley, 1998).

Carbon tab

Aluminium stub
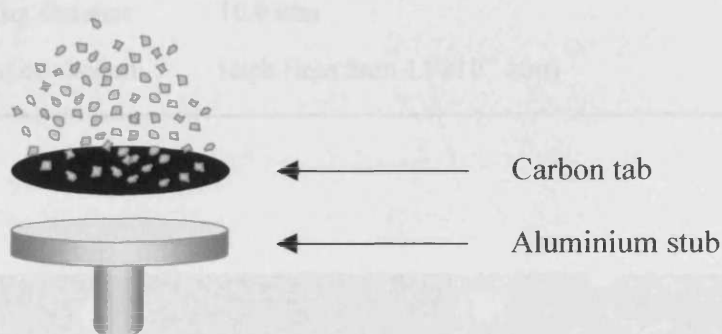
Figure 2. 1 Diagram of preparation of specimen for E-SEM.

2. 2. 3 Size of particles

The operating conditions of the E-SEM are shown in Table 2. 2. The back scattered electron (BSE) images for each particle specimen were taken at low magnification (x2,500) in order to observe relatively large particles (ESD>2.0 μm). At higher magnification (x15,000), smaller particles (ESD<1.0 μm) were easily detected. The sizes of all individual particles including those, which were attached to bigger particles, were measured using BSE images and an image analysis system (Leica Qwin, Leica Micro system imaging solutions Ltd, UK). Digitised images of selected particles were converted to a green colouration using the image analysis system. The size (ESD) was then calibrated using the length derived from measuring the scale bar on each image (Figure 2. 2).

Table 2. 2 Running condition of SEM

	Condition	Comment
SEM	Philips E-SEM	
Detector	Back-scattered electron detector (BSE)	
Aperture	5	Range: 1-6
Operating voltage	20.0 keV	
Spot size	3	Range: 1-4
Working distance	10.0 mm	
Degree of vacuum	High (less then 1.0×10^{-5} atm)	
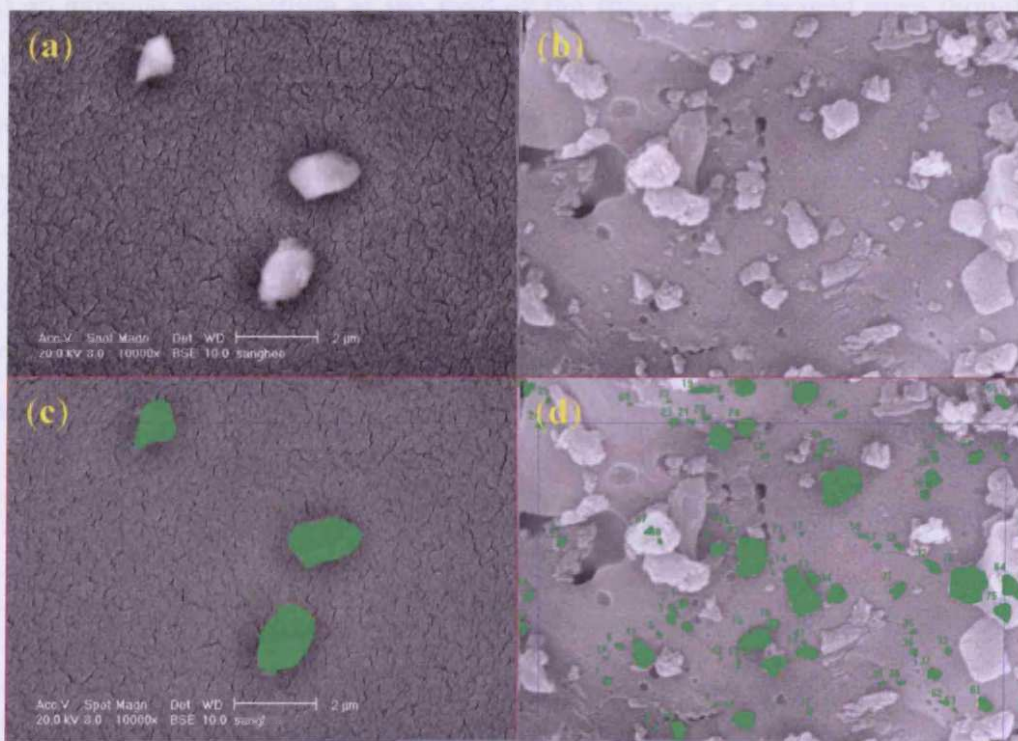
Figure 2. 2 The digitised BSE images of particles (a, and b) and the image (green, c and d) converted by an image analysis system for sizing purposes.

2. 2. 4 The atomic and molecular composition of particles

There are two ways to analyse the composition of the specimens, namely a mapping method and a pinpoint analysis. A pinpoint analysis gives the opportunity to select regions where only particles are located in isolation from interfering material. There are three ways to carry out a pinpoint analysis. The first way is to analyse grid points, which divide a square drawn over the image evenly, and the second is from spectra obtained from the points dividing a line drawn over the image evenly by an operator. With these two methods the operator can specify the number of divisions. The third way consists of the points selected manually and randomly. Twenty-five grid spectra from each field were chosen to be analysed using EDX at a low magnification (x2,500) in order to avoid subjectivity (Figure 2. 3). All the values from these analyses (the first way) were recorded and the average value was then calculated. The same fields were then analysed by a mapping method. A mapping method was employed to find an average composition of the field of the specimen examined even though this value could include the composition of the blank carbon (C) tab (background signal). A total of nine fields were analysed by the pinpoint and mapping methods. All the values from both the pinpoint analysis and the mapping method were calibrated using the ratio between the atomic percentages of the C and other atoms resulting from analysis of a blank carbon tab without particles. The compositions of the specimens were expressed as mean atomic percentages based on the standard compounds (Table 2. 3).
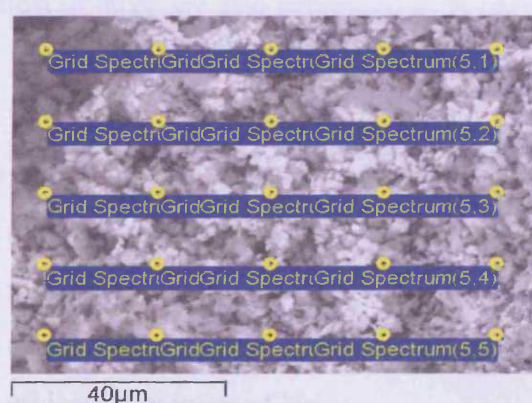
Figure 2. 3 Twenty-five grids points on the BSE image employed for a pinpoint analysis.

Table 2. 3 Standard oxide compound and formulae for each atom

Atom	Standard oxide compound and Formula
Al	Al_2O_3
Ca	CaO
K	K_2O
Si	SiO_2
Fe	FeO
Na	Na_2O

The molecular composition of MA was then extrapolated by stoichiometric approaches based on the atomic ratio of silicon (Si), aluminium (Al) and feldspar-specific atoms such as potassium (K), sodium (Na) or calcium (Ca) under the hypothesis that MA is composed of four materials namely a crystalline silica (SiO_2), alkali feldspars from orthoclase ($KAlSi_3O_8$) to albite ($NaAlSi_3O_8$) and plagioclase feldspars anorthite, ($CaAl_2Si_2O_8$) (White A. F. and Brantley S. L (1995). The serial equations were set up in order to find the relative amount of each kind of silica containing mineral dust. The molecular composition of the specimen is expressed as a weight percentage (% (w/w)) in order to make it easy to compare with other data from the literature since most of those are also expressed as % (w/w).

The hypothesis is

MA = a (SiO_2) + b ($KAlSi_3O_8$) + c ($NaAlSi_3O_8$) + d ($CaAl_2Si_2O_8$)
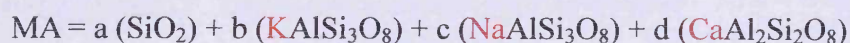
total relative molecular number of Si=(a+3b+3c+2d)

total relative molecular number of Al=(b+c+2d)

total relative molecular number of K=b

total relative molecular number of Na=c

total relative molecular number of Ca=d

if total relative molecular number of x is expressed as (x)

Therefore,

$(Si) = (Al) + 2x(K) + 2x (Na) + a$

$a = (Si) - (Al) - 2x(K) - 2x(Na) =$ relative molecular number of (SiO_2) in MA

$b = (K) =$ relative molecular number of $(KAlSi_3O_8)$ in MA

$c = (Na) =$ relative molecular number of $(NaAlSi_3O_8)$ in MA

$d = (Ca) =$ relative molecular number of $(CaAl_2Si_2O_8)$ in MA

if relative weight of x is expressed as X

$X = (x) \times$ molecular weight of x

and these values were then converted to percentages (w/w)

$$\text{percentages (w/w)} = \frac{X}{MA} \times 100$$

2. 3 Results

2. 3. 1 The BSE images of the particles uncoated and coated with gold

The particle specimen was coated with gold in order to get clear image since the conductivity of mineral dust is very low. The coating process with high conductivity material such as carbon or gold prevents charging and produce clear images (Figure 2. 4). With this process, it was much easier to recognise the smaller particles aggregated with the larger ones.
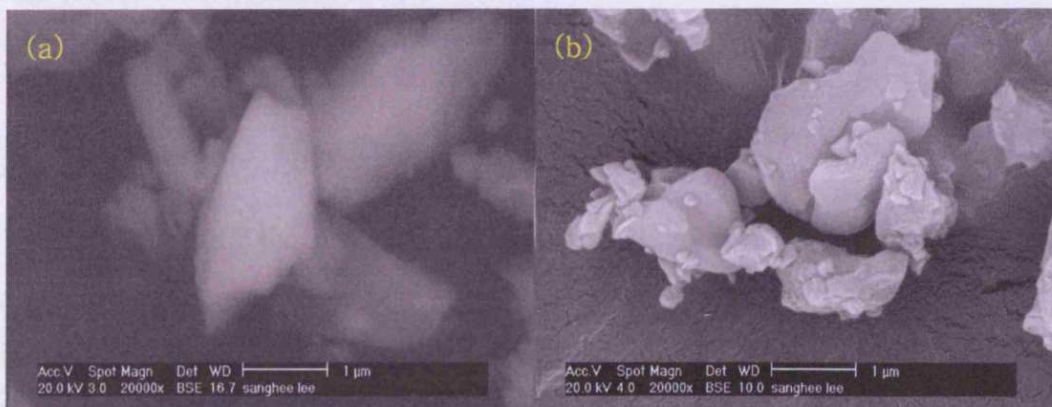
Figure 2. 4 The BSE images of the MA uncoated (a) and coated with gold (b). A scale bar is on each image.

2. 3. 2 BSE and SE images

BSE images were chosen (Table 2. 2) since the higher density or higher atomic numbered material gives the stronger signal (Krinsley, 1998). The BSE images expressed higher numbered material such as silicon and other metals which are major components of mineral dusts as white (Figure 2. 5). BSE images seem to be clearer than secondary electron (SE) ones under higher magnification (x15,000). The particles were not recognised from a SE (yellow circles) image were distinguishable against another particles in BSE images.
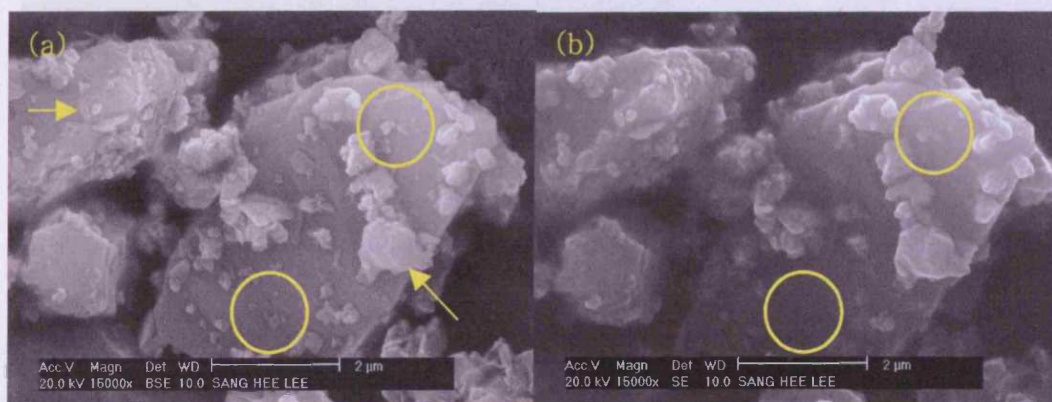
Figure 2. 5 The BSE (a) and SE (b) images of the CRS particles. The arrows depict the particles attached to the larger particles. The particles in the circles were visible on the BSE image (a) but not on the SE image (b).

2. 3. 3 The morphology of the particles

The morphology of the particles is shown in a Figure 2. 6. A number of smaller particles were attached to the larger ones in all specimens and clearly detectable under high magnification (x15,000). From the BSE images, the sizes of the particles attached to the larger CRS aggregates seem to be smaller than those which were attached to equivalently larger MA or ANR particles (see below).
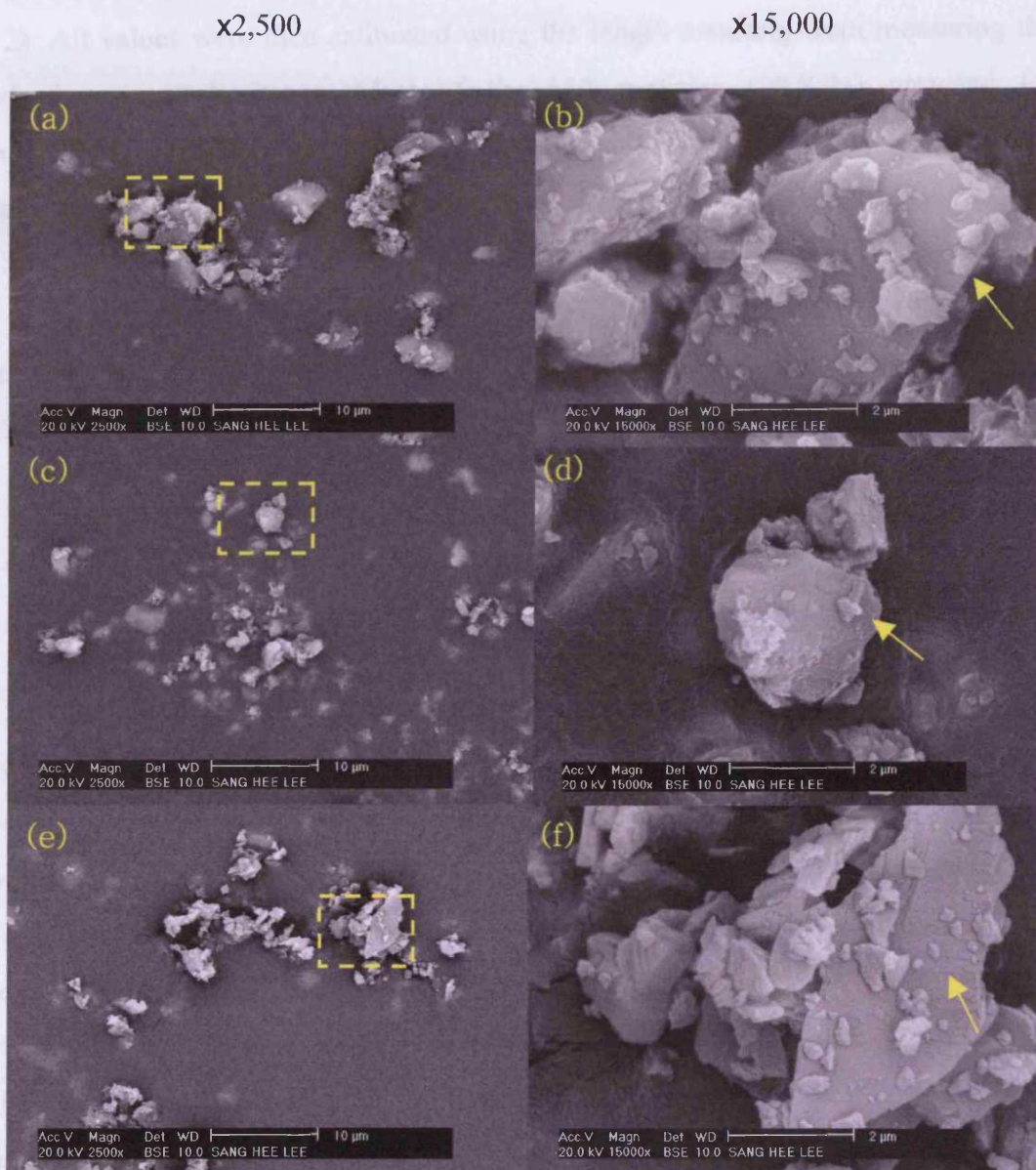
x2,500   x15,000

Figure 2. 6 The BSE images of the CRS (a), and (b), ANR (c) and (d) and MA (e) and (f) at low (x2,500) and high (x15,000) magnifications. The square depicts the region where the BSE image was taken under higher magnification and the arrows depict small particles, which were attached to the larger ones. A scale bar is given for each image.

2. 3. 4 The size of particles

The sizes (ESD) of the particles were measured using an image analysis system (see 2. 2. 2). All values were then calibrated using the length resulting from measuring the scale bar on each image. Most of the MA particles (99.87%) prepared for toxicological studies were respirable of which equivalent spherical diameter (ESD) is less than 2.5 μm (Figure 2. 7). Furthermore, 5.15% of the particles were ultrafine (ESD< 0.1 μm). Most of the ANR particles (94.86%) were also respirable and 4.39% of these are ultrafine. The respirable fraction of CRS is 97.60% and 32.19% of these are ultrafine. The percentages of the CRS particles of ESD range between 0.1-0.3 and 0.3-0.5 were relatively lower than the percentages observed for the MA or the ANR.

2. 3. 5 The composition of particles

2. 3. 5. 1 The composition of the carbon tab using a pinpoint analysis and a mapping method (Blank value)

The blank signal was obtained by analysing a carbon tab without any dust sample in order to deduce any background interference contributed by the carbon tab components. The relative amount of each atom was expressed as atomic percentages (Figure 2. 8). As expected the major signal came from carbon (C) and oxygen (O). However, the carbon tab contains Na, which is also found in albite ($NaAlSi_3O_8$). This apart, there is no sign of the existence of any other component of the MA, CRS or ANR such as Si, Al or other feldspar-specific atoms such as K and Ca on the blank carbon tab.

2. 3. 5. 2 The composition of particles using pinpoint analysis

All particle specimens were analysed and the atomic composition was expressed in the same way as detailed above (section 2. 2. 3). The atomic percentage of sodium (Na) in the specimen was calibrated considering the ratio of the atomic percentages between Na and carbon (C) from the background signal since the carbon tab itself contains Na (Figure 2. 8). The atomic composition of each mineral dust was expressed as an average value.

(a) MA
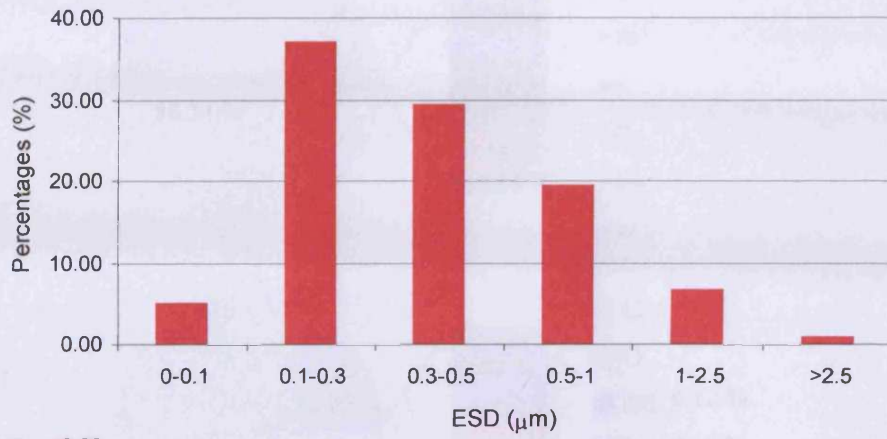
CRS
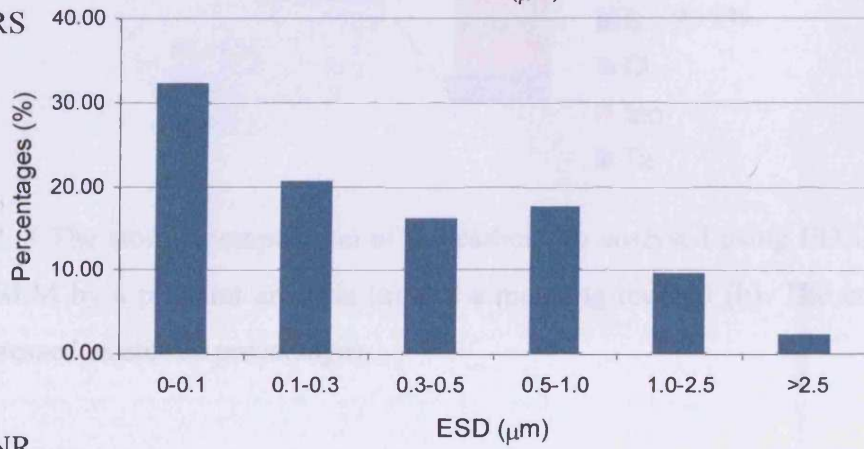
ANR
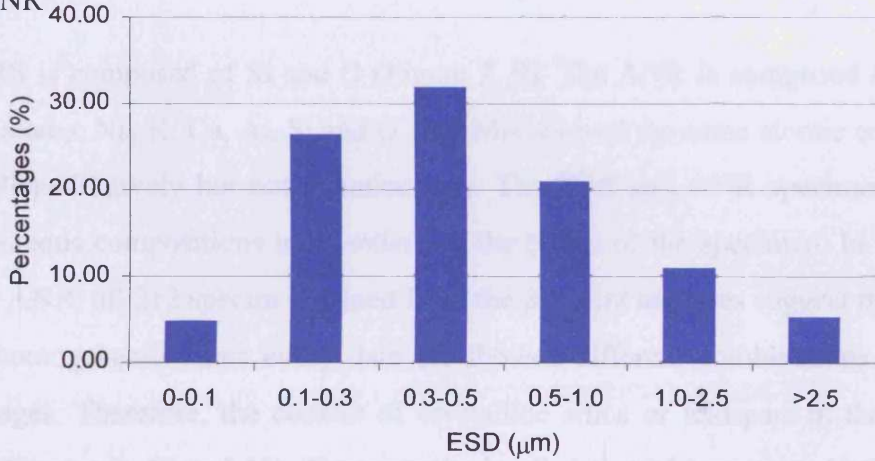
Figure 2. 7 Size distributions of MA, CRS, and ANR determined from BSE images and an image analysis.

(a)

(b)
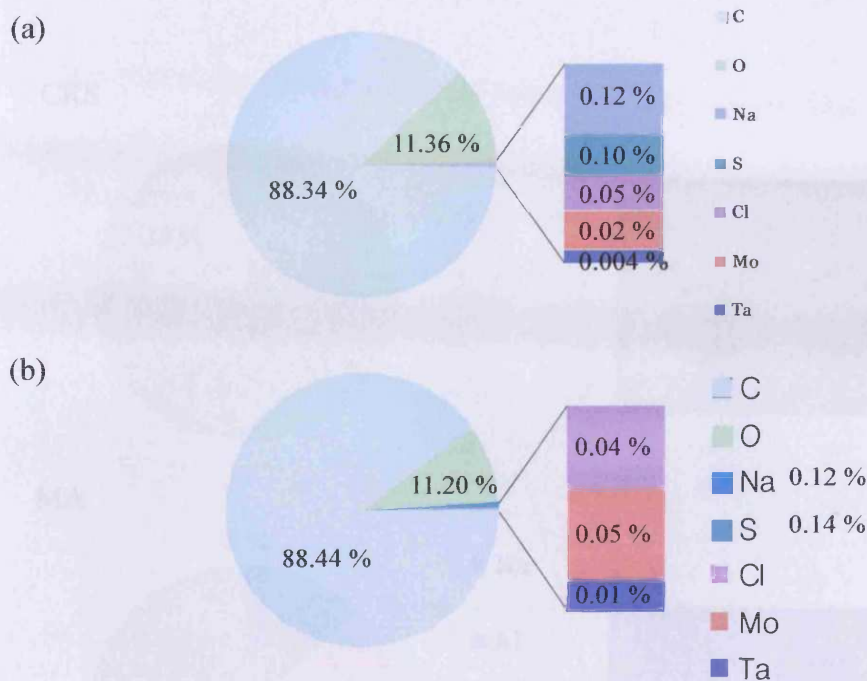
Figure 2. 8 The atomic composition of the carbon tab analysed using EDX combined with E-SEM by a pinpoint analysis (a) and a mapping method (b). The composition was expressed as atomic percentages.

The CRS is composed of Si and O (Figure 2. 9). The ANR is composed of feldspar related atoms; Na, K, Ca, Al, Si and O. The MA showed the same atomic composition as ANR qualitatively but not quantitatively. The CRS and ANR specimens showed homogeneous compositions independent of the points of the specimen. In contrast to CRS or ANR, all 212 spectra obtained from the pinpoint analyses suggest that the MA is not homogeneous since every data set showed different combinations of atomic percentages. Therefore, the content of crystalline silica or feldspars in the MA also varied (Figures 2. 10 and 11). These results implied that MA contains 19.73% (w/w) of crystalline silica and the most abundant component would be albite (42.91% (w/w)).

CRS
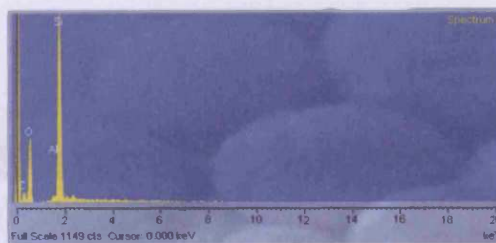
MA
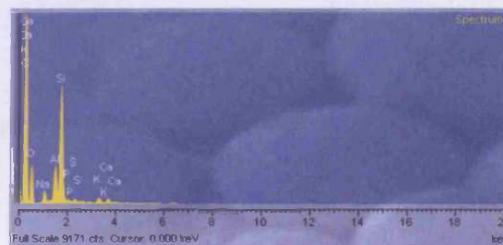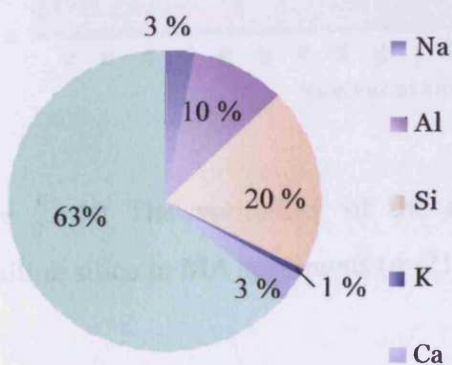
ANR
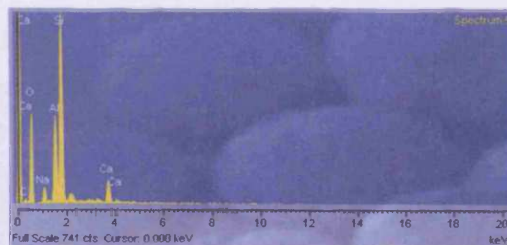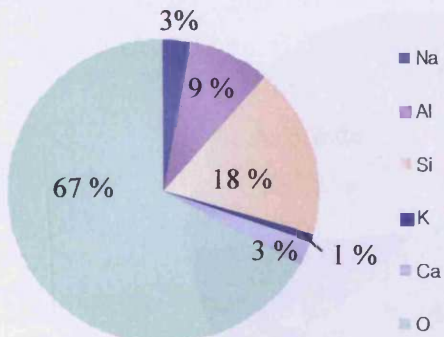
Figure 2. 9 The average atomic composition of CRS, MA and ANR decided by a pinpoint analysis using EDX combined with E-SEM. The composition was expressed as atomic percentages (n=210).

Figure 2. 10 The variability of the amount of albite, anorthite, orthoclase and crystalline silica in MA specimens (n=211).
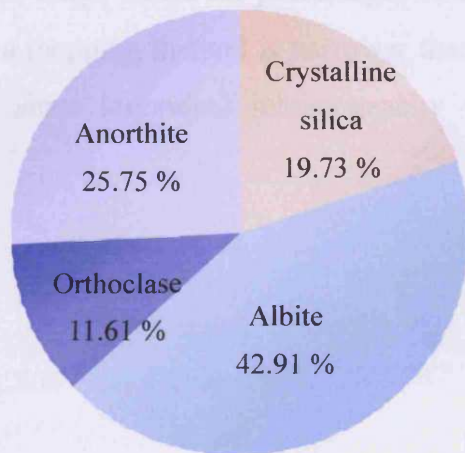
Figure 2. 11 The average molecular composition of the MA calculated by stoichiometric approaches based on the atomic composition from pinpoint analyses. The composition was expressed as a weight percentage of each molecule.

2. 3. 5. 3 The composition of particles using mapping

The compositions of particles were also investigated using a mapping method. The same field already analysed by a pinpoint analysis was again examined by a mapping method. This method gives the average composition of the field of the specimen analysed. These analyses proved again that CRS a pure compound composed of Si and O without any other atom (Figure 2. 12). ANR is made up of various atoms such as Si, K, Ca, Na, Al, and O, which are components of feldspars. The atomic percentages of the MA suggested the similarity between the atomic compositions of MA and ANR since the MA also contained feldspar specific atoms such as Al, Na, K, and Ca.

The molecular composition of the MA was calculated by stoichiometric approaches (Figures 2. 13 and 14) as explained previously (see 2. 2. 3). The results from the mapping method showed that the MA contains approximately 23.55% crystalline silica (Figure 2. 14). This value is higher than that obtained from the pinpoint analysis (19.73% (w/w)) (Figure 2. 11). Mapping analyses again showed the inhomogeneity of the MA without detecting any preponderance of crystalline silica or feldspars (Figure 2. 13). However, the range where the percentages of crystalline silica (17.55-29.61%) were spread from a mapping method is narrower than the range (0.99-78.53%) from pinpoint analyses since individual inhomogeneity was counterbalanced by other particles.

CRS
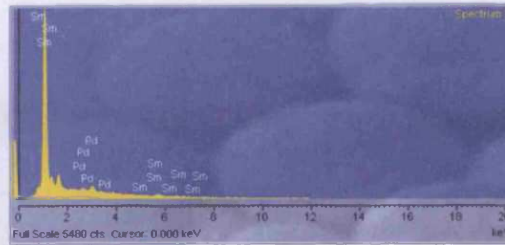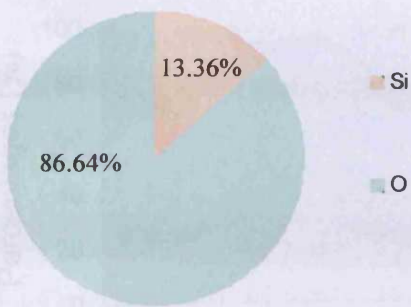
MA
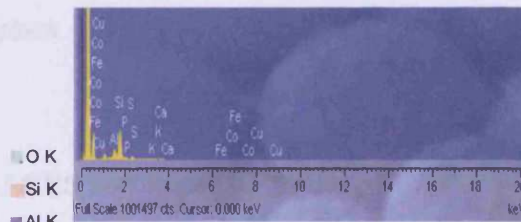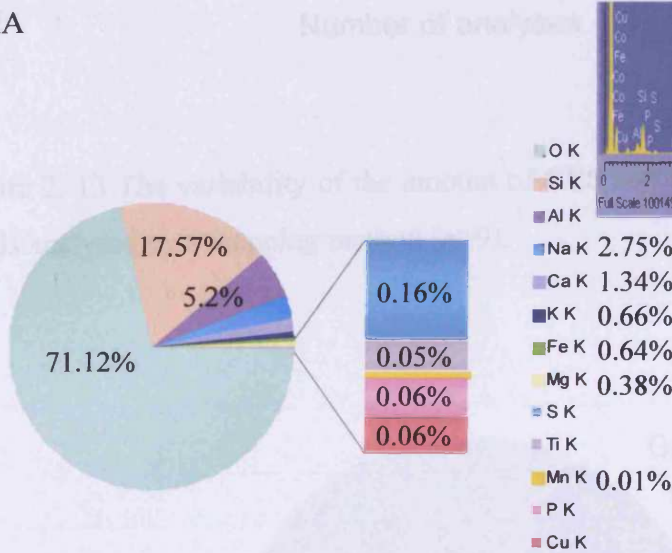
ANR
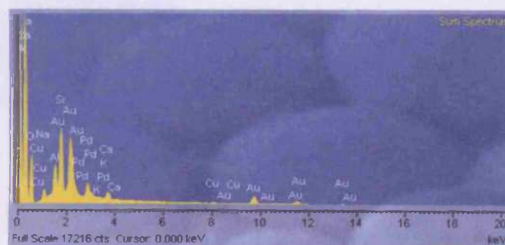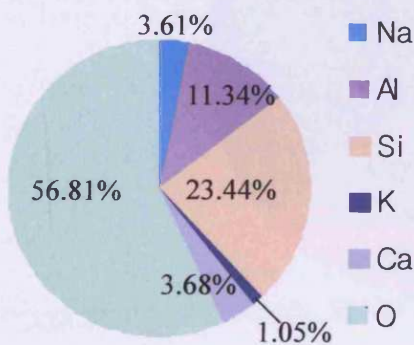
Figure 2. 12 The atomic compositon of CRS, MA and ANR determined by a mapping method using EDX combinded with E-SEM. The compositions were expressed as atomic percentages. The spectra of the CRS, MA and ANR gained from a mapping method (n=9).
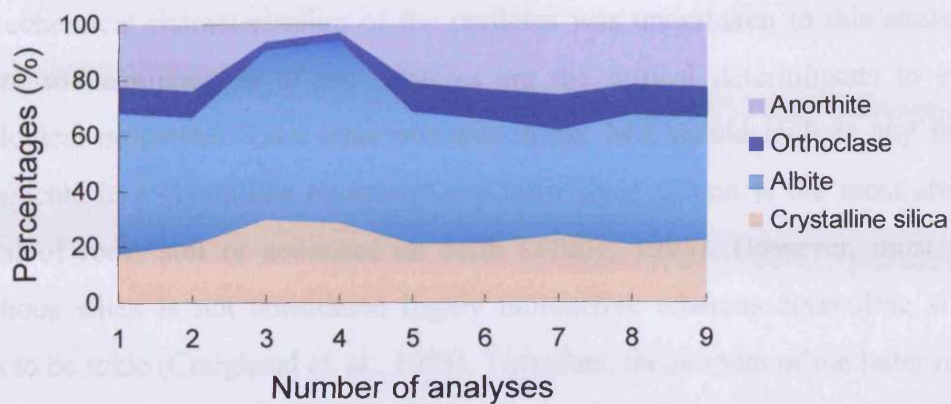
Figure 2. 13 The variability of the amount of CRS and feldspars in the MA specimen fields analysed by a mapping method (n=9).
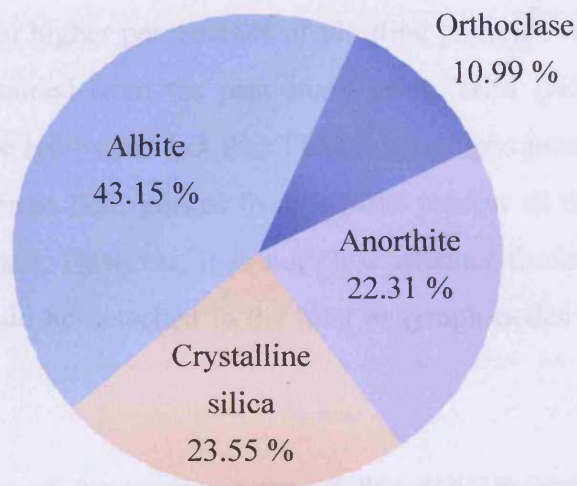
Figure 2. 14 The mean molecular composition of the MA obtained using a mapping method, atomic composition and stoichiometric approaches. The composition was expressed as a weight percentage of each molecule; albite, orthoclase, anorthite or crystalline silica.

2. 4 Discussion

Physicochemical characterisation of the particles was undertaken in this study since the size and composition of the particles are the critical determinants to explain toxicological properties. Like other volcanic ashes, MA would include any form of silica/silicate in a crystalline or amorphous form since silicon is the most abundant material of rock, soil or sediment on earth (White, 1995). However, most of the amorphous silica is not considered highly bioreactive whereas crystalline silica is known to be toxic (Craighead et. al., 1983). Therefore, the amount of the latter mineral in the ash would be critical in deciding the toxicity of the volcanic ash. Another decisive factor implicated in toxicity would be the size of the ash since only a respirable fraction could reach the deeper lung such as alveolar units and have a chance to cause changes in the lung. Therefore, it is important to find the proportion of crystalline silica known to be toxic and its respirable fraction in the ash sample.

In this study, the sizes of the particles, which are attached to larger one, were also measured resulting in higher percentages of ultrafine particles when compared to the size distribution obtained from the past study using TEM (Housley *et. al.*, 2002). These differences are led by the fact that TEM micrographs present those particles as one big particle whereas BSE images from E-SEM present all the particles including attached ones in detail. However, it is not clear whether those particles aggregated with larger ones could be detached in the lung or lymph nodes during the exposure-period.

The size distribution of the specimen was deduced by measuring the ESD of the particles from the BSE images using an image analysis system. Each diameter was then calibrated by measuring the scale bar on the image. These studies showed that mineral dust, the CRS, the ANR, and the MA prepared for the toxicological studies are mostly respirable. Therefore, it implies that compositional analyses also examined in this study were carried out for the respirable fraction of the MA, the CRS and the ANR.

Strictly speaking, it would be questionable whether the physicochemical properties of several specimens can represent the general physicochemical properties of the MA in the atmosphere. There are several factors, which affect the relative amount of the MA or crystalline silica in the air. Firstly, the amount of ash generated per unit period affects the concentration. Secondly, the ash generated via pyroclastic flows normally contains a higher content of crystalline silica than that via explosive eruptions (Jones, 2000). Thirdly, the re-suspension of already deposited ash by mechanical activities would happen more often in dry seasons resulting in increases in the concentration of the ash or a crystalline silica in the air (Searl et. al., 2002). Therefore, it is always important to find information about the generation and collecting conditions of the MA in detail since its composition will vary depending on those conditions.

Thus, there are a number of potential sizes and chemical compositions of MA and each sample should be physicochemically characterised prior to use by toxicologists. In this study, a respirable fraction representative of pyroclastic flow and a dry season of July 1997 was chosen for investigation. This sample, already partially characterised by others (Pooley, 2000; Housley et. al, 2002) was further investigated using differential techniques.

Both a pinpoint analysis and a mapping method were employed to find the composition of the particles using EDX combined with E-SEM. A pinpoint analysis produced twenty-five grid spectra in each field and the same field was again analysed using a mapping method (n=9). Both analyses produced slightly different atomic compositions of the MA specimen. Interestingly, the proportion of silicon dioxide believed to be crystalline silica seemed to be higher in the studies using a mapping method compared to those from pinpoint analyses. Furthermore, iron (Fe) was detected from the mapping analyses but it was not detectable using pinpoint analyses. These observations implied that compositional analysis would vary slightly with the method chosen.

In spite of minor differences, the results from both methods of analysis identified two findings of the molecular compositions of the MA. Firstly, the deduced molecular composition was albite> anorthite> crystalline silica> orthoclase with albite being the most abundant material in the MA specimen. Secondly, the composition of the MA is not homogeneous since variations were recognisable among the atomic compositions from either pinpoint or mapping analyses. Therefore, the content of the crystalline silica also varies. The inhomogeneity could result from differences in the composition of individual particles or a preponderance of crystalline silica or feldspar particles in the specimen. However, the grid spectra from the pinpoint analyses suggested that the particles are spread in a random manner. Moreover, the results from mapping methods did not show any affinity among crystalline silica/feldspar particles.

In summary, size distribution of the CRS, ANR and MA specimens showed that the particles prepared for toxicological surveys are mostly respirable. The MA contains approximately 20 % crystalline silica. However, the MA is not homogeneous and any preponderance of crystalline silica or feldspars was not recognisable. Furthermore, it was suggested that most of individual particles of MA contained both crystalline silica and feldspars.

3 Quantitative biochemical and cellular changes

in the rat lung instilled with

Montserrat volcanic ash or

its two major components; anorthite and cristobalite

3. 1 Introduction

The Soufriere Hills volcano in the island of Montserrat, believed as dormant, made the first documented eruption in 1995. The volcanic activity has involved and continuous to the explosive eruption, dome growing, dome collapse or pyroclastic flow/surge and continues to the present time. The latest big event happened as a hybrid earthquake swarm and pyroclastic flow during the period 9-12th July, 2003. Heavy ash and rock fragments falls then followed on 13th July (http://www.volcano.si.edu).

Generally, volcanic ash from a pyroclastic flow contains a high content of a crystalline silica, classified as a human carcinogen by the International Agency for research on Cancer (IRAC) (IRAC, 1997). Indeed, some Montserrat volcanic ash (MA) has been reported to contain a crystalline silica in the form of cristobalite (CRS) (Baxter *et. al.,* , 1999). Moreover, the risk of cumulative exposure to the dust caused by both continuous ash generation due to on going volcanic activities and resuspension of the MA already deposited by wind or mechanical activities raises further concerns. These two characteristics of the situation in Montserrat raised the concerns about the health of residents. Therefore, risk assessments including toxicological studies were required to find out more about the bioreactivity of the MA.

To date, few toxicological studies with MA have been reported. One *in vitro* study suggested that a high dose (30 mg/mL) of MA from an explosive eruption has mild haemolytic activity (Wilson *et. al.,* 2000). Such a finding indicated that this particular sample of MA exhibited a low bioreactivity. Similarly, a short-term *in vivo* study showed that 1 mg instillation of MA from pyroclastic flows in rat lung had little inflammatory potential compared to the same dose of pure preparation of CRS (Housley *et. al,* 2002). Such findings indicate a low risk to residents inhaling MA despite alternative suggestions to the contrary that exposure to MA with a high CRS could lead to lung fibrosis (Baxter *et. al.,* 1999). The earlier *in vivo* studies by Housley *et. al.,* (2002) did have limitations. Firstly, they were conducted short term (11 weeks maximum exposure) and therefore could not provide information on lung fibrosis as this scarring event is unlikely to occur in the absence of inflammation noted in these studies. Secondly, the dose of 1 mg instilled into the rats, whilst being a mass that is

recognised to produce inflammation if the dust is bioreactive (Henderson *et. al.*, 1995; Murphy *et. al.*, 1998) may well have been too low to produce any damaging effects.

The objective of the present study was to determine the long-term toxic potential of a respirable fraction of MA, containing 20 % CRS, obtained from pyroclastic flows in 1997 (as used by Housley *et. al.*, 2002). In addition, other animal groups were to receive instillations of CRS and anorthite (ANR). ANR, feldspar, is a major component of MA (see Chapter 2). Three different doses of ash, ANR and CRS were selected for the present study. The lowest dose (1.0 mg) was chosen since this amount of mineral dust could cause inflammation within 12 weeks if it is bioreactive and for comparison with other dust materials (Henderson *et. al.*, 1995; Murphy *et. al.*, 1998). The highest dose used (5.0 mg) was chosen because instillation of this mass into rats can lead to fibrogenic effects in the lung in the long-term (Richards and Curtis, 1984). In addition, as 5.0 mg of MA would contain 1.0 mg of crystalline silica, further comparisons between treated groups would be possible to determine if the CRS was equally bioreactive in the presence or absence of ANR. As good toxicological practice, an intermediate instilled dose of 2.5 mg was also selected for all three exposed groups. Sham-treated (control) animals received the vehicle instillate (0.15 M sodium chloride (NaCl)) only.

Alterations in lung biochemistry were assessed (Richards and Curtis. 1984; Murphy *et. al.*, 1998; Richards *et. al.*, 1991) using measurements of lung permeability (lung: body weight, lavage surface protein), inflammation (lavage free cell numbers, differential counts), parenchymal proliferation (dried lung weight) and fibrogenesis (hydroxyproline). The parameters measured in lung and lung lavage fluid are shown in Table 3. 1 with details of the biological endpoints such as oedema, specific effects on epithelial cells, inflammation and fibrogenesis. Further information on each parameter measured is given in the materials and methods section.

Table 3.1 Biological endpoints

Biological Endpoint	Comment on Health Effect
Parenchymal wet lung: body weight	Early increases above control indicate increased lung permeability. Later increases indicate cell replication/fibrogenesis
Total protein (1,000g lavage)	Early increases denote changes in epithelial permeability with protein accumulation at the lung surface (oedema)
Acid phosphatase activity in free cells lavaged from the lung	High activity represents the increase in a number of active macrophages (MACs).
Differential cell count	An increase in the number of MACs alone is usually indicative of a mild inflammation. A persistent, proportionate increase in the number of PMNs is associated with a more severe inflammatory response.
γ-Glutamyl transpeptidase (300 g lavage)	Increases denote epithelial type 2 and Clara cell damage
Alkaline phosphatase activity (300 g lavage)	Increase indicates type 2 cell changes
Total pulmonary surfactant complex (lavage)	Early small increases/decreases show changes in type 2 cells. Later more extensive increases indicate lipoproteinosis
Dried lung weight	Increases denotes cell proliferation
Hydroxyproline level in the lavaged lung	Elevation indicates fibrogenesis in the lung

3. 2 Materials and methods

3. 2. 1 Instillation

Male, CD 1 strain rats (approximately 170 g, Charles River, UK), specific pathogen free, were kept in wire-bottomed cages for one week before treatment. The animals were anaesthetised with halothane (Merial Animal Health Ltd.) and exposed to particles by non-invasive intratracheal instillation using a syringe with sterile 0.15 M sodium chloride (NaCl) solution (0.5 mL) inserted through a glass tube (Richards and Curtis, 1984). Three doses (1.0, 2.5 or 5.0 mg) of mineral dust (MA, CRS, and ANR) were instilled into 5 animals of each group. These dusts were prepared as explained in 2. 2. 2 and the physicochemical properties of each mineral dust were characterised in 2. 3. A sham-treated group was instilled with sterile 0.15 M NaCl solution only. Each group was sacrificed at 6, 13, 25 or 49 weeks post-treatment.

3. 2. 2 Lung indices – Lung and body weight ratio and dried lung weight.

The rats were sacrificed by a lethal intraperitoneal injection of euthatal (pentobarbitone sodium B. P., 200 mg/mL, Rhone Animal Health Ltd. UK). The body weight of each rat was recorded before dissection. The blood free lung was obtained by perfusion with the sterile NaCl solution (0.15 M) via the pulmonary artery. The lung was detached from the cavity and weighed. After lavage, the trachea was cut from the lung and briefly dried and its weight was recorded. The weight of lung parenchyma was deduced as total weight minus the weight of the trachea. The parenchymal lung was then blot dried and each lobe was excised. The *lobus dexter cranialis* was weighed. The lobe was dried in an oven at 75 °C for 1 week and its dried (constant) weight was recorded. Based on the wet weight, the dried weight of the whole of the lung could then be calculated.

3. 2. 3 Lung lavage

The lung lavage, which contains all the proteins secreted by epithelial lining cells, surfactant, and free cells (mostly macrophages in sham exposed animals) was collected by washing the inner lining of the lung with sterile 0.15 M NaCl solution (7~10 mL) five times. The pooled lavage fluid was centrifuged at 300 g for 10 minutes at 10 °C to remove cells and 8x1 mL of the supernatant (300 g) was taken and

dispensed to 8 Eppendorf tubes for storage. The remaining supernatant was centrifuged again at 1,000 g for 1 hour at 4 °C and 5x1 mL of the supernatant (1,000 g) was taken and dispensed to 5 Eppendorf tubes for storage. The pellet was then processed to obtain surfactant (see below 3. 2. 10). All the samples were frozen in liquid nitrogen and stored at -80 °C (Richards and Curtis, 1984).

3. 2. 4 Acellular protein in the lavage fluid (1,000 g supernatant)

Bovine serum albumin solution (2mg/mL in 0.9 % NaCl solution, Sigma) was employed as a standard to quantify the amount of acellular protein in the lavage fluid. The solution was diluted to the range; 1.25 to 20 µg/mL with phosphate buffered saline solution without magnesium (Mg) and calcium (Ca) ion (PBS, pH 7.4). The PBS was employed as a blank. A diluted (10 times or 20 times) sample, 1,000 g lavage fluid (200 µL), with PBS was added to the each well of a 96 well plate. Bradford reagent (50 µL) was then added. The absorbance at 590 nm was read using a plate reader (Bradford, 1976). Assays for each lavage and standard solution were performed in triplicate and the total mean value for protein was calculated for each animal.

3. 2. 5 Free cell number

The free cell fraction was obtained as a pellet by centrifuging the lung lavage at 300 g for 10 minutes (see above). The pellet was resuspended with 0.15 M NaCl solution (3 mL) and then added to the cell counting chamber (Weber Scientific International Ltd., England). The number counted under the microscope (x) was converted to the total free cell number per lung by multiplying by the whole volume of cell suspension (x x 10^4 x 3).

3. 2. 6 Differential cell counting

The cell suspension containing 100,000-cell/ mL from each animal was prepared by adding sterile saline solution (0.15 M NaCl) to the pellet resuspension depending on the number of free cells counted. The solution (6x1.0 mL) was centrifuged in a cytospin for 6 minutes at 12,000 rpm onto glass slides, which were air-dried. The slides were fixed and stained with Rapi diff kit (Raymond A. Lamb Ltd., UK). The

stained slides were mounted with DPX (containing dibutylphthalate and xylene, BDH Laboratory supplies, England) and then the numbers of MACs and PMNs were counted under a light microscope. MACs appeared as large and relatively round. Their nuclei were stained blue and cytoplasm red. PMNs seemed to be relatively smaller than MACs and their cytoplasm was hardly visible. The multiple lobulated nucleus was stained as blue as found with MACs (Bain, 1989).

3. 2. 7 Acid phosphatase activity in the free cell population

Acid phosphatase, located in the lysosome-rich compartment of the alveolar macrophage provides an additional quantitative marker to differential counting of this cell population (Kwok-wai Lam et. al., 1982). An Eppendorf containing 1×10^6 frozen (-80 °C) free cells was thawed at 37 °C, and 0.15 M NaCl solution (1.0 mL) added to the sample. Approximately 12,500 cells were required for analyses (deduced from pilot studies). To release latent acid phosphatase activity the cells were sonicated for 1 minute at 0 °C.

Acid phosphatase was measured by adapting Sigma kit (No. 104-LL) used to measure alkaline phosphatase. This adaptation involves the replacement of 2-amino-2-methyl-1-propanol buffer (1.5 M, pH 10.3) with citrate buffer (citrate 90 mM and chloride 10 mM, pH 4.8). One unit of acid phosphatase activity is defined as nmol p-nitrophenol released for 1 hour at 37°C. Data were expressed as total activity for the whole population of free cells lavaged from the lung surface. Assays for each lavaged free cell population were performed in triplicate and the mean value was calculated for each animal.

3. 2. 8 γ-glutamyl transpeptidase activity in lavage fluid (300 g supernatant)

γ-glutamyl transpeptidase (γGT) acts as a good marker enzyme for bronchiolar Clara and alveolar type 2 cells (Dinsdale et. al., 1992). The majority of the enzyme protein structure is found in the extracellular region of these cells in the close proximity with the epithelial lining fluid (Devlin, 1993). Thus, high levels of this enzyme in lavage fluid would indicate damage to the surface of Clara and type 2 epithelial cells. Lavage fluid (300 g, 25 μL) was used for analyses. γGT activity was measured by adapting a 96 well plate with Sigma kit (No. 545A). One unit of activity is defined as p-

nitroaniline (nmol) generated per minute at 37°C. Data were expressed as total activity for whole lavaged fluid from the lung surface (at pH 9.0). Assays for each lavage were performed in triplicate and the mean value was calculated for each animal.

3. 2. 9 Alkaline phosphatase assay in lavage fluid (300 g supernatant)

Alkaline phosphatase is also a good marker for Clara cells and type 2 cells and therefore any damage to these cells will result in alkaline phosphatase released into the epithelial lining fluid and its detection in lavage. Alkaline phosphatase was measured using Sigma kit (104-LL). The reaction scale was modified for a 96 well plate. One unit of activity is defined as nmol p-nitrophenol released for 1 hour at 37 °C. The data were expressed as total activity for the whole lavaged fluid from the lung surface. Assays for each lavage were performed in triplicate and the mean value was calculated for each animal.

3. 2. 10 Surfactant

The complex of pulmonary surfactant, the major product secreted by type 2 cells was quantified from lavage samples by the method described by Richards and Curtis (1984). Excessive accumulation of this material at the lung surface results in the disease process known as lipoproteinosis (Eskenasy, 1989; Governa et. al., 1986; Khubchandani and Snyder, 2001). The five pellets of the group of animals treated with the same dose of the same dust for the same period were obtained after two centrifugations of lavage fluid (300 g and 1,000 g) and resuspended with 4 M NaCl solution (10.0 mL). These solutions were centrifuged at 1,500 g for 30 minutes. The white pellicle, which floated to the top of the tube, was collected and dialysed against distilled water for approximately 50 hours with stirring at 4 °C. The water was changed twice. The dialysed solution containing pure surfactant was freeze-dried for two or three days and weighed. The data were expressed as a mean value per animal lung.

3. 2. 11 Hydroxyproline

Hydroxyproline is an unusual aminoacid, which acts as a marker for collagen-like proteins. During interstitial matrix repair (fibrogenesis) or lung scarring (fibrosis), the amount of collagen in the lung increases. The hydroxyproline level in the lavaged lung was measured using a method modified from that of Huszar *et. al.,* (1980). The dried lung was ground and the powder was digested with 4 M sodium hydroxide solution at 100 °C for 1 hour. The assays were performed in triplicate and the mean value was calculated for each animal.

3. 2. 12 Data analyses

The Kruskal-Wallis test, which is appropriate for a non-parametric data set due to its low degree of freedom and large variances, was applied in order to find statistical distinction between two different groups (at 95 % confidence level) using Minitab (13.0).

3. 3 Results

3. 3. 1 Exposure time and dose effects

3. 3. 1. 1 General health aspects

There was no animal loss during the instillation treatment. After treatment, the general health of the treated animals was checked regularly based on the body weight changes, any sign of malaise, excessive respiratory rates or nasal discharge. No sign of these symptoms was noted in any animal during the 49-week exposure period. The growth curves set by each treated group did not show any significant differences between sham and particle-instilled groups (Figure 3. 1).

3. 3. 1. 2 Oedema

The permeability changes (lung leakage or oedema) can be indicated by early increases in wet lung and body weight ratios or the amount of the acellular protein recovered from the lung lavage. The sham-exposed groups maintained the ratios with small ranges for all four sacrifice-time points (Figure 3. 2). In contrast, lung and body weight ratios increased and displayed a large distribution range in CRS-instilled
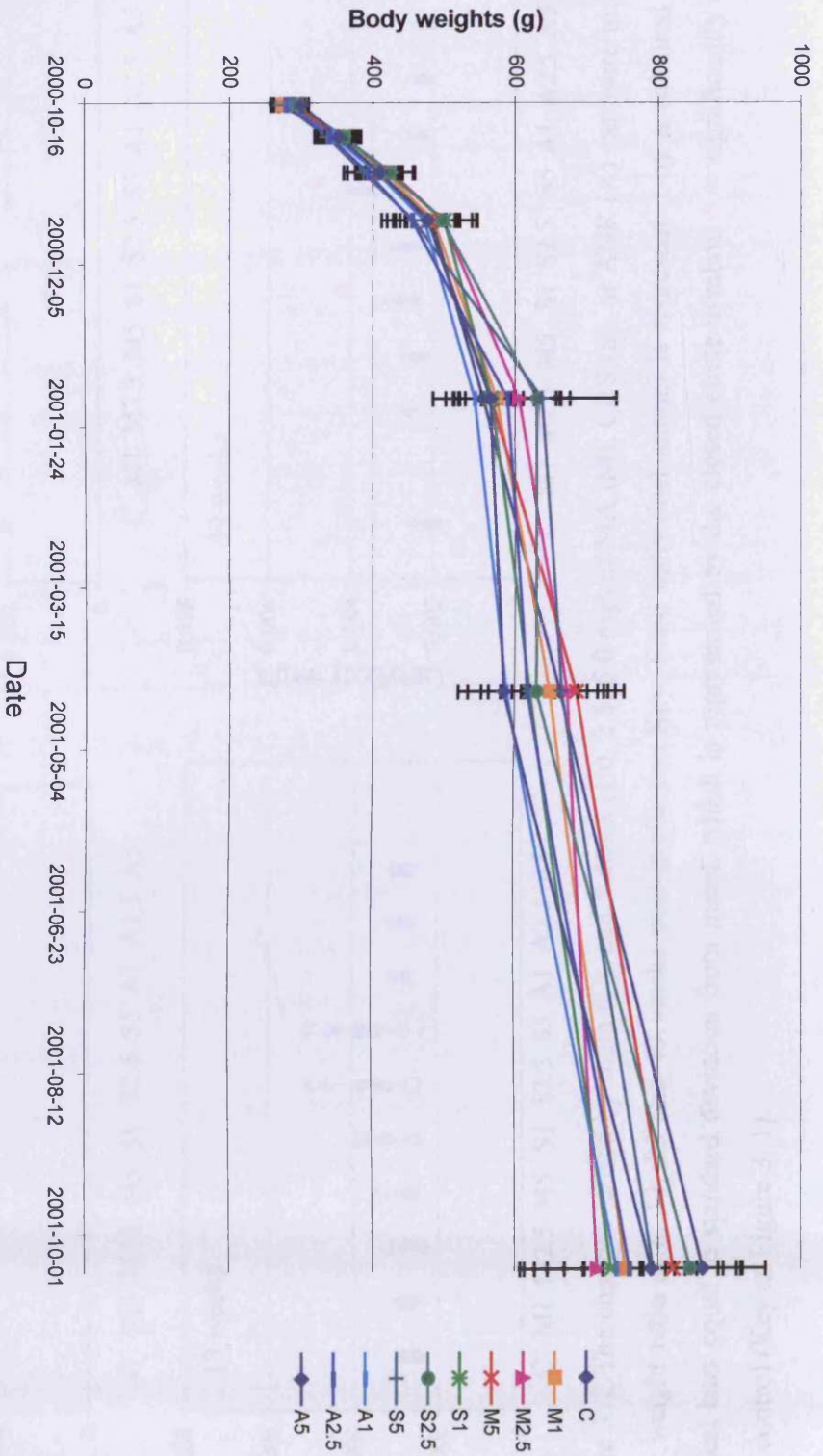
Figure 3. 1 Mean body weight with time post-instillation for all the treatment groups (C=sham-treated control rats, M (1, 2.5 and 5) = Montserrat volcanic ash at 3 doses (mg) A= anorthite; S=cristobalite.). The vertical bars represent standard deviation.
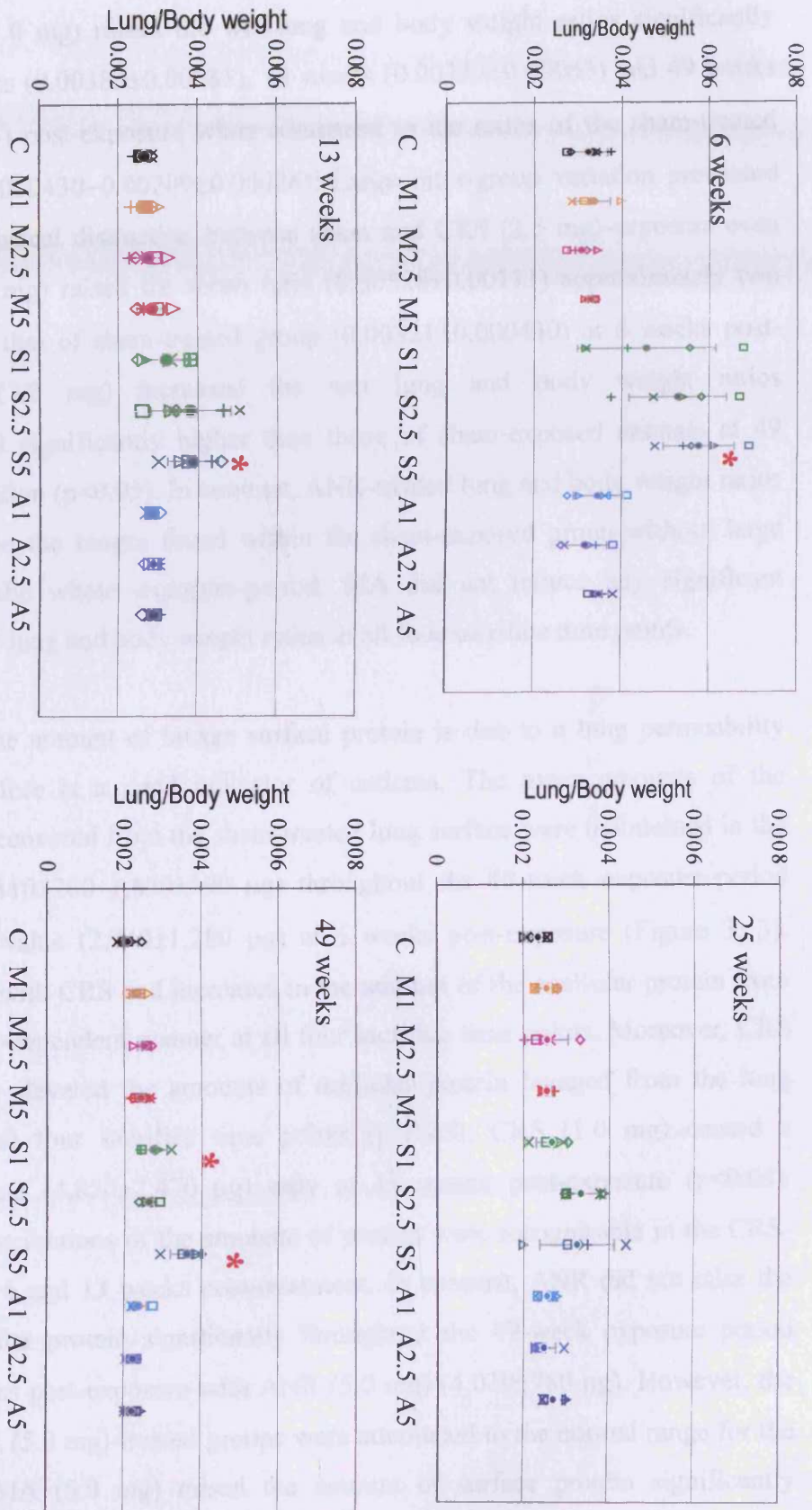
Figure 3. 2 The changes caused by sham (C), and 3 doses (1.0, 2.5, 5.0 mg) of MA (M), CRS (S), or ANR (A) exposure in lung and body weight ratio at 6, 13, 25 and 49 weeks post-instillation Key. Each individual animal is represented by a coloured symbol. Vertical bars equal to standard deviation from mean, which is represented by the closed circle symbol. * = significantly different from control (Key as Figure 3.1).

animals. Clear dose dependent effects were noticed at 6 weeks post-instillation. Moreover, CRS (5.0 mg) raised the wet lung and body weight ratios significantly ($p<0.05$) at 6 weeks (0.00383 ± 0.00081), 13 weeks (0.00323 ± 0.00063) and 49 weeks (0.00360 ± 0.00043) post-exposure when compared to the ratios of the sham-treated group (0.00321 ± 0.000430–0.00209 ± 0.00026). Large intra-group variation prevented the finding of statistical distinction between sham and CRS (2.5 mg)-exposure even though, CRS (2.5 mg) raised the mean ratio (0.00528 ± 0.00111) approximately two times higher than that of sham-treated group (0.00321 ± 0.000430) at 6 weeks post-exposure. CRS (1.0 mg) increased the wet lung and body weight ratios (0.00273 ± 0.00034) significantly higher than those of sham-exposed animals at 49 weeks post-instillation ($p<0.05$). In contrast, ANR-treated lung and body weight ratios were maintained in the ranges found within the sham-exposed group without large variation during the whole exposure-period. MA did not induce any significant increase in the wet lung and body weight ratios at all four sacrifice time points.

The increase in the amount of lavage surface protein is due to a lung permeability change and therefore is a good indicator of oedema. The mean amounts of the acellular protein recovered from the sham-treated lung surface were maintained in the narrow range ($1,310\pm200$–$1,870\pm390$ μg) throughout the 49-week exposure-period except the mean value ($2,740\pm1,280$ μg) at 6 weeks post-exposure (Figure 3. 3). Animals instilled with CRS had increases in the amount of the acellular protein from the lung in a dose-dependent manner at all four sacrifice time points. Moreover, CRS (2.5 and 5.0 mg) elevated the amounts of acellular protein lavaged from the lung significantly at all four sacrifice time points ($p<0.05$). CRS (1.0 mg) caused a significant increase ($4,850\pm2,470$ μg) only at 13 weeks post-exposure ($p<0.05$). Broad-ranging distributions of the amounts of protein were recognisable in the CRS-treated groups at 6 and 13 weeks post-treatment. In contrast, ANR did not raise the amount of acellular protein significantly throughout the 49-week exposure period except at 25 weeks post-exposure with ANR (5.0 mg) ($4,020\pm780$ μg). However, the values from ANR (5.0 mg)-treated groups were attenuated to the normal range for the last 24 weeks. MA (5.0 mg) raised the amount of surface protein significantly
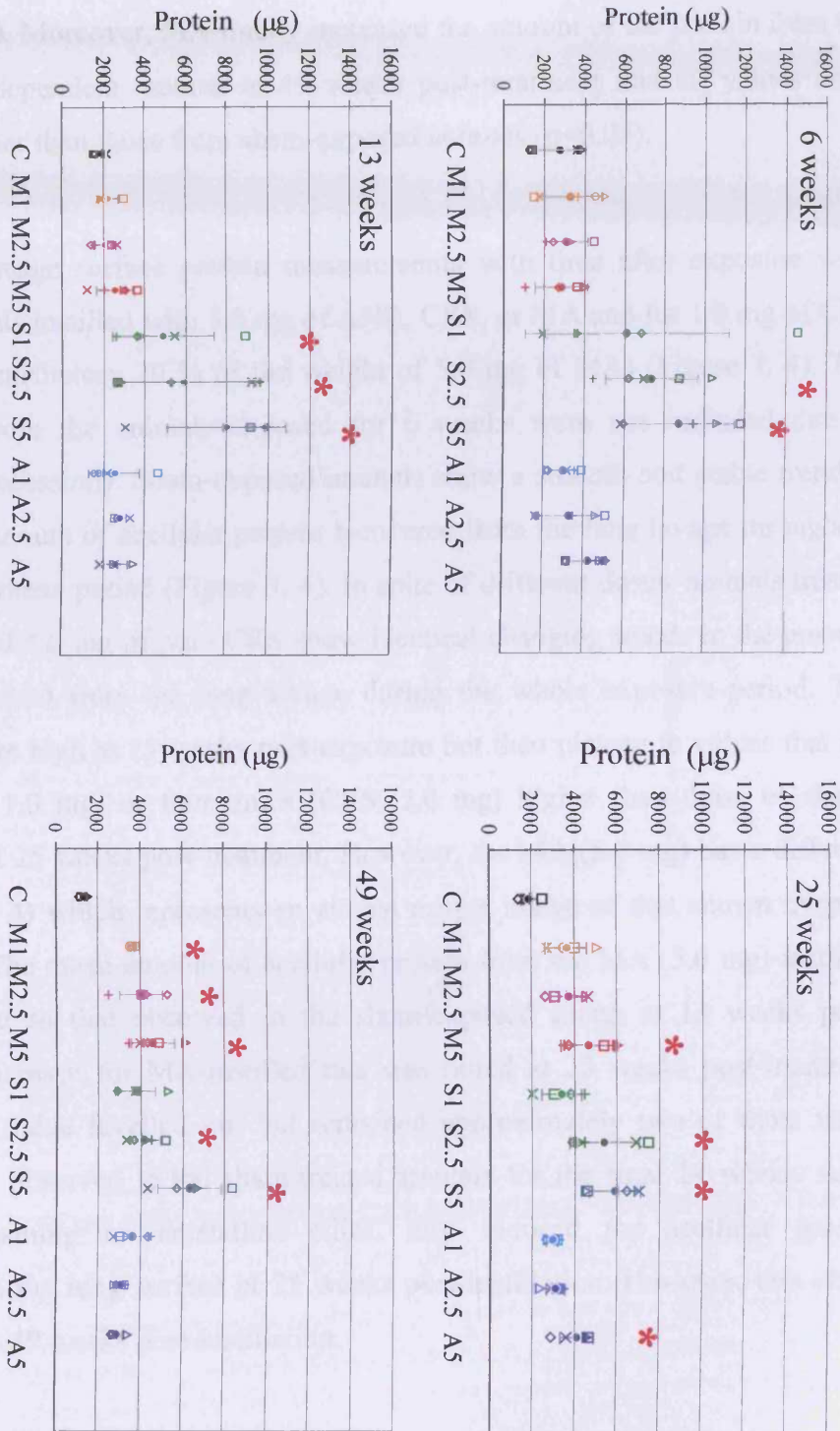
Figure 3. 3 The changes caused by sham (C), and 3 doses (1.0, 2.5, 5.0 mg) of MA (M), CRS (S), or ANR (A) exposure in the amount of acellular protein (1,000 g supernatant) recovered from the lung lavage at 6, 13, 25 and 49 weeks post-instillation (Key as Figure 3. 1 and 2).

Protein (µg)

6 weeks

C M1 M2.5 M5 S1 S2.5 S5 A1 A2.5 A5

Protein (µg)

13 weeks

C M1 M2.5 M5 S1 S2.5 S5 A1 A2.5 A5

Protein (µg)

25 weeks

C M1 M2.5 M5 S1 S2.5 S5 A1 A2.5 A5

Protein (µg)

49 weeks

C M1 M2.5 M5 S1 S2.5 S5 A1 A2.5 A5

(4,620±1,240 µg) at 25 weeks post-instillation (p<0.05) when compared to the values from the sham-exposed group and maintained this effect for the last 24 weeks (4,530±1,020 µg). Moreover, MA finally increased the amount of the protein from the lung in a dose dependent manner at 49 weeks post-treatment and all values were significantly higher than those from sham-exposed animals (p<0.05).

The trends of lavage surface protein measurements with time after exposure were plotted for animals instilled with 5.0 mg of ANR, CRS, or MA and for 1.0 mg of CRS (found as the contributory 20 % of the weight of 5.0 mg of MA) (Figure 3. 4). The data obtained from the animals exposed for 6 weeks were not included due to infection (see discussion). Sham-exposed animals show a smooth and stable trend in changes in the amount of acellular protein recovered from the lung lavage throughout the 49-week exposure period (Figure 3. 4). In spite of different doses, animals treated with both 1.0 and 5.0 mg of pure CRS show identical changing trends in the amount of protein recovered from the lung lavage during the whole exposure-period. The mean amounts are high at 13 weeks post-exposure but then plateau to values that are still two (CRS, 1.0 mg) or four times (CRS, 5.0 mg) higher than those of sham-exposed group at 25 weeks post-treatment. However, the MA (5.0 mg) has a different curve (Figure 3. 4) which represents an almost mirror image of that shown by pure CRS (1.0 mg). The mean amount of acellular protein from the MA (5.0 mg)-instilled lung was similar to that observed in the sham-exposed group at 13 weeks post-exposure. An increase for MA-instilled rats was noted at 25 weeks post-treatment after which the value levelled out but remained approximately two or three times higher than that observed in the sham-treated animals for the final 24 weeks. ANR (5.0 mg), containing no crystalline silica, also induced the acellular protein accumulation on the lung surface at 25 weeks post-instillation. However, this effect did not persist to 49 weeks post-instillation.
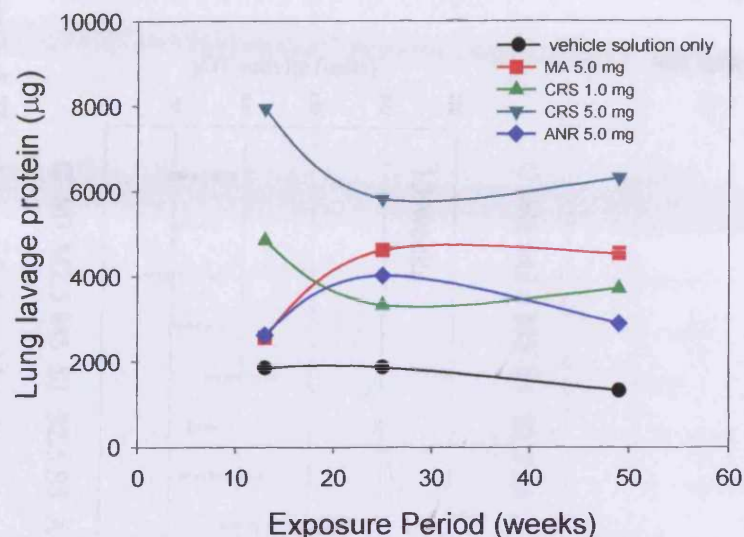
Figure 3. 4 The changing trends in the amount of acellular lung surface protein from the sham or MA (5.0 mg), CRS (1.0 or 5.0 mg), or ANR (5.0 mg) instilled lung with increasing time of exposure.

3. 3. 1. 3 Epithelial cell damage

Increases in γGT or alkaline phosphatase activities indicate epithelial cell proliferation or functional damage. Generally, sham treated animals show a mean of γGT activities in narrow ranges (58.2±19.1–63.5±18.7 units) throughout the 49-week exposure period (Figure 3. 5). Increases in the γGT activities (86.7±21.9–127.2±38.9 units) were caused by a high dose (5.0 mg) of pure CRS-exposure for 49 weeks and individual animal fluctuations in enzyme activities were recognisable from CRS (1.0 and 2.5 mg)-treated lung. CRS (2.5 and 5.0 mg) elevated the activities significantly when compared to the values from the sham-treated animals at 25 weeks post-exposure ($p < 0.05$). The CRS (5.0 mg) increased the mean activity (142.3±55.4 and 107.5±21.1 units) approximately two times higher than those of the sham-exposed group (58.2±19.1 and 63.5±11.3 units) at 6 and 49 weeks post-treatment but the large intra group variances prevent the finding of a statistical difference between the sham and the CRS (5.0 mg)-instilled group. In contrast, ANR did not induce any significant
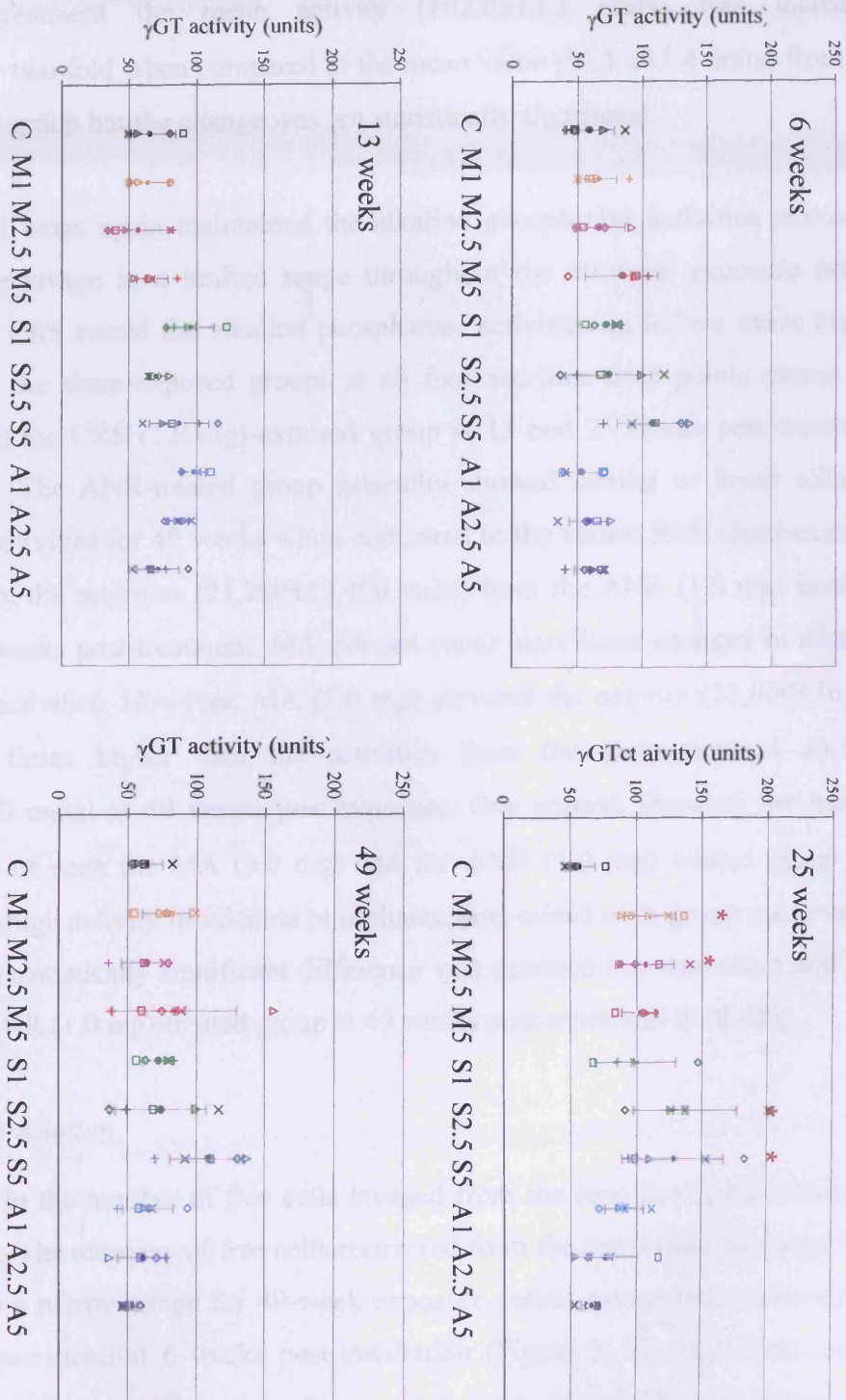
Figure 3. 5 The changes induced by sham or MA, CRS or ANR instillation in epithelial lining fluid γGT activity total per lung at 6, 13, 25, and 49 weeks post-exposure. (Key as Figure 3. 1 and 2).

increase in γGT activities at any sacrifice time point. However, MA raised the γGT activities and a statistical difference was noticeable between sham and MA (1.0 and 2.5 mg)-exposed group at 25 weeks post-instillation ($p<0.05$). For MA (5.0 mg) at 25 weeks post-treatment the mean activity (102.0 ± 13.2 units) was increased approximately two fold when compared to the mean value (65.1 ± 11.4 units) from the sham-exposed group but the change was not statistically significant.

Sham-exposed lungs again maintained the alkaline phosphatase activities recovered from the lung lavage in a limited range throughout the 49-week exposure period (Figure 3. 6). CRS raised the alkaline phosphatase activities up to two times higher than those of the sham-exposed groups at all four sacrifice time points except the activities from the CRS (1.0 mg)-exposed group at 13 and 25 weeks post-treatment (Figure 3. 6). The ANR-treated group generally showed similar or lower alkaline phosphatase activities for 49 weeks when compared to the values from sham-exposed animals except the activities ($21,200\pm17,400$ units) from the ANR (1.0 mg) instilled group at 49 weeks post-treatment. MA did not cause significant changes in alkaline phosphatase activities. However, MA (5.0 mg) elevated the activity ($33,900\pm36,500$ units) three times higher than the activities from the sham-exposed animals ($12,100\pm3,800$ units) at 49 weeks post-exposure. One animal, showing the highest γGT activity, of each the MA (5.0 mg) and the ANR (1.0 mg) treated group had outlying very high activity of alkaline phosphatase and raised each group mean value. As a result, a statistically significant difference was detected between sham and MA (5.0 mg) or ANR (1.0 mg)-treated group at 49 weeks post-treatment ($p<0.05$).

3. 3. 1. 4 Inflammation

The increase in the number of free cells lavaged from the lung is a good marker for inflammation. The numbers of free cells recovered from the sham-exposed lungs were distributed in a narrow range for 49-week exposure period except the numbers from the animals sacrificed at 6 weeks post-instillation (Figure 3. 7). This sham-control value ($11.79\times10^6\pm4.21\times10^6$) at 6 weeks post-exposure was significantly higher than those ($5.89\times10^6\pm2.15\times10^6$ and $5.63\times10^6\pm0.4\times10^6$) obtained from the lung exposed for 13 or 25weeks ($p<0.05$). Furthermore the number of free cells lavaged from the
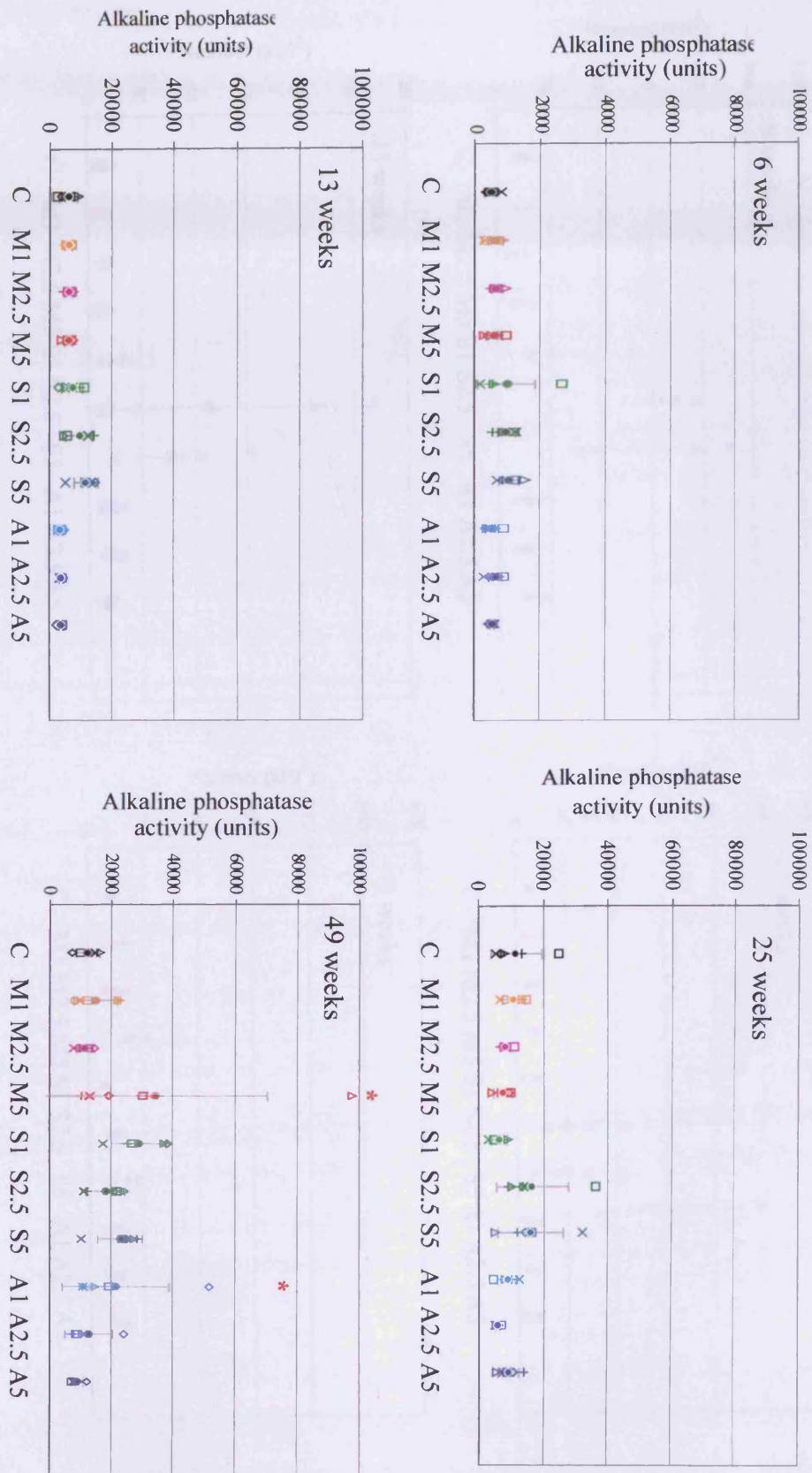
Figure 3. 6 The changes induced by sham or MA, CRS or ANR instillation in epithelial lining fluid alkaline phosphatase activity total per lung at 6, 13, 25, and 49 weeks post-exposure. (Key as Figure 3. 1 and 2).
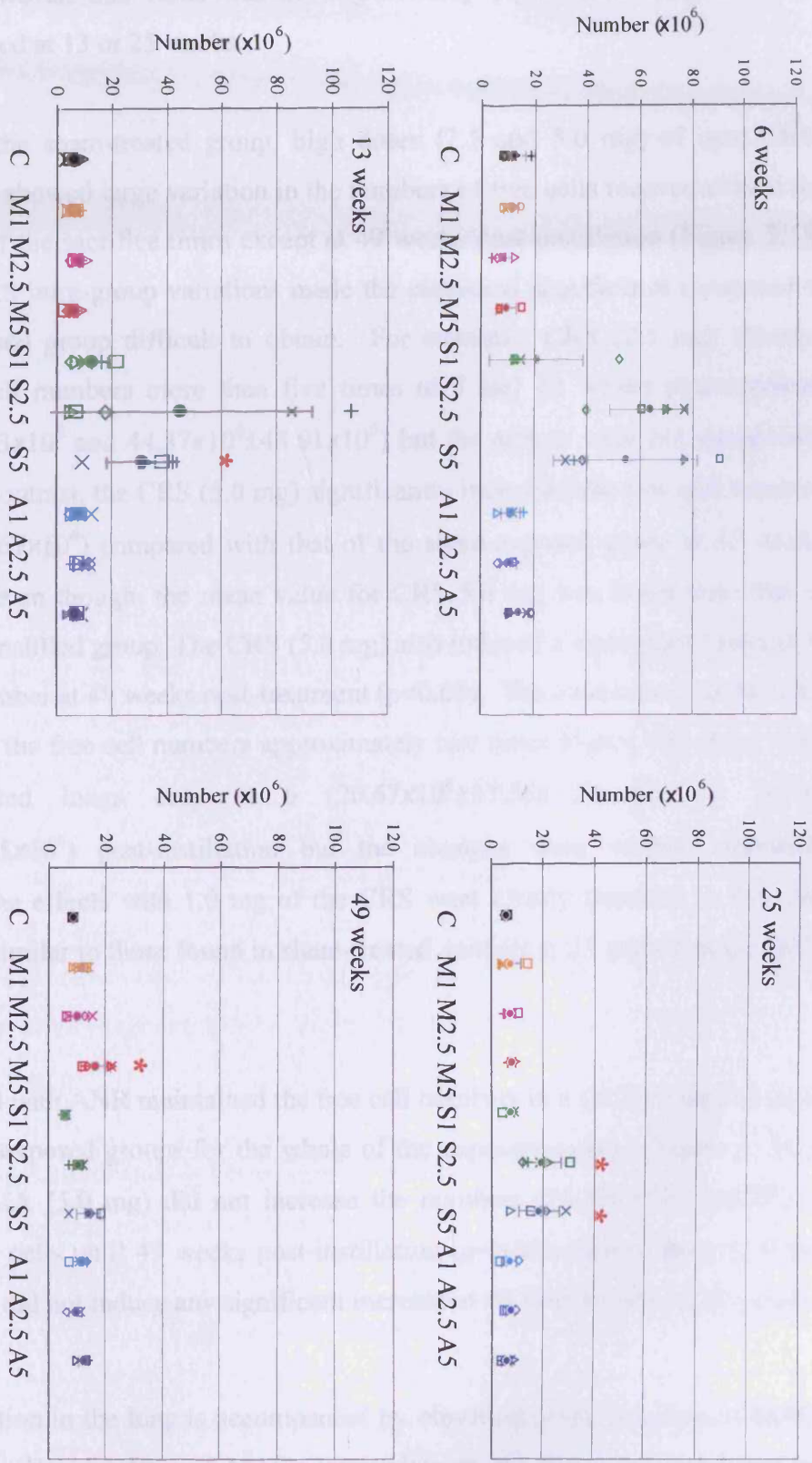
Figure 3. 7 The increases induced by sham, or 3 doses (1, 2.5, or 5.0 mg) of MA, CRS, or ANR exposure in the number of free cells recovered from lung lavage at 6, 13, 25, 49 weeks post-instillation. (Key as Figure 3. 1 and 2).

sham-treated lungs was also increased ($8.42 \times 10^6 \pm 0.33 \times 10^6$) at 49 weeks post-instillation. However, this value was not significantly higher than those from the animals sacrificed at 13 or 25 weeks.

In contrast to the sham-treated group, high doses (2.5 and 5.0 mg) of pure CRS-instilled groups showed large variation in the numbers of free cells recovered from the lungs at most of the sacrifice times except at 49 weeks post-instillation (Figure 3. 7). These large CRS intra-group variations made the statistical significance compared to the sham-exposed group difficult to obtain. For example, CRS (2.5 mg) elevated average free cell numbers more than five times at 6 and 13 weeks post-exposure ($63.2 \times 10^6 \pm 14.63 \times 10^6$ and $44.37 \times 10^6 \pm 48.01 \times 10^6$) but the effects were not statistically significant. In contrast, the CRS (5.0 mg) significantly increased the free cell numbers ($30.75 \times 10^6 \pm 12.67 \times 10^6$) compared with that of the sham-exposed group at 13 weeks post-exposure even though, the mean value for CRS 5.0 mg was lower than that of CRS (2.5 mg)-instilled group. The CRS (5.0 mg) also induced a significant increase in the free cell number at 49 weeks post-treatment ($p < 0.05$). The lowest dose of the CRS (1.0 mg) raised the free cell numbers approximately two times higher than those from the sham-treated lungs only at 6 ($20.67 \times 10^6 \pm 17.56 \times 10^6$) and 13 weeks ($12.17 \times 10^6 \pm 6.65 \times 10^6$) post-instillation but the changes were without statistical significance. The effects with 1.0 mg of the CRS were clearly transient as free cell numbers were similar to those found in sham-treated animals at 25 and 49 weeks post-exposure.

Animals treated with ANR maintained the free cell numbers in a similar range to those from the sham-exposed groups for the whole of the exposure-period (Figure 3. 7). A high dose of MA (5.0 mg) did not increase the numbers ($16.30 \times 10^6 \pm 5.16 \times 10^6$) of lavageable free cells until 49 weeks post-instillation ($p < 0.05$). Lower doses (1.0 and 2.5 mg) of MA did not induce any significant increase at all four sacrifice time points.

Mild inflammation in the lung is accompanied by elevation in the numbers of MACs in lavage fluid. The numbers of MACs lavaged from the sham-exposed lungs are distributed in a narrow range during the whole exposure-period except the numbers

from the animals sacrificed at 6 weeks post-treatment (Figure 3. 8). The numbers from this group ($10.27 \times 10^6 \pm 3.59 \times 10^6$) were significantly higher than the values from the sham-exposed animals ($5.89 \times 10^6 \pm 2.15 \times 10^6$ and $5.56 \times 10^6 \pm 0.40 \times 10^6$) sacrificed at 13 or 25 weeks post-instillation ($p < 0.05$). The numbers of MACs from the sham-exposed lungs were raised at 49 weeks post-exposure ($8.42 \times 10^6 \pm 0.33 \times 10^6$) but it was not significantly higher than the values from the other sham-exposed groups sacrificed at 13 or 25 weeks post-instillation.

Pure CRS generally elevated the numbers of MACs from the lung in a dose dependent manner. The CRS (5.0 mg) caused significant increases in the number of MACs at 13 and 25 weeks post-treatment ($19.26 \times 10^6 \pm 6.33 \times 10^6$ and $10.89 \times 10^6 \pm 3.69 \times 10^6$) when compared to the numbers from the sham-treated lung ($p < 0.05$). CRS (2.5 mg) also substantially raised the number of MACs. Large intra-group variances, which made it difficult to gain statistical significances, were also recognised at 13 ($23.07 \times 10^6 \pm 22.75 \times 10^6$) and 25 weeks post-exposure ($13.81 \times 10^6 \pm 4.60 \times 10^6$). CRS (1.0 mg) increased the values only at 6 ($15.55 \times 10^6 \pm 14.75 \times 10^6$) and 13 ($9.35 \times 10^6 \pm 4.62 \times 10^6$) weeks post-treatment without significance. In contrast, ANR showed dose and time independent effects on the increases in the numbers of MACs throughout the 49-week exposure period. However, ANR (5.0 mg) did not raise the numbers of MACs ($11.55 \times 10^6 \pm 1.78 \times 10^6$) recovered from the lung lavage significantly when compared to those of sham treated groups at 49 weeks post-instillation ($p < 0.05$). The high dose (5.0 mg) of MA raised the number of MACs ($11.96 \times 10^6 \pm 3.56 \times 10^6$) substantially when compared to the sham-exposed groups at 49 weeks post-exposure but was without statistical significance.

Acid phosphatase activity is a good marker enzyme for MACs, which may be responding to ingested particles. These "activated" MACs are then believed to contribute to the inflammatory response. The results from acid phosphatase activity measurements of free cells from the lung lavage correlated closely with the changes in the number of MACs recovered from the sham or dust-exposed lung at all four sacrifice time points (Figures 3. 8 and 9). Sham-exposure again maintained the free cell acid phosphatase activities at a limited range throughout the 49-week exposure
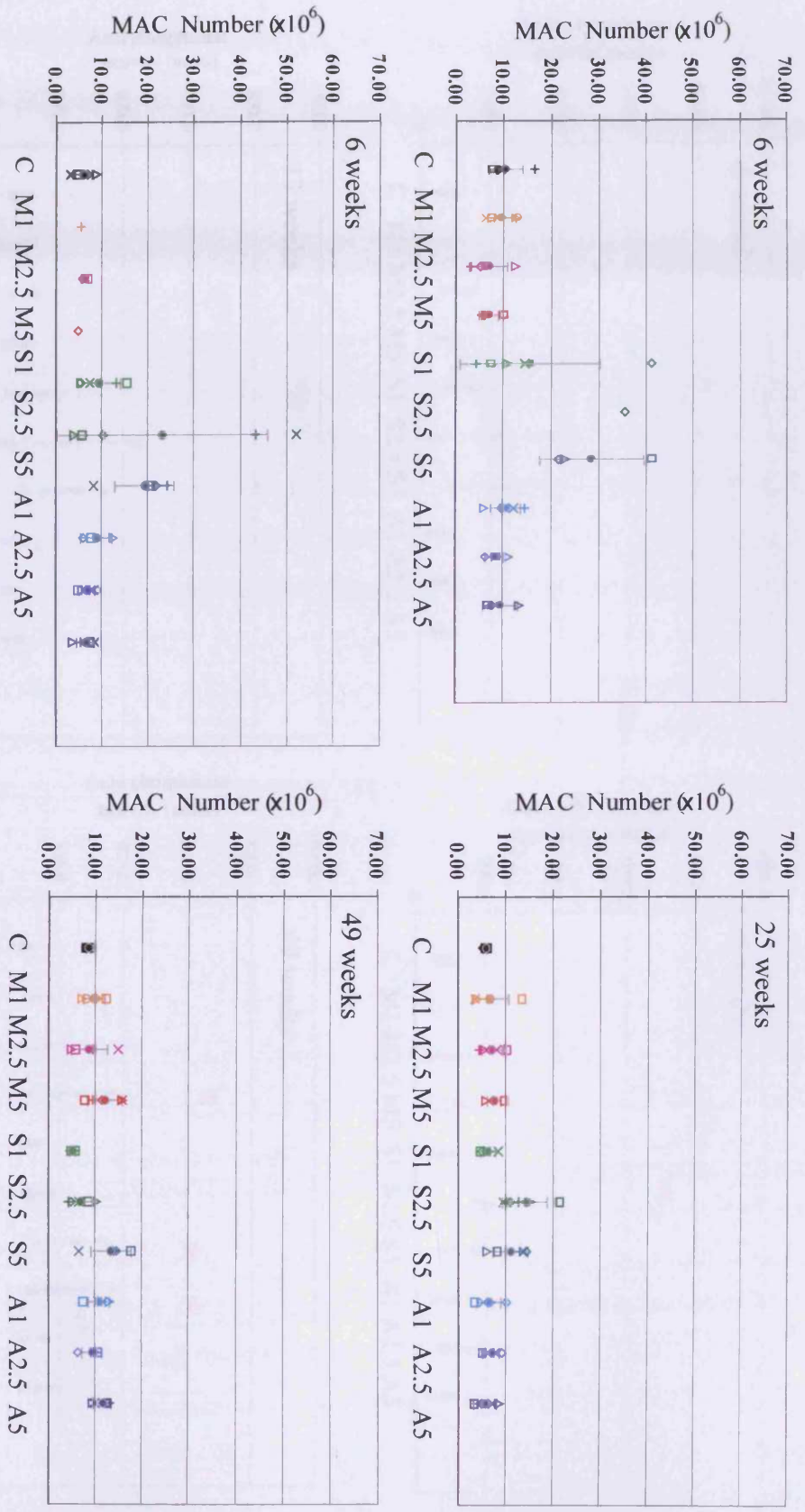
Figure 3. 8 The increases induced by sham, or 3 doses (1, 2.5, or 5.0 mg) of MA, CRS, or ANR exposure in the number of MACs recovered from lung lavage at 6, 13, 25 and 49 weeks post-instillation. (Key as Figure 3. 1 and 2).

70
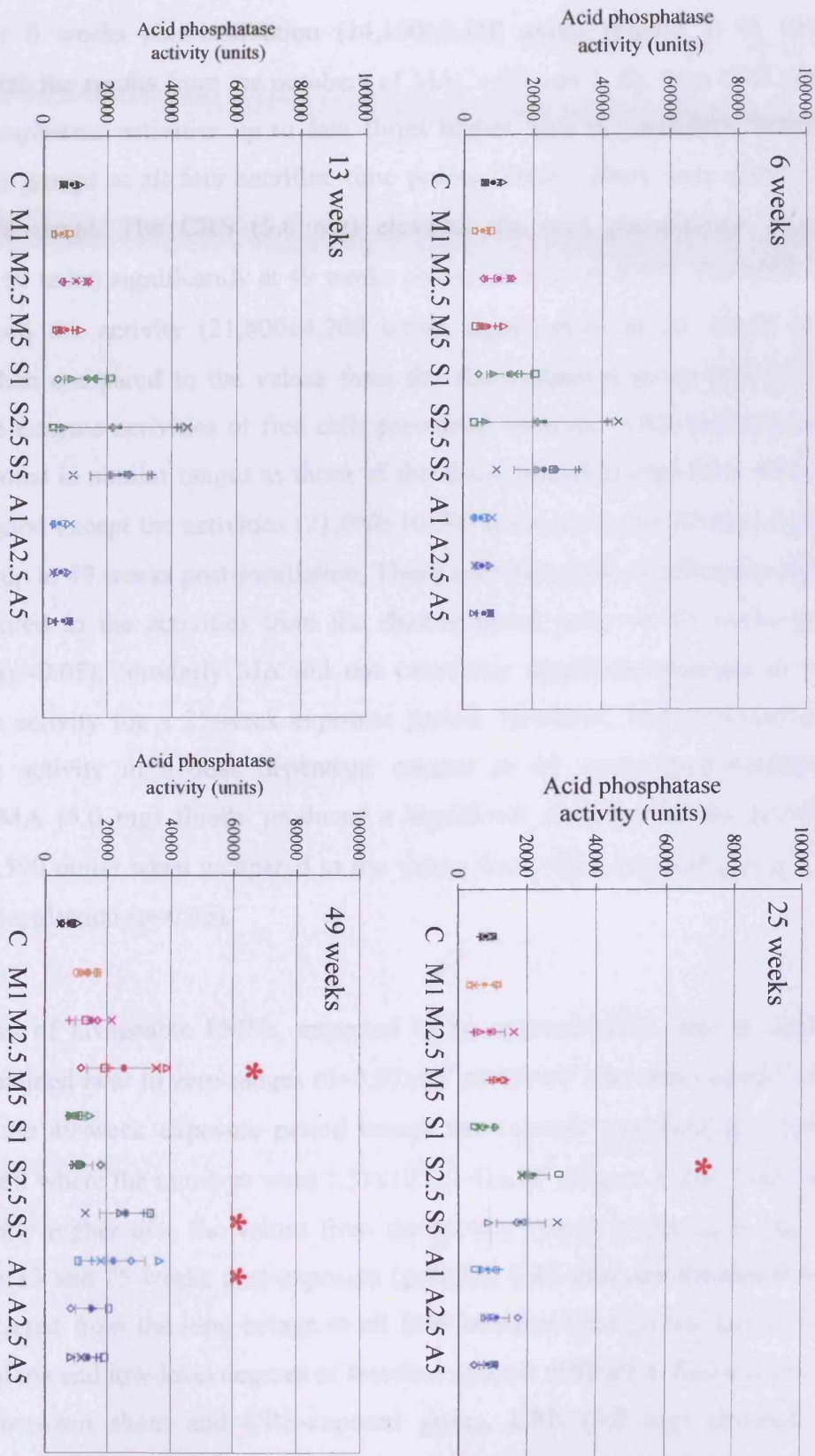
Figure 3. 9 The changes induced by sham or 3 doses (1, 2.5 and 5 mg) of MA, CRS, or ANR exposure in acid phosphatase activity from free cells at 6, 13, 25, and 49 weeks post-instillation (Key as Figure 3. 1. and 2).

period (7,450±2,260 −8,390±2,260 units) except the values from the animals sacrificed at 6 weeks post-instillation (14,190±8,480 units) (Figure 3. 9) which correlates with the results from the numbers of MACs (Figure 3. 8). Pure CRS raised the acid phosphatase activities up to four times higher than the activities from the sham-treated groups at all four sacrifice time points. These values were distributed over a wide range. The CRS (5.0 mg) elevated the acid phosphatase activity (25,800±8,160 units) significantly at 49 weeks post-treatment (p<0.05). The CRS (2.5 mg) increased the activity (21,800±4,200 units) significantly at 25 weeks post-exposure when compared to the values from the sham-exposed group (p<0.05). In contrast, the enzyme activities of free cells recovered from the ANR-instilled lungs were distributed in similar ranges as those of the sham-treated groups for a 49-week exposure period except the activities (21,600±10,500 units) from the ANR (1.0 mg)-instilled group at 49 weeks post-instillation. These activities were significantly higher when compared to the activities from the sham-exposed lungs at 49 weeks post-instillation (p<0.05). Similarly MA did not cause any significant changes in acid phosphatase activity for a 25-week exposure period. However, MA increased acid phosphatase activity in a dose dependant manner at 49 weeks post-instillation. Moreover, MA (5.0 mg) finally produced a significant elevation of the activities (33,900±36,500 units) when compared to the values from sham-exposed group at 49 weeks post-instillation (p<0.05).

The numbers of lavageable PMNs, expected to be approximately zero in healthy animals, remained near to zero ranges ($0-0.07 \times 10^6 \pm 0.08 \times 10^6$) in sham-treated lungs throughout the 49-week exposure period except the animals sacrificed at 6 weeks post-treatment where the numbers were $1.51 \times 10^6 \pm 1.41 \times 10^6$ (Figure 3. 10). This value is significantly higher than the values from the groups treated in the same way but sacrificed at 13 and 25 weeks post-exposure (p<0.05). CRS elevated the numbers of PMNs recovered from the lung lavage at all four sacrifice-time points. Large intra-group variations and low-level degrees of freedom make it difficult to find a statistical difference between sham and CRS-exposed group. CRS (5.0 mg) elevated the numbers ($11.49 \times 10^6 \pm 6.87 \times 10^6 - 0.60 \times 10^6 \pm 0.43 \times 10^6$) significantly (p<0.05) at every
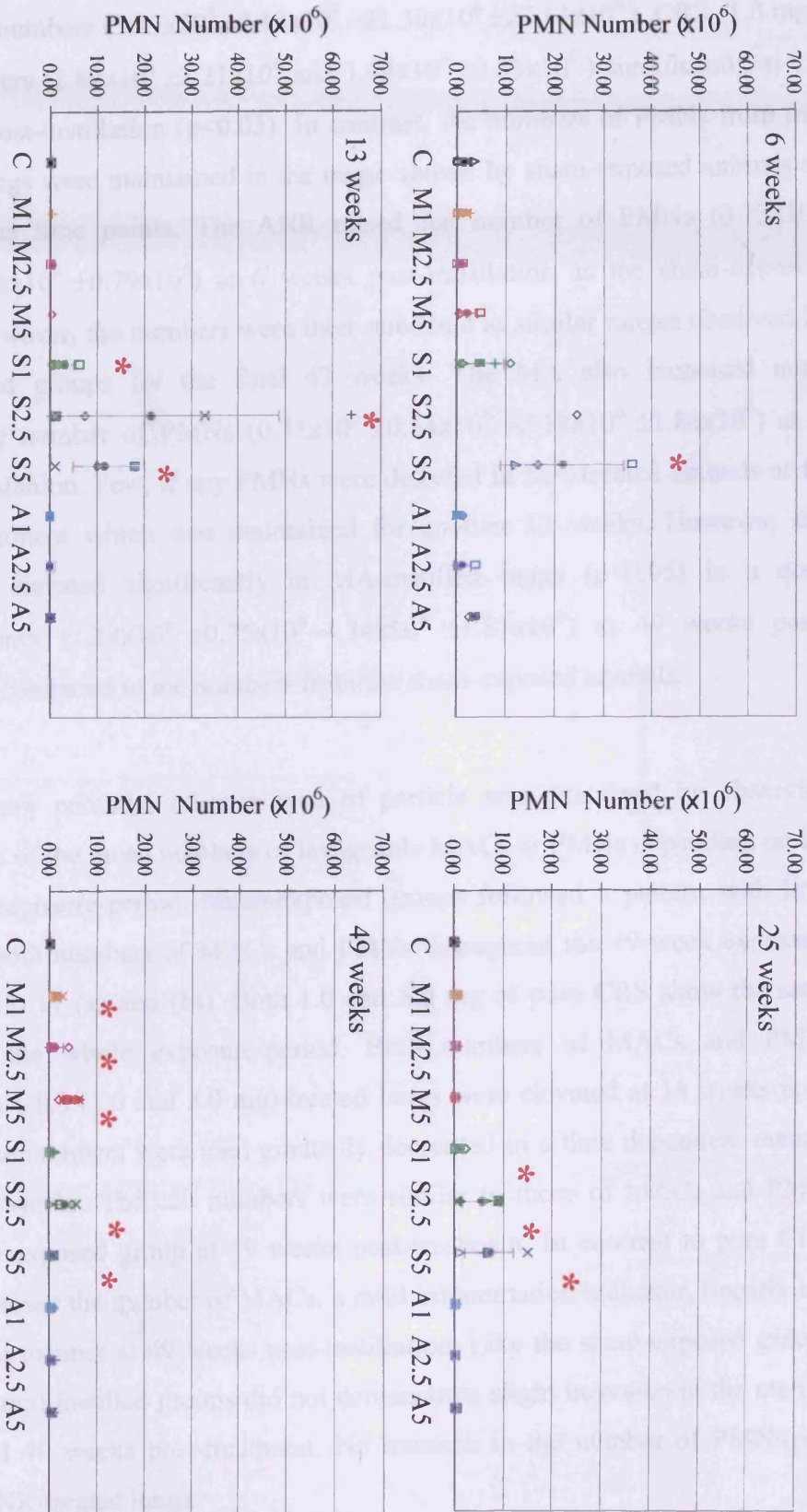
Figure 3. 3. 1. 10 The increases induced by sham, and 3 doses (1, 2.5, or 5.0 mg) of MA, CRS, or ANR exposure in the number of PMNs recovered from lung lavage at 6, 13, 25 and 49 weeks post-instillation. (Key as Figure 3. 3. 1. 1 and 2).

sacrifice time point when compared to the values from the sham-exposed groups. CRS (2.5 mg) raised numbers $(3.23 \times 10^6 \pm 2.13 \times 10^6 - 21.30 \times 10^6 \pm 27.13 \times 10^6)$. CRS (1.0 mg) raised the numbers $(2.82 \times 10^6 \pm 2.21 \times 10^6$ and $1.04 \times 10^6 \pm 0.83 \times 10^6)$ significantly at 13 and 25 weeks post-instillation $(p < 0.05)$. In contrast, the numbers of PMNs from the ANR-treated lungs were maintained in the range shown by sham-exposed animals at all four sacrifice time points. The ANR raised the number of PMNs $(0.73 \times 10^6 \pm 0.67 \times 10^6 - 3.48 \times 10^6 \pm 0.79 \times 10^6)$ at 6 weeks post-instillation as the sham-exposed animals did. However, the numbers were then stabilised at similar ranges observed in the sham-treated groups for the final 43 weeks. The MA also increased non-significantly the number of PMNs $(0.71 \times 10^6 \pm 0.54 \times 10^6 - 2.18 \times 10^6 \pm 1.86 \times 10^6)$ at 6 weeks post-instillation. Few, if any PMNs were detected in MA-treated animals at 13 weeks post-treatment which was maintained for another 12 weeks. However, the numbers were elevated significantly in MA-instilled lungs $(p < 0.05)$ in a dose dependent manner $(1.28 \times 10^6 \pm 0.75 \times 10^6 - 4.34 \times 10^6 \pm 1.87 \times 10^6)$ at 49 weeks post-exposure when compared to the numbers from the sham-exposed animals.

The inflammatory potential of each type of particle was examined by observing changing trends of the mean numbers of lavageable MACs or PMNs depending on the length of the exposure-period. Sham-exposed groups followed a pattern with little fluctuation in both numbers of MACs and PMNs throughout the 49-week exposure-period (Figure 3. 11 (a) and (b)). Both 1.0 and 5.0 mg of pure CRS show the same trends during the whole exposure-period. Both numbers of MACs and PMNs recovered from CRS (1.0 and 5.0 mg)-treated lungs were elevated at 13 weeks post-exposure. These numbers were then gradually decreased in a time dependent manner for the last 36 weeks. The cell numbers were similar to those of MACs and PMNs from the sham-exposed group at 49 weeks post-treatment. In contrast to pure CRS, MA (5.0 mg) raised the number of MACs, a mild inflammation indicator, linearly in a time dependent manner at 49 weeks post-instillation. Like the sham-exposed groups, the ANR (5.0 mg)-instilled groups did not demonstrate slight increases in the number of MACs until 49 weeks post-treatment. No increase in the number of PMNs was observed in ANR-treated lungs.
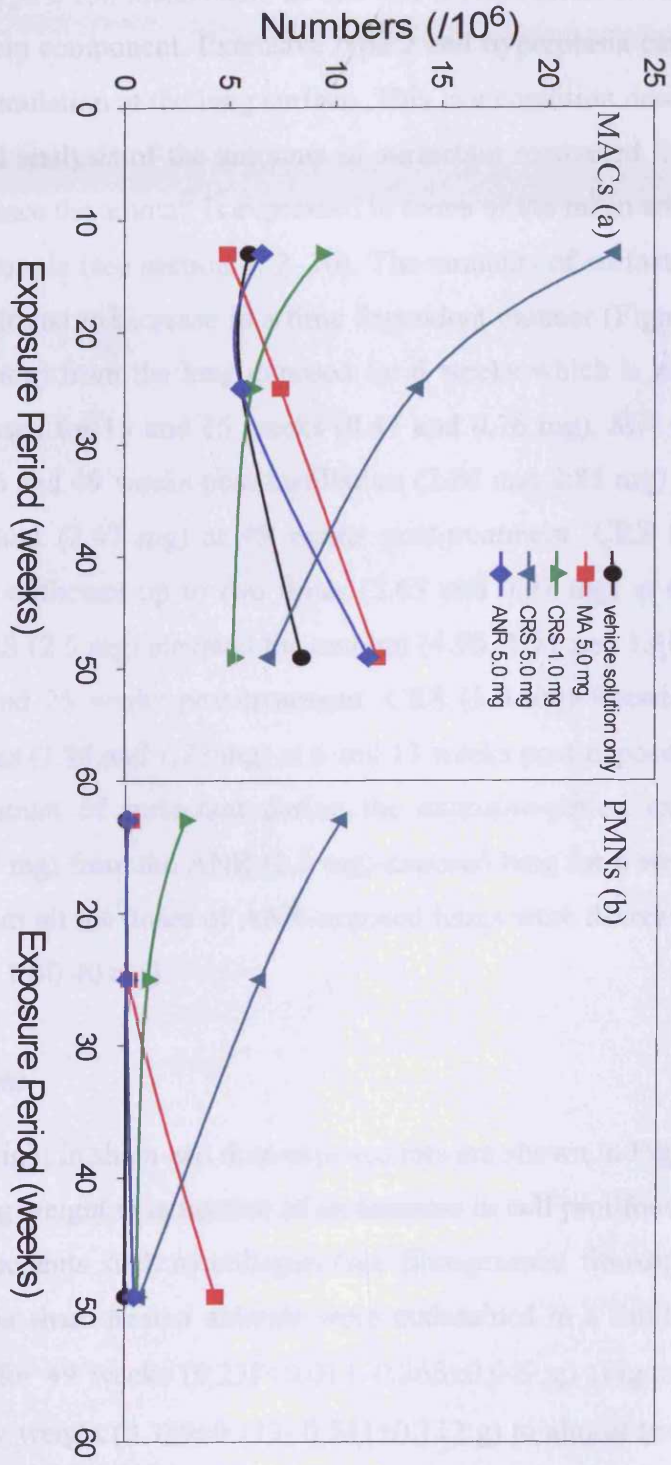
Figure 3. 11 The changing trends in the number of MACs (a) and PMNs (b) from the sham or MA (5.0 mg), CRS (1.0 or 5.0 mg), or ANR (5.0 mg) instilled lung depending on the exposure period.

3. 3. 1. 6 Lipoproteinosis

The amount of surfactant recovered from the lung lavage was employed as an indicator for changes in type 2 cell metabolism as this cell is responsible for the direct secretion of this lipoprotein component. Extensive type 2 cell hyperplasia can lead to excessive surfactant accumulation at the lung surface. This is a condition described as lipoproteinosis. Statistical analysis of the amounts of surfactant recovered from lung lavage is not applicable since the amount is expressed in terms of the mean amount for each group as a pooled sample (see section 3. 2. 10). The amounts of surfactant from sham-treated lungs were found to increase in a time dependent manner (Figure 3. 12) except the amount (1.17 mg) from the lung exposed for 6 weeks which is larger that those from the lung exposed for 13 and 25 weeks (0.47 and 0.76 mg). MA (2.5 mg) increased the amount at 6 and 49 weeks post-instillation (2.86 and 2.85 mg) and MA (5.0 mg) raised the amount (2.47 mg) at 49 weeks post-treatment. CRS (1.0 mg) increased the amount of surfactant up to two times (2.63 and 0.97 mg) at 6 and 13 weeks post-exposure. CRS (2.5 mg) elevated the amount (4.98, 1.71 and 1.40 mg) up to four times at 6, 13, and 25 weeks post-treatment. CRS (5.0 mg) likewise raised surfactant up to three times (3.94 and 1.72 mg) at 6 and 13 weeks post-exposure. ANR did not increase the amount of surfactant during the exposure-period except the amount of surfactant (2.7 mg) from the ANR (2.5 mg)-exposed lung for 6 weeks. The amounts of surfactant from all the doses of ANR-exposed lungs were decreased at 25 weeks post-instillation (0.19-0.40 mg).

3. 3. 1. 7 Dried lung weight

Changes in dried lung weight in sham and dust-exposed rats are shown in Figure 3. 13. An elevation in dried lung weight is indicative of an increase in cell proliferation and/ or a rise in matrix components such as collagen (see fibrogenesis/ fibrosis below). Dried lung weights of the sham-treated animals were maintained in a limited range without any fluctuation for 49 weeks (0.228±0.013–0.265±0.049 g) (Figure 3. 13). CRS raised the dried lung weight (0.339±0.112–0.541±0.112 g) to almost twice those of the sham treated lung weight during the whole exposure-period (49 weeks). However, it was difficult to obtain statistical significance for this elevation in the CRS (5.0 mg)-treated lungs because of large intra-group variations.
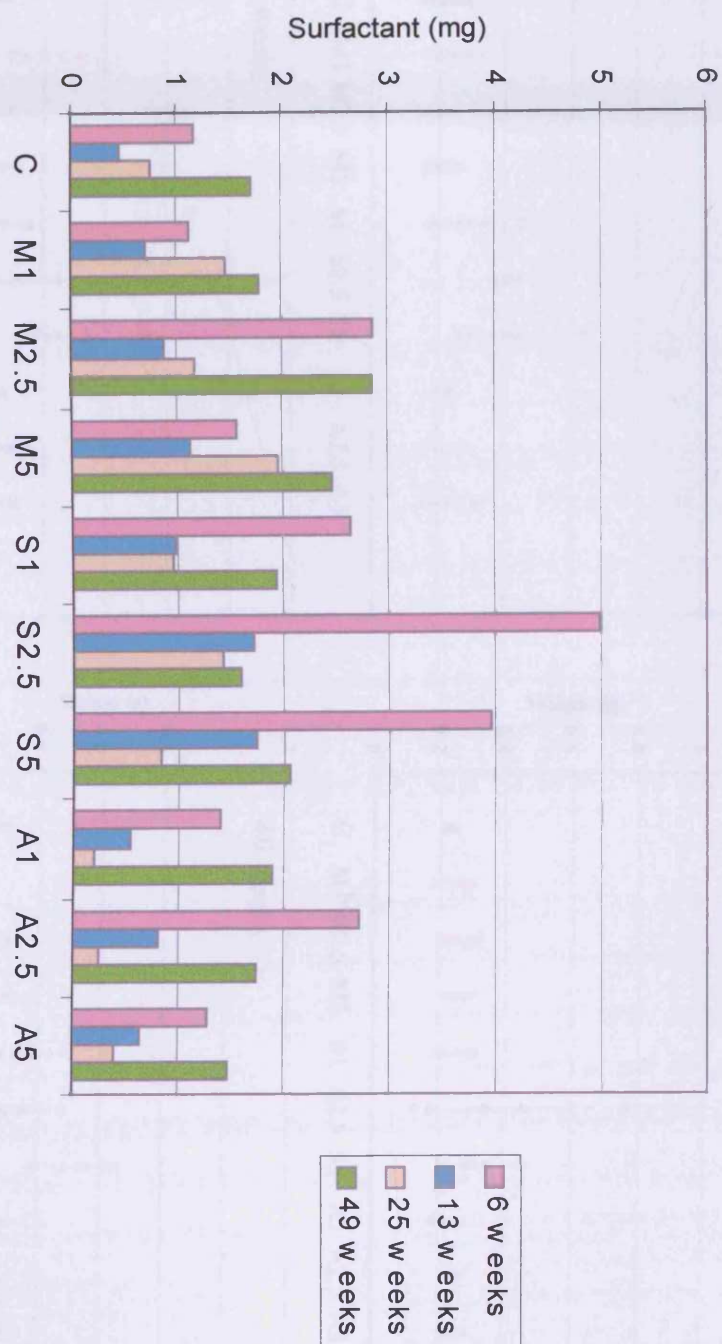
Figure 3. 12 The changes induced by sham or 3 doses (1, 2.5 and 5 mg) of MA, CRS, or ANR exposure in the amounts of surfactant from lung lavage at 6, 13, 25, and 49 weeks post-instillation. Key as Figure 3. 1.
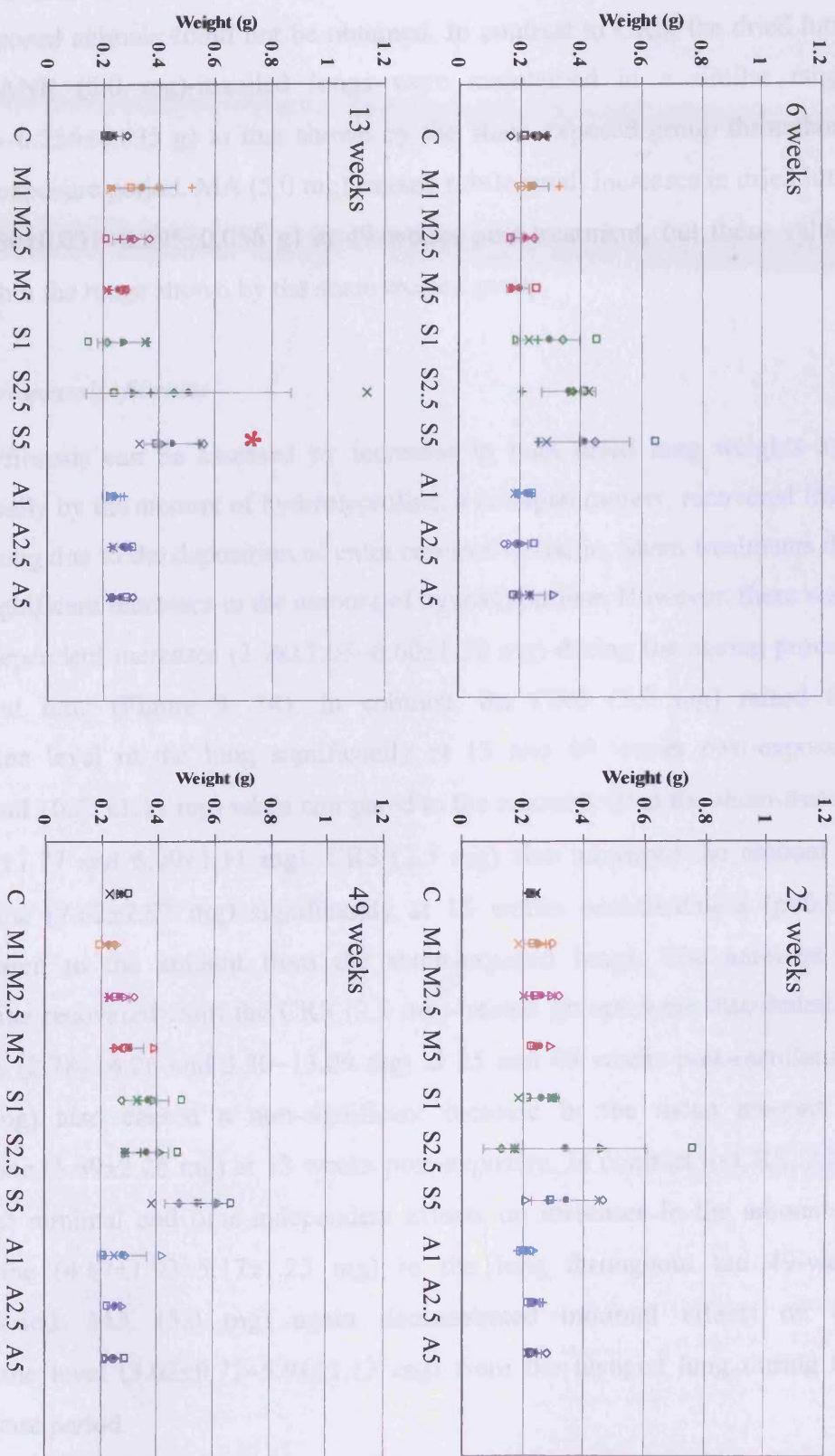
Figure 3. 13 The increases caused by sham or 3 doses (1.0, 2.5, or 5.0 mg) of MA, CRS, or ANR exposure in the dried lung weight at 6, 13, 25, and 49 post-treatment. (Key as Figure 3. 1 and 2).

CRS (2.5 mg) also raised dried lung weights (0.336±0.268–0.501±0.366 g) but for similar reasons as above, statistical differences between the values from CRS (2.5 mg) and sham-exposed animals could not be obtained. In contrast to CRS, the dried lung weights of ANR (5.0 mg)-instilled lungs were maintained in a similar range (0.238±0.026–0.256±0.035 g) to that shown by the sham-exposed group throughout the 49-week exposure period. MA (5.0 mg) caused subtle small increases in dried lung weights (0.250±0.031–0.295±0.056 g) at 49 weeks post-treatment, but these values were still within the range shown by the sham-treated group.

3. 3. 1. 8 Fibrogenesis/fibrosis

Fibrogenesis/fibrosis can be assessed by increases in both dried lung weights and more specifically by the amount of hydroxyproline, a collagen moiety, recovered from the lavaged lung due to the deposition of extra connective tissue. Sham treatments did not induce significant increases in the amount of hydroxyproline. However, there were slight time-dependent increases (3.78±1.05–6.60±1.20 mg) during the ageing process in normal rat lung (Figure 3. 14). In contrast, the CRS (5.0 mg) raised the hydroxyproline level in the lung significantly at 13 and 49 weeks post-exposure (6.82±1.77 and 10.22±1.11 mg) when compared to the amounts from the sham-treated lungs (3.78±1.77 and 6.60±1.11 mg). CRS (2.5 mg) also increased the amount of hydroxyproline (7.62±2.97 mg) significantly at 13 weeks post-treatment ($p < 0.05$) when compared to the amount from the sham-exposed lungs. The amounts of hydroxyproline recovered from the CRS (2.5 mg)-treated groups were distributed in broad ranges (2.78–14.26 and 3.30–13.09 mg) at 25 and 49 weeks post-instillation. CRS (1.0 mg) also caused a non-significant increase in the mean amount of hydroxyproline (5.59±2.26 mg) at 13 weeks post-exposure. In contrast to CRS, ANR (5.0 mg) had minimal and time-independent effects on increases in the amount of hydroxyproline (4.17±1.93–5.17±1.25 mg) in the lung throughout the 49-week exposure period. MA (5.0 mg) again demonstrated minimal effects on the hydroxyproline level (3.02±0.72–5.91±1.13 mg) from the lavaged lung during the whole exposure period.
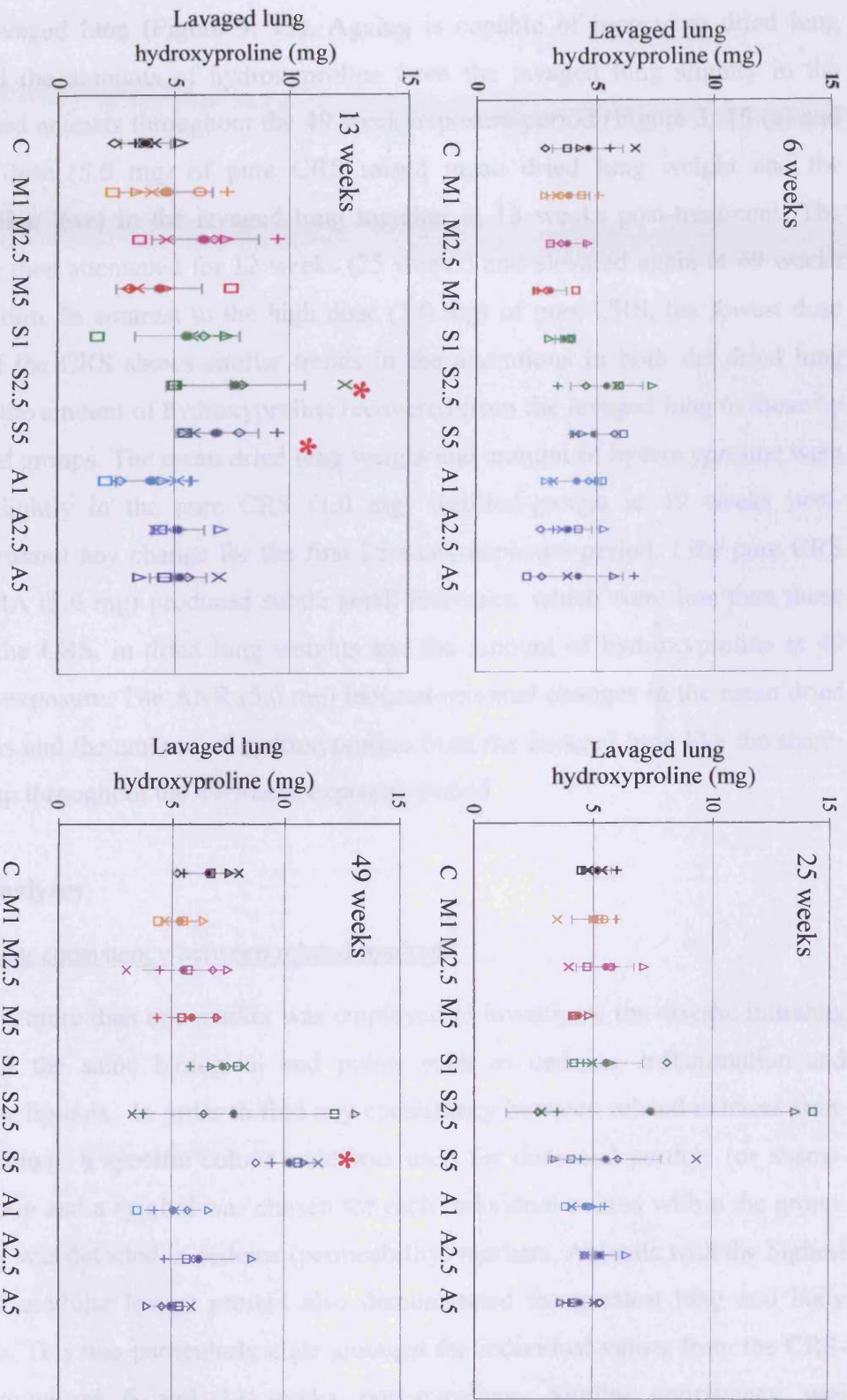
Figure 3. 14 The changes caused by sham, or 3 doses (1.0, 2.5, or 5.0 mg) of MA, CRS, or ANR instillation in the amount of hydroxyproline from the lavaged lung. (Key as Figure 3. 1 and 2).

The fibrogenic potential of particles was assessed by observing the trends of exposure-period changes in the mean dried lung weight and mean amount of hydroxyproline from the lavaged lung (Figure 3. 15). Ageing is capable of increasing dried lung weights and the amounts of hydroxyproline from the lavaged lung slightly in the sham-exposed animals throughout the 49-week exposure-period (Figure 3. 15 (a) and (b)). High dose (5.0 mg) of pure CRS raised mean dried lung weight and the hydroxyproline level in the lavaged lung together at 13 weeks post-treatment. The values were then attenuated for 12 weeks (25 weeks) and elevated again at 49 weeks post-instillation. In contrast to the high dose (5.0 mg) of pure CRS, the lowest dose (1.0 mg) of the CRS shows similar trends in the alterations in both the dried lung weight and the amount of hydroxyproline recovered from the lavaged lung to those by sham-treated groups. The mean dried lung weight and amount of hydroxyproline were increased slightly in the pure CRS (1.0 mg) instilled-groups at 49 weeks post-treatment without any change for the first 25-week exposure-period. Like pure CRS (1.0 mg), MA (5.0 mg) produced subtle small increases, which were less than those caused by the CRS, in dried lung weights and the amount of hydroxyproline at 49 weeks post-exposure. The ANR (5.0 mg) induced minimal changes in the mean dried lung weights and the amount of hydroxyproline from the lavaged lung like the sham-treated group throughout the 49-weeks exposure-period.

3. 4 Data analyses

3. 4. 1 Finding consistency between related markers

In this study, more than one marker was employed to investigate the disease initiating potential for the same biological end points such as oedema, inflammation and fibrogenesis/ fibrosis. In order to find any consistency between related markers from the same animal, a specific colour code was used for dose and particle (or sham)-exposed group and a symbol was chosen for each individual animal within the group. Consistency was detected in oedema (permeability) markers. Animals with the highest amounts of acellular lavage protein also demonstrated the greatest lung and body weight ratio. This was particularly clear amongst the individual values from the CRS-instilled groups at 6 and 13 weeks post-exposure. Similar consistency was recognisable in the inflammation markers. Data from a number of groups/exposure
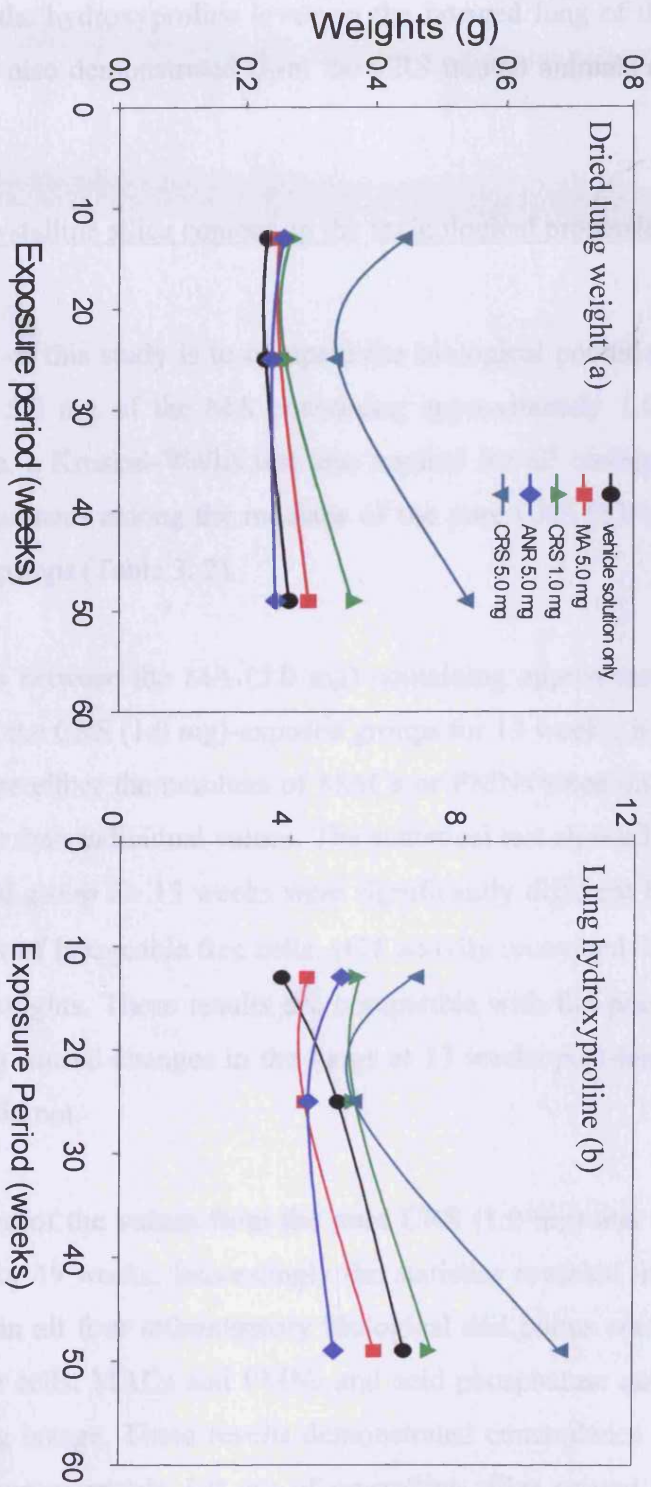
Figure 3.15 The changing trends in the dried lung weight (a) and the amount of hydroxyproline from the lavaged lung (b) of the sham or MA (5.0 mg), CRS (1.0 or 5.0 mg), or ANR (5.0 mg) instilled lung depending on the exposure period.

times showed that rats with high numbers of MACs also showed high activities of acid phosphatase, a lysosomal marker for MACs. Interestingly there were good correlations between the amounts of acellular protein recovered from the lung lavage of individual animals and the hydroxyproline levels in the lavaged lung of the same rats. The correlations were also demonstrated from the CRS treated animals at 6 and 13 weeks post-exposure.

3. 4. 2 The effects of the crystalline silica content on the toxicological properties of the particles

One of the important aims of this study is to compare the biological potential of 1.0 mg of the pure CRS and 5.0 mg of the MA containing approximately 1.0 mg of crystalline silica. Therefore, a Kruskal-Wallis test was applied for all biological end points in order to find differences among the medians of the pure CRS (1.0 mg) and the MA (5.0 mg)-exposed groups (Table 3. 2).

The first comparison set is between the MA (5.0 mg) containing approximately 1.0 mg of crystalline silica and the CRS (1.0 mg)-exposed groups for 13 weeks. In this set, it is not possible to compare either the numbers of MACs or PMNs since only mean values were recorded rather than individual values. The statistical test showed that the pure CRS (1.0 mg)-exposed group for 13 weeks were significantly different from the MA (5.0 mg) in the number of lavageable free cells, γGT activity recovered from 300 g lavage, and dried lung weights. These results are compatible with the phenomena that the pure CRS (1.0 mg) caused changes in the lungs at 13 weeks post-instillation whereas the MA (5.0 mg) did not.

The second set is composed of the values from the pure CRS (1.0 mg) and the MA (5.0 mg)-exposed groups for 49 weeks. Interestingly the statistics revealed that there are significant differences in all four inflammatory biological end points such as the numbers of lavageable free cells, MACs and PMNs and acid phosphatase activity of the free cells from the lung lavage. These results demonstrated concordance that the MA (5.0 mg) containing approximately 1.0 mg of crystalline silica caused delayed inflammation in the lung whereas the lung inflammation caused by the CRS (1.0 mg) was attenuated at 49 weeks post-treatment.

Table 3. 2 P values from statistical comparisons between changes in the biological end points caused by the pure CRS (1.0 mg) and the MA (5.0 mg) containing approximately 1.0 mg of CRS using a Kruskal-Wallis test. (Key. If p<0.05, these two groups are significantly different from each other, shown in red).

Biological endpoints	P values		
	CRS (1.0 mg) and MA (5.0 mg) at 13 weeks	CRS (1.0 mg) and MA (5.0 mg) at 49 weeks	CRS (1.0 mg) and MA (5.0 mg, 13 weeks) and MA (5.0 mg, 49 weeks)
Parenchymal wet lung: body weight	0.465	0.076	0.327
Total protein (1,000g lavage)	0.076	0.175	0.221
Free cell number	0.047	0.009	0.086
The number of MACs	Not available	0.014	0.221
The number of PMNs	Not available	0.016	0.462
Acid phosphatase activity	0.175	0.016	0.086
γGT activity (300 g lavage)	0.028	0.917	0.221
Alkaline phosphatase activity (300 g lavage)	0.465	0.465	0.016
Dried lung weight	0.016	0.175	0.462
Hydroxyproline level from the lavaged lung	0.143	0.076	0.221

84

The pure CRS (1.0 mg)-exposed group for 13 weeks and the MA (5.0 mg) for 49 weeks were selected for the third comparison set since in spite of different exposure-periods, both groups had demonstrated inflammatory changes in the lung. In contrast to the results from both the previous comparison sets, the significant difference between groups appeared in only one out of ten biological end points, which is alkaline phosphatase activity from 300 g lung lavage. These results imply that in spite of the different exposure-period and doses, the stage of the lungs from both the MA (5.0 mg) containing approximately 1.0 mg of CRS and the pure CRS (1.0 mg)-exposed groups were not significantly different in most of the biological endpoints.

3. 5 Discussion

The present study was initiated in order to investigate the toxicological properties of MA as MA contains up to 23 % (w/w) of CRS, a known toxic crystalline silica (Baxter *et. al.,* 1999). This particular composition of the ash is found as pyroclastic flow/surge and as such raised concerns about the health of residents on the island. Toxicological properties of MA were studied comparing those of positive (pure CRS) and negative control mineral dust (ANR), both of which are major components of MA. The investigations were focused on four important increasingly severe biological end points in the lung; oedema (lung surface permeability change), inflammation, lipoproteinosis and fibrosis/fibrogenesis. To this end an animal model, an intratracheal instillation technique was used and a study carried out for biochemical markers in lung lavage and lavaged lung tissue.

The rats were exposed to three doses (1.0, 2.5 or 5.0 mg) of each particle (MA, CRS or ANR) during four different exposure-periods (6, 13, 25 or 49 weeks) to study dose or time effects in order to minimise the risk of data misinterpretation caused for example by casual infection at a single time point. However, this experimental design required employing a large number (over two hundred) of rats. Such a study would be more difficult using an inhalation exposure technique requiring the commitment of numerous inhalation chambers for long periods of time. The costs of such inhalation facilities would also be prohibitively expensive. Moreover, the inhalation procedure can cause a continuous stress since the rats cannot move freely if kept in a chamber-

closed (nose only exposure) system. Therefore, in the present study the intratracheal instillation technique was employed and it was possible to treat 263 animals during a minimum duration (approximately 3 days for this study). Using this non-invasive instillation technique all the animals were found to recover rapidly (3-5 minutes) and suffer minimal stress (no failure to gain body weight). Arguably, there is a difference between instillation and natural inhalation in that the particles would not make contact with the nasal and upper respiratory tract with the former technique. The invasive characteristics of the instillation treatment is controlled by setting up sham-exposed animal groups for each exposure-period in order to find any side effects from the treatment or any possible infection during the experimental period.

Earlier studies (Henderson et. al., 1995) have established that approximately 1.0 mg mass as a single dose into a rat lung could provide a standard method to study pulmonary inflammation. However, previous studies by Housley et. al., (2002) have indicated that MA may have low bioreactivity in that 1.0 mg instillation of this material caused very little effect over a 11-week exposure period. Therefore, in the present studies, this dose was increased substantially to 2.5 and 5.0 mg. It is possible that the Housley et. al. studies could also have missed effects because of the short-term of their studies. Thus, in the present investigation it was decided to increase the exposure time to approximately one year. As the animals were three months old prior to instillation a one-year exposure-period would take them through to approximately half of their lifetime.

Rats were sacrificed and the changes in the lung were assessed analysing lung lavage with biochemical markers. The data gained from the biochemical approaches were dealt with in three ways. Firstly, consideration was given to intra-group variability of response and whether or not the extent of change in any biological marker was related to another measurement in the same animal. Secondly, a statistical analysis of group data was undertaken. Thirdly, comparison of high dose treatments and the CRS 1.0 mg group with exposure time was investigated to see if any trends could be determined with respect to transient or progressive changes in lung permeability, inflammation and fibrosis. One time point (6 weeks) was not considered for this third aspect relating to trend data. This was because at 6 weeks it was felt there was evidence for a mild infection in this animal population at this time. The seventy-one

rats in the 6-week groups were instilled at a different time (June, 2001) and housed in a separate room from the remainder of the treated animals (instilled October, 2000). It was particularly noticeable that these 6-week sham-treated control rats had higher numbers of free cells and higher and more variable levels of acellular lavage protein than normally observed in 'clean' animals and indeed in the control rats at all the other sacrifice time points. Both of the above observations suggest a mild inflammation and a potential increase in lung permeability. Coupled with this, differential counts of the free cell population from the 6-week sham-treated animals, showed that they had PMNs present. PMNs are rarely, if ever, detected in 'clean' control animals. Thus, whilst the 6-week sham-treated rats were included in examining group variability and the statistical analysis to see the effects of the particles, the data were not included in the trend analysis. The potential for mild infection is always present in a large-scale experiment of this nature. However, in this instance it has been recognised (it is rarely reported in literature) and was fortunately confined only to the early time point of 6 weeks.

The infection factor made it difficult to investigate the short-term effects of the particles. However, CRS (5.0 mg)-instilled animals demonstrated significant elevations in oedema markers and severe inflammation markers when compared to the values from the infected sham-exposed group at 6 weeks post-treatment. CRS (2.5 mg) raised only the amount of acellular protein significantly at 6 weeks post-exposure. CRS (1.0 mg) did not show any statistical difference against values from the sham-treated animals at 6 weeks post-instillation. Therefore, CRS showed dose-dependent effects in inducing lung oedema and inflammation markers at 6 weeks post-exposure. These toxicological properties of the CRS, especially dose dependent effects, indicated that CRS could induce oedema and inflammation in the lung at 6 weeks post-exposure without consideration of underlying infection. In contrast to CRS, MA, containing approximately 20 % (w/w) crystalline silica, did not cause any significant increase in any biological end points when compared to the values from the sham-exposed group at 6 weeks post-instillation. These results supported the fact that in spite of its crystalline silica content (20 % (w/w)), the MA would not cause acute effects on normal lungs or synergetic effects on infected lungs. ANR did not show any significant increase or dose dependent effects on any changes in the biological endpoints in the lungs at 6 weeks post-treatment. Therefore, ANR did not cause any

synergetic effects on initiating disease in the lung without any dose-related responses. These results support the opinion that the ANR is minimally bioreactive.

The ANR remained as minimally bioreactive throughout the 49-week exposure-period implying that animals can cope with a 5.0 mg of single instillation for a 49-week exposure-period if the mineral dust was poorly water-soluble and non-toxic. Nevertheless, the long-term study for 49 weeks revealed a different level of bioreactivity for the pure CRS and the MA. The highest dose (5.0 mg) of the pure CRS did not demonstrate fibrogenic changes such as increases in the hydroxyproline level in the lungs until 49 weeks post-instillation. These phenomena suggested that the exposure to a high dose ($\geq$5.0 mg) of toxic particles like CRS for a long period ($\geq$ 49 weeks) would be a prerequisite to initiating fibrosis in the rat lung. In direct contrast, the MA was not fibrogenic when delivered as a single instillation (up to 5.0 mg) for a 49-week exposure-period. Fibrogenesis apart, all doses of the MA demonstrated inflammatory changes such as significant increases in the numbers of lavageable PMNs in the lung at 49 weeks post-exposure. The interesting feature is that such inflammatory changes were delayed and occurred 43 weeks later than those in the pure CRS-exposed lung.

Where does the delay factor come from if the inflammatory changes in the lung were caused by the crystalline silica component in the MA? Several hypotheses can be suggested. Firstly, the minimally reactive feldspar component of MA, present in high quantities in the volcanic ash complex, can competitively interfere with the processing/clearance of the CRS. This competitive interferences can cause disease development in the lung to be retarded resulting in a delayed inflammation (at 49 weeks post-instillation) which developed much earlier when caused by the pure preparation of CRS (at 6 weeks). The competitive interferences in drainage to thoracic lymph nodes by MACs or any possible inactivation process in the lung, allow the crystalline silica component in MA to stay or remain active in the lung longer than pure CRS. It would be the reason in spite of longer-term (49 weeks) exposure, why 5.0 mg of the MA containing approximately 1.0 mg of crystalline silica can mimic the effects in the lung of a 1.0 mg of dose of the pure CRS at 13 weeks post-exposure.

Secondly, the CRS in the MA generated during vigorous seismic activity under high temperature and/or pressure conditions, may have different properties such as hydrophilicity or free radical generation. It was reported that heat-treated CRS is less hydrophilic or generates less radicals than pure CRS (Fubini and Arean, 1999; Fubini et. al., 1999). The more hydrophilic a mineral dust the more easily it interacts with biomolecules and these interactions could induce membranolysis and possibly acute inflammation. Therefore, MA containing crystalline silica could be less hydrophilic or generate less free radicals than pure CRS resulting in a lower toxicity for the volcanic ash. Equally, there may be some differences between artificial heating conditions and volcanic ash generation conditions.

Thirdly, during seismic activity, a variety of potential contaminants (trace metal, organometallic compounds, organic polymer or volcanic glass) could act as masking agents against crystalline silica or its active sites in MA thus reducing the toxicity of the crystalline silica component of the MA. For example, aluminium lactate treated quartz demonstrated lower fibrogenecity than untreated quartz (Fubini et, al., 1995). Moreover, as mentioned in chapter 2, physicochemical investigations using E-SEM and EDX suggested that individual MA particles contain both crystalline silica and feldspars. However, it is not clear whether the feldspars links with the crystalline silica component by chemical bonding or if they just merge with each other. Nevertheless, the ANR could act as a masking agent against the crystalline silica component. Therefore, the actual probability of changes in the lung caused by this crystalline silica component of the ash could be lower than expected. It is also possible that following MA deposition in the lung, changes could take place in its surface properties and especially in the crystalline silica component. It was reported that both feldspar and silica mixture in soil can be dissolved under acidic conditions by weathering effects (see Chapter 1). The persistent or long-term processing in the acidic environment of lysosomes in the MACs could change the crystalline silica surface by separating the other contaminants from the crystalline silica components in the MA particles. This procedure could restore the bioreactivity of the crystalline silica component in the MA, which was masked or lost by other minimally bioreactive material thus explaining the delayed inflammation in the lungs caused by MA.

In summary, sham-treatment or the instillation of up to 5.0 mg doses of durable ANR dust particles has minimal effects on the rat lung for period of exposure of approximately one year. In addition, MA containing approximately 20 % (w/w) of crystalline silica will produce a delay inflammatory response in the lung (one year post-instillation). Such an inflammatory effect was seen much earlier (6 weeks post-instillation) when 1.0 mg of a pure CRS sample (equivalent to the dose in 5.0 mg of MA) was used. MA does not initiate any fibrogenic reaction in the lung over 49 weeks, which contrasts with the effects noted with 5.0 mg of pure CRS.

4 Gross morphological

and quantitative histological changes in the lung

and thoracic lymph nodes from Montserrat volcanic ash,

anorthite or cristobalite-exposed rats

4.1 Introduction

A crystalline silica or a crystalline silica containing mineral dust is known to be bioreactive in the lung as described before (see Chapters 1 and 3). The quantitative cellular and biochemical investigations into the bioreactivity of MA and its two major components, CRS and ANR (see Chapter 3), suggested MA is inflammatory and CRS is fibrogenic in the lungs after long-term exposure up to 49 weeks. For the most part these quantitative investigations centred on the use of lung lavage although some studies were carried out on lung dried weight and a fibrotic marker, lung tissue hydroxyproline. Broncho-alveolar lavage techniques are very useful but can suffer certain disadvantages. Once a disease process is underway airways can shut down and alveoli become more difficult to wash out as cellular and lipoprotein components accumulate. In addition, lavage technique provides little information on cellular or interstitial changes accompanying the disease process. Thus, to both compliment and add further information to the manner in which CRS, MA or ANR could affect the lung a histopathological study, reported in this chapter, was performed

It was also previously reported that crystalline silica could cause thoracic lymph node enlargements containing granulomas since the lymph node is the organ where the dust particles that had been instilled or inhaled were translocated (Adamson and Prieditis, 1998; Davis et. al., 2001; Friedetzky et. al., 1998; Garn et. al., 1997). Such structural changes were often found in the nodes from animals demonstrating fibrotic symptoms in the lung.

Thus, the aims of this study were to investigate changes in (a) the gross morphology of the lung or lymph nodes at four different sacrifice time points (6, 13, 25 and 49 weeks) (b) areas covered by free cells in the alveoli units which could be comparable to the number of lavageable free cells as a good marker of inflammation (c) the areas of the connective tissue components especially collagen in the interstitial region related to hydroxyproline level in the lung as a marker of fibrosis (d) the sizes of thoracic lymph nodes and (e) the areas of granuloma in the nodes using an image analysis system.

4.2 Material and methods

4. 2. 1 The size of the lymph nodes

One to four tracheobronchial lymph nodes, chosen at random from each animal were pooled together in a petri dish (3.0 mm dia) and a digitised image was recorded. Comparative analysis of the size of the lymph nodes from all sham and dust-exposed animals was carried out using image analysis based on the projected area of the nodes in the digitised photograph. The lymph node size was then calibrated from the diameter of the petri dish.

4. 2. 2 Preparation of the lungs and lymph nodes for histopathlogy

Immediately after sacrifice, the lungs were removed intact (without saline perfusion) and 10% neutral buffered formalin (pH 7.0) was introduced by gravity feed into a tracheal cannula and embedded in paraffin wax using a Leica EG1140Hocq Embedding Centre. Sections were then cut at a thickness of 5µm and mounted on uncoated slides. The sections were stained with haematoxylin and eosin (a general purpose stain) or Massons' trichrome used to visualise collagen. Identical preparations were made from the pooled lymph nodes collected from each group of animals.

4. 2. 3 Quantification of specific regions in the lung or lymph nodes using an image analysis system.

Digitised pictures of the lung or thoracic lymph node sections were obtained and the area was quantified based on its colour or shape using an image analysis system (Leica Qwin, Leica Micro system imaging solutions Ltd, UK, Figure 4. 1). The free cell accumulation was measured in the area covered by free cells in the alveoli units. This area was then calibrated by dividing it by the total area of alveoli units from each digitised picture. The interstitial collagen was quantified by detecting blue-green coloured areas since collagen is stained blue-green by Massons' trichrome. The area was then calibrated by the total interstitial area in each picture. The area of the granuloma of the lymph nodes was also measured using the image analysis system.
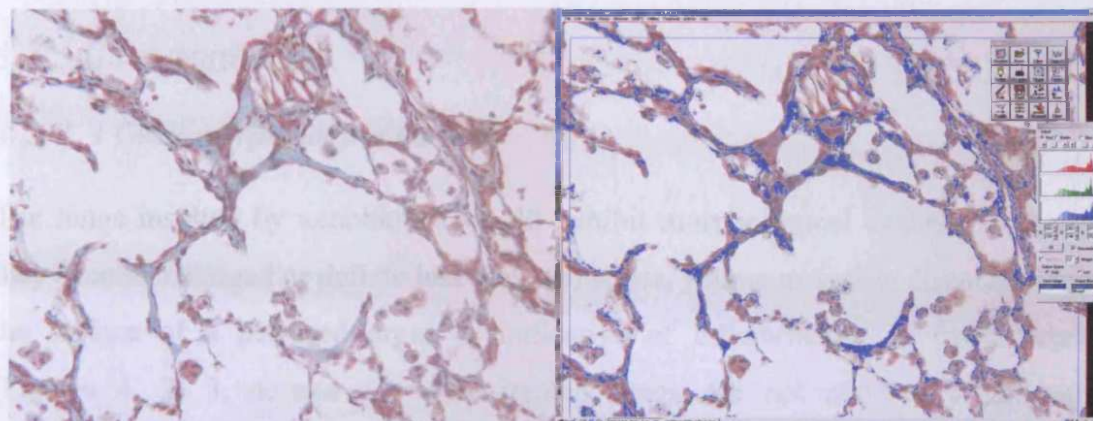
Figure 4. 1 The digitised micrographs of the CRS (5.0 mg)-exposed lung 49 weeks and the image (blue) converted by an image analysis system for colour-detecting purposes

4. 2. 4 Morphology of the free cells lavaged from the lung

The cytospin slides of the free cell population were prepared as described before (Chapter 3) and digitised images were recorded.   The diameter of the MACs was measured using the image analysis system. Approximately 200 cells per group were studied.

4. 2. 5 Data analysis

The Kruskal-Wallis test, which is appropriate for a non-parametric data set due to its low degree of freedom and large variances, was applied in order to find statistical distinction between two different groups (at 95 % confidence level) using a software package (Minitab 13.0).

4. 3 Results

4. 3. 1 Gross morphology

4. 3. 1. 1 Gross morphology of the lung

The lungs insulted by xenobiotics would exhibit morphological changes in that (a) they become enlarged or deflate less well, (b) white, yellow or brown discoloration on the surface of a perfused organ is indicative of inflammation or lipoprotenosis (Figures 4. 2, 3, 4, and 5). Sham-treated lungs did not show any noticeable morphological changes during the 49-week exposure-period. Enlarged and brown discolorations were noticed in the CRS (2.5 or 5.0 mg)-exposed groups at all four-sacrifice time points. All doses of the MA or the ANR did not cause any noticeable enlargement or discoloration in the lung for the first 25 weeks. However, grey discoloration indicating particle deposition was observed on the lung parenchyma from all doses of the MA and the CRS and the highest dose (5.0 mg) of the ANR-exposed animals at 49 weeks post-exposure.

Saline only   1.0 mg   2.5 mg   5.0 mg

ANR   CRS   MA
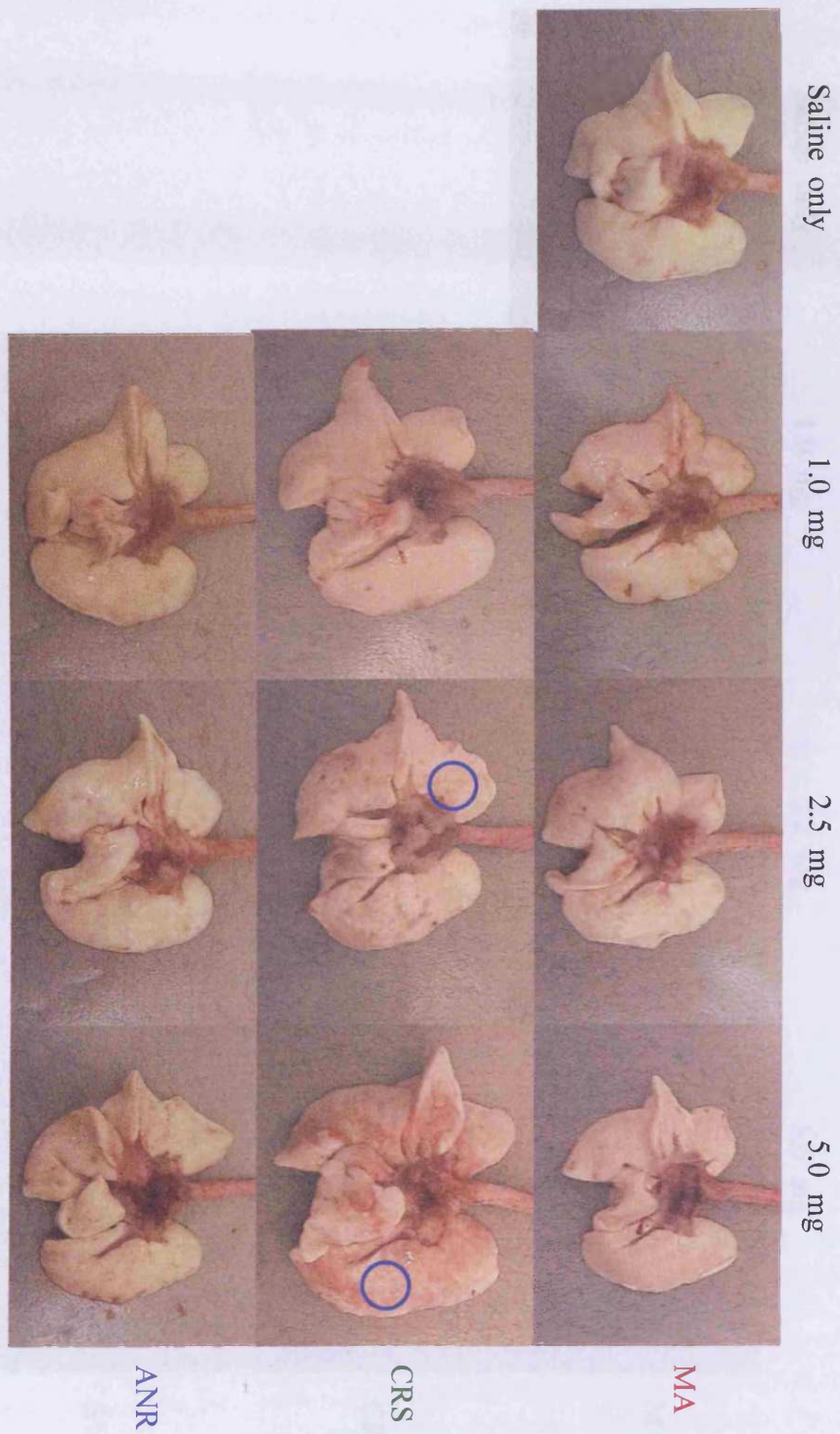
Figure 4. 2 The digitised photographs of gross lung morphology at 6 weeks post-instillation. Yellow or brown discolorations in blue circles indicate inflammation/ lipoproteinosis in the lung.
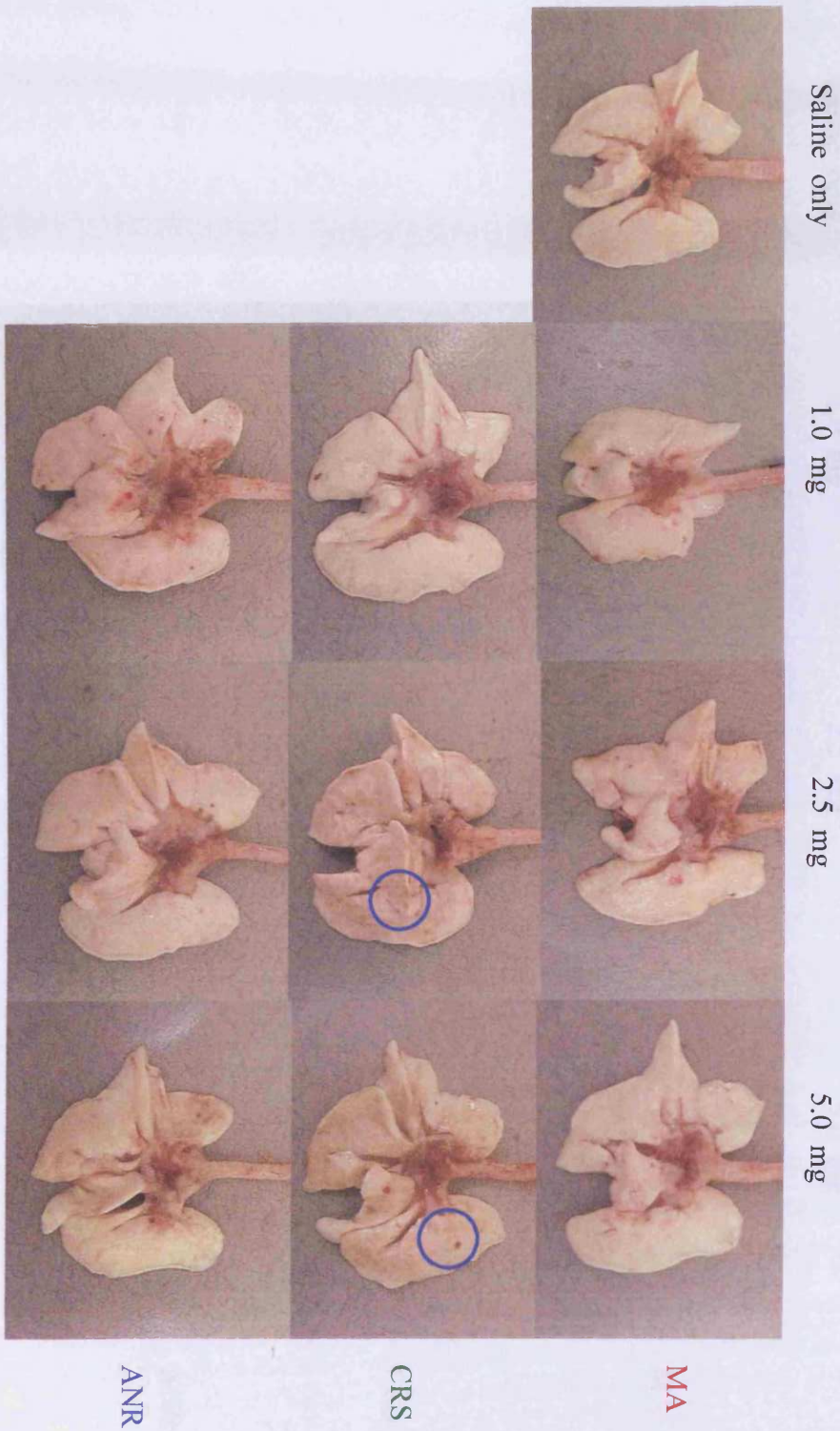
Figure 4. 3 The digitised photographs of gross lung morphology at 13 weeks post-instillation. The yellow discolouration on the lung surface in blue circles indicates inflammation or lipoproteinosis.
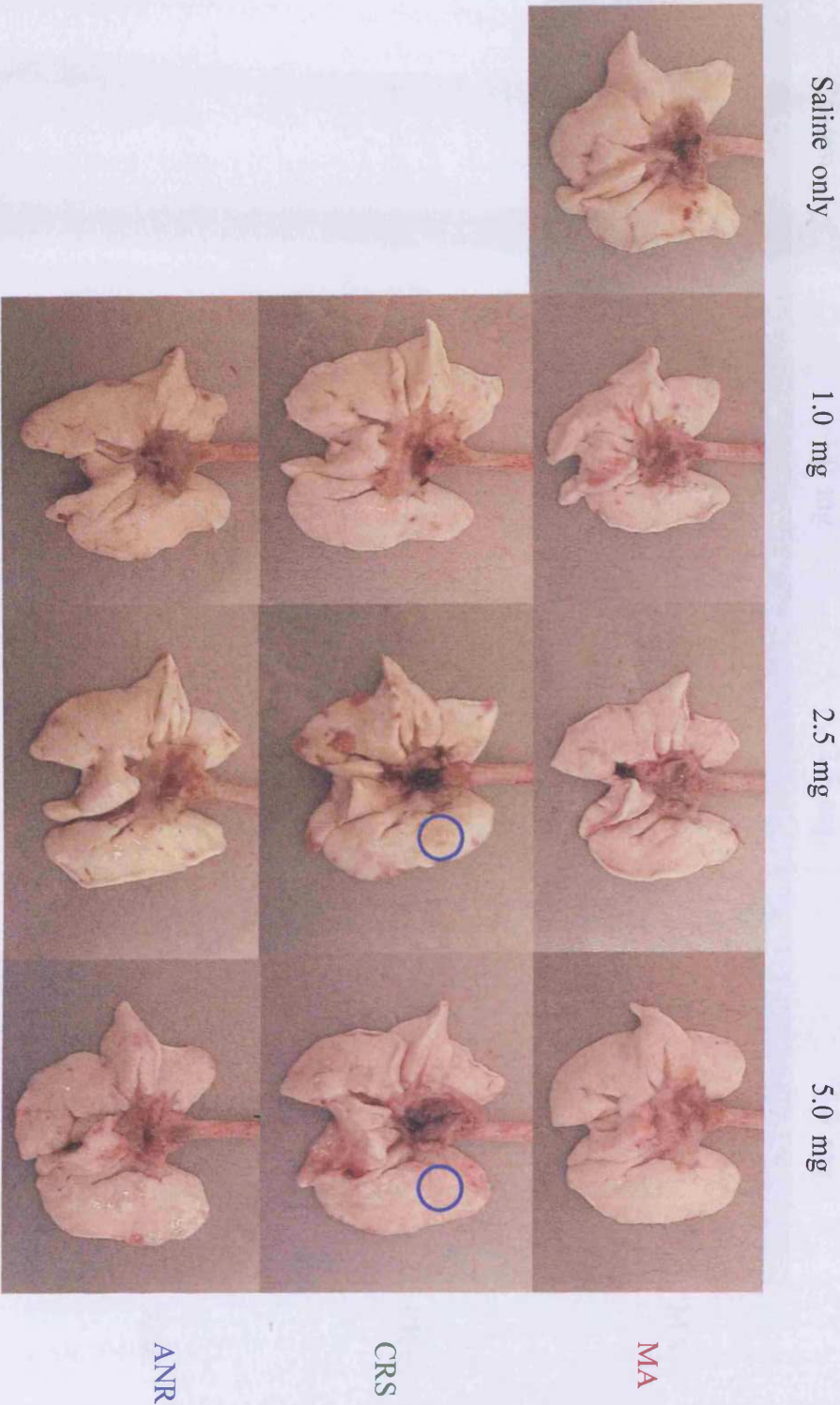
Figure 4. 4 The digitised pictures of gross lung morphology at 25 weeks post-instillation. Brown discolourations in blue circles indicate lipoproteinosis.
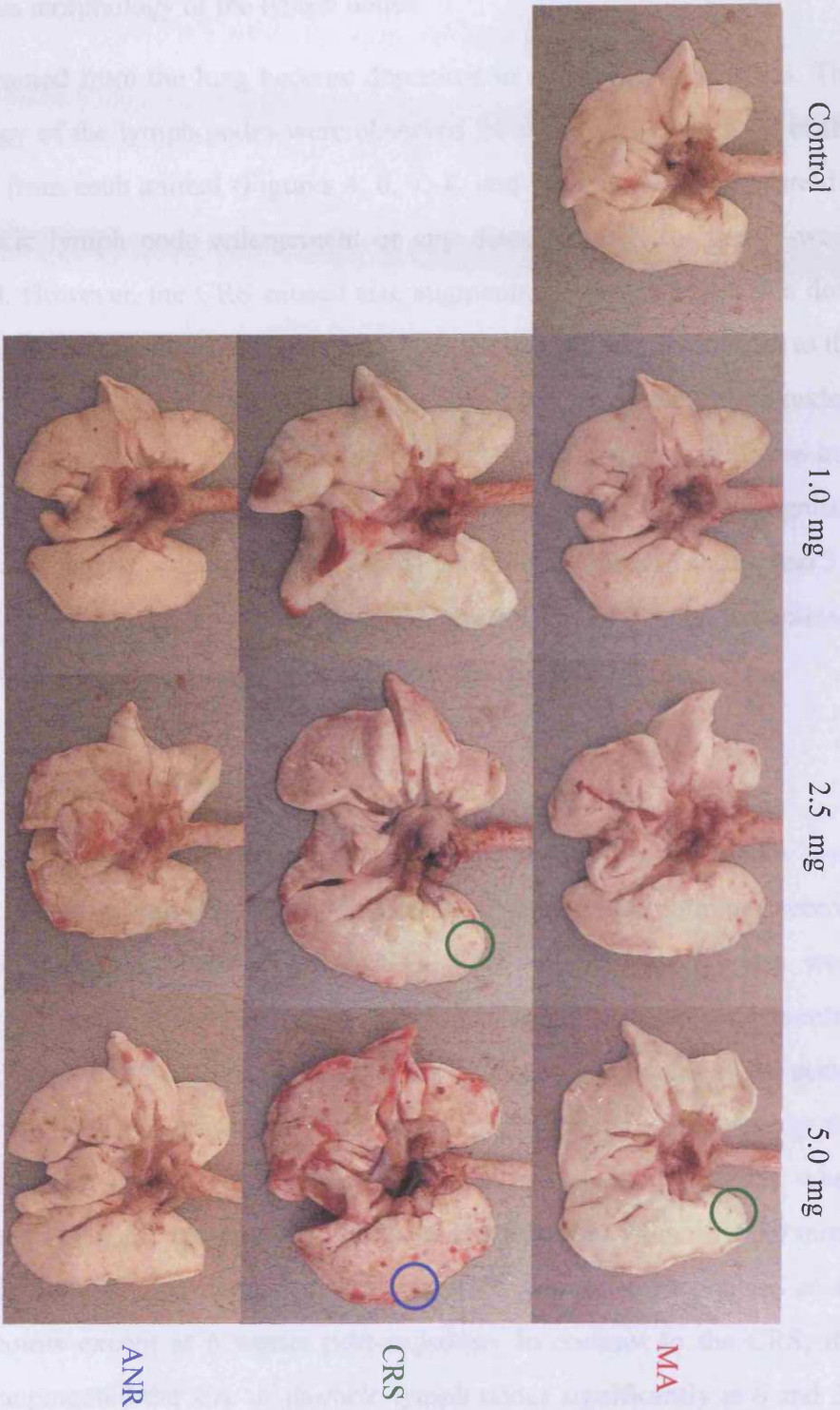
Figure 4. 5 The digitised pictures of gross morphology of the lungs at 49 weeks post-instillation. Grey discolorations in green circles indicate dust deposition in the lung and brown discolouration in a blue circle suggests lipoproteinosis.

4. 3. 1. 2 Gross morphological changes in the lymph nodes

4. 3. 1. 2. 1 Gross morphology of the lymph nodes

The particles drained from the lung become deposited in thoracic lymph nodes. The gross morphology of the lymph nodes were observed from the digitised image of the nodes collected from each animal (Figures 4. 6, 7, 8, and 9). The sham exposure did not cause thoracic lymph node enlargement or any discolouration for the 49-week exposure-period. However, the CRS caused size augmentation in the nodes in a dose and time dependent manner at all four different sacrifice time points. In contrast to the CRS, the ANR did not trigger any changes in the size of the thoracic lymph nodes. The MA finally led to size augmentation in the nodes at 49 weeks post-instillation in a dose dependent manner (Figure 4. 9). Moreover, grey discolorations were recognised from the digitised images of the thoracic lymph nodes from all doses (1.0, 2.5, and 5.0 mg) of the CRS or the MA or the highest dose (5.0 mg) of the ANR-exposed animals for 49 weeks indicating particle deposition in the nodes.

4. 3. 1. 2. 2 The size of the lymph nodes

The structural alterations in the sham or dust-exposed thoracic lymph nodes were represented by size augmentation or appearance/disappearance of germinal centres and granulomatous area formation instead. The sizes of the lymph nodes were measured using the digitised images and an image analysis system and are presented in Figure 4. 10. Sham-exposure did not lead to any changes in the sizes of the nodes during a 49-week exposure-period. The CRS caused significant size increases in the thoracic lymph nodes at all four different sacrifice time points ($p < 0.05$) when compared to the sizes of the lymph nodes from the sham-treated animals (6.50 mm^2, Figure 4. 10). Moreover, time dependent size increases were also recognised at all sacrifice time points except at 6 weeks post-exposure. In contrast to the CRS, the ANR (5.0 mg) augmented the size of thoracic lymph nodes significantly at 6 and 25 weeks post-instillation ($p < 0.05$) but the enlargement did not continue for the last 24 weeks.
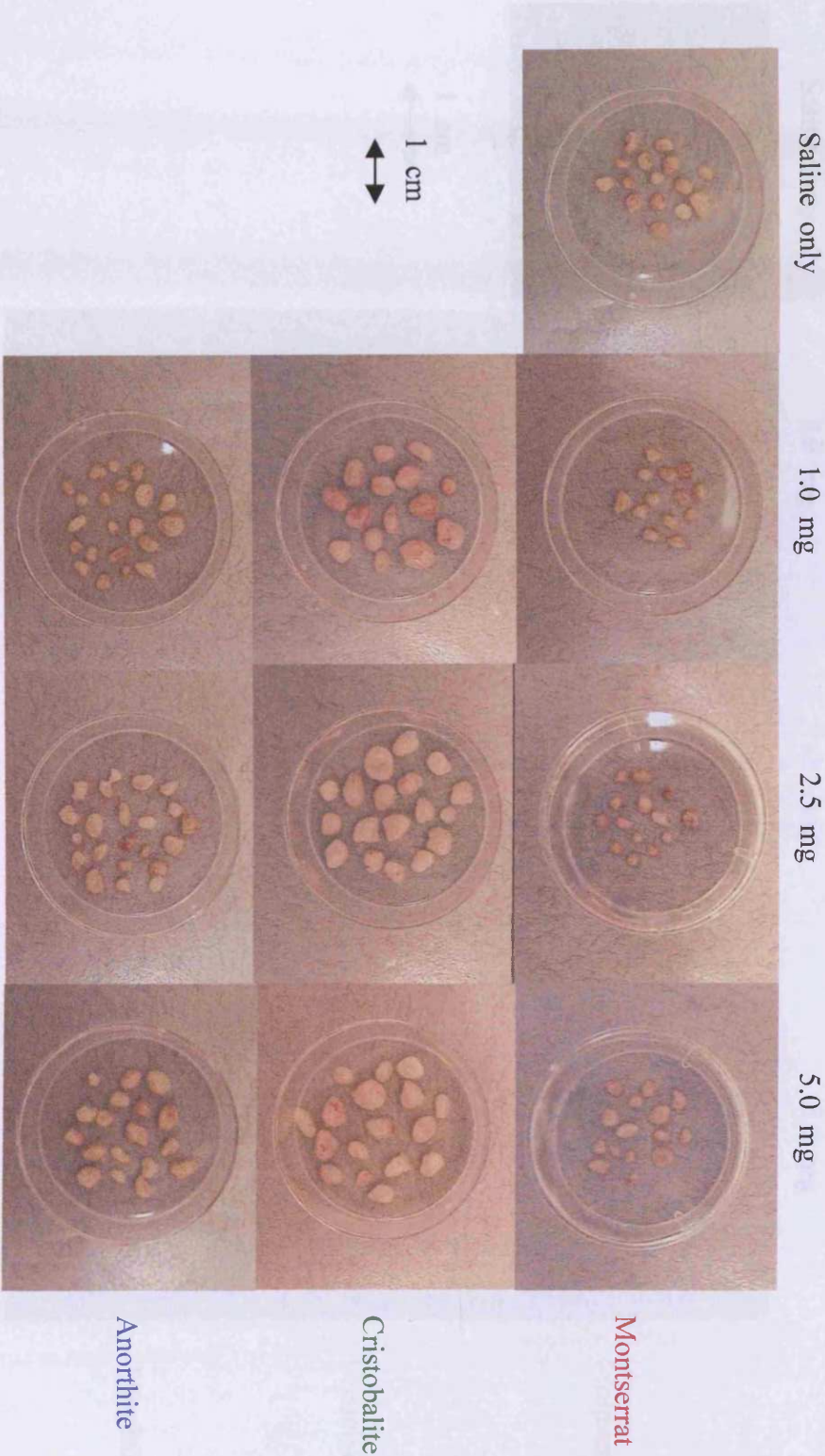
Figure 4. 6 The digitised pictures of lymph node morphology at 6 weeks post-instillation. The nodes are dissected randomly from the tracheo-bronchial region during removal of the intact lung.
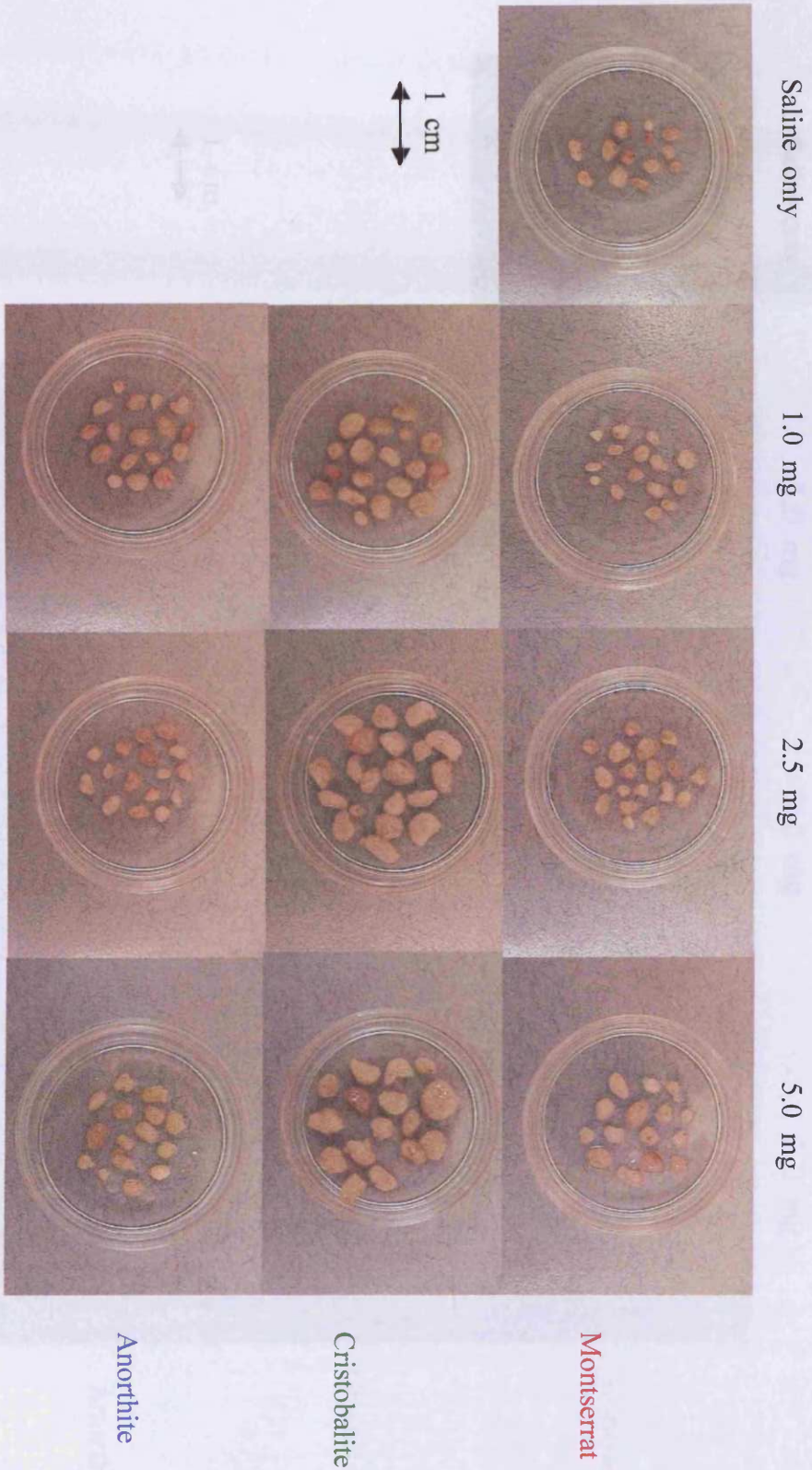
Figure 4.7 The digitised pictures of lymph node morphology at 13 weeks post-instillation. The nodes are dissected randomly from the tracheo-bronchial region during removal of the intact lung.
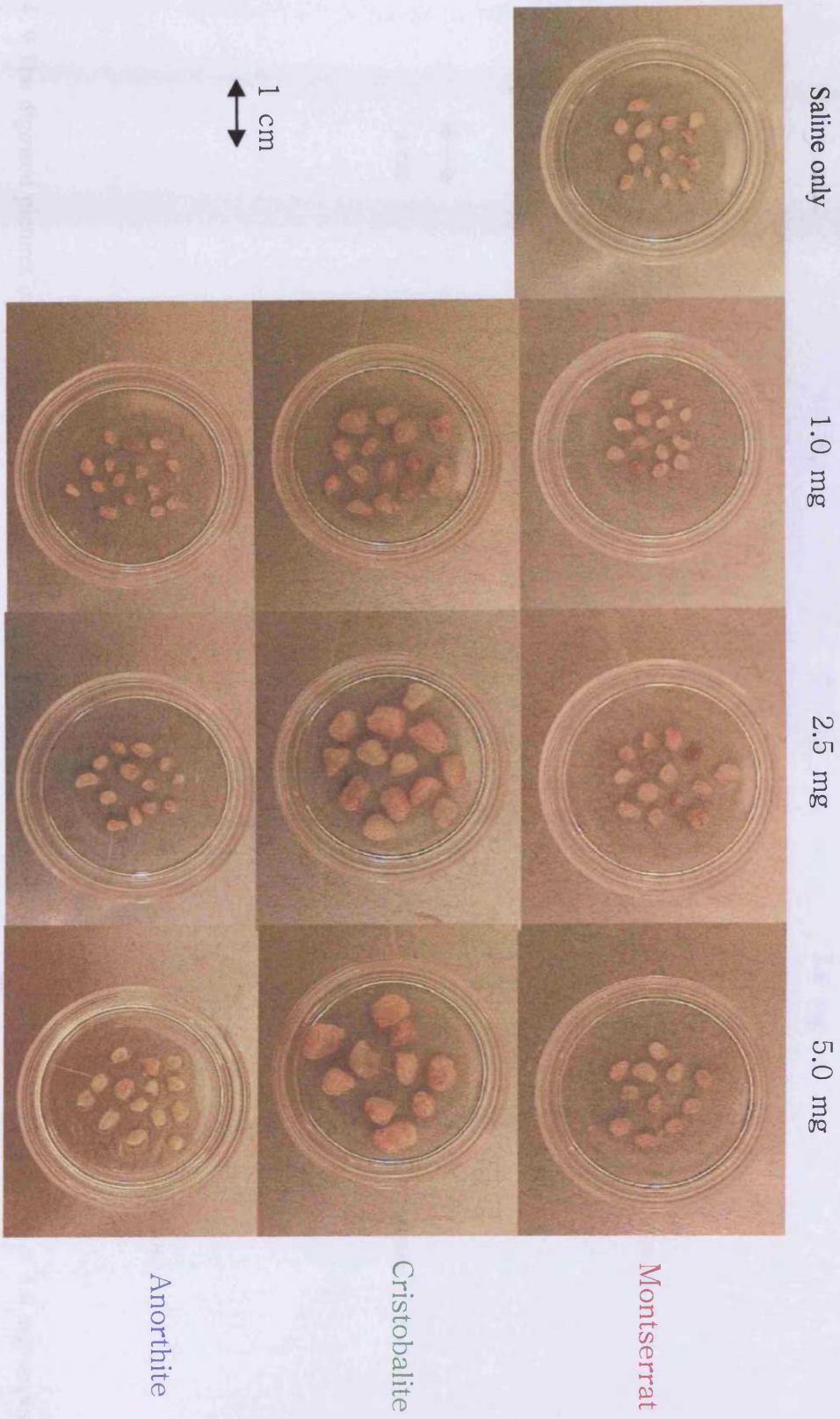
Figure 4. 8 The digitised pictures of the thoracic lymph nodes from sham, MA, CRS or ANR-exposed rat lungs at 25 weeks post-instillation
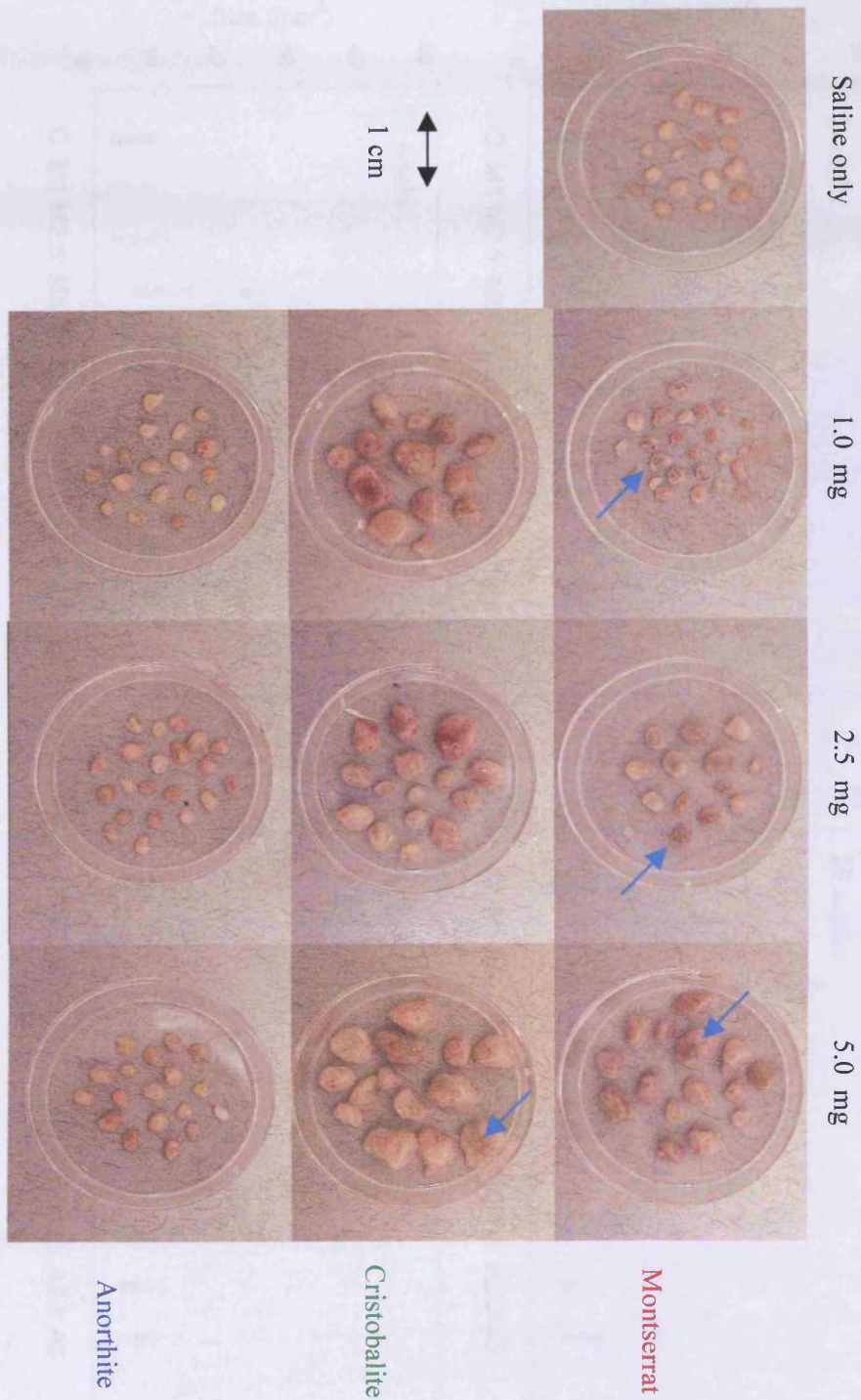
Figure 4. 9 The digitised pictures of gross morphology of the thoracic lymph nodes from sham, MA, CRS or ANR (1.0, 2.5 or 5.0 mg)-exposed animals] for 49 weeks. Grey discouloration (green arrows) indicates particle deposition.
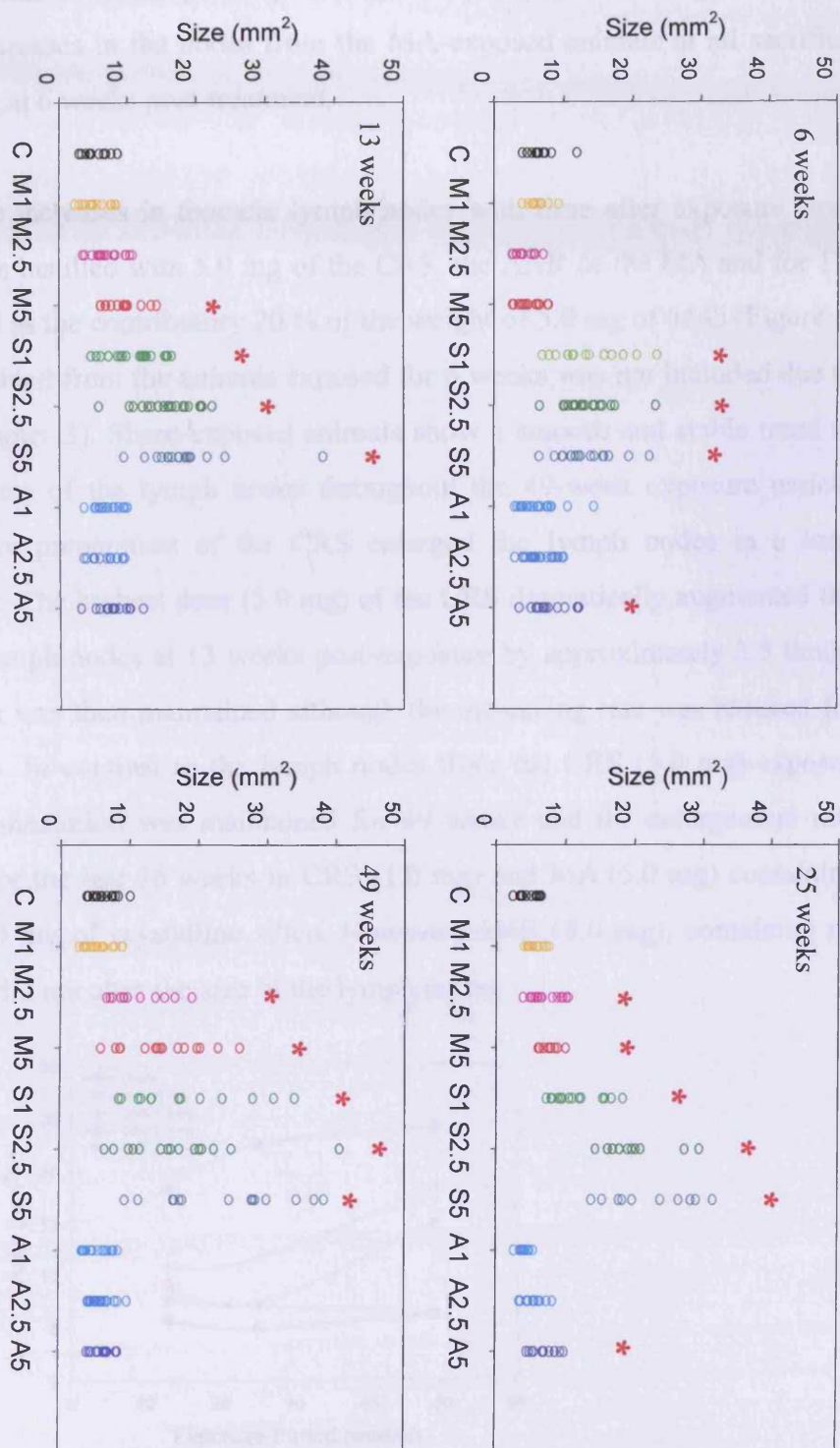
Figure 4. 10 The changes in the sizes of the lymph nodes from the sham, 1.0, 2.5 and 5.0 mg of the MA, the CRS, and the ANR -exposed animals for 6, 13, 25 and 49 weeks . (C=sham-treated control rats, M (1, 2.5 and 5) = Montserrat volcanic ash at 3 doses (mg) A= anorthite; S=cristobalite.) (* = a significant increase compared with control value, p<0.05).

However, the MA (5.0 mg) enlarged the lymph nodes significantly at 13, 25 and 49 weeks post-instillation (p<0.05). A lower dose of MA (2.5 mg) caused the enlargement at 25 and 49 weeks post-exposure (p<0.05). These results suggested dose dependent size increases in the nodes from the MA-exposed animals at all sacrifice time points except at 6 weeks post-treatment.

The trends of size increases in thoracic lymph nodes with time after exposure were plotted for animals instilled with 5.0 mg of the CRS, the ANR or the MA and for 1.0 mg of CRS (found as the contributory 20 % of the weight of 5.0 mg of MA) (Figure 4. 11). The data obtained from the animals exposed for 6 weeks was not included due to infection (see Chapter 3). Sham-exposed animals show a smooth and stable trend in changes in the sizes of the lymph nodes throughout the 49-week exposure period. However, the pure preparation of the CRS enlarged the lymph nodes in a time dependent manner. The highest dose (5.0 mg) of the CRS dramatically augmented the size of thoracic lymph nodes at 13 weeks post-exposure by approximately 3.5 times. The augmentation was then maintained although the increasing rate was reduced for the last 36 weeks. In contrast to the lymph nodes from the CRS (5.0 mg)-exposed animals, size augmentation was maintained for 49 weeks and the enlargement rate was accelerated for the last 36 weeks in CRS (1.0 mg) and MA (5.0 mg) containing approximately 1.0 mg of crystalline silica. However, ANR (5.0 mg), containing no crystalline silica, did not alter the size of the lymph nodes.
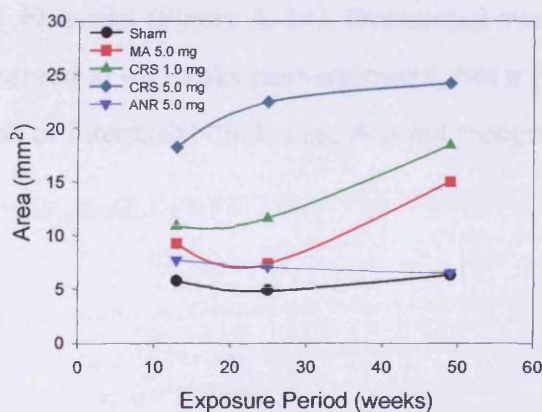
Figure 4. 11 The trends of the changes in the sizes of lymph nodes from sham, the MA (5.0 mg), the CRS (1.0 or 5.0 mg) or the ANR (5.0 mg)-exposed animals depending on the exposure period.

4. 3. 2 Histopathology

4. 3. 2. 1 Histopathological changes in the mineral dust-instilled lungs

Crystalline silica containing mineral dusts can cause inflammation indicated by free cell influx into the alveoli units or fibrosis recognised from connective tissue proliferation resulting in collagen deposition in interstitial regions. Massons' trichrome staining presents the nuclei as blue-black and collagen, cartilage and mucin as blue-green. Sham-treated lungs demonstrated clean alveoli units with thin alveolar walls appearing to be slightly green implying little collagen deposition in the interstitial area for 49 weeks (Figures 4. 12, 13 and 14). However, all doses of the CRS led to an influx of free cells in the alveoli units resulting in group accumulations at 13 weeks post-instillation. Moreover, alveolar wall thickening was also noticeable with enlarged alveolar septa stained as green. These changes were not so noticeable in 1.0 mg CRS-exposed lungs at 49 weeks post-instillation (Figure 4. 14). However, the highest dose (5.0 mg) of the CRS caused interstitial thickening with collagen deposition even though the cell influx in alveoli units were less prominent at 49 weeks post-instillation. In contrast to the CRS, all doses of the ANR did not induce any free cell influx, alveolar wall thickening or collagen deposition in the interstitial region in the lungs for 49 weeks. Low dose (1.0 mg) of MA-exposed lungs for 13 or 49 weeks resulted in relatively clear alveoli units and thin alveolar walls with little collagen deposition. The highest dose (5.0 mg) of the MA did not induce free cells influx in alveoli units until 49 weeks (Figure 4. 14). Occasional swollen alveolar septa stained as green were observed at 49 weeks post-treatment, but a fibrogenic response such as collagen deposition or interstitial thickening was not recognised with the MA.
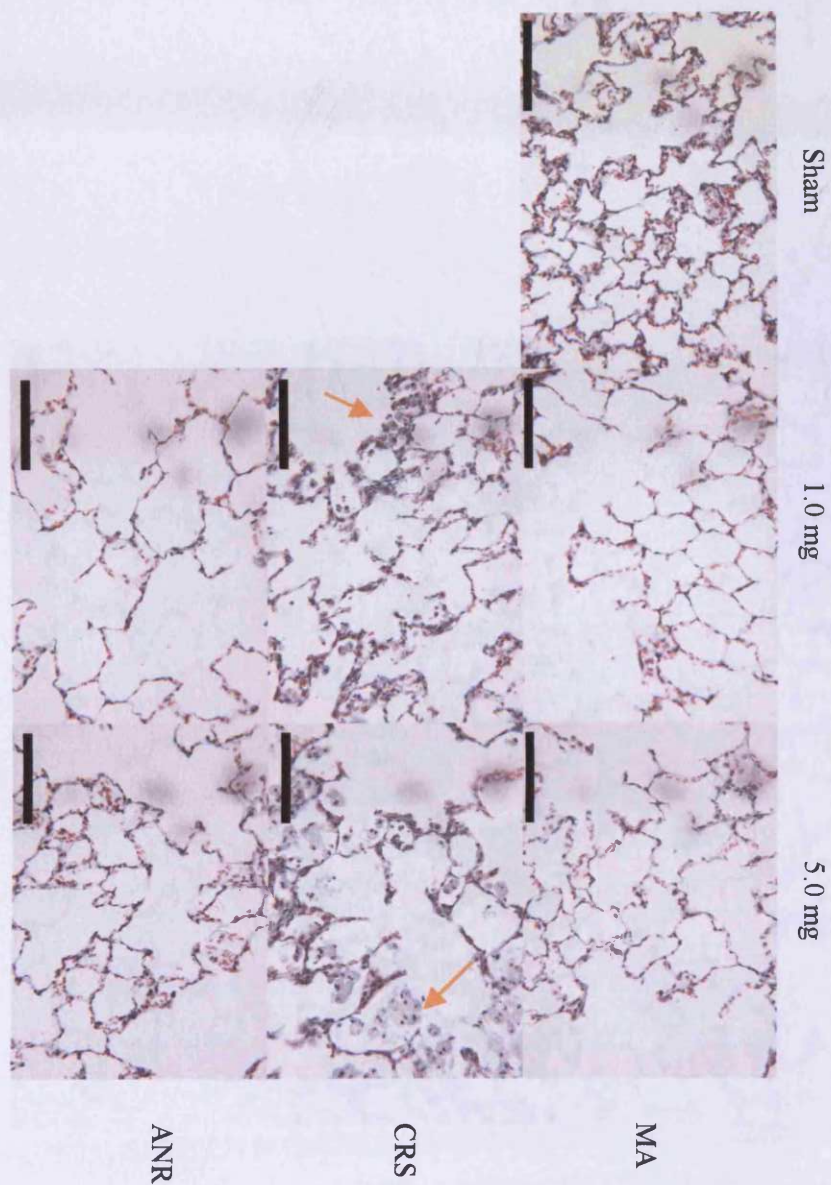
Figure 4. 12 The micrographs of the sham, the MA, the ANR or the CRS (1.0 or 5.0 mg)-exposed lung section. Masson's trichrome staining at 6 weeks post-exposure. Arrows depict free cell influx in alveoli units. A scale bar=108 μm
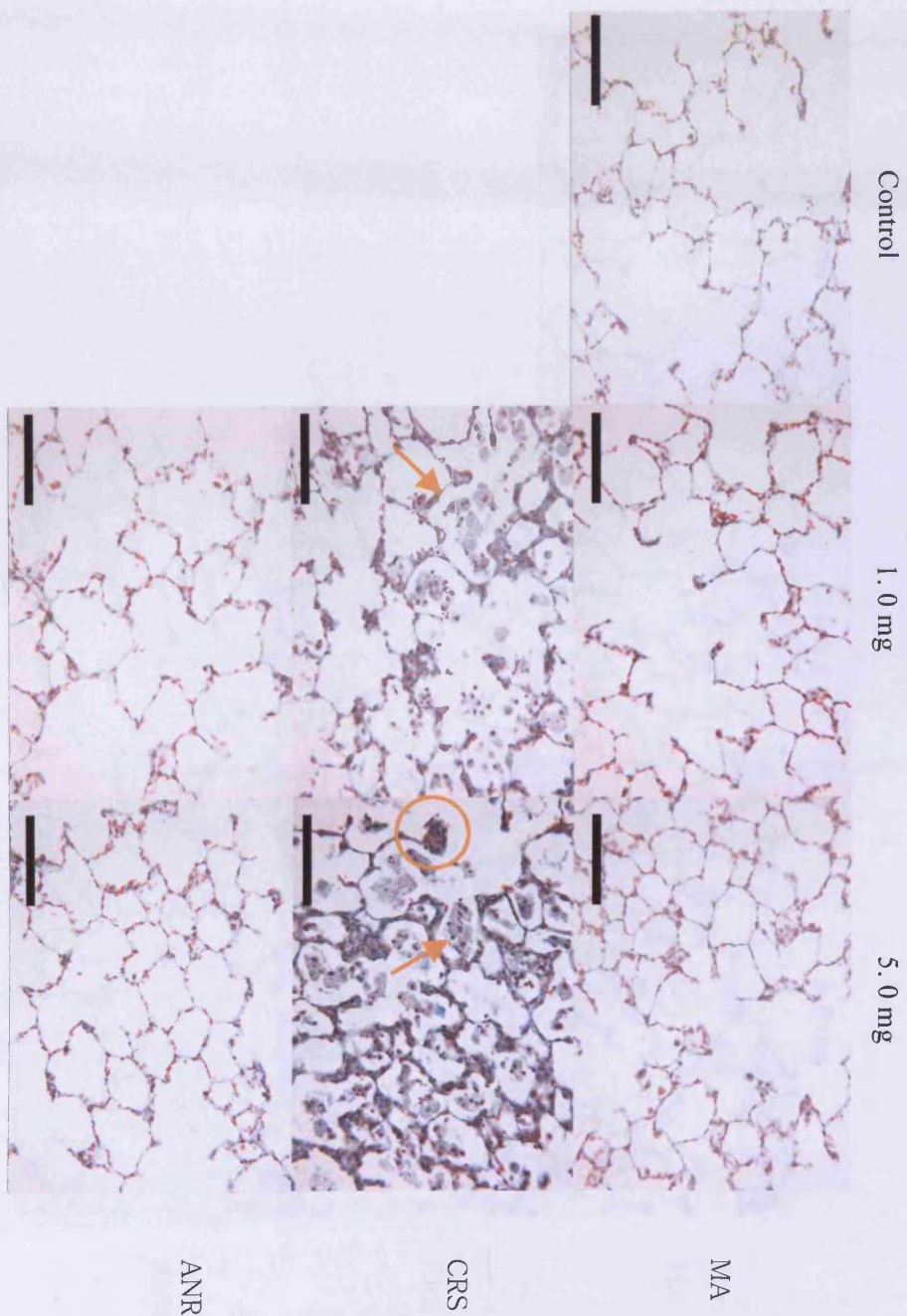
Figure 4. 13 The micrographs of the sham, the MA, the ANR or the CRS (1.0 or 5.0 mg)-exposed lung section. Masson's trichrome staining at 13 weeks post-exposure. Arrows depict free cell influx in alveoli units and a circle denotes swollen aveolar septum. (A scale bar=108 μm)
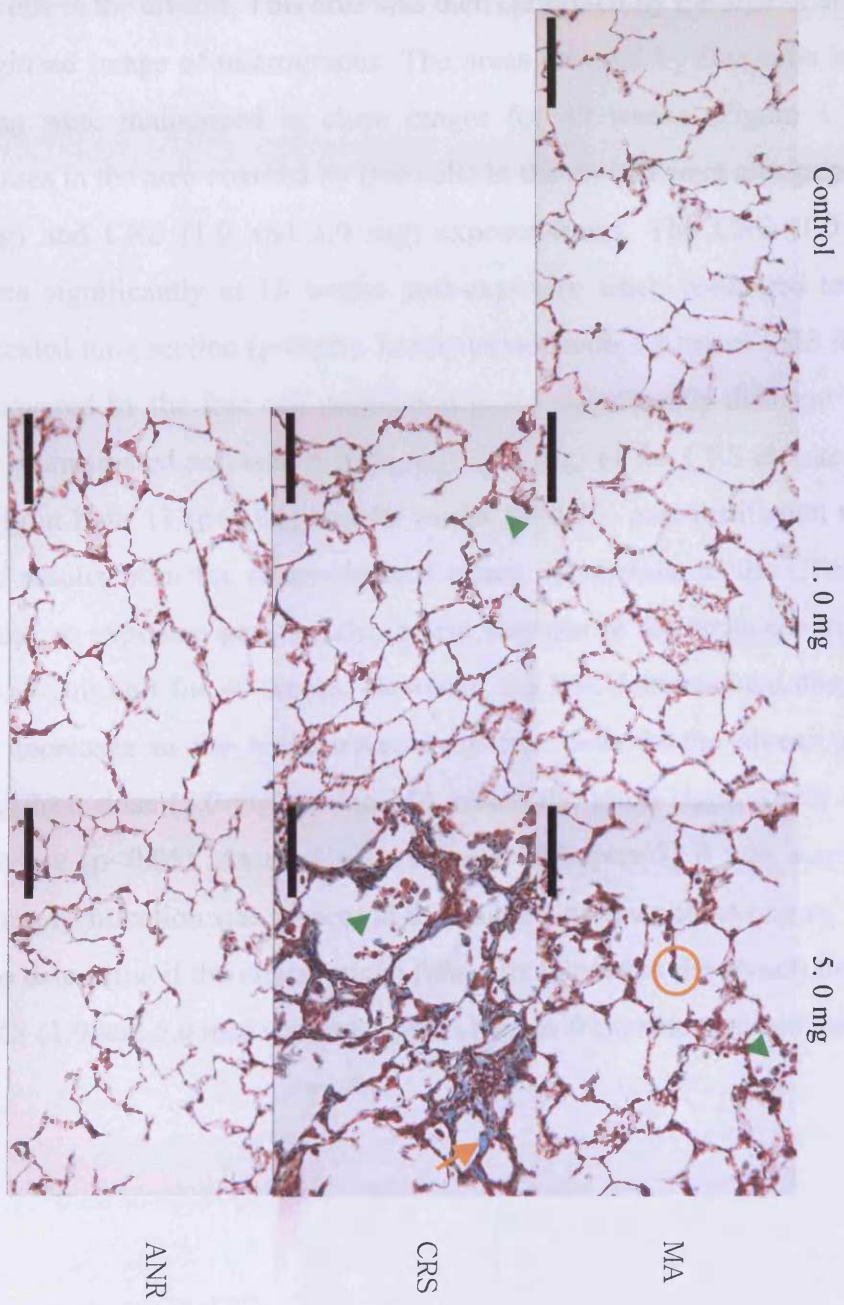
Figure 4. 14 The micrographs of the sham, the MA, the ANR or the CRS (1.0 or 5.0 mg)-exposed lung section. Masson's trichrome staining at 49 weeks post-exposure. The arrow depicts collagen deposition in the interstitial area, arrow heads depicts free cells influx and circle depicts green coloured alveolar septa. A scale bar=108 μm

4. 3. 2. 2 Quantification of alveolar free cells and interstitial collagen

One of the typical inflammatory responses of the lung is free cell influx in the alveolar region. The degree of free cell-influx was semi-quantified by measuring the area covered by free cells in the alveoli. This area was then calibrated by the area of alveoli units in each digitised image of micrographs. The areas covered by free cells in the sham-treated lung were maintained in close ranges for 49 weeks (Figure 4. 15). Significant increases in the area covered by free cells in the alveoli were recognised in the MA (5.0 mg) and CRS (1.0 and 5.0 mg) exposed-lungs. The CRS (1.0 mg) increased the area significantly at 13 weeks post-exposure when compared to that from the sham-treated lung section ($p<0.05$). In rats treated with 1.0 mg of CRS for 49 weeks the area covered by the free cell population is not significantly different from that observed in sham-treated animals. A high dose (5.0 mg) of the CRS elevated the areas significantly at both 13 ($p<0.01$) and 49 weeks ($p<0.05$) post-instillation when compared to the results from the sham-exposed group. In contrast to the CRS, the ANR showed dose or exposure period independent changes in the areas covered by free cells in the alveoli unit for 49 weeks. However, the MA demonstrated dose and time dependent increases in the areas covered by free cells in the alveoli units. Moreover, the highest dose (5.0 mg) of the MA raised the areas significantly at 49 weeks post-exposure ($p<0.05$). As detailed previously (Chapter 3) it was suspected that a mild respiratory infection was present in the rats at 6 weeks post-exposure. Thus, it was difficult to determine if the elevations in free cells located in the alveoli for MA (5.0 mg) and CRS (1.0 and 5.0 mg) represent time changes from sham-treated animals.
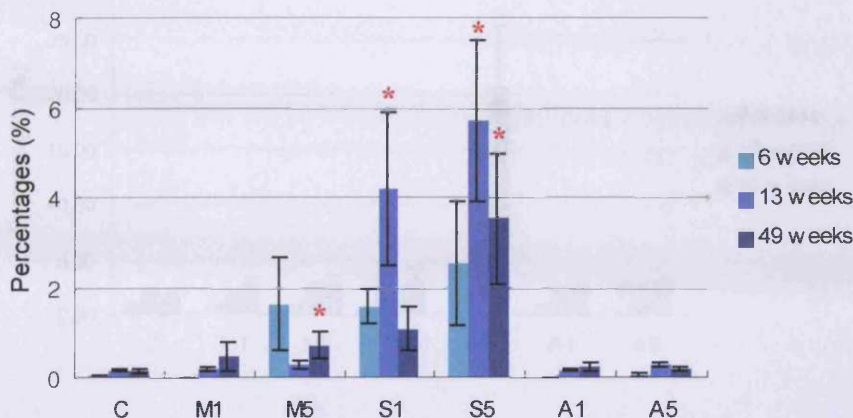
Figure 4. 15 The area covered by free cells in the alveoli unit in the lung. (Key: C=sham-treated control rats, M (1 and 5) = MA at 2 doses (1.0 and 5.0 mg) A= ANR; S=CRS. Red asterisks indicate significant increases compared to the results from the sham-treated groups (p<0.05, n=15))

The augmentation of the interstitial collagen is a good indicator for fibrogenic changes in the lung. The interstitial collagen was measured using an image analysis system since collagen was stained blue-green by Masson's trichrome. The area of blue-green coloured interstitial region was then calibrated by interstitial area of each digitised picture and any green coloured region in the alveolar region including MACs was excluded. The blue-green coloured areas in the sham-exposed lungs were maintained in close ranges for 49 weeks (Figure 4. 16). MA (1.0 mg) and CRS (1.0 mg) increased the blue-green coloured area significantly at 6 weeks post-instillation and these could be due to infection (see chapter 3). A high dose (5.0 mg) of the CRS raised the interstitial collagen deposited area significantly both at 13 and 49 weeks post-instillation in a time dependent manner (p<0.001). In contrast to the CRS, the ANR did not cause any significant changes in the green coloured areas for 49 weeks. The MA containing approximately 20 % (w/w) of crystalline silica did not cause dose or time related changes in the collagen deposited area in the interstitial region for 49 weeks.
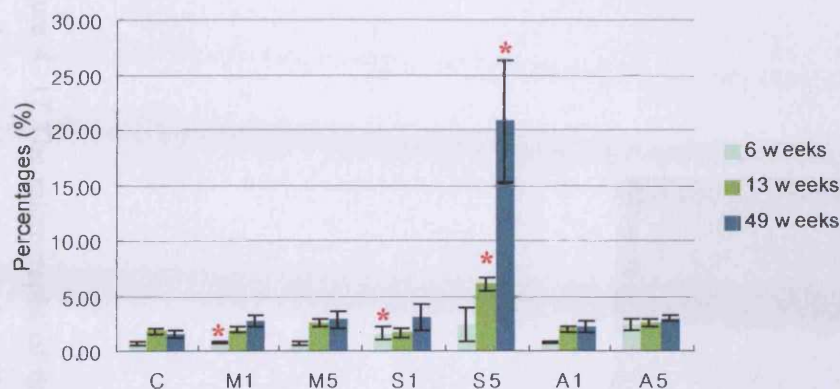
Figure 4. 16 The areas stained green in the interstitial region of the lungs by Masson's trichrome. (n=15, Key as Figure 4. 15)

4. 3. 2. 3 Histopathology of the lymph nodes

Thoracic lymph nodes are the organs where instilled/inhaled particles are cleared and deposited by MACs (Adamson and Prieditis, 1998; Davis et. al., 2001; Friedetzky et. al., 1998; Garn et. al., 1997). Therefore, if the instilled particles were toxic, structural changes in the nodes would be expected. The lymph nodes from sham-treated animals demonstrated compact links among cells without the appearance of germinal centres (Figures 4. 17, 18 and 19). However, the CRS caused granulomatous areas appearing as a loose connection among the cells in the nodes at 6 weeks post-instillation and the changes were maintained throughout another 43 weeks. The ANR did not cause any granulomatous effects in the nodes at 13 weeks post-exposure. Only one of the nodes collected from 5 animals randomly and examined, showed a granuloma at 49 weeks post-instillation. The highest dose (5.0 mg) of the MA induced granuloma in the nodes at 13 weeks post-exposure and the symptom became more severe at 49 weeks post-instillation. Moreover, granulomatous areas also appeared in the nodes from the 1.0 mg of MA-exposed animals for 49 weeks. Local particle depositions were also recognisable in the nodes from the mineral dusts-exposed animals and most of the particles were found in the granulomatous areas.

113
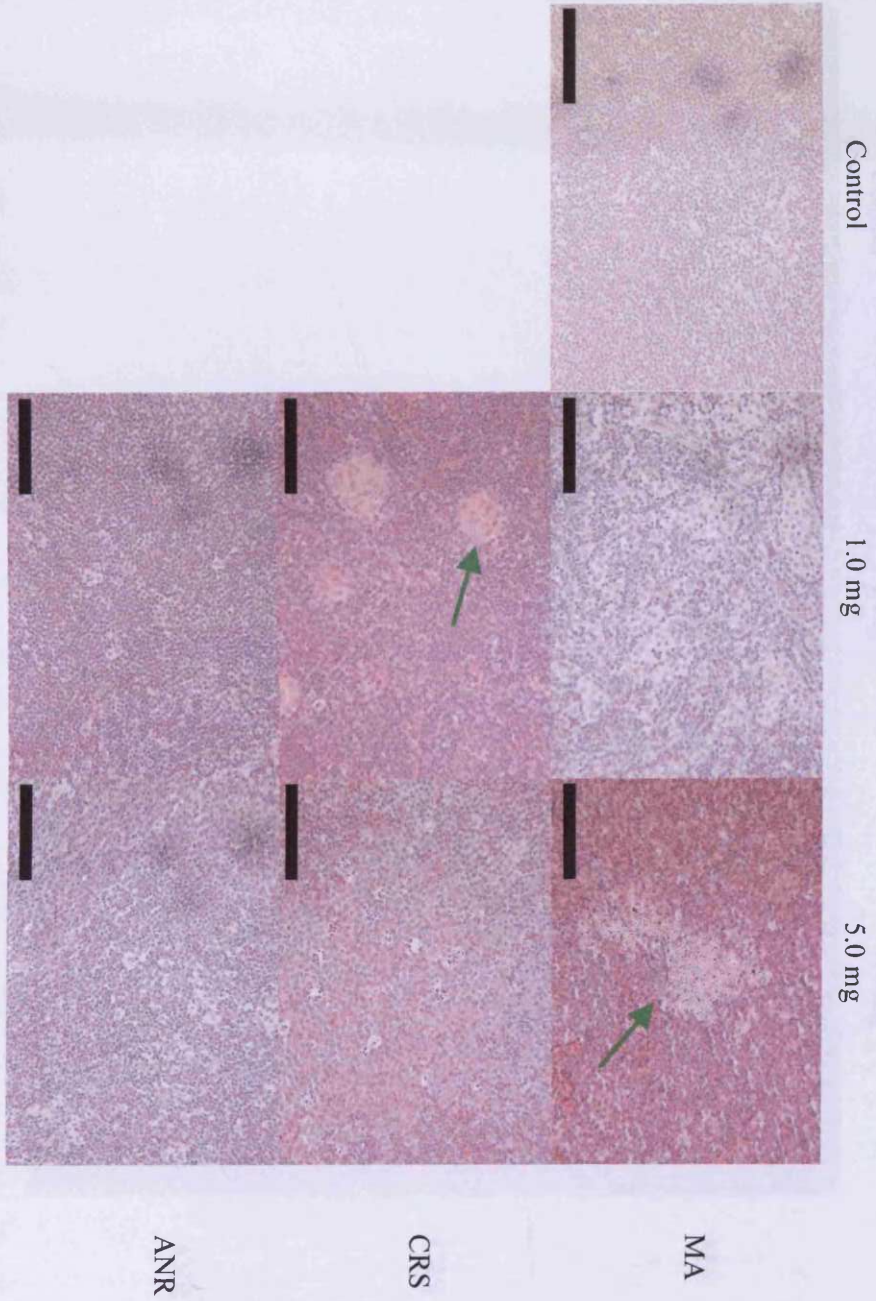
Figure 4. 17 The micrographs of the lymph nodes from the sham, the MA, the CRS or the ANR exposed animals for 6 weeks. Arrows depict granulomatous areas. A scale bar=108 μm.
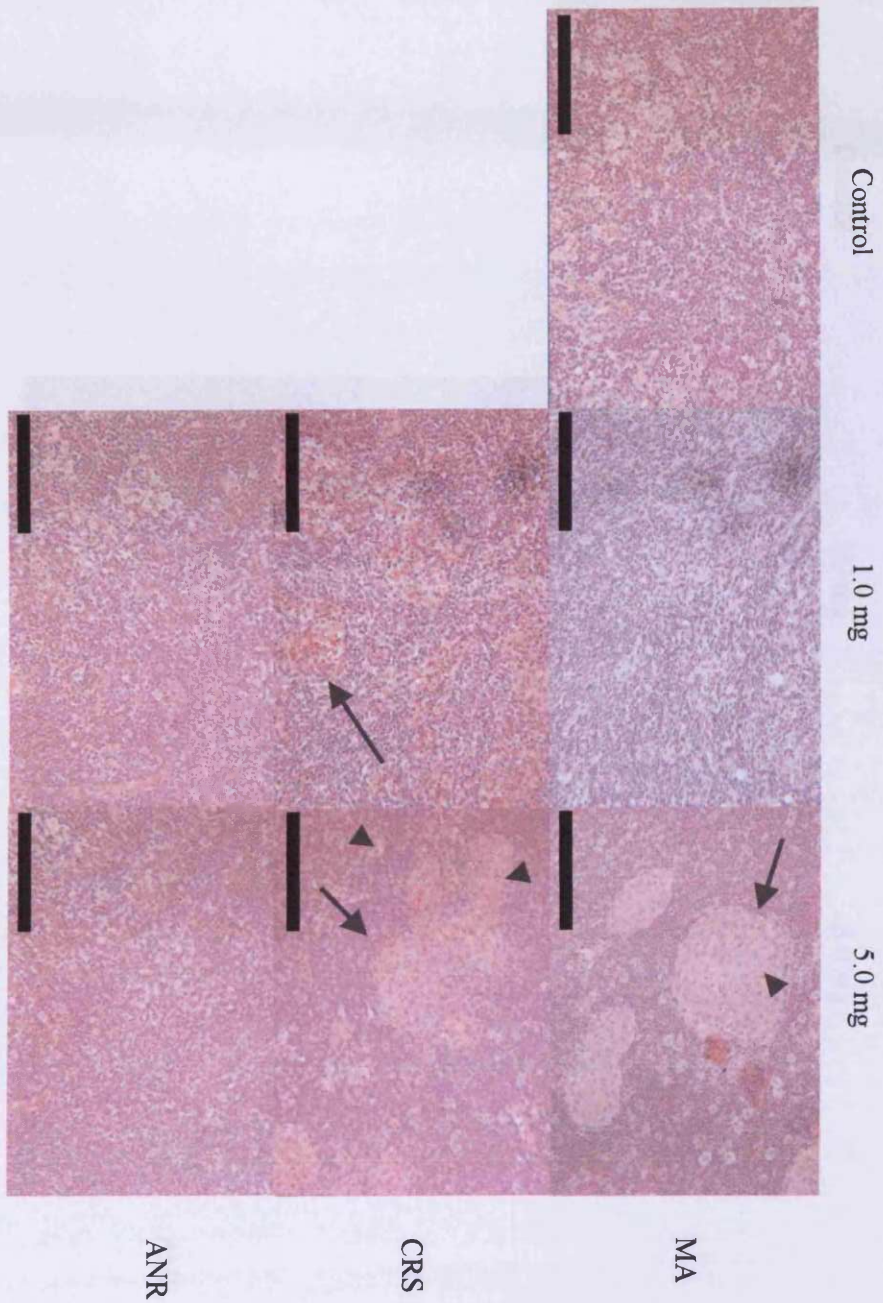
Figure 4. 18 The micrographs of the lymph nodes from the sham, the MA, the CRS or the ANR exposed rats for 13 weeks. The sections were stained with Haematoxylin and eosin. Arrows depict granulomatous area and arrowheads indicate the particles deposited in these area. A scale bar=108 μm.
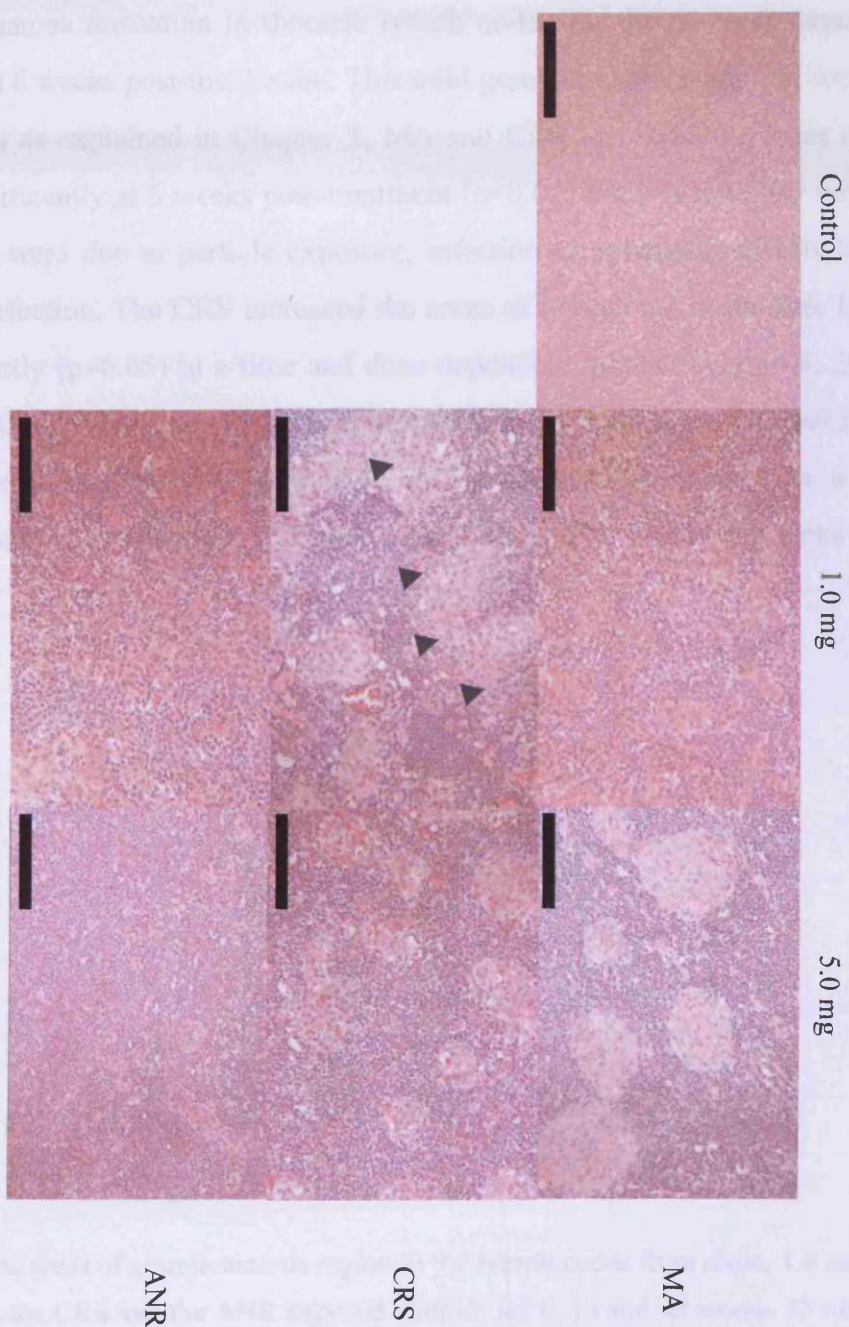
Figure 4. 19 The micrographs of the lymph nodes from the sham, the MA, the CRS or the ANR exposed animals for 49 weeks. The sections were stained with Haematoxylin and eosin. Arrowheads indicate the particles deposited in these area. A scale bar=108 μm.

4. 3. 2. 4 Quantification of the granulomatous area in the lymph nodes

The sizes of granuloma taken to be zero in the nodes from healthy animals were measured using the image analysis system (Figure 4. 20). Sham-exposure did not cause granulomatous formation in thoracic lymph nodes for the 49-week exposure-period except at 6 weeks post-instillation. This mild granulomatous symptom could be due to infection as explained in Chapter 3. MA and CRS increased the areas of the granuloma significantly at 6 weeks post-treatment ($p < 0.05$) but it is not clear whether these increases were due to particle exposure, infection or synergetic effects led by exposure and infection. The CRS increased the areas of granuloma in thoracic lymph nodes significantly ($p < 0.05$) in a time and dose dependent manner (Figure 4. 20). In contrast to the CRS, ANR showed little granulomatous formation for 49 weeks. The MA (5.0 mg)-exposure increased the size of the granulomatous area in a time dependent manner with statistic significance ($p < 0.05$) both at 13 and 49 weeks post-instillation.
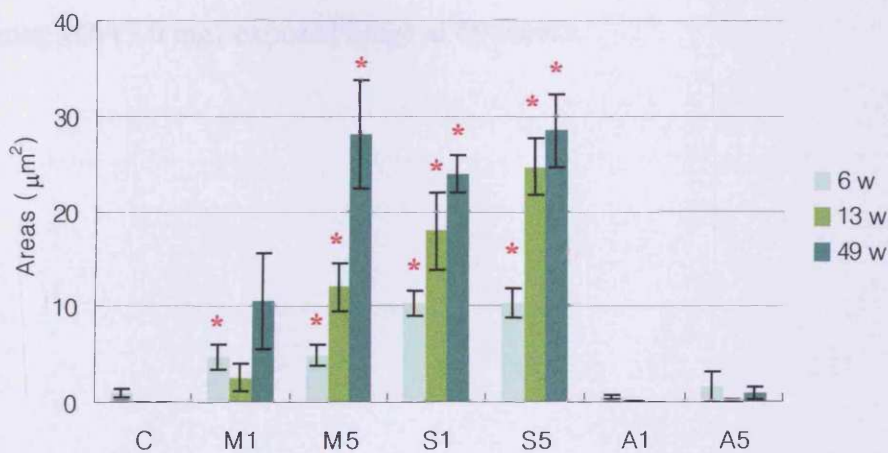
Figure 4. 20 The areas of granulomatous region in the lymph nodes from sham, 1.0 and 5.0 mg of the MA, the CRS and the ANR exposed-animals for 6, 13 and 49 weeks. 15 random areas of section per group were investigated. (Key as Figure 4. 15)

4. 3. 2. 5 The morphology of the free cells lavaged from the lung

The morphology of the lavageable free cells such as MACs or PMNs stained with Rapi-diff were investigated. The free cells from the sham-exposed lungs for 13 or 49 weeks were mainly composed of MACs and their size did not vary (Figures 4. 21, 22 and 23). However, multinucleated giant cells appeared in the lavageable free cells from the CRS-exposed lungs at 13 weeks post-instillation. Moreover, foamy MACs, which are normally found in the lung showing lipoproteinosis and PMNs, which hardly appeared in the healthy lung, were also observed in the free cells recovered from the lung lavage from CRS-exposed animals for 13 weeks. The numbers of the multinucleated giant cells and PMNs were reduced in the CRS-exposed lungs at 49 weeks post-instillation. In contrast, most of free cells recovered from ANR-exposed lungs were MACs and their sizes did not vary at both 13 and 49 weeks post-instillation. A few multinucleated giant cells were found in the free cells from the MA (1.0 mg)-exposed lung for 13 weeks without PMNs' appearing. PMNs, good markers of inflammation, did not appear in the lavageable free cells from the MA-exposed lungs until 49 weeks post-treatment. More foamy MACs also appeared in the free cells from MA (5.0 mg)-exposed lungs at 49 weeks.
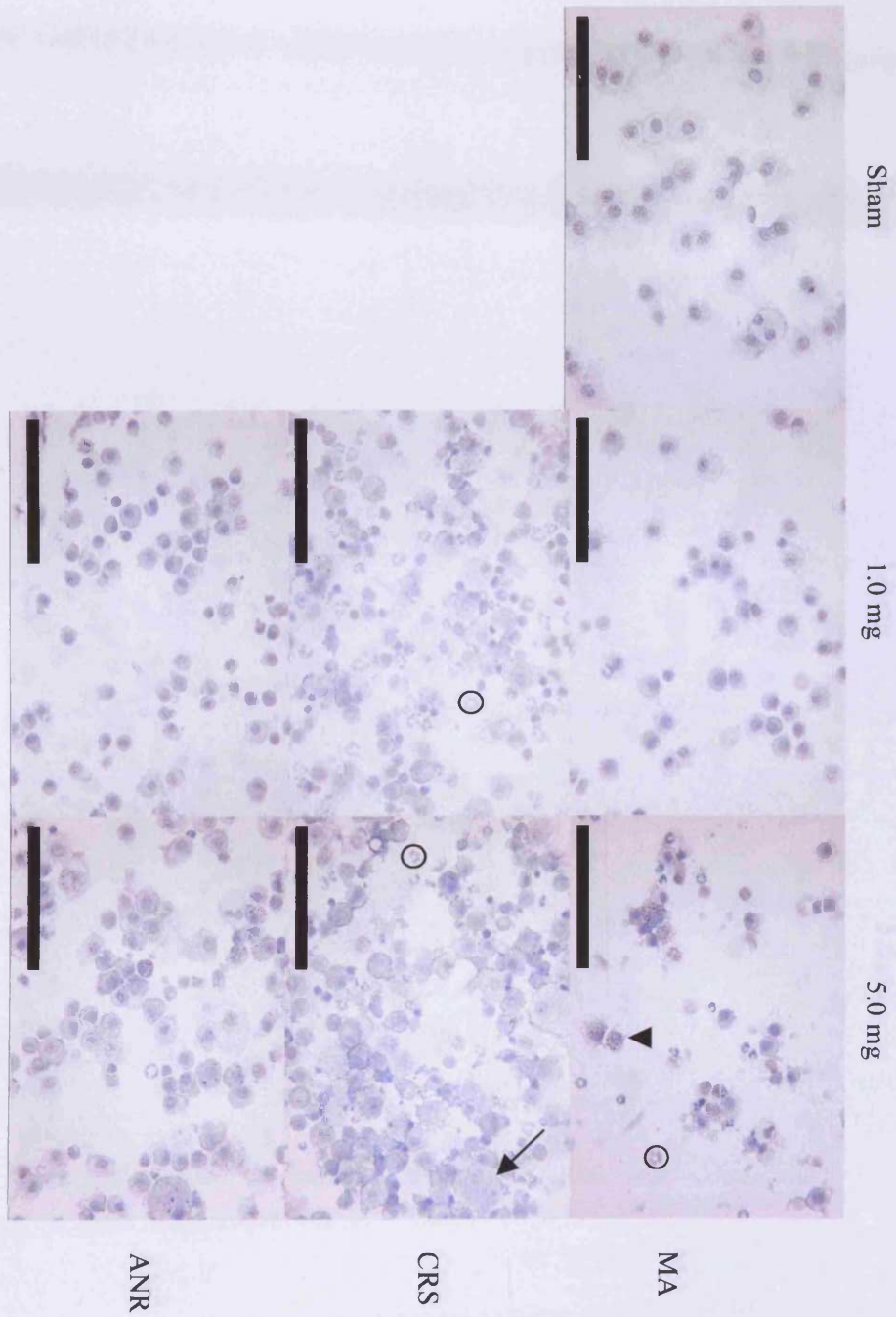
Figure 4. 21 The digitised images of the micrographs of the lavageable free cells from sham, MA, CRS or ANR (1.0 or 5.0 mg)-exposed lung for 6 weeks. Circles depict PMNs, arrows depict foamy MACs and arrowheads indicate the particles in MACs. A scale bar=100 μm
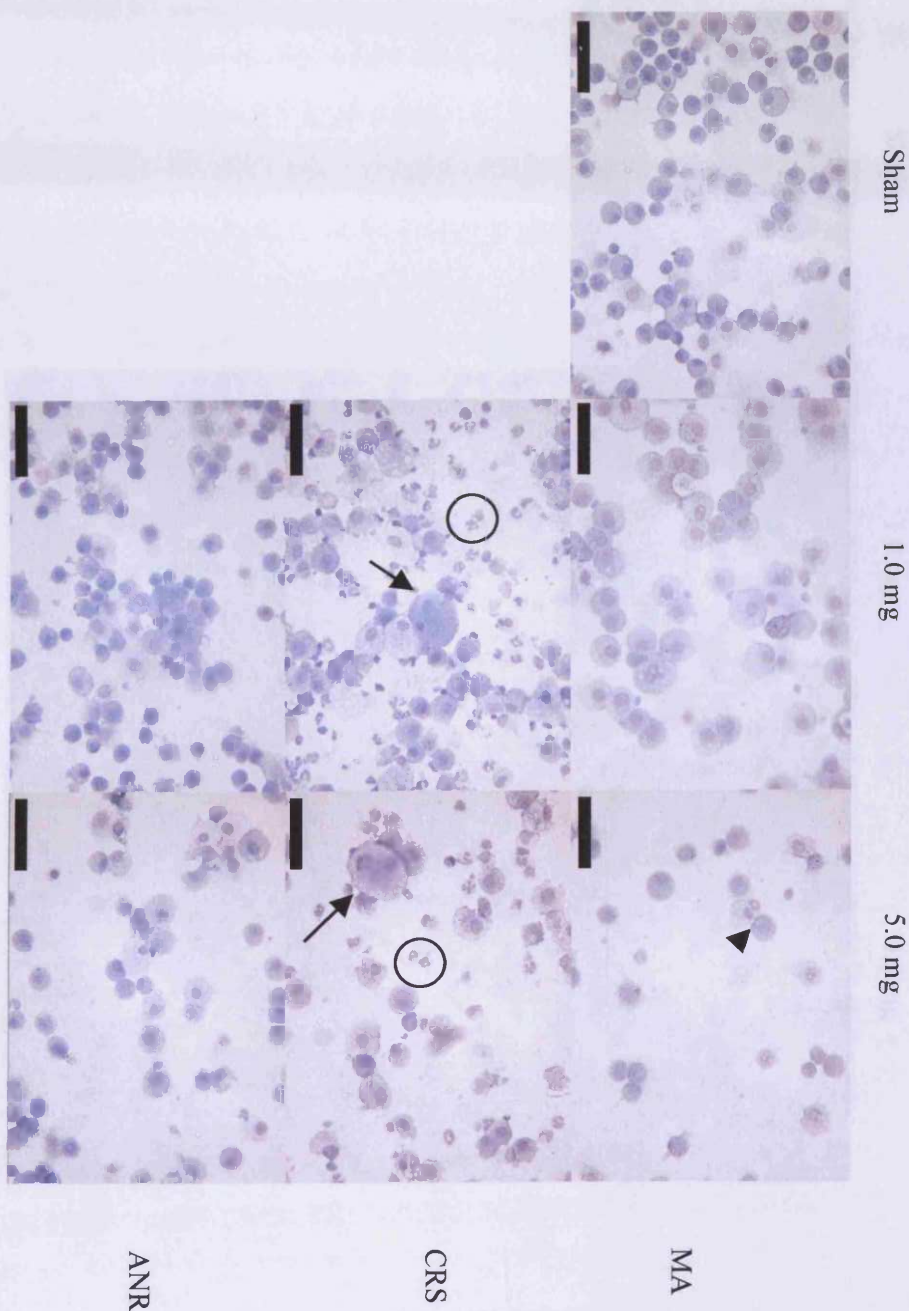
Figure 4. 22 The digitised images of the micrographs of the lavageable free cells from sham, MA, CRS or ANR (1.0 or 5.0 mg)-exposed lung for 13 weeks. Circles depict PMNs, arrows depict foamy MACs and arrowheads indicate the particles in MACs. A scale bar=50 μm
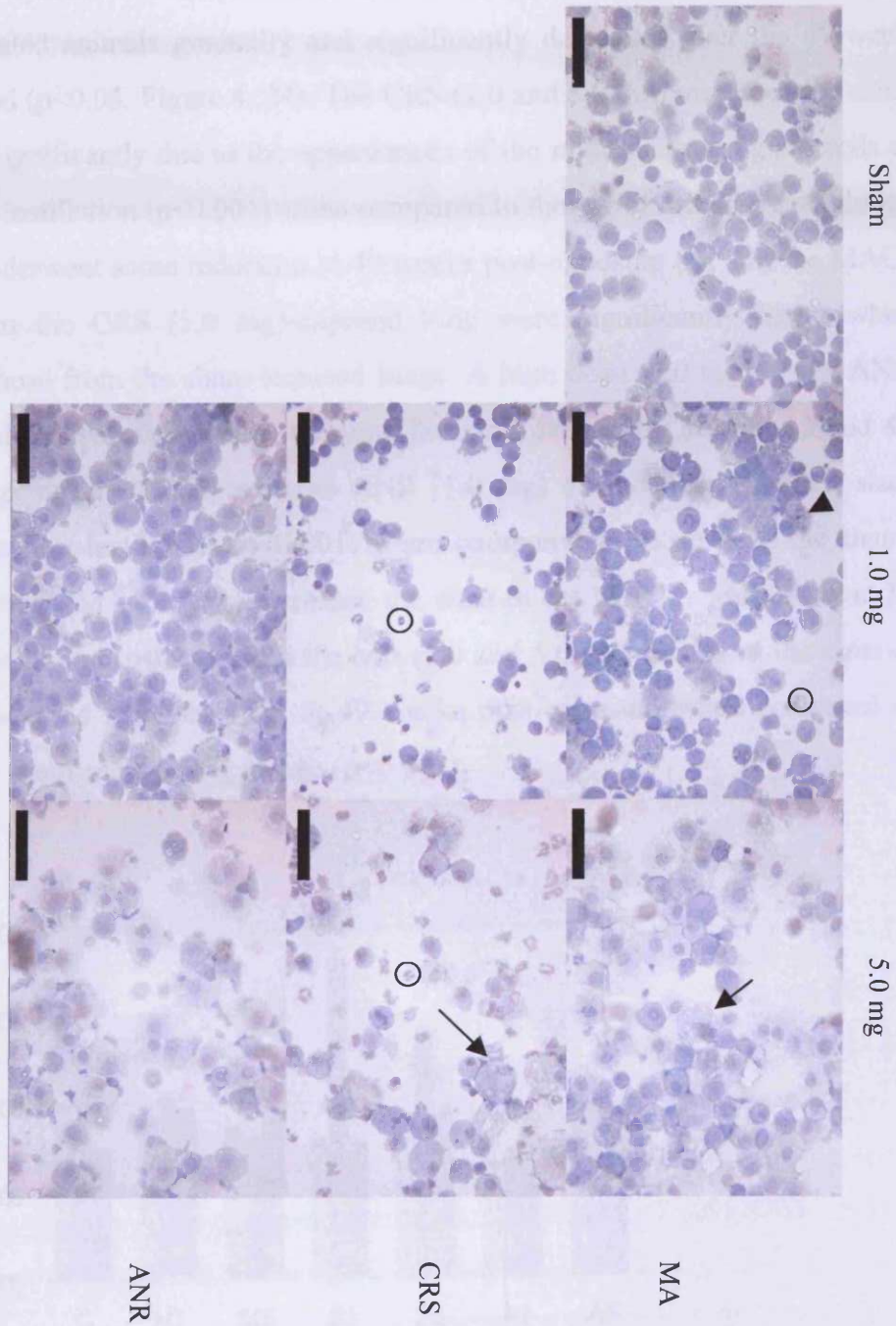
Figure 4. 23 The digitised images of the micrographs of the lavageable free cells from sham, MA, CRS or ANR (1.0 or 5.0 mg)-exposed lung for 49 weeks. Circles depict PMNs, arrows depict foamy MACs and arrowheads indicate the particles in MACs. A scale bar=50 μm

4. 3. 2. 6 The size of the MACs lavaged from the lung

The equivalent spherical diameters (ESD) of the MACs were measured using the image analysis system. The diameters of the MACs recovered from the lung lavage from sham-treated animals gradually and significantly decreased over the 49-week exposure-period ($p < 0.05$, Figure 4. 24). The CRS (1.0 and 5.0 mg) increased the sizes of the MACs significantly due to the appearances of the multinucleated giant cells at 13 weeks post-instillation ($p < 0.001$) when compared to those from sham-treated lungs. These sizes underwent some reduction at 49 weeks post-exposure but still the MACs recovered from the CRS (5.0 mg)-exposed lung were significantly larger when compared to those from the sham-exposed lungs. A high dose (5.0 mg) of the ANR enlarged the MACs recovered from the lung lavage significantly at both 13 and 49 weeks post-exposure ($p < 0.001$) whereas ANR (1.0 mg) did not increase their sizes until 49 weeks post-instillation ($p < 0.001$) when compared to those from the sham-treated lung lavage. MA (1.0 mg) increased the sizes of the MACs significantly at 13 weeks post-instillation ($p < 0.001$) and the MA (1.0 and 5.0 mg) increased the sizes of the MACs recovered from the lung at 49 weeks post-exposure when compared to those from the sham-treated lung lavage ($p < 0.001$).
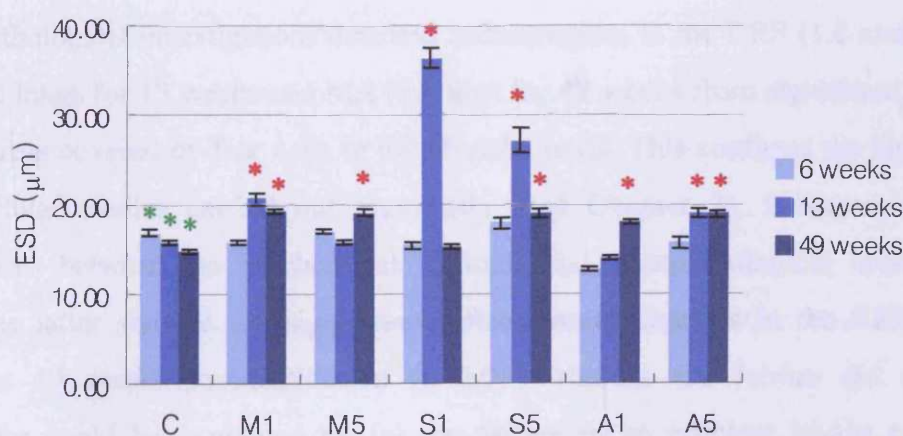
Figure 4. 24 The changes in the sizes of the MACs induced by MA, CRS or ANR instilled into the lungs (Key as Figure 4. 15, At least 180-200 cells were counted on each cytospin). Green asterisk indicates significant decreases between sham-exposed groups for 6 and 13 weeks and 13 and 49 weeks ($p < 0.05$).

122

4. 4 Discussion

Semi quantitative histopathology was employed to investigate morphological or structural changes in the lung or thoracic lymph nodes caused by mineral dust-instillation. Previous biochemical and cellular investigations (Chapter 3) focused on the changes at the lung surface since lung lavage samples were employed for most of the investigations. However, the lavage process does not always reflect the changes in the lung under certain circumstances for example when lipoprotein accumulation and interstitial wall thickening are so severe that the alveoli may not be washed out efficiently. Moreover, biochemical and cellular investigations were not carried out for thoracic lymph nodes. Therefore, histopathological investigation was employed to detect the changes in the lung or thoracic lymph nodes, which were not analysed from biochemical or cellular approaches.

Gross morphology of the lungs particularly those exposed to CRS, resulted in yellow or brown surface discoloration indicative of inflammation or lipoproteinosis. However, these observations were limited to the surface of the lungs and therefore, semi quantitative histopathological investigations were employed to find the changes in the parenchyma caused by mineral dust-instillation.

Histopathological investigations detected inflammation in the CRS (1.0 and 5.0 mg)-exposed lungs for 13 weeks and MA (5.0 mg) for 49 weeks from significant increases in the areas covered by free cells in the alveolar units. This confirms the biochemical and cellular studies carried out previously (see Chapter 3). However, there are differences between the biochemical/ cellular and histopathological investigations since the latter showed the significant inflammatory changes in the CRS-exposed lungs at 49 weeks post-instillation ($p < 0.05$) whereas the former did not. This difference could be explained by (a) the failure in an efficient lavage process in former studies or (b) that in histopathological image analysis, there is a reduced chance of pinpointing an alveolar space area because of increased wall thickening.

Semi-quantitative histopathological investigations also showed that CRS (5.0 mg) caused collagen accumulation in the lungs at 13 and 49 weeks post-instillation. These results agreed with biochemical and cellular studies detecting increases in the hydroxyproline level in these lungs previously (Chapter 3). However, there are some differences in the distribution of stain between the CRS-exposed lungs for 13 and 49 weeks. A blue-green colour was detected mainly in swollen alveolar septa at 13 weeks post-instillation where surfactant containing epithelial type 2 cells accumulated. This blue-green coloration could result from collagen fibre required for additional connective support for the cells in the septal structure. In addition to this the image analysis clearly showed a blue-green deposition in MACs located in the alveoli (5.0 mg CRS, 13 weeks). It is possible that such MACs contain the collagen moiety of surfactant proteins and thus have an important cellular role in the breakdown of the lipoprotein complex (Crouch et. al., 1991; Mason et. al., 1998; Khubchandani and Snyder, 2001). The histopathological data support the suggestion that only long-term (49 weeks) exposure to high dose (5.0 mg) of toxic CRS can cause a true fibrogenic response in the lung as previously shown from the quantitative biochemical and cellular investigations.

Histopathology also showed that MA caused delayed inflammation in the lung detectable at 49 weeks post-treatment without any fibrogenic response. However, at 13 weeks post-instillation MA (5.0 mg) was capable of producing significant thoracic lymph node enlargement (p<0.05) and an inflammatory granulomatous response in the lymph nodes. Moreover, micrographs revealed that the MA particles removed from the lungs were deposited in granulomatous area of the nodes. This suggested that the focal concentration of MA in small areas of the lymph nodes at 13 weeks post-instillation could cause inflammation. Thus, size changes and histopathological examination for granuloma formation provided the earliest biomarker of MA toxicity. This toxicity was then detected much later in the lung parenchyma tissue.

Interestingly ANR, which forms some 80 % by mass of the MA produce none of these effects on thoracic lymph nodes or the lungs. This was further evidence that the CRS component of MA (20 % w/w) was responsible for both the early (13 weeks) effect on the nodes and late inflammatory responses (49 weeks) in the lung parenchyma. In order to confirm this, further work was warranted on the physicochemical characterisation of the particles deposited in granulomatous regions of the nodes and in lung parenchymal tissue. These investigations are reported in Chapter 5.

5 The fate of the particles instilled into the lung

5.1 Introduction

Histopathology data showed that volcanic ash and other particles instilled into the lung were deposited in the alveolar macrophages (MACs), the lung parenchyma or granulomatous areas in thoracic lymph nodes (see Chapter 4). Other researchers have already reported that particles containing silica can be drained from the lung to thoracic lymph nodes by MACs (Adamson and Prieditis, 1998; *Davis et. al.,* 2001; Friedetzky *et. al.,* 1998; Garn *et. al.,* 1997). However, to date it is unknown as to whether the physicochemical properties of the Montserrat volcanic ash (MA) such as compositions or size distributions of the particles are altered during lymphatic drainage when compared to those of the original ones instilled.

Previous studies have proposed that the more toxic particles would be carried to the lymph nodes more quickly (Adamson and Prieditis, 1998; Davis *et. al.,* 2001; Friedetzky *et. al.,* 1998; Garn *et. al.,* 1997). It can be surmised that physicochemical compositional changes are possible in the crystalline silica component of the MA depending on whether the particles are located in MACs, lung parenchyma or thoracic lymph nodes. Phagocytosis by MACs followed by lysosomal location with processing under acidic conditions may readily induce compositional alterations or change surface properties of MA since such conditions are very similar to those of weathering in the soil (see in Chapter 1).

Alveolar MACs could have an affinity with the smaller particles during the draining of the particles from the lung to thoracic lymph nodes in order to avoid steric hindrances among cell organelles and the particles in the MACs. This affinity could lead to changes in the size distribution of the particles remaining in the lung or deposited in the lymph nodes in a time dependent manner when compared to that of the original particles instilled.

The aims of this study were to find whether there were (a) any chemical changes in the MA found in the lung or lymph nodes compared to the composition of the original particles and (b) any changes in the particle size distribution following the drainage to

the lymph nodes by MACs. The lungs and thoracic lymph nodes from a single dose of 5.0 mg of MA, cristobalite (CRS) or anorthite (ANR) instilled animals were chosen for investigation in order to maximise the detection of the particles. Two different time points (13 and 49 weeks post-exposure) were chosen to assess any time effects on the compositions or size distributions of the particles. Back scattered electron (BSE) images from environment scanning electron microscopy (E-SEM 300, Phillips) and an image analysis (Leica Qwin, Leica Micro system imaging solutions Ltd, UK) system were employed to obtain the size distributions of the particles remaining in the lungs or deposited in thoracic lymph nodes. The compositional changes in the particles instilled into the lung were studied using electron dispersive X-ray analysis (EDS; Oxford Isis 300, UK) combined with E-SEM.

5. 2 Materials and methods

5. 2. 1 Preparation of a specimen

Lung and lymph node sections prepared for histopathology were cut at a thickness of 5 μm and mounted on a carbon disk (dia. 25 mm, thickness=3 mm, Agar scientific Ltd., UK). This disk was then attached to an aluminium stub using a carbon tab (Figures 5. 1 and 2). It was not necessary to coat tissue specimens with carbon or gold in contrast to particle samples which needed to be coated as reported previously (Vallyathan and Green, 1985; Kriensley *et. al.,* 1998, Chapter 2).

Specimen

Carbon disk

Carbon tab

Aluminium stub
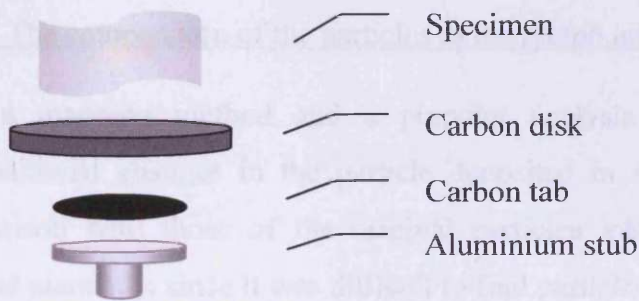
Figure 5. 1 Diagram of tissue specimen preparation for E-SEM.

A carbon disk with lung or lymph node section

An aluminium stub

A back-scattered electron detector
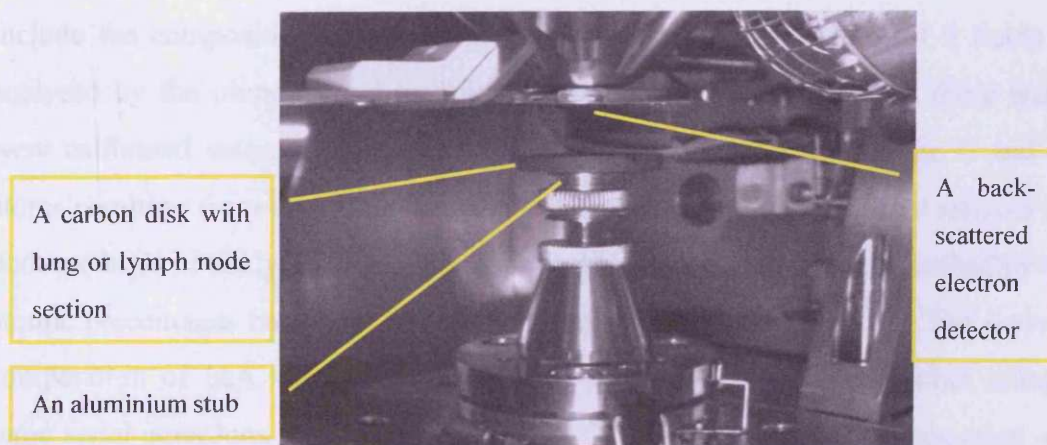
Figure 5. 2 The specimen inside the chamber

5. 2. 2 The sizes of the particles in the lymph nodes or lungs

The Back scattered electron (BSE) images for each tissue specimen were taken. Difficulty was encountered in accurate size measurement for some particles as their edges were covered by tissue. The sizes of all individual particles including those, which were attached to bigger particles, were measured using BSE images and an image analysis system. The particle size was then calibrated using the scale bar on each image. The characterisation method has previously been explained in detail (see section 2. 2. 2). The operating conditions of the E-SEM were the same as those in Chapter 2 (Table 2. 2).

5. 2. 3 The composition of the particles in the lymph nodes or lungs

Both a mapping method and a pinpoint analysis were employed to find the compositional changes in the particle deposited in the lung and lymph nodes for comparison with those of the original particles instilled. Pinpoint analyses were selected manually, since it was difficult to find particle-dominated fields in the lung or lymph nodes, especially from ANR-exposed animals. All the values from these analyses were recorded and the average value was then calculated. The same fields were then analysed by a mapping method, which was employed to find an average composition of the field of the specimen examined recognising that this method would include the composition of the tissue (background signal). A total of 9 fields were analysed by the pinpoint and mapping methods. All the values from these analyses were calibrated using the ratio between the atomic percentages of the C and other atoms resulting from analysing lung or lymph nodes from sham-treated animals using both methods of analysis. The compositions of the specimens were described by mean atomic percentages based on the standard compounds (see Table 2. 3). The molecular composition of MA was then extrapolated by stoichiometric approaches using the same serial equations as in Chapter 2 (see 2. 2. 3). The molecular composition of the specimen is expressed as percentages (% (w/w)) in order to facilitate comparison with other data from the literature. The standard oxide compounds for compositional analyses are the same as those used in Chapter 2 (see Table 2. 3)

5. 3 Results

5. 3. 1 The morphology of the lung and lymph nodes

Back scattered electron (BSE) images were chosen since higher atomic numbered material gives a stronger signal or a brighter white image (Krinsley et. al, 1998). Therefore, it is easier to distinguish between tissue, which is a lower atomic numbered material, and particles, which are higher atomic numbered materials in the lung or thoracic lymph nodes (Figure 5. 3).

5. 3. 1. 1 The BSE images of the lung

The BSE images of the sham-treated lungs showed clear alveolar units and septa without any higher atomic numbered materials or MACs (Figure 5. 4)

In contrast to the BSE images of the sham-exposed lungs, the images of the particle-instilled lungs showed bright white-coloured materials in the MACs or interstitial regions (Figures 5. 4, 5, 6 and 7). Moreover, local and dense deposition makes it easier to distinguish the particles against the tissue background. The morphology of the white coloured images appeared identical to those observed for the original instilled particles. This correlation was configured from compositional analysis using EDX combined with E-SEM (Figure 5. 8).

The BSE images of the lungs exposed to the ANR for 13 weeks showed different images from those of the sham-treated lungs (Figure 5. 4). Focal particle accumulation was recognised in the ANR-exposed lungs for 13 weeks and BSE images obtained under high magnification (x10,000) revealed most of the particles were densely packed in the alveolar MACs. After long-term (49 weeks) exposure, few particles were found in the interstitial region of the ANR-exposed lung without any thickening (Figure 5. 5).

The BSE images of the lungs exposed to the CRS for 13 weeks showed different images from those of the sham-treated lungs (Figures 5. 4 and 6). The interstitial region was slightly thickened following CRS treatment and some of the MACs were

131
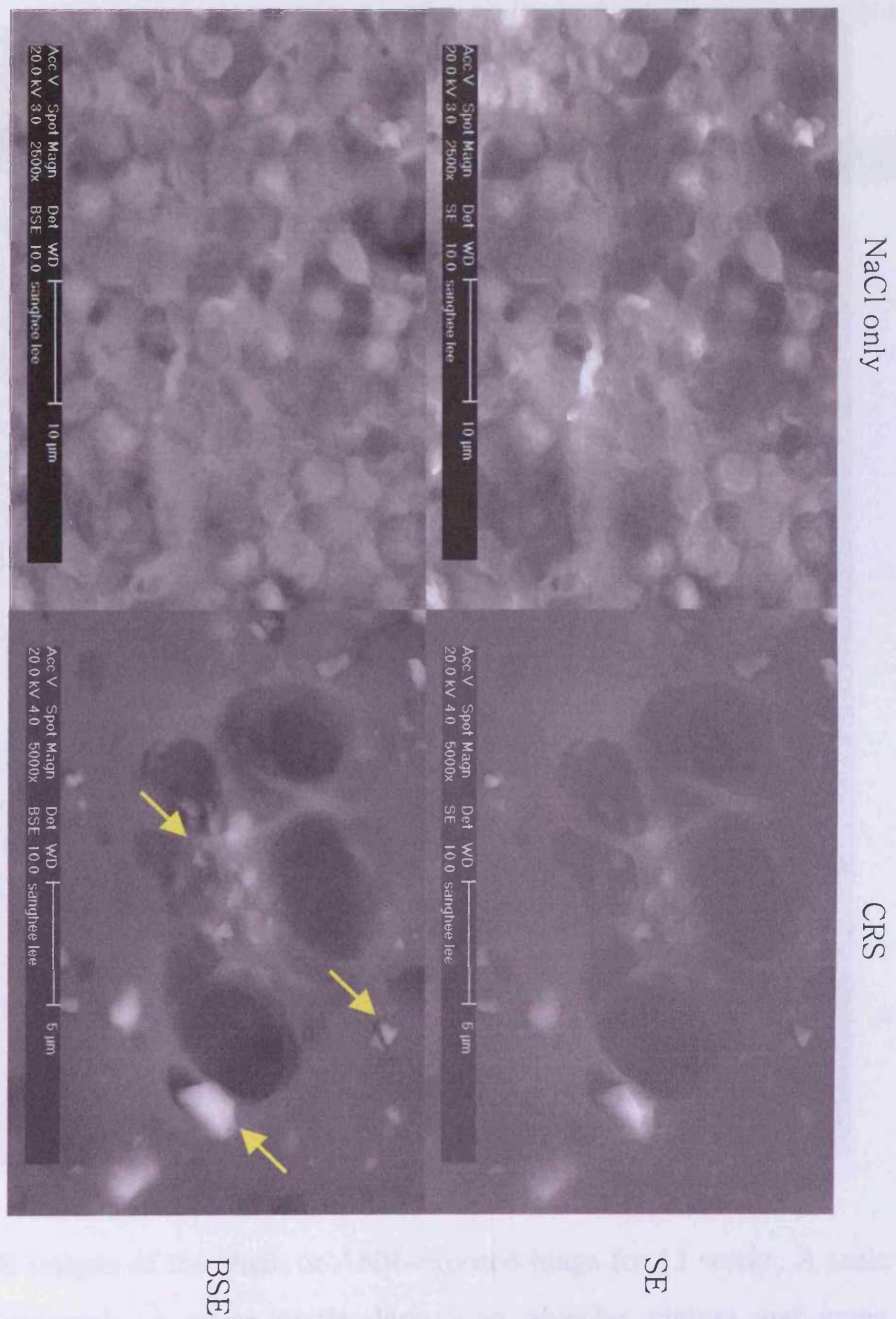
Figure 5. 3 The SE and BSE images of the lymph nodes from the sham or CRS-exposed animals for 13 weeks. A scale bar is on each micrograph. Yellow arrows depict particles deposited in the lymph nodes.

Sham-treated   ANR
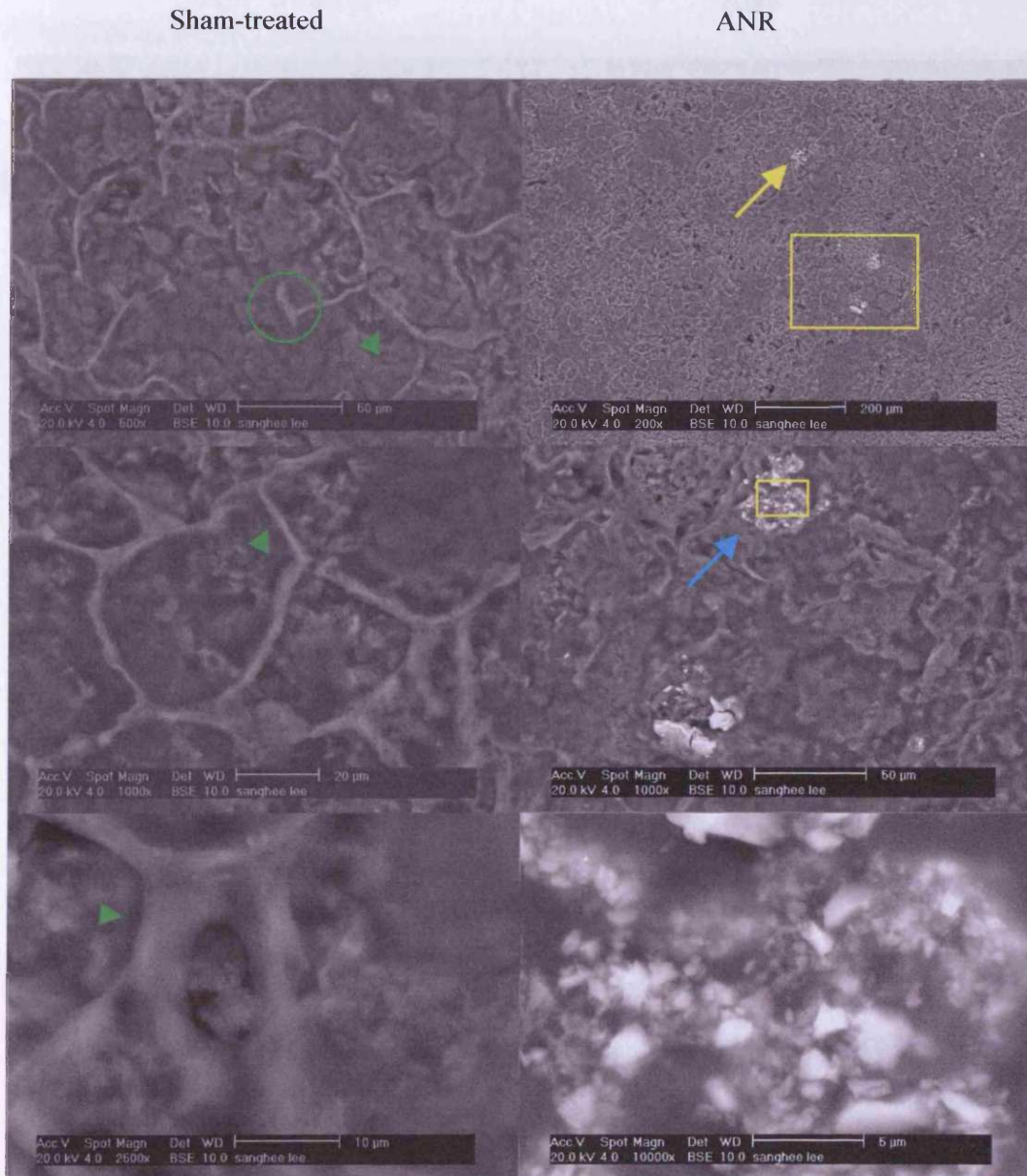
Figure 5. 4 The BSE images of the sham or ANR-exposed lungs for 13 weeks. A scale bar is on each micrograph. A green circle depicts an alveolar septum and green arrowheads depict alveolar walls. Yellow arrows depict particle deposition in the lung and the blue arrow shows particle deposition in MACs.

Sham-treated   ANR
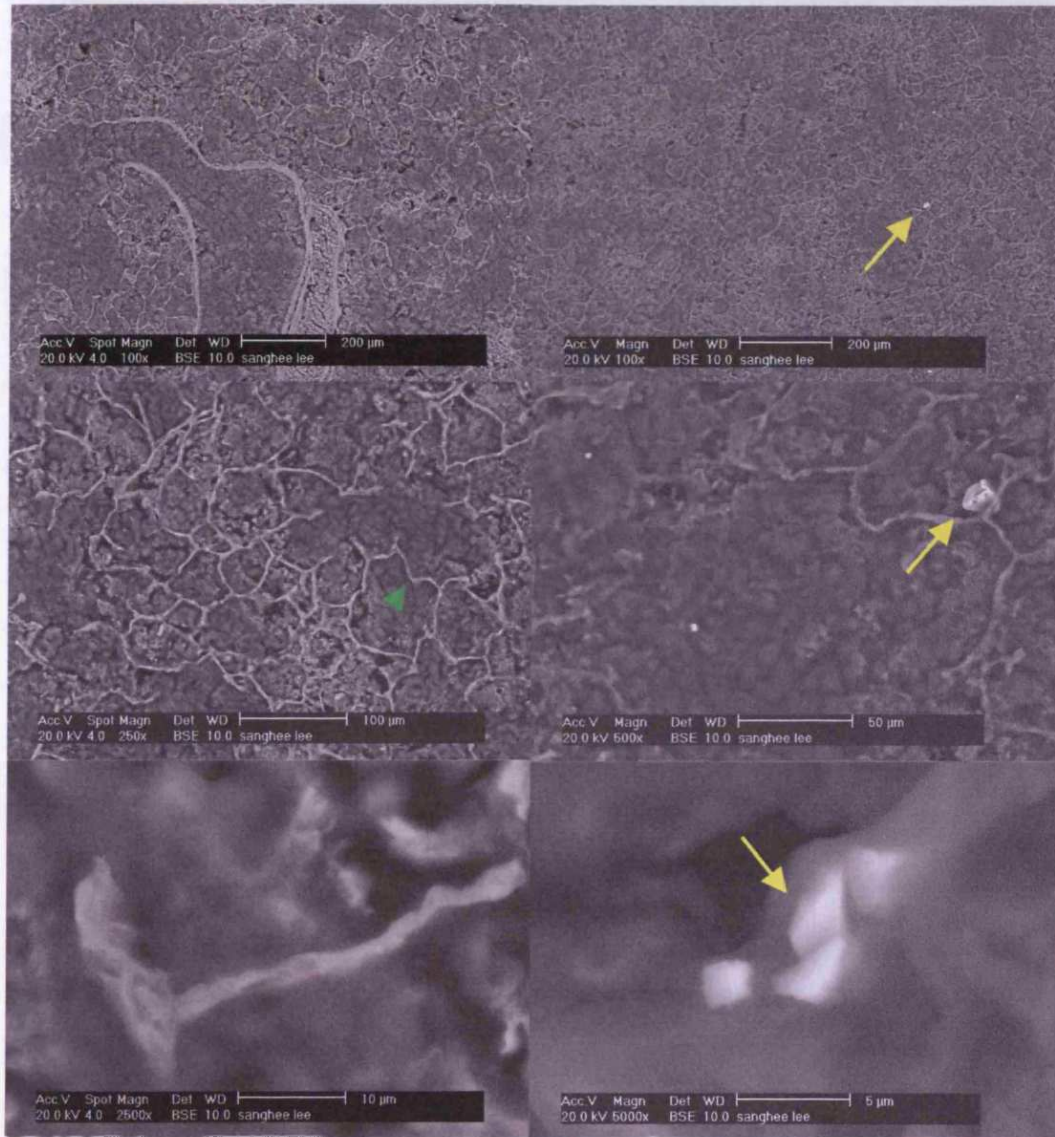
Figure 5. 5 The BSE images of the sham or ANR-exposed lungs for 49 weeks. A scale bar is on each micrograph. A green arrowhead depicts alveolar wall. Yellow arrows depict particle deposition in the lung.

CRS   MA
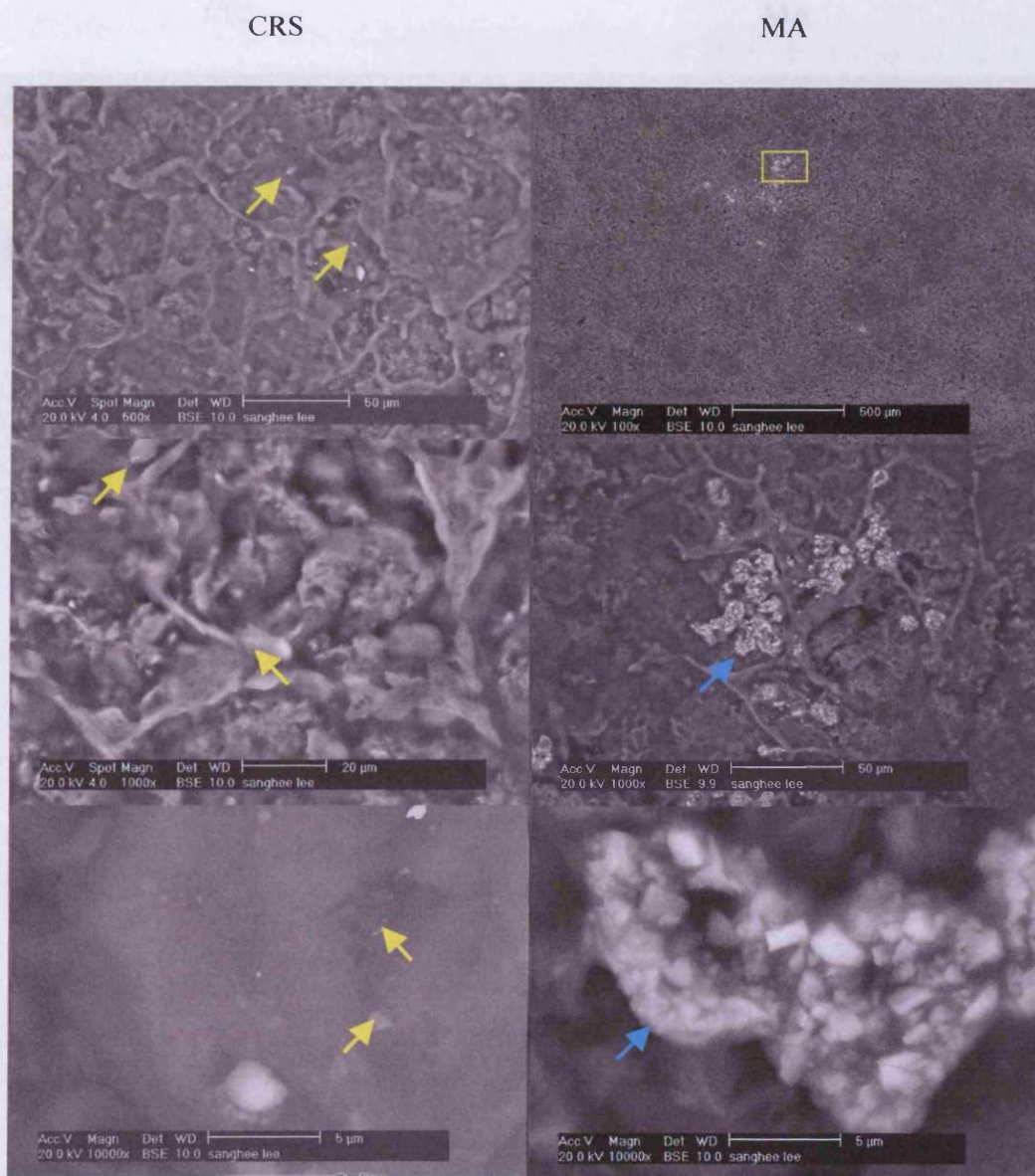
Figure 5. 6 The BSE image of the CRS or MA-exposed lung for 13 weeks. A scale bar is on each micrograph. Yellow arrows depict the CRS and blue arrows depict the MA remaining in the lung.
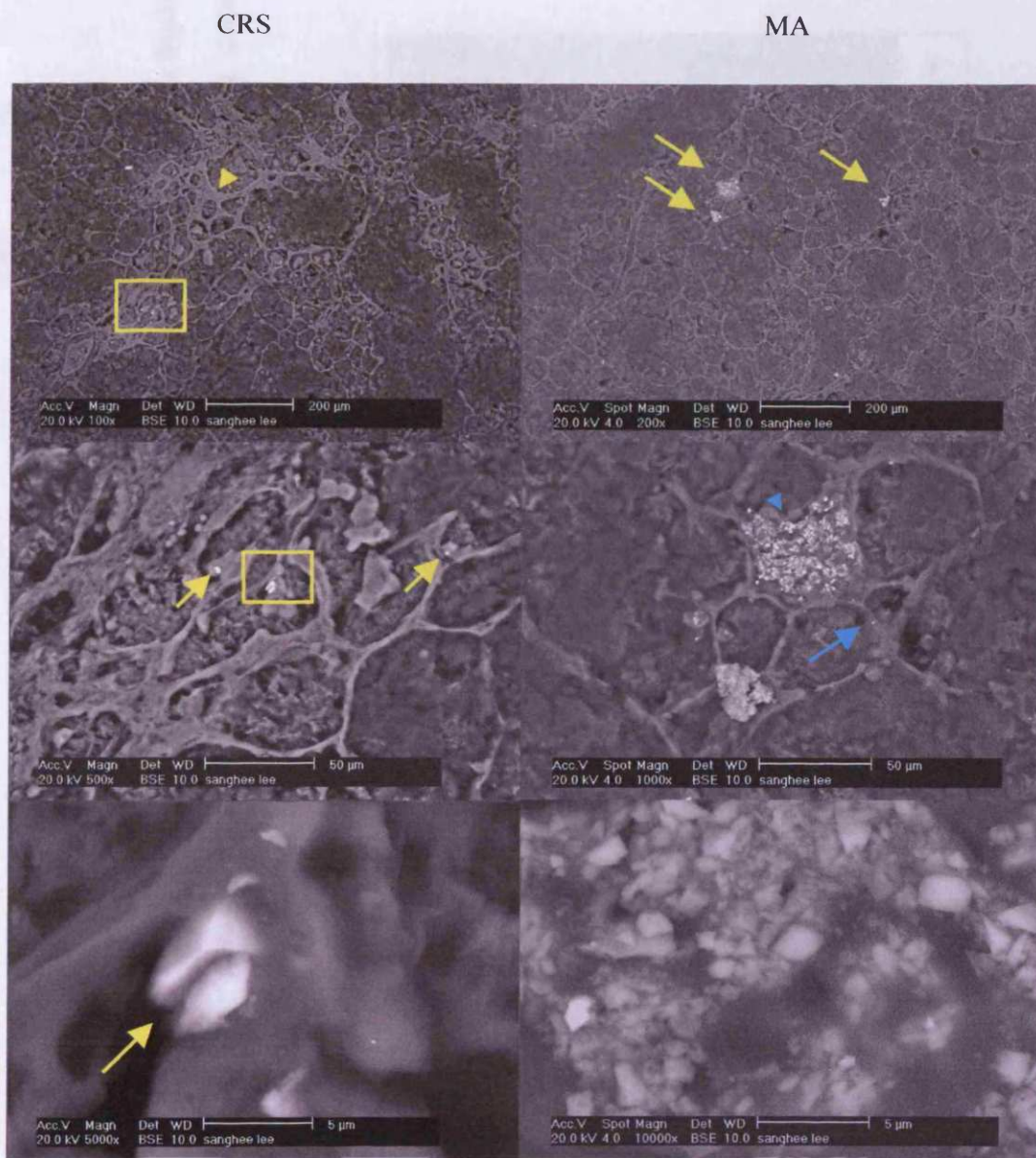
CRS   MA

Figure 5. 7 The particles deposited in the lung from the CRS or MA-exposed animals for 49 weeks. A scale bar is on each micrograph. Yellow arrowhead depicts interstitial thickening and yellow arrows depict the CRS/MA deposited in the lungs. Blue arrow depicts the particles in the interstitial region. Blue arrowhead depicts the macrophages containing the MA.
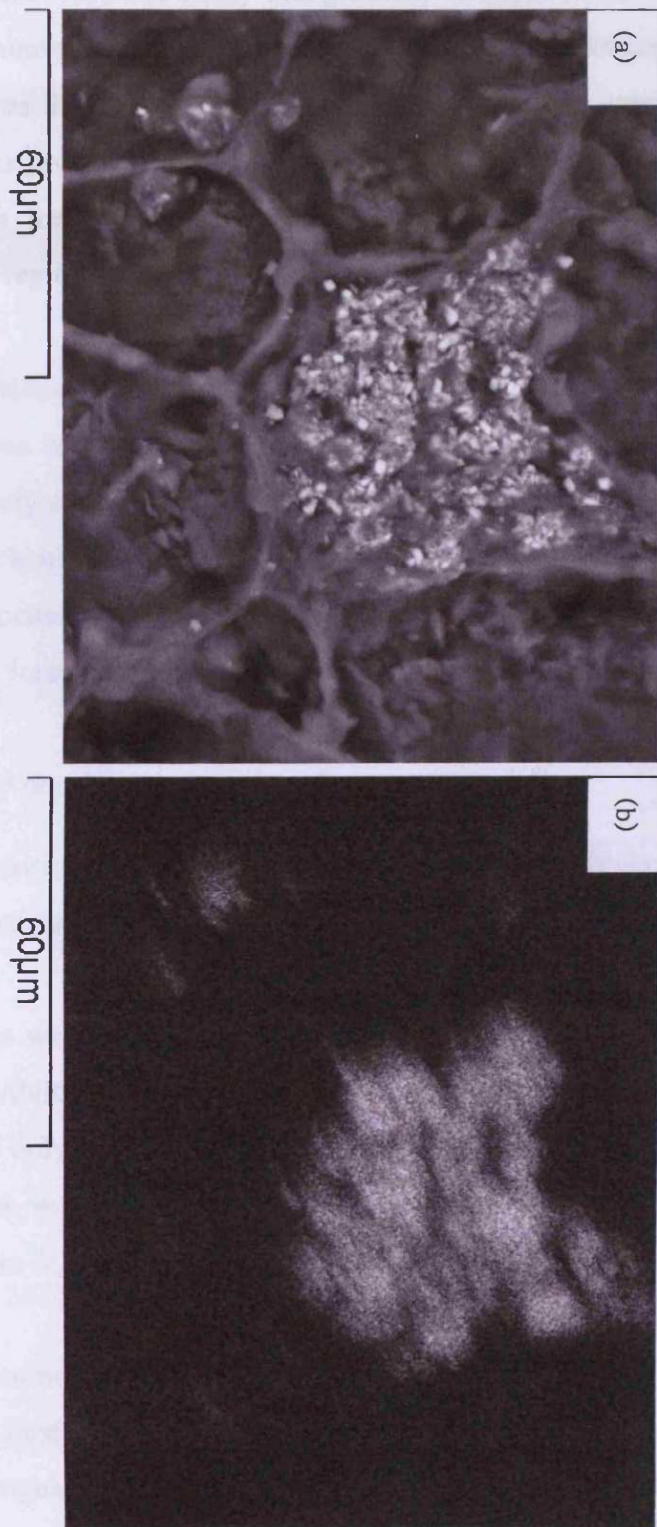
Figure 5. 8 The BSE image shows MA deposition in the MACs in the MA-exposed lungs for 49 weeks (a) and the map obtained by a mapping method using EDX combined with ESEM shows silicon white (b).

visible in the alveolar units at 13 weeks post-exposure. In contrast to ANR, the MACs densely packed with the CRS were not easily recognisable at either 13 or 49 weeks post-instillation since the numbers of CRS particles were not easily detected under lower magnification (Figures 5. 4 and 6). Nevertheless, CRS particles were mostly found in MACs at 13 weeks post-instillation. The thickening of the interstitial region of the CRS-exposed lungs for 49 weeks became more distinct and most of the particles were found in this region (Figure 5. 7).

The BSE images of the MA-exposed lungs for 13 weeks showed a much larger amount of particle-deposition in the lung than that of the CRS (Figure 5. 6). Most of the MA particles were densely packed in the MACs but did not cover the nucleus area. Some focal interstitial thickening was recognised in the MA-exposed lung for 49 weeks. Some particles deposited in this interstitial area could be recognised but most particles were still found in focal groupings of the MACs (Figure 5. 7).

5. 3. 1. 2 The BSE images of the thoracic lymph nodes

The BSE images of the thoracic lymph nodes from sham-treated animals showed cell compaction without any particles (Figure 5. 9).

Any morphological changes were not noticed at either 13 or 49 weeks post-treatment (Figures 5. 9 and 10). The ANR deposition in the nodes was hardly recognisable at 13 weeks post-instillation and only few particles were found in the nodes (Figure 5. 9). Local and dense deposition was then noticed in the nodes from the ANR-exposed animals for 49 weeks (Figure 5. 10).

CRS particle deposition was not readily distinguishable against the tissue under low magnification at 13 weeks post-exposure since the amount of the dust deposited was not large enough to be recognised or that the particles deposited in an area were not detectable on size parameters (Figure 5. 11). However, the BSE image under high magnification revealed some white imaged material, which was confirmed as a silicon
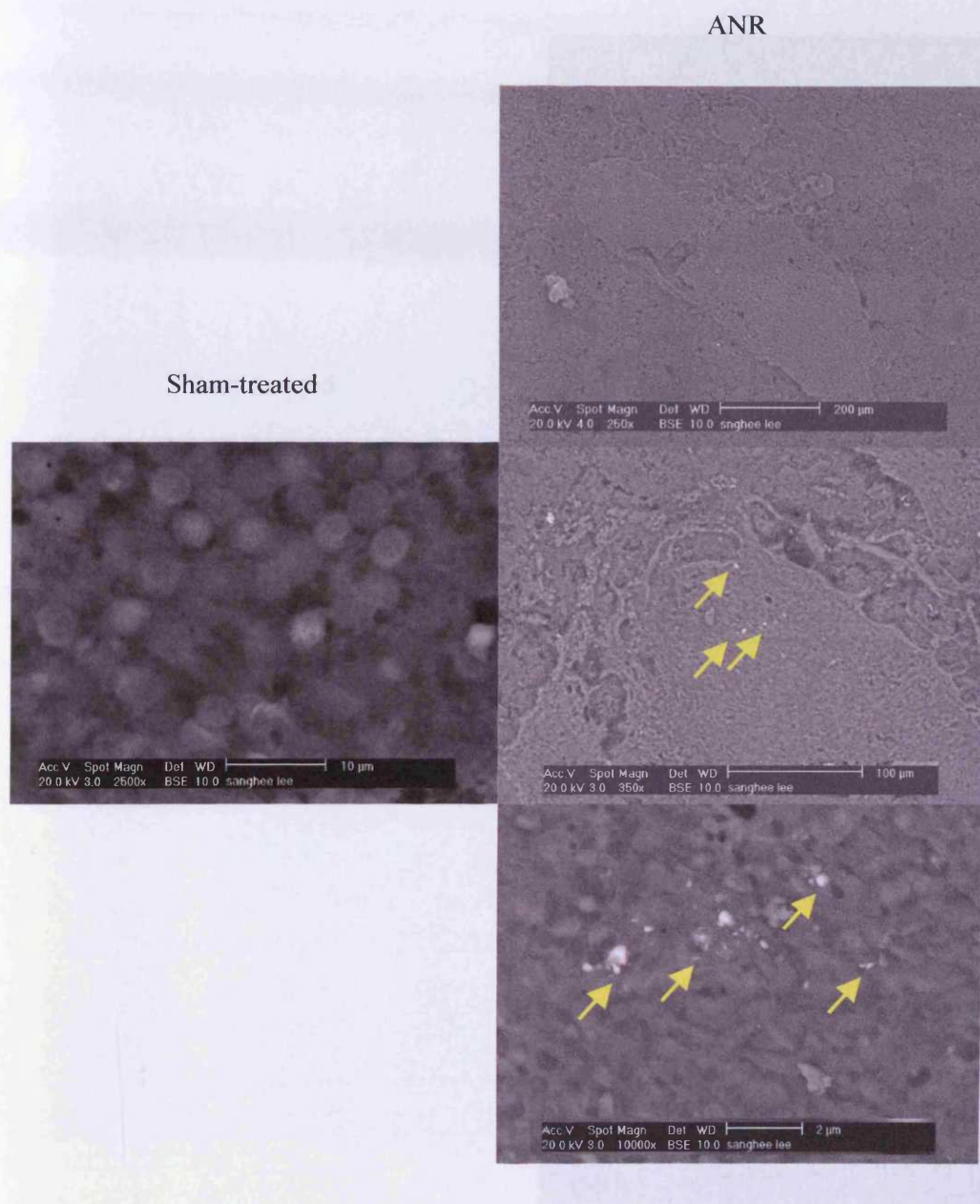
Figure 5. 9 The BSE images of the lymph nodes collected from the sham and ANR-exposed rats for 13 weeks. Yellow arrows depict particle deposition in the nodes.
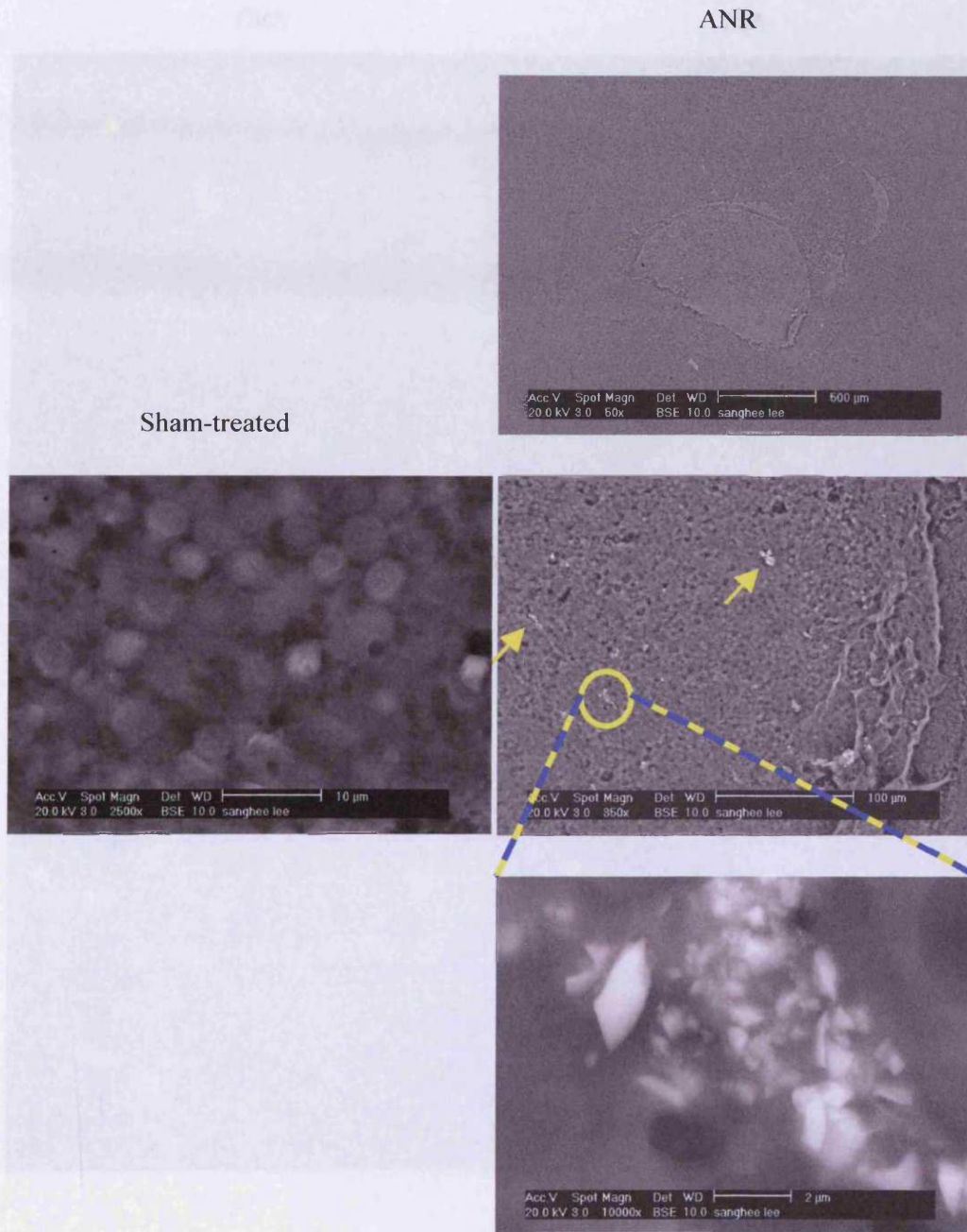
Figure 5. 10 The micrographs of the lymph nodes from the sham and ANR-exposed animals for 49 weeks. Yellow arrows depicts particle deposition in the lymph nodes.
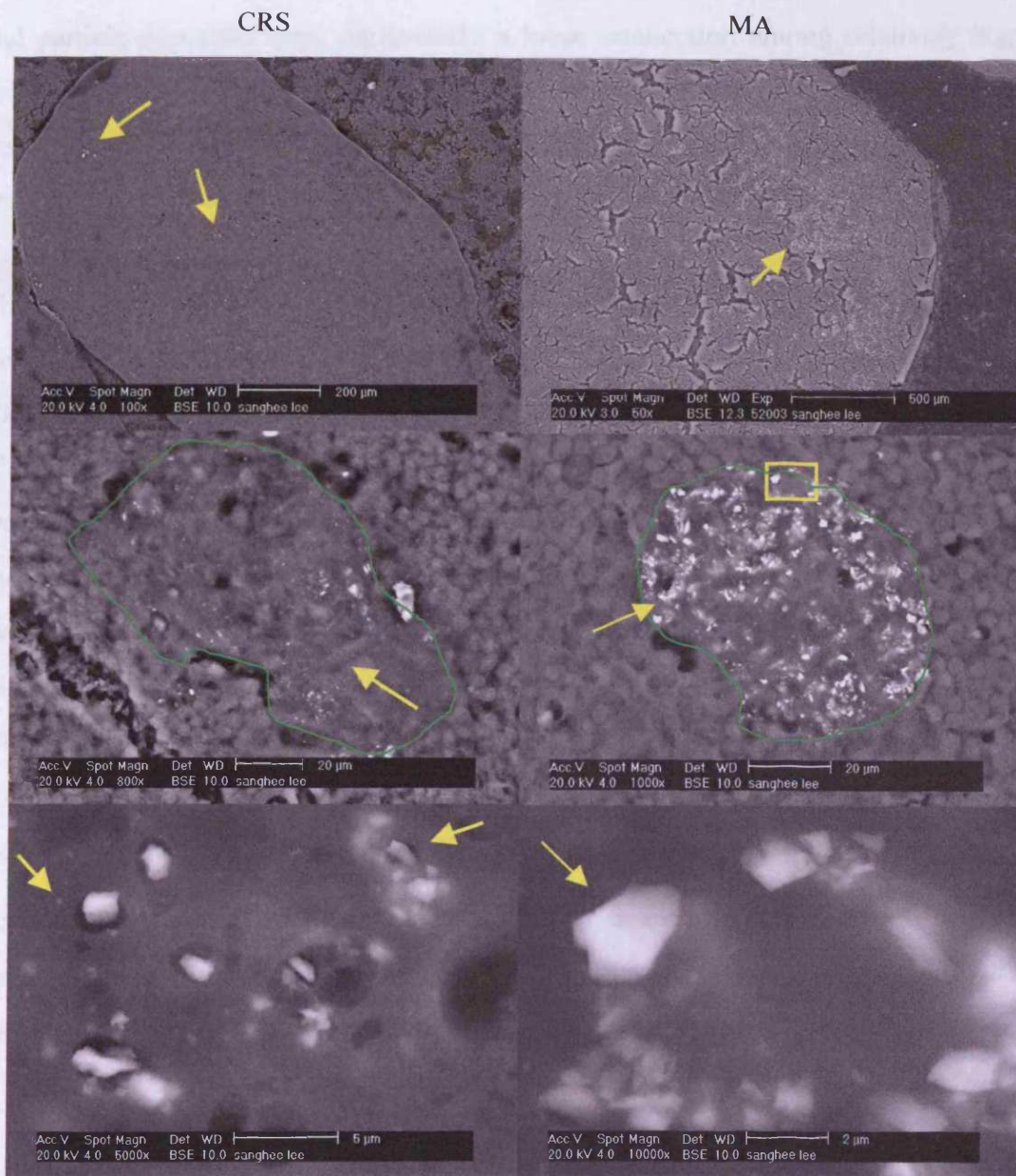
CRS   MA

Figure 5. 11 The BSE images of the lymph nodes collected from the CRS or MA-exposed animals for 13 weeks. Yellow arrows depict the CRS/MA deposited in the lymph nodes. Green lined areas are granuloma regions. A scale bar is on each image.

141

containing material from the compositional analyses (Figure 5. 12). These images (Figure 5. 11 and 12) also demonstrated morphological changes in the oval-shaped and particle-deposited area, particularly a loose connection among relatively bigger cells suggesting granulomatous changes in thoracic lymph nodes at 13 weeks post-instillation (Figure 5. 11). More particles were found in the lymph nodes as more granulomatous areas were observed at 49 weeks post-instillation (Figure 5. 13).

The MA deposition was more distinct than the CRS or ANR from BSE images under a low magnification since the amount of the MA particles was larger than that of the CRS. In addition, areas of MA deposition were larger than those observed for ANR (Figures 5. 12 and 13). Therefore, white oval-shaped MA deposits in the lymph nodes were recognisable at both 13 and 49 weeks post-exposure. Moreover, high magnification images (Figures 5. 12 and 13) suggested that dense deposition of MA caused similar granulomatous changes in the lymph nodes to the CRS. This confirmed the quantitative histological studies, which showed that the average size of the nodes was augmented by the MA at 49 weeks post-exposure (see Chapter 4).

5. 3. 2 The size distribution of the particles in the lungs or the lymph nodes

Each size distribution of the MA, CRS and ANR remaining in the lung and deposited in the thoracic lymph nodes and original MA, CRS and ANR is displayed in Figure 5. 14.

5. 3. 2. 1 The size distribution of the MA in the lung or the lymph nodes

The overall size distributions of the MA in the lungs and thoracic lymph nodes at 13 and 49 weeks post-exposure were different from that of the original particles instilled (Figure 5. 14). The size distribution of the MA remaining in the lungs at 13 weeks post-instillation was a near mirror image of that of the original MA. The percentages of the MA in the size ranges of 0-0.1, 0.1-0.3 and 0.3-0.5 μm in the lungs and lymph nodes (except the ultrafine particles deposited in the lymph nodes) were all lower than those from the original particles (Figure 5. 14). In contrast, the percentages of the MA (ESD>0.5 μm) in the lung were higher than those of the original particles.
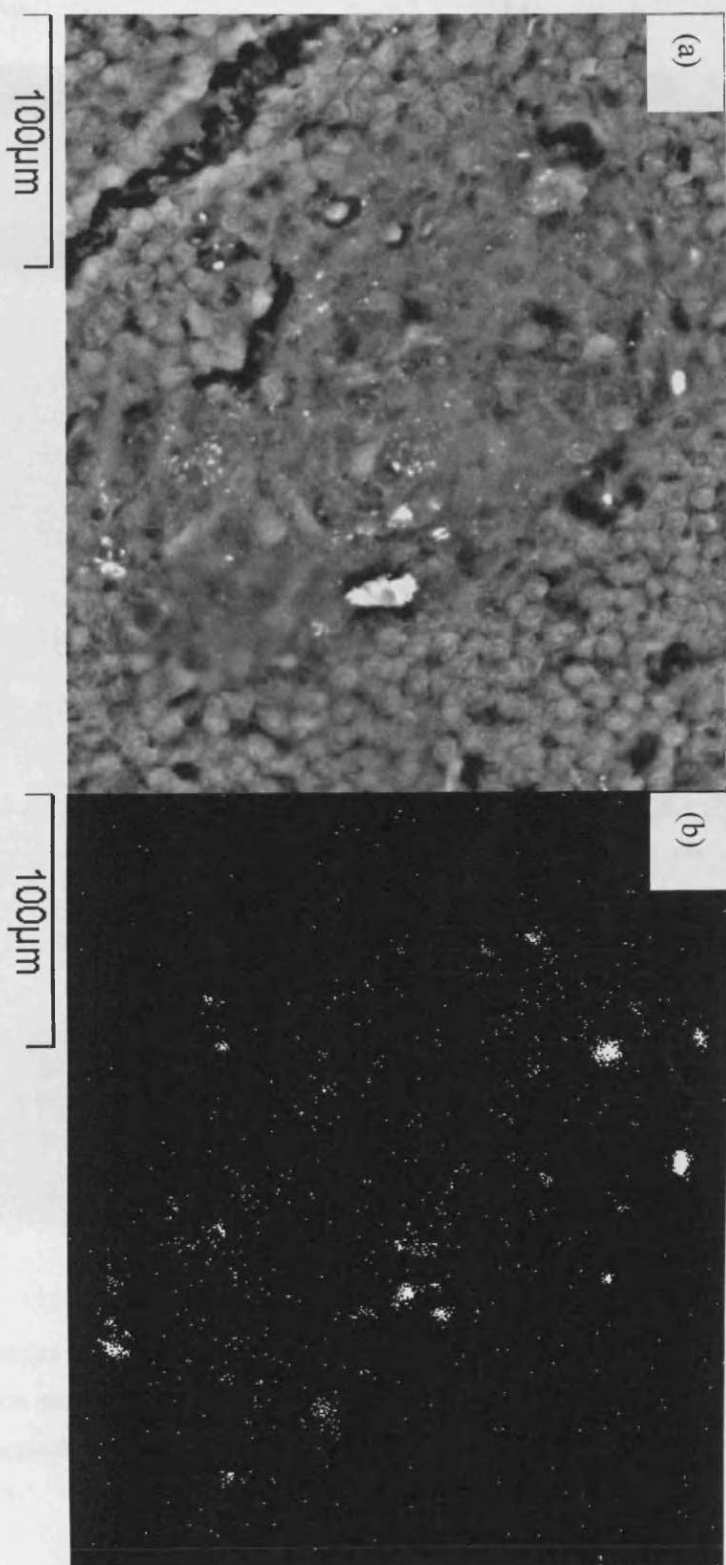
Figure 5. 12 The BSE image of the lymph nodes from the CRS-exposed animals for 13 weeks shows granulomatous area (a) and same area from a mapping method using EDX shows silicon white (b).

CRS   MA
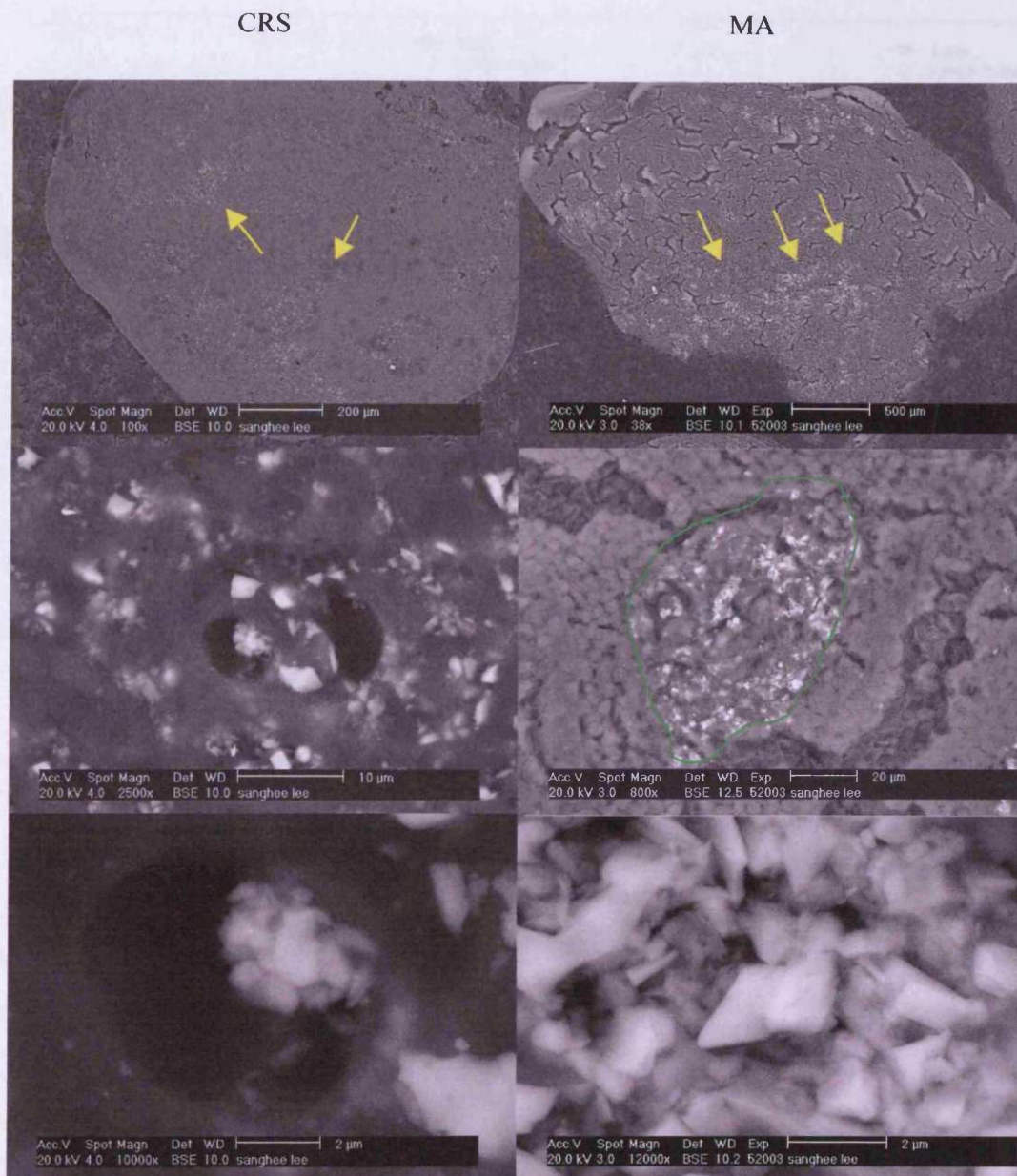
Figure 5. 13 The BSE images of the lymph nodes from the CRS or MA-exposed animals for 49 weeks. A scale bar is on each micrograph. Yellow arrows depicts particle deposition in the nodes. Green lined area is granuloma

(a) MA

(b) CRS

(C) ANR
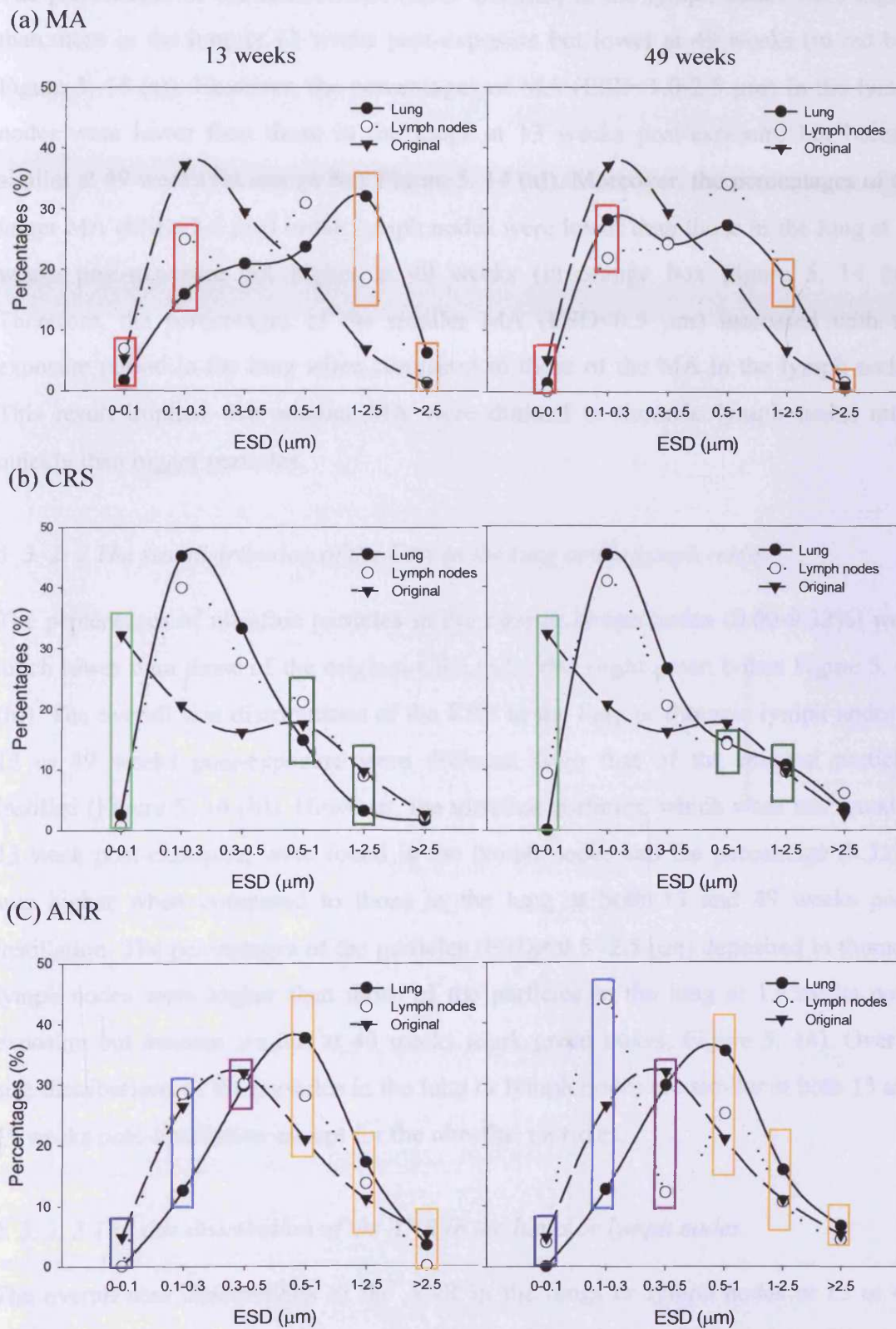
Figure 5. 14 The size distributions of the MA (a), CRS (b) and ANR (c) remaining in the lung or deposited in the thoracic lymph nodes at 13 and 49 weeks post-instillation and original ones.

The percentages of the smaller MA (ESD<0.3 µm) in the lymph nodes were higher than those in the lung at 13 weeks post-exposure but lower at 49 weeks (in red box Figure 5. 14 (a)). However, the percentages of MA (ESD=1.0-2.5 µm) in the lymph nodes were lower than those in the lungs at 13 weeks post-exposure but became similar at 49 weeks (in orange box Figure 5. 14 (a)). Moreover, the percentages of the larger MA (ESD>2.5 µm) in the lymph nodes were lower than those in the lung at 13 weeks post-exposure but higher at 49 weeks (in orange box Figure 5. 14 (a)). Therefore, the percentages of the smaller MA (ESD<0.5 µm) increased with the exposure period in the lung when compared to those of the MA in the lymph nodes. This result implied that smaller MA were drained to thoracic lymph nodes more quickly than bigger particles.

5. 3. 2. 2 The size distribution of the CRS in the lung or the lymph nodes

The percentages of ultrafine particles in the lung or lymph nodes (0.00-9.32%) were much lower than those of the original CRS (32.19%) (light green boxes Figure 5. 14 (b)). The overall size distributions of the CRS in the lung or thoracic lymph nodes at 13 or 49 weeks post-exposure were different from that of the original particles instilled (Figure 5. 14 (b)). However, the ultrafine particles, which were not found at 13 week post-exposure, were found in the lymph nodes and the percentage (9.32%) was higher when compared to those in the lung at both 13 and 49 weeks post-instillation. The percentages of the particles (ESD =0.5 -2.5 µm) deposited in thoracic lymph nodes were higher than those of the particles in the lung at 13 weeks post-exposure but became similar at 49 weeks (dark green boxes, Figure 5. 14). Overall size distributions of the particles in the lung or lymph nodes are similar at both 13 and 49 weeks post-instillation except for the ultrafine particles.

5. 3. 2. 3 The size distribution of the ANR in the lungs or lymph nodes

The overall size distributions of the ANR in the lungs or lymph nodes at 13 or 49 weeks post-exposure were different from those of the original ANR particles (Figure 5. 14). Higher percentages of the larger ANR (ESD>0.5µm) in the lung were recognised compared with those of the original ANR particles at both 13 and 49 weeks post-

instillation (yellow boxes Figure 5. 14). In contrast, percentages of the smaller ANR (ESD<0.5μm) in the lung were lower than those of original particles (blue and purple boxes). In spite of those differences, both size distributions of the ANR remaining in the lung at 13 and 49 weeks post-instillation look similar. The percentages of the particles (ESD=0.1-0.3 μm) in the lymph nodes (28.44% at 13 weeks or 43.83% at 49 weeks) were always higher than those from the lung (12.46% at 13 weeks or 12.62% at 49 weeks) at both 13 and 49 weeks post-instillation (a blue box Figure 5. 14). Moreover, the percentage of the particles (ESD=0.1-0.3 μm) in the lymph nodes becomes higher in a time dependent manner.

5. 3. 3 The compositional analysis of the particles in the lung or lymph nodes

5. 3. 3. 1 The composition of the particles remaining in the lung

5. 3. 3. 1. 1 The atomic composition of the sham-treated lung; blank value

The blank signal was obtained by analysing the sham-treated lung in order to take account of any background interference contributed by lung components. The relative amount of each atom was expressed as an atomic percentage (Figure 5. 15). As expected, the major signal came from carbon (C) and oxygen (O). However, the sham-treated lungs contain sodium (Na) and calcium (Ca), which are components in albite [$NaAlSi_3O_8$] and anorthite [$CaAl_2Si_2O_8$]. This apart, there is no sign of the existence of any other component of the MA, CRS or ANR such as silicon (Si), aluminium (Al) or an orthoclase specific atom such as K.

5. 3. 3. 1. 2 The composition of the CRS remained in the lung

All the particles remaining in the lung were analysed and the atomic composition was expressed in the same way as detailed above (5. 2. 3 and 5. 3. 3. 1. 1). The atomic percentages of Na, Ca, phosphorus (P), sulphur (S) were calibrated considering the ratio of the atomic percentage between any specific atom and C from the background signal since lung tissue itself contained these atoms and a large area did not include any particles. Extra P, S, Ca, and potassium (K) were detected by a pinpoint or mapping method in the CRS in the lung exposed for 13 weeks (Figure 5. 16). Interestingly, iron (Fe) was detected by both a pinpoint and a mapping method in the

CRS particles in the lung at 49 weeks post-instillation. In spite of the fact that such extra atoms were detected, there is no indication of the existence of other silica containing minerals such as anorthite, orthoclase or albite.

(a)

(b)
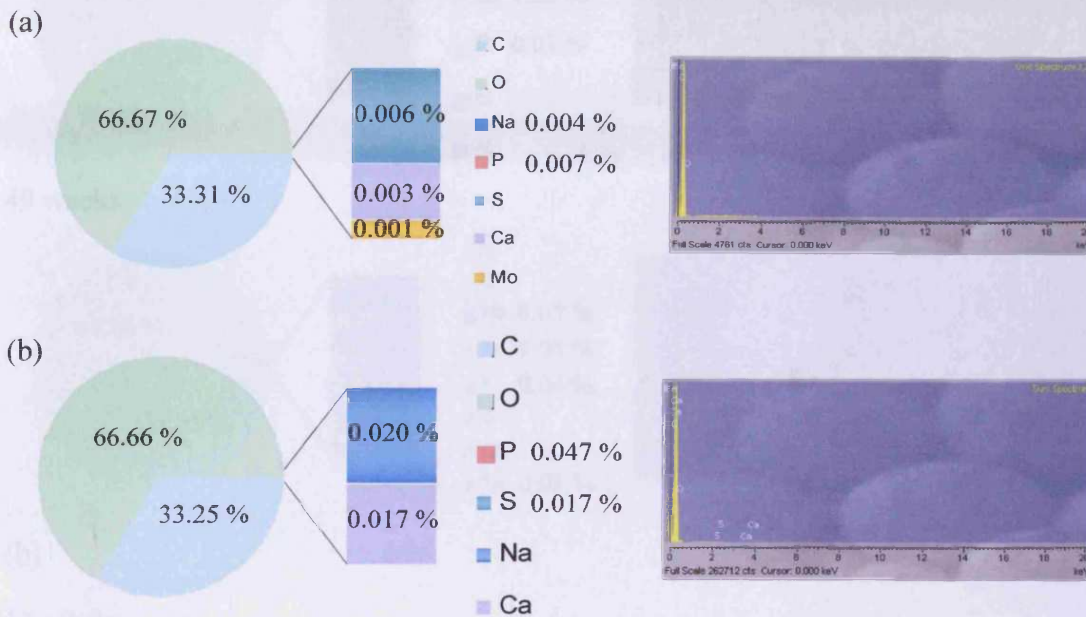
Figure 5. 15 The atomic composition of the sham-instilled lung was analysed using EDX associated with E-SEM. The atomic percentages were decided by (a) a pinpoint analysis or (b) a mapping method.

5. 3. 3. 1. 3 The composition of the ANR deposited in the lung

The atomic compositions of the ANR remaining in the lung exposed for 13 or 49 weeks were analysed and expressed in the same way as detailed in 5. 2. 3 and 5. 3. 3. 1. 1. The percentages of atoms such as P, S, Na, or Ca, which are shared with the sham-treated lung tissue, were calibrated as detailed above (5. 3. 3. 1. 2). Extra traces of atoms such as P, S, titanium (Ti), magnesium (Mg), or Fe were detected (Figure 5. 17). Moreover, a trace of Fe detected was positively related to the amount of Si detected except for the results from the ANR-exposed lungs for 49 weeks by a mapping method. This result suggested that Fe was included in the ANR particle rather than from external contaminants.

(a)

13 weeks

66.71 %

33.20 %

0.010 %
0.010 %
0.006 %

■ C
■ O
■ Si 0.52 %
■ P 0.01 %
■ S
■ K

49 weeks

66.70 %

32.25 %

0.11 %

0.02 %

■ C
■ O
■ Na 0.03 %
■ Si 1.90 %
■ P 0.04 %
■ S
■ Ca
■ Fe 0.01 %

(b)

13 weeks

66.68 %

33.23 %

0.02 %

0.01 %

■ C
■ O
■ Si
■ S

49 weeks

66.67 %

33.13 %

0.04 %

0.05 %

0.01 %

■ C
■ O
■ Na 0.02 %
■ Mg 0.01 %
■ Si
■ S
■ Fe
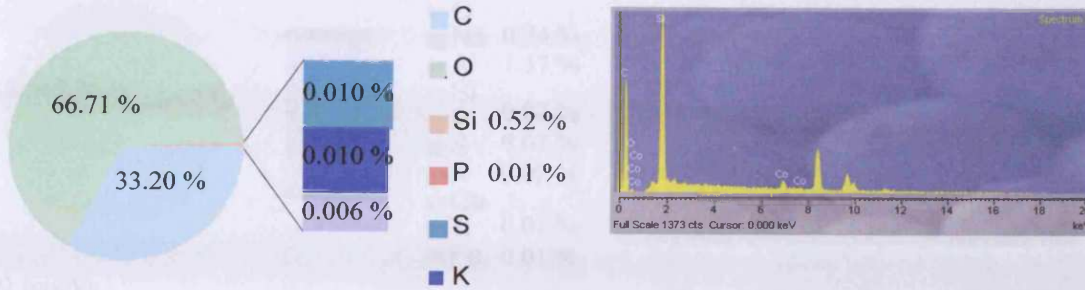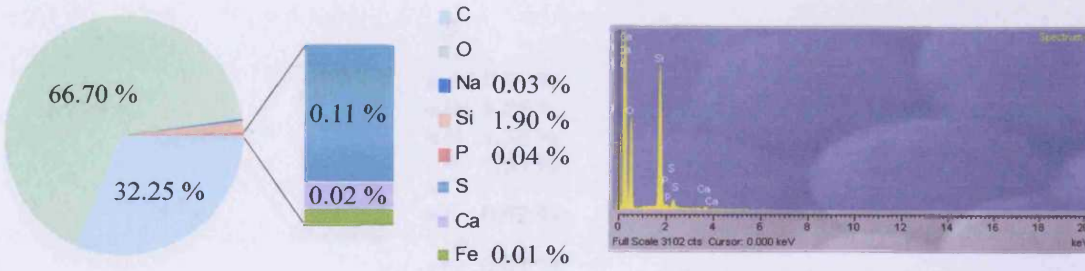
Figure 5. 16 The atomic compositions of the CRS remained in the lung exposed for 13 and 49 weeks decided using a pinpoint (a) and mapping (b) method. The atomic compositions are expressed as atomic percentages.

(a)

13 weeks

65.96 %   2.44 %   0.35 %

29.25 %

C
O
Na 0.74 %
Al 1.37 %
Si
P   0.02 %
S   0.01 %
K   0.02 %
Ca
Ti 0.01 %
Fe 0.01 %

49 weeks

65.99 %

0.05 %

0.53 %

29.74 %

C
O
Na 0.81 %
Mg 0.85 %
Al 1.36 %
Si 1.53 %
P
K   0.02 %
Ca
Fe 0.02 %

(b)

13 weeks

66.56 %

0.02 %

0.05 %

32.65 %

C
O
Na 0.09 %
Al 0.21 %
Si 0.35 %
P   0.02 %
S
K   0.005
Ca
Fe 0.005

49 weeks

66.61 %

0.04 %

0.02 %

0.04 %

32.96 %

C
O
Na 0.03 %
Mg 0.01 %
Al 0.09 %
Si 0.15 %
P
S
Ca
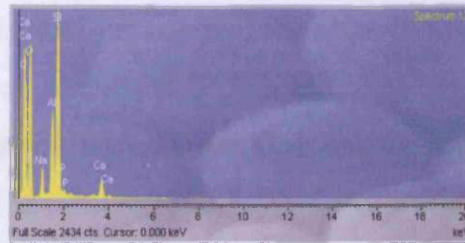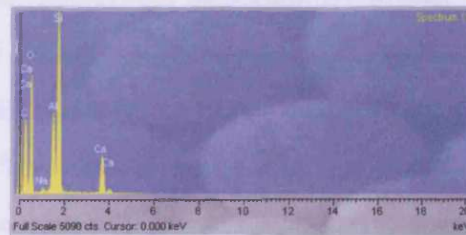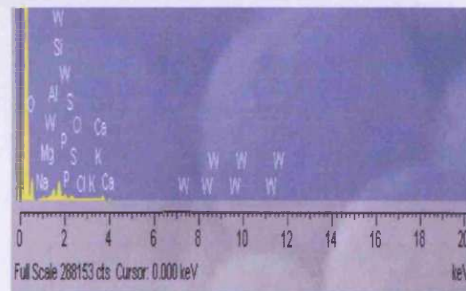
Figure 5. 17 The atomic composition of the ANR remained in the lung exposed for 13 or 49 weeks. These atomic percentages were gained by a pinpoint (a) and a mapping (b) method.

5. 3. 3. 1. 4 The composition of the MA deposited in the lung

The atomic compositions of the MA remaining in the lung exposed for 13 or 49 weeks were analysed and expressed in the same way as detailed in 5. 2. 3 and 5. 3. 3. 1. 1. The percentages of the atoms such as P, S, Na, or Ca, which are shared with the sham-treated lung tissue, were calibrated as detailed above (5. 3. 2. 1. 2). Extra traces of atoms such as P, S, Ti, molybdenum (Mo) or Fe were detected (Figure 5. 18). Specifically, a trace of Fe was detected in both of the lungs exposed for 13 or 49 weeks by both pinpoint and mapping methods. Moreover, as noted previously the amount of Fe was positively proportional to the amount of Si and the relative amounts of Fe from the lungs exposed for 49 weeks were higher than those from the lungs for 13 weeks. The molecular compositions of the MA were calculated by stoichiometric approaches based on the ratio of the atomic percentages of Si, Al and feldspar specific atoms such as Na, K and Ca (Figure 5. 19). The weight percentages of crystalline silica found using mapping methods were lower compared to those resulting from pinpoint analyses at both 13 and 49 weeks post-exposure. Both pinpoint and mapping methods indicated that the average content of crystalline silica in the MA from the lungs exposed for 13 weeks (19.25 or 9.65 % (w/w)) was higher than that from the lungs for 49 weeks (11.77 or 8.77 % (w/w)). Interestingly, the crystalline silica content of the MA in the lung was lower than that of the original MA independent of the exposure periods. Orthoclase $[KAlSi_3O_8]$ and anorthite $[CaAl_2Si_2O_8]$ contents from the lung exposed for 13 weeks were lower than those from the lungs for 49 weeks.

(a)

13 weeks

65.09 %	C
2.34 %	O
30.09 %	Na 0.42 %
0.07 %	Mg 0.06 %
0.15 %	Al 0.68 %
0.05 %	Si
	P 0.03 %
	K
	Ca
	Fe

49 weeks

66.13 %	C
3.36 %	O
27.57 %	Na 0.74 %
0.14 %	Mg 0.10 %
0.38 %	Al 1.34 %
0.18%	Si
	P 0.08 %
	S 0.05 %
	K
	Ca
	Ti 0.02 %
	Fe
	Mo 0.01 %

(b)

13 weeks

66.55 %	C
32.60 %	O
0.02 %	Na 0.09 %
0.03 %	Mg 0.01 %
0.01 %	Al 0.20 %
	Si 0.45 %
	K
	Ca
	Fe

49 weeks

66.55 %	C
32.92 %	O
0.01 %	Na 0.04 %
0.02 %	Mg 0.01 %
0.01 %	Al 0.09 %
	Si 0.21 %
	K
	Ca
	Fe
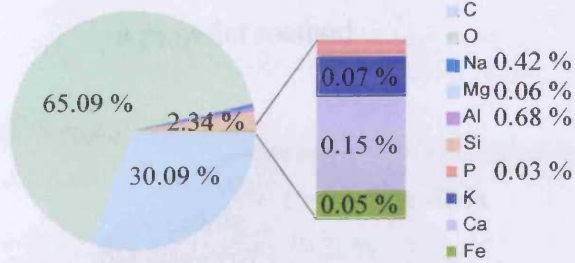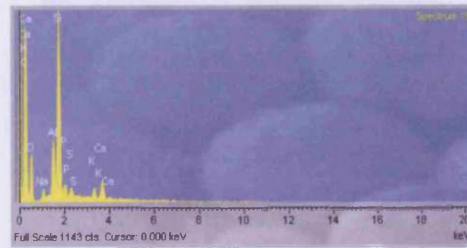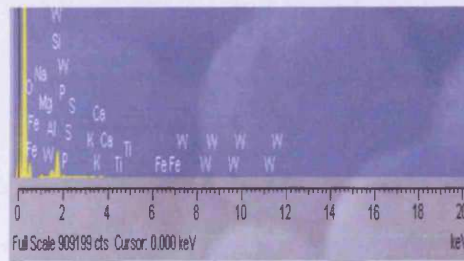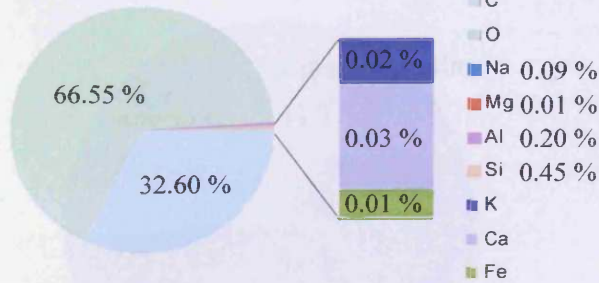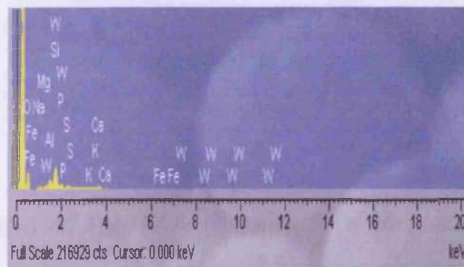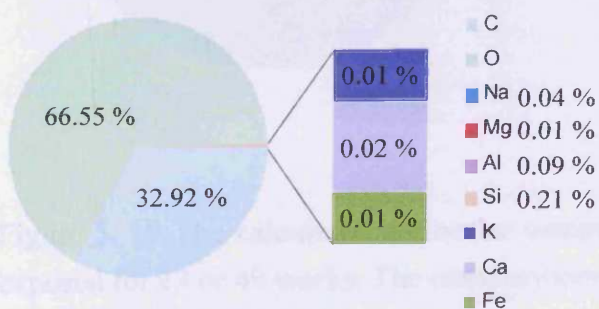
Figure 5. 18 The atomic compositions of the MA remained in the lung exposed for 13 or 49 weeks. The compositions were expressed as atomic percentage and decided by pinpoint (a) or mapping (b) methods.

13 weeks
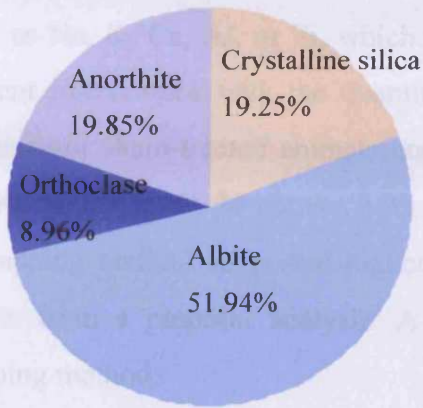
a pinpoint method   a mapping method
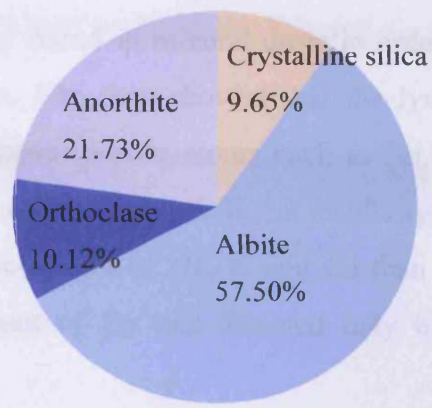
49 weeks
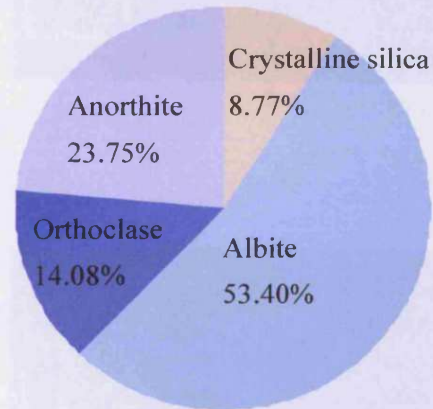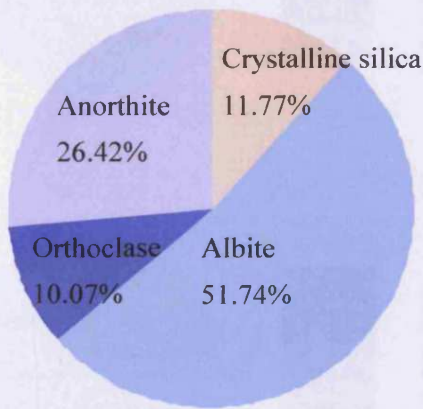
Figure 5. 19 The calculated molecular composition of the MA remained in the lung exposed for 13 or 49 weeks. The compositions were expressed as weight percentages.

5. 3. 3. 2 The composition of the particles deposited in the thoracic lymph nodes

5. 3. 3. 2. 1 The atomic composition of lymph nodes from the sham-treated animals

It is important to find whether the sham-exposed lymph node specimen shares atoms such as Na, K, Ca, Al, or Si, which are normally found in mineral dusts in order to prevent interference with the quantitative results. The data showed that the lymph nodes from sham-treated animals contained feldspar-specific atoms such as Na, Ca and K (Figure 5. 20). Moreover, both methods of analyses gave different results again. A mapping method suggested higher atomic percentages of Na, K and Ca than the results from a pinpoint analysis. A small amount of Fe was detected only by a mapping method.

(a)

(b)
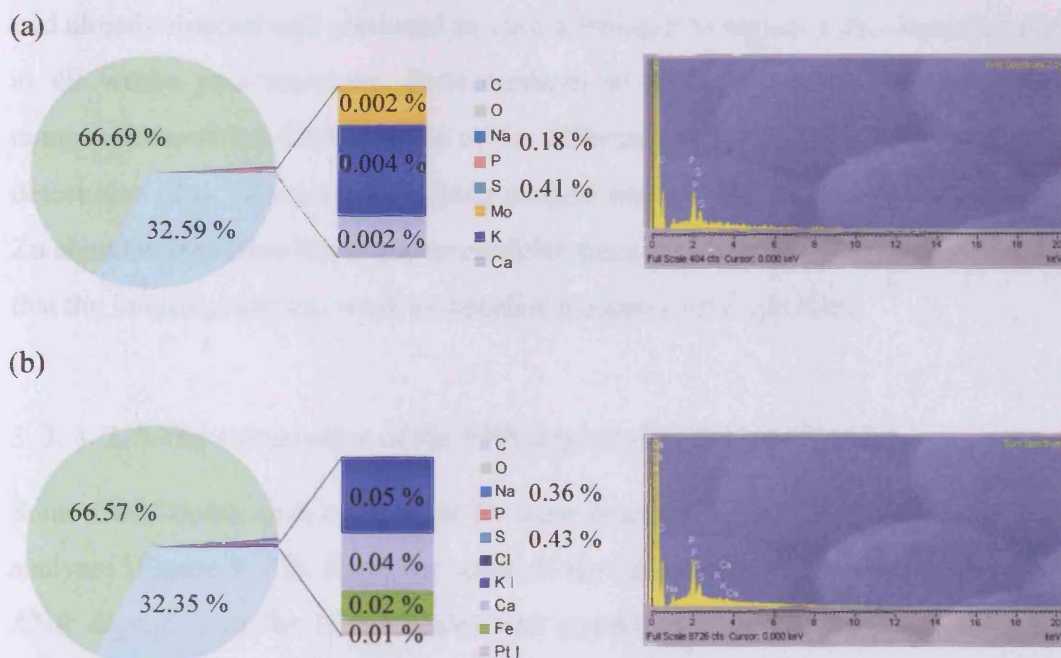
Figure 5. 20 The atomic compositions of the lymph nodes from the sham-exposed animals decided by a pinpoint analysis (a) and a mapping method (b).

154

5. 3. 2. 2. 2 The composition of the CRS deposited in the lymph nodes

BSE images (Figures 5.11 and 13) showed that CRS particles were deposited locally and the areas of deposition are much smaller that the tissue only area. Therefore, most of the atoms were detected from tissue material rather than particles. All the values were calibrated using the ratio between C and other atoms resulting from analysing the lymph nodes from the sham-treated animals. The results after calibration suggested that none of the feldspar specific atoms such as Na, K or Ca was detected from the particles deposited (Figure 5. 21). Pinpoint analysis suggested that the percentages of Si increased from 2.22% at 13 weeks post-instillation to 8.29% at 49 weeks whereas the mapping method did not show any increases (Figure 5. 21). These results imply that the CRS would be drained to the region where other CRS particles had already drained and produced as such a stronger Si signal in the deposited region at 49 weeks post-treatment. Both methods of analyses present slightly different compositions of the CRS. In spite of the different results, both methods were able to detect zinc (Zn). However, a mapping method was not able to distinguish whether the Zn signal comes from the tissue or particles since the quantity of Zn was so small and that the intensity was too weak to visualise it against a background.

5. 3. 3. 2. 3 The composition of the ANR deposited in the lymph nodes

Some trace atoms such as P, S, or Fe were detected by both pinpoint and mapping analyses (Figure 5. 22). However, after all the calibrations, the results imply that the ANR deposited in the lymph nodes was composed of Si, Al and feldspar specific atoms such as Na, K, and Ca. In contrast to the observation with CRS, pinpoint analysis suggested little changes in the percentages of Si between 13 and 49 weeks post-exposure. In spite of the different compositions of the ANR depending on analysis methods, the ratios between Si and Al, Na, K or Ca were very similar for both methods employed.
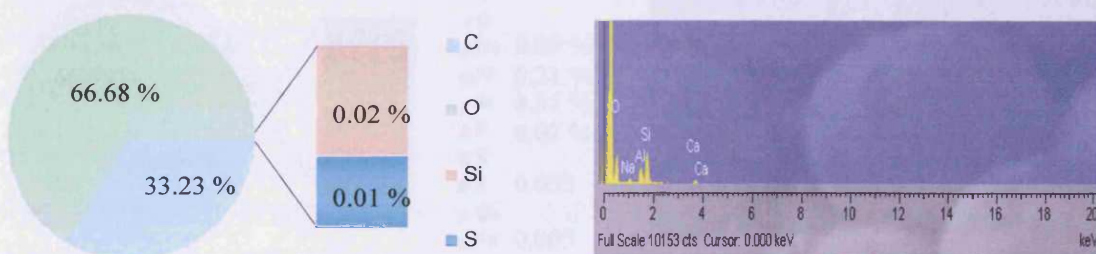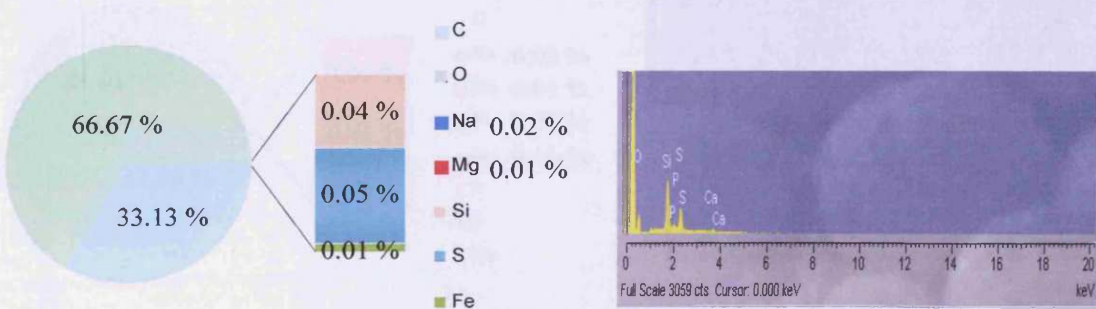
(a)

13 weeks

49 weeks

(b)
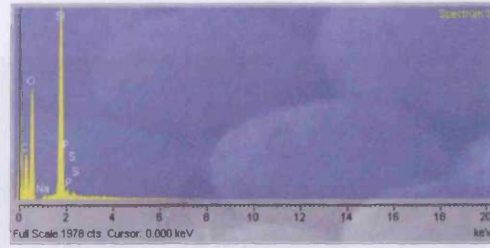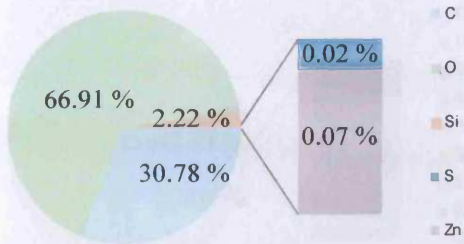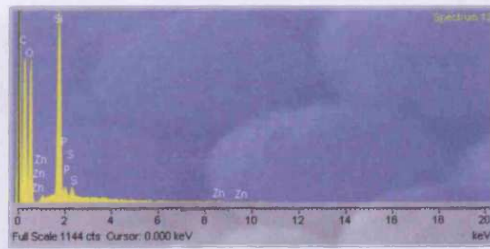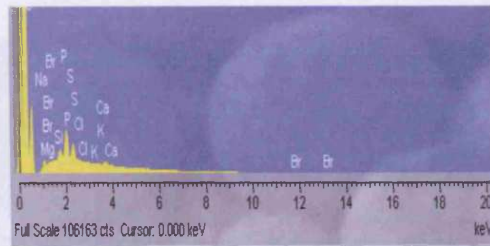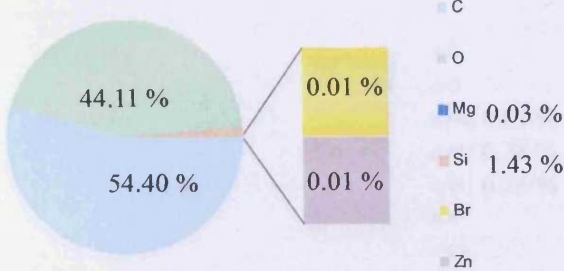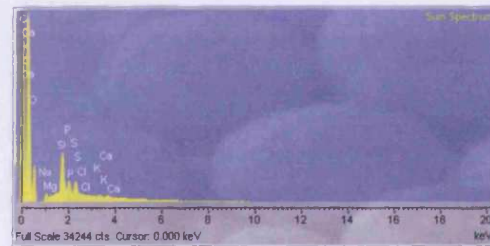
13 weeks

49 weeks

Figure 5. 21 The atomic compositions of the CRS deposited in the lymph nodes at 13 weeks post-instillation. The atomic percentages were decided by a pinpoint analysis (a) and a mapping method (b).

(a)

13 weeks

C
O
Na 0.7 %
Mg 0.01 %
Al 2.28 %
Si
S 0.02 %
K
Ca
Ti 0.01 %
Fe 0.05 %

68.19 %
3.49 %
22.67 %
0.18 %
0.46 %

49 weeks

C
O
Si
Al 2.28 %
Na
K 0.07 %
Ca

65.86 %   4.39 %
26.06 %
0.64 %
0.69 %

(b)

13 weeks

C
O
Mg 0.03 %
Al 0.26 %
Si 0.26 %
K
Ca
Ti 0.004 %

66.53 %
32.15 %
0.01 %
0.03 %

49 weeks

C
O
Si
Al 1.55 %
Na
K 0.06 %
Ca

66.39 %   3.00 %
28.05
0.48 %
0.48 %
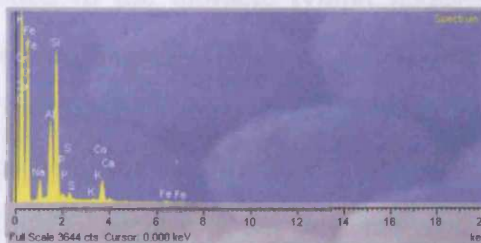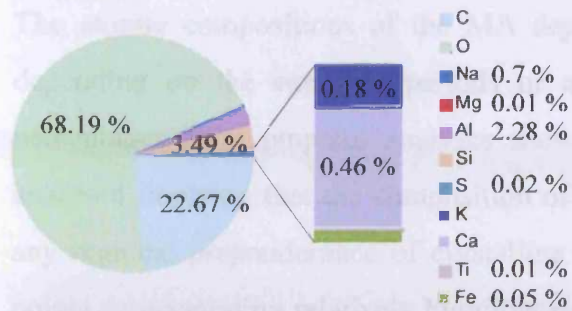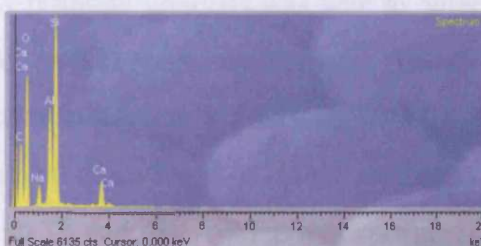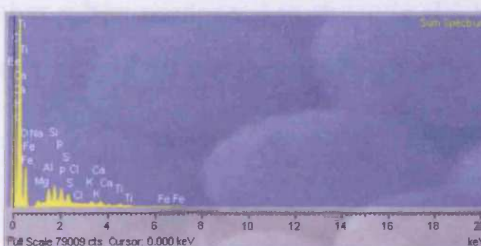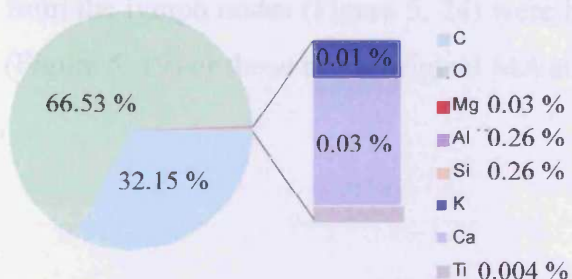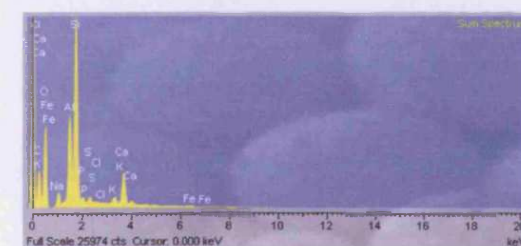
Figure 5. 22 The atomic composition of the ANR depositied in the lymph nodes from the ANR exposed animals for 13 or 49 weeks. The atomic percentages were decided by a pin-point analysis (a) or a mapping method (b).

5. 3. 3. 2. 4 The composition of the MA deposited in the lymph nodes

The atomic compositions of the MA deposited in the thoracic lymph nodes vary depending on the exposure periods or analysis methods (Figure 5. 23). Atomic percentages from pinpoint analyses showed different values depending on points analysed implying that the composition of the MA was not homogeneous. However, any regional preponderance of crystalline silica/feldspar was not detected since the points demonstrating relatively high/low percentages of crystalline silica, were found in the field scanned in a random manner. Only pinpoint analysis was able to detect Fe from the lymph nodes at both 13 and 49 weeks post-instillation. The atomic percentage of the Fe at 49 weeks post-exposure was lower than that at 13 weeks. Interestingly, the weight percentages of crystalline silica from mapping methods were higher than those from pinpoint analysis at both 13 and 49 weeks post-exposure. Both analysis methods showed that the crystalline silica contents of the MA deposited in the lymph nodes from the animals sacrificed at 13 weeks post-exposure were higher than those at 49 weeks (Figure 5. 24). Moreover, the crystalline silica contents in the MA from the lymph nodes (Figure 5. 24) were higher when compared to those in the lung (Figure 5. 19) or those of the original MA at both 13 and 49 weeks post-instillation.
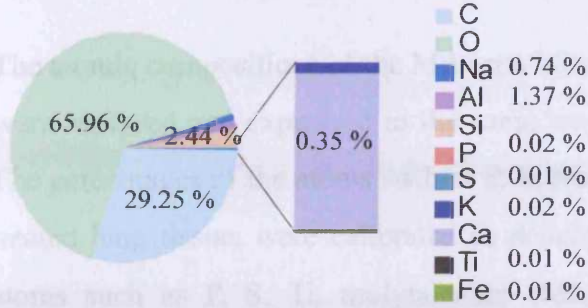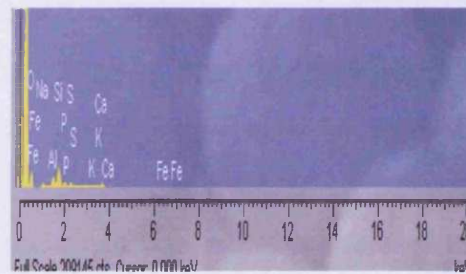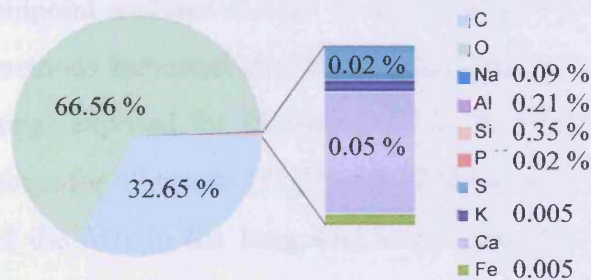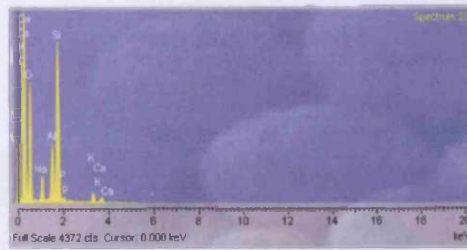
(a)

13 weeks

49 weeks

(b)
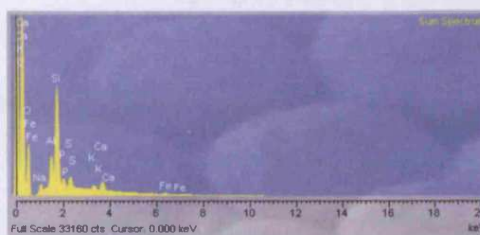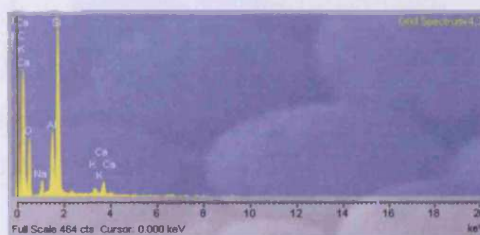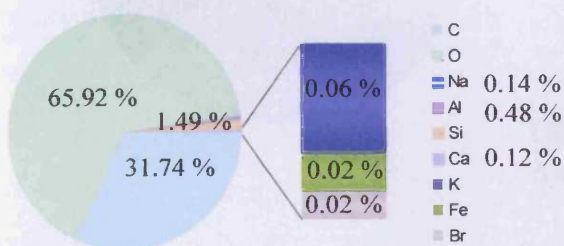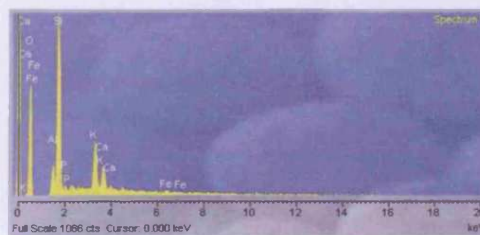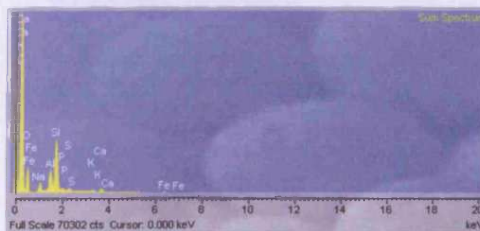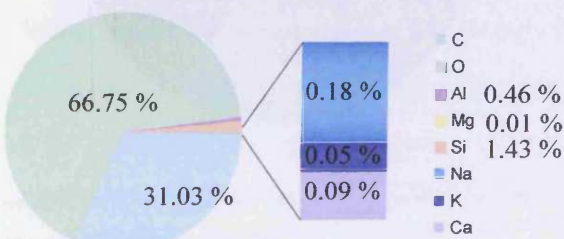
13 weeks

49 weeks

Figure 5. 23 The atomic composition of the MA deposited in the lymph nodes at 13 and 49 weeks post-instillation decided by a pin-point analysis (a) and a mapping method (b).

159

13-week

a pinpoint analysis   a mapping method
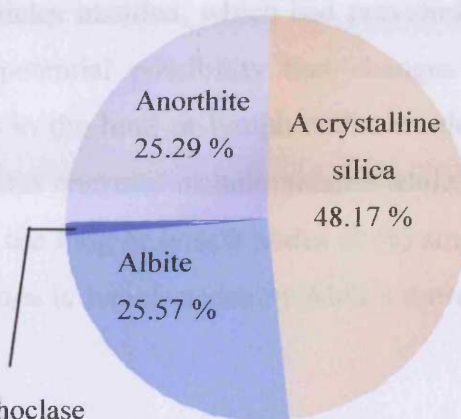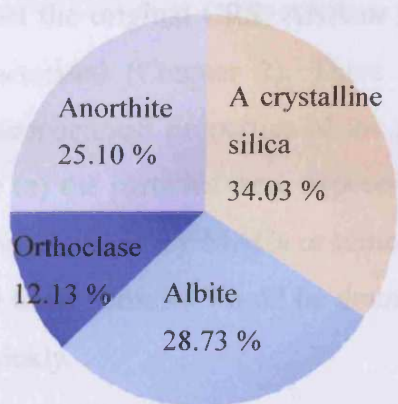
49-week

a pinpoint analysis   a mapping method
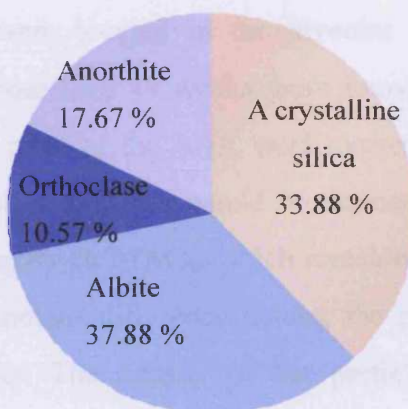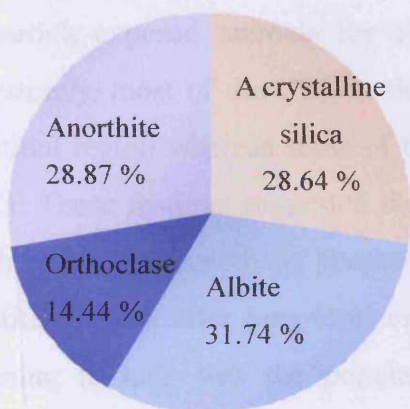
Figure 5. 24 The molecular composition of the MA deposited in the lymph nodes from the animals at 13 and 49 weeks post-exposure. The compositions were analysed by both a pinpoint analysis and a mapping method and expressed as percentages (w/w).

5. 4 Discussion

The study was initiated in order to find any differences in the size distribution or composition of the particles remaining in the lung or deposited in the lymph nodes against the original CRS, ANR or MA particles instilled, which had previously been characterised (Chapter 2). There was a potential possibility that changes in the physicochemical properties of the particles in the lung or lymph nodes would occur since (a) the particles were exposed to various enzymes or antioxidants while carried or phagocytosed by MACs or remaining in the lung or lymph nodes or (b) smaller or more toxic particles would be drained to thoracic lymph nodes by MACs more easily or quickly.

E-SEM, BSE image, and EDX with pinpoint and mapping methods were chosen to characterise the particles in the lung or the lymph nodes. BSE images made it easier to distinguish particles against the tissue since the higher atomic numbered material produced more detectable back scattered electrons and thus was expressed as a white image. The images showed most of the MA, CRS or ANR remaining in the lungs from the particle-exposed animals for 13 weeks were located in the alveolar MACs. Interestingly, most of the CRS in the lung exposed for 49 weeks were found in the interstitial region whereas some of the MA or most of the ANR were located in the MACs. These features suggested that the instilled particles would be drained to the lymph nodes or alternatively phagocytosed by alveolar MACs, which remained in the interstitial region after long-term exposure. Another difference among the particles remaining in lung was the population density. The density of the particles was ANR>MA>CRS in order whereas the sizes of the area where the particles were deposited gave the opposite order; CRS>MA>ANR. The higher density coverage were thus obtained from the less toxic material. This result implied that MACs are less likely to retain a large amount of a more toxic material such as CRS. Therefore, only a small amount of the CRS would be carried by MACs.

The same population density order was recognised among the particles deposited in the lymph nodes. It was very difficult to find ANR particles since the particle-deposited area was very small and it was detected in only 1 or 2 lymph nodes from the group. Morphological changes in the lymph nodes from rats treated with ANR were not seen even though the particles were concentrated in a very focal area. In contrast to the ANR, the oval shaped area in the lymph nodes from the MA or the CRS-instilled animals contained large numbers of particles. This suggested that most of the MA or the CRS were located in a granulomatous region associated with reduction in cell compaction.

Figure 5. 25 The BSE images of the MA remaining in the lung at 49 weeks post-exposure. Blue circles depict the particles attached to a larger one. Yellow circle depict the particles, which are not attached to any other particles.

In spite of the good contrast between the particles and tissue, the resolution among individual particles in tissues, which were mostly densely packed in local areas, was not as good as that from the original particle-specimen. A lesser number of the smaller particles attached to the larger ones were found in the BSE images of the MA remaining in the lungs at 49 weeks post-instillation (Figure 5. 25) when compared to

the original MA (Figure 2. 6). Several hypotheses could be suggested. Firstly, the smaller particles aggregated with the larger ones would be detached during the exposure period. Secondly, the edge of the particle image was not always clear enough to define the morphology of the ultrafine particles since the signal was interfered with by the back-scattered electron from the tissue material. This effect was further compounded by the fact that the signals from the ultrafine particles were weak. This resulted in inaccurate measurement particularly of ultrafine particles in the lung or the lymph nodes. The second hypothesis can also explain why the percentages of the ultrafine CRS in the lung or lymph nodes were nearly zero even though original instilled material contained 32.19 % ultrafine particles.

Thus, ultrafine CRS particles were much reduced in number in lung and lymphatic tissue compared with those of the original instillation. In spite of this observation, the size distributions of the CRS deposited in the lung and thoracic lymph nodes were very similar at both time points. In contrast, the size distributions of the MA were quite different in lung and thoracic lymph nodes. The percentages of the particles (ESD<0.3 μm) deposited in the thoracic lymph nodes were higher than those of the particles in the lung at 13 weeks post-exposure and then these differences were reversed at 49 weeks. These phenomena implied that smaller particles (ESD<0.3 μm) would be drained to the lymph nodes more quickly than larger ones.

Furthermore, both methods of analysis suggested that there was a higher crystalline silica content of the MA deposited in the lymph nodes than that in the original MA or the MA remaining in the lung at both 13 and 49 weeks post-exposure. In contrast, the crystalline silica content of the MA remaining in the lungs was lower than that in the original MA at 13 and 49 weeks post-instillation. These results suggested that the crystalline silica, the most toxic material in the MA, would be drained more easily and quickly to the lymph nodes than other ash components such as feldspars. A rapid drainage of the crystalline silica component of the MA to the lymph nodes may explain why formation of granuloma was the first recognised change in the lymph nodes prior to lung inflammation (at 49 weeks post-instillation) (Chapter 3 and 4). There are two possible explanations for the delay of the lung inflammation. Firstly, the

163

low crystalline silica content of the MA in the lung would require a longer time to trigger changes in the lung if there were competitive interferences with feldspar components in initiation/development of inflammation in the lung as discussed previously (Chapter 3). Secondly, the granulomatous symptoms, which became more severe in a time dependent manner, could cause functional stress in the lung resulting from failure of efficient clearance to the lymph nodes.

In conclusion, physicochemical properties such as size distribution and chemical composition of the particles instilled into the lung were changed during the exposure period. Furthermore, these changes in the physicochemical properties were affected by the region where the instilled particles remained/deposited and exposure period since the smaller and more toxic particles could be drained to thoracic lymph nodes more easily or quickly. BSE images and results from compositional analysis using EDX associated with E-SEM suggested that most of the MA drained from the lung was deposited in the granulomatous regions in thoracic lymph nodes and the crystalline silica content of the MA in this region was higher when compared to those of the MA remaining in the lung or the original MA instilled. These phenomena could explain why the first changes caused by the MA instilled into the lung was recognised in thoracic lymph nodes 36 weeks earlier than the inflammation in the lung.

6. The changes in mRNA expression during inflammation and fibrogenesis induced in lung by Montserrat volcanic ash or pure cristobalite

6. 1 Introduction

The toxicological properties of Montserrat volcanic ash (MA), anorthite (ANR) and cristobalite (CRS) were investigated previously using quantitative biochemical techniques (Chapter 3) and histopathology (Chapter 4). These investigations showed that the mineral dust produced different biological endpoints relating to both dose (1.0, 2.5 or 5.0 mg) and time post-instillation (13, 25 or 49 weeks).

The major objective of the present study was to employ modern genomic macroarray analysis to see if individual genes or gene group clusters were involved during (1) inflammatory events in lung parenchyma or (2) fibrogenesis. The general scheme of this project is presented in Figure 6. 1.

Inflammation was not noted from conventional toxicological analysis with MA (5.0 mg, containing approximately 1.0 mg of crystalline silica) until 49 weeks post-instillation and yet it was detected at 13 weeks post-exposure using 5.0 mg of pure CRS. The quantitative biochemical and cellular and semi-quantitative histopathological studies showed that most of the parameters such as the numbers of free cells, MACs or PMNs and the area of alveolar units covered by free cells of the MA (5.0 mg)-exposed lungs for 49 weeks were approximately two or three times higher than those from the CRS (5.0 mg)-exposed lungs for 13 weeks. However, there were no statistical differences between groups. Thus, genomic comparison between the two groups was considered in order to find any similarities/dissimilarities in gene profiling in terms of mechanism. Equally, fibrogenesis was detected by conventional analysis at 49 weeks with 5.0 mg CRS and not at all with 5.0 mg MA at 49 weeks. Thus, genomic comparisons between these data sets could perhaps provide information on the differences between inflammatory and fibrogenic responses at the level of gene expression.

All the genomic changes needed to be related to a control group of animals i.e. those sham-treated with 0.15 M NaCl vehicle. As gene changes might be expected during the animal ageing process, a further comparison set was needed for 13 and 49 week

166

sham-exposed groups to assess the changes in mRNA expression occurring in the lung as a result of ageing.

To date, there are few agreed rules or principles for the interpretation of the huge data sets generated by macroarray analysis. In this study, the view taken was simplistic with the attempt to identify important candidate genes or gene group clusters that may be important in inflammation and fibrosis. To this end, a simple analysis using commercial software to detect gene changes of greater than five fold (compared to the sham-exposed group) in any treated group were considered. A second analysis (K-means clustering) was also adapted to classify the genes, which showed similar trends in   dust-exposure and thus possibly related by their function (Brent, 1999). Moreover, this second method could recognise smaller changes in the genes, which were rejected from the simple analysis but may still be important in inflammation, lipoproteinosis and fibrogenesis in the lung.

Biological sample selection:
Ageing, Inflammation, fibrosis

mRNA extraction and
Hybridisation and
Target preparation

Macroarray scanning

Re-scaling/Macroarray adjustment

Simple quantitative analysis

Standardisation

High-level analysis: K-means clustering

Figure 6. 1 An algorithm of the methods and data analysis (modified from Tamayo and Ramaswamy, 2002)

6. 2 Materials and Methods

6. 2. 1 Extraction of mRNA from the lavaged lung tissue

mRNA was extracted from lavaged lung tissue and all procedures followed the manual from the RNeasy kit (Qiagen Ltd. UK). The lung, snap frozen in liquid nitrogen (-196°C) and stored at -70°C, was ground with a pestle and mortar under a liquid nitrogen atmosphere (-196°C). The lung powder was then homogenised and lysed with lysis buffer (buffer RLT containing guanidine thiocyanate, 600 μL) and β-mercaptoethanol (10 μL/mL of buffer RLT). Both guanidine thiocyanate and β-mercaptoethanol are involved in inactivation of RNase during the lysis procedure. QIAshredder (Qiagen Ltd. UK) was employed to lyse homogenised lung tissue powder efficiently since some of the fibrotic lung contained relatively large amounts of connective tissue. The lysate was then centrifuged at maximum speed for 5 minutes. The supernatant was poured to Eppendorf tubes containing the same volume of 70 % (v/v) of ethanol (abs. Sigma, UK) as that of the lysis buffer used and then mixed by gentle inversion (10 times). The mixture, including precipitate, was applied to the RNeasy mini column and centrifuged at 13,000 rpm for 15 seconds. The column was washed with wash buffer (buffer RW1, 300 μL) and the flow-through was discarded. The genomic DNA in the sample was then digested with RNase free DNase (RNase-free DNase set, Qiagen Ltd.) for 20 minutes in iced water and washed again with buffer RW1 (300μL) and DNA free mRNA was bound to the membrane during washing with buffer RPE (500 μL) twice. The column was centrifuged at maximum speed for 15 seconds again in order to remove any liquid remaining. The RNA was then eluted with RNase free water. The quality and quantity were checked by the ratio between absorbance at 260 nm and 280 nm using a spectrophotometer. The concentration of mRNA larger than 500 μg/μL was chosen and its quality was assessed using electrophoresis (0.5 % agarose gel, tris-EDTA (TE) buffer, at 70 mV, 30 minutes). Ethidium bromide (Sigma, UK) was employed to visualise the mRNA under UV light.

6. 2. 2 Macroarray

Approximately 2 µg of mRNA isolated from each lavaged lung was employed for each nylon membrane (details below). The mRNA was converted to ^{32}P labelled cDNA using [α-^{32}P] ATP (Amersham Ltd., UK) and cDNA synthesis (CDS)-primer mix (BD Biosciences, UK). Incorporated labelled ATP ([α-^{32}P] ATP) was then removed using nucleospin columns (BD Biosciences, UK). The cDNA was employed in order to hybridise with the cDNA of 1,185 genes on the nylon membrane (Atlas rat toxicology array 1.2, BD Biosciences, UK) using ExpressHyb solution (BD Biosciences, UK) at 68 °C overnight. These membranes were washed with 2xsaline-sodium citrate buffer (SSC 300 mM sodium chloride 39 mM trisodium citrate, pH 7.0), 1% (w/w) sodium dodecyl sulphate (SDS) solution until the counts per minute (cpm) became less than 50. The membranes were washed again using 0.1xSSC, 0.5% (w/w) SDS solution until the counts became between 7-15 cpm. Each membrane was kept in a sealed bag in order to prevent drying out and it was then exposed to a phosphorous image screen (Kodak) for up to 2 weeks.

6. 2. 3 A simple quantitative analysis of array data

The membrane was exposed on a phosphoimage screen for a period of up to 14 days to get quantifiable data. The screen was then scanned using a Quantity One 4. 1. 1 (Bio-Rad, UK). The data were quantified using commercial software (AtlasImage 2.01). All the arrays were cross-compared to avoid the misanalysis caused by instability of the data resulting from experimental error or systematic errors. Furthermore, this method maximised the number of comparison sets. The gene changes were only considered after the both the conditions were satisfied namely, that the difference of its intensity between a control group and a treated group larger than 5,000 with the change ratio more than 5 fold except the case that if the intensity difference was larger than 10,000, the gene was considered as up/downregulated. The fold changes are presented in the table and in the case of downregulation, 1/X fold change is expressed as X (Table 6.1-6.5).

6. 2. 3 K-means clustering

The K-means clustering method was employed to classify genes, which may functionally related using a statistical programme Minitab 13.0 (Quinn and Keough, 2002). This method chooses one gene randomly and then finds other genes which shows similar trends from comparative data based on the changes in the mRNA expressional level. For this analysis, all the values were converted to log values and then standardised.

6. 3 Results

6. 3. 1 Raw array data and reproducibility

In spite of the individual animal genetic variances and the instability and the high sensitivity of the technique, three arrays from the sham-exposed animals at 49 weeks showed acceptable reproducibility (Figure 6. 2). In terms of reproducibility it can be seen that genes with red boxes are of quite similar intensity in each array. However, this did not apply for every gene in each array. As an example, variable intensities between arrays are shown by the genes designated with a blue box (Figure 6. 2). Further examples of arrays following visualisation of gene expression intensity are shown in Figure 6. 3. Even without software analysis, it is clear by eye that certain genes in lungs treated with MA or CRS were up/downregulated in comparison with sham-treatments.

6. 3. 2 The mRNA expressional changes

6. 3. 2. 1 Ageing; comparison of mRNA expression profile of the lungs from the sham-exposed rats for 13 and 49 weeks

Two different control groups; sham-exposed animals for 13 and 49 weeks were employed to examine any differences in gene expression caused by the ageing process (Table 6. 1). From simple quantitative analysis, changes in 12 genes were noted from a total of 1,185 genes screened in the macroarray. Eight of these were upregulated, and four downregulated. With K-means clustering analysis with a more relaxed

171
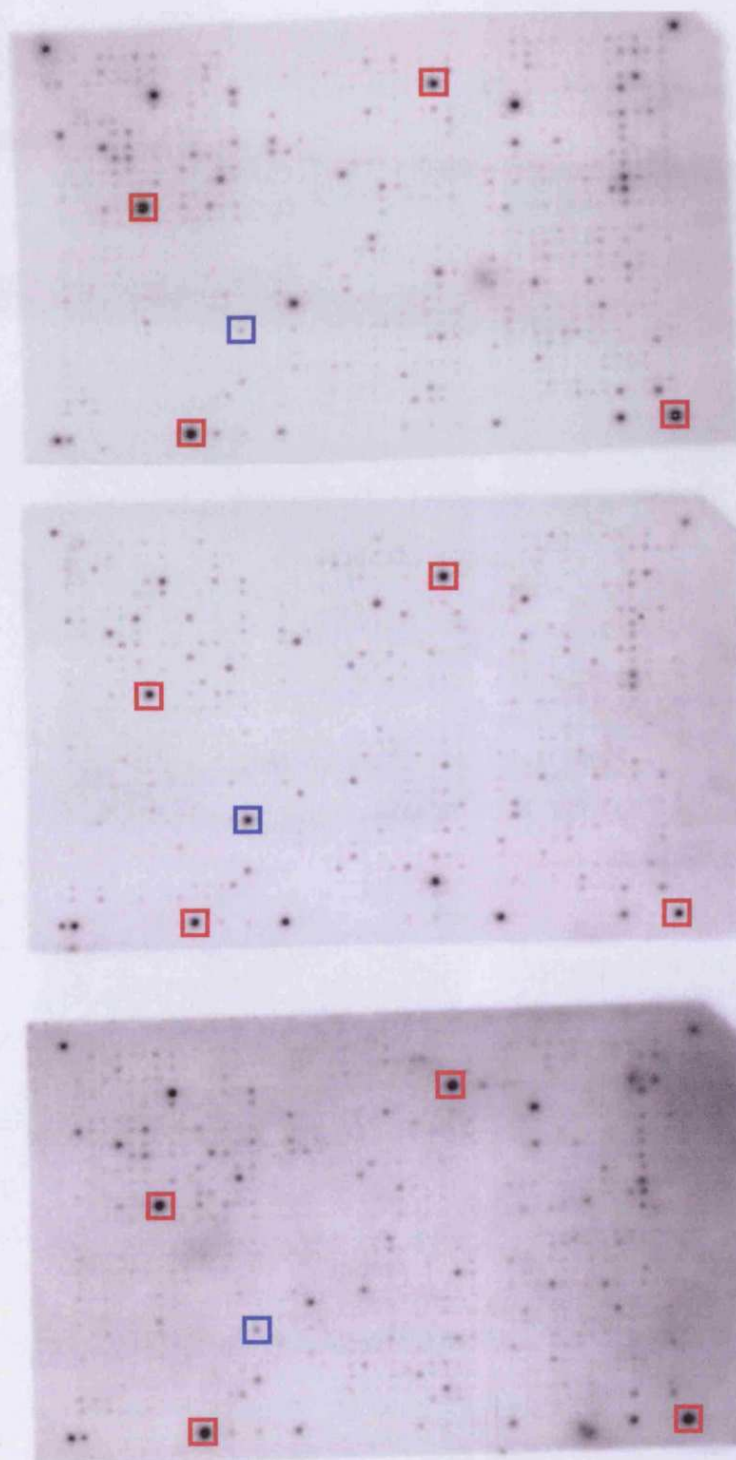
Figure 6. 2 The digitised pictures of the nylon membranes containing cDNA hybridised from the mRNA isolated from three sham-exposed lungs at 49 weeks post-instillation. The genes in red boxes with relatively higher intensity were detected in all three membranes but those in blue boxes show individual variances.
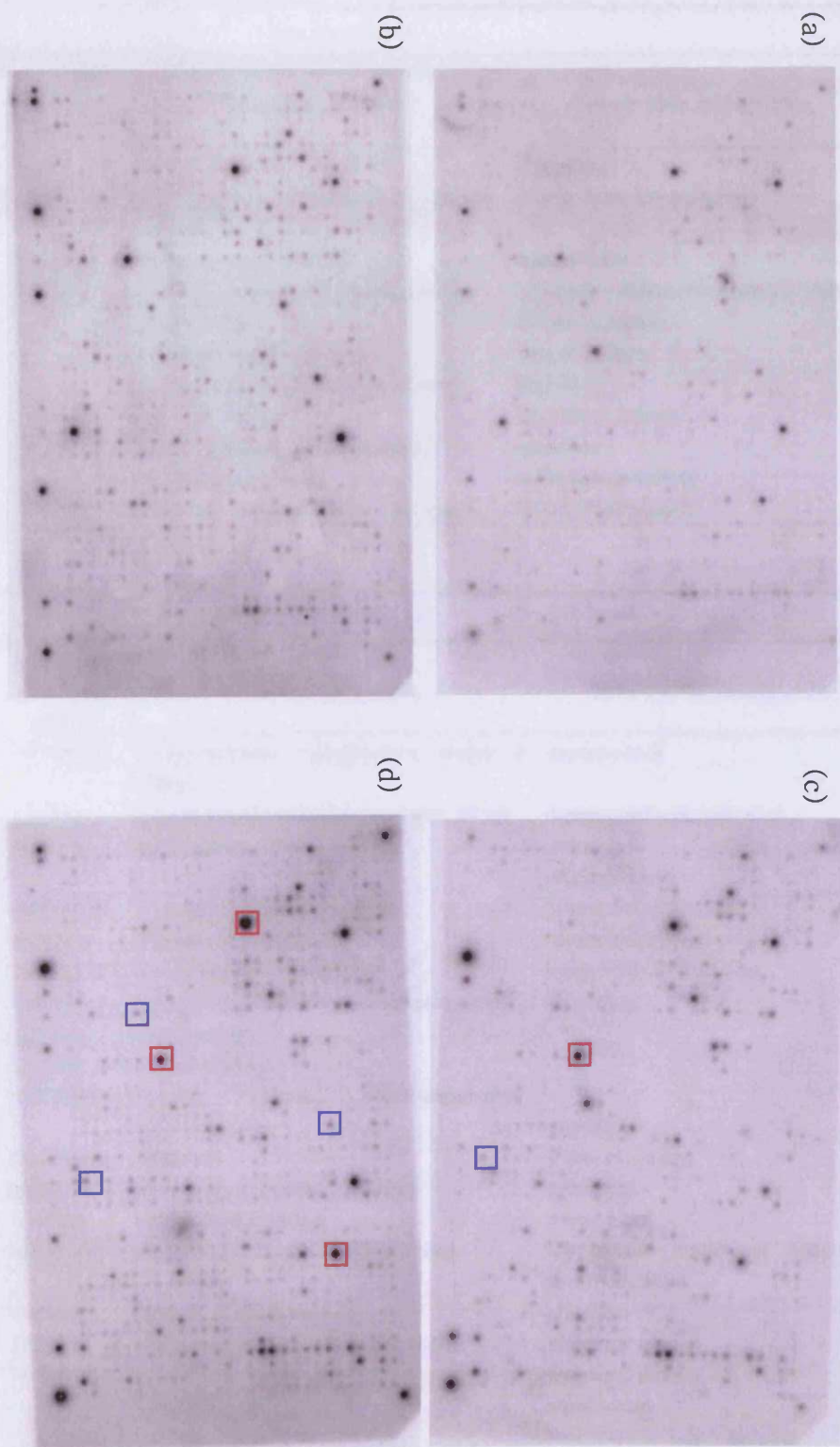
Figure 6. 3. The digitised pictures of the nylon membranes containing cDNA hybridised from the mRNA isolated from the sham-exposed lungs for 13 (a) and 49 weeks (b) and CRS-exposed lung for 13 weeks (c) and MA-exposed lung for 49 weeks (d). The genes in red boxes were recognised as upregulated and in the blue boxes were down regulated when (c) compared to (a) and (d) to (b).

Table 6. 1 The list of the up/down regulated genes caused by the ageing process (key: the genes in bold characters are also recognised as up/down regulated from both a simple quantitative analysis and K-means clustering)

Upregulated

A simple quantitative analysis	K means clustering method	Gene/protein name	Gene/protein classification
L29090	L29090	transducin beta 3 subunit	signalling
M65008	M65008	Zinc-finger transcription factor NGFI-C	Transcription/translation
X59051	X59051	Ribosomal protein S29	metabolism
X72914	X72914	cartilage oligomeric matrix protein	Cartilage oligomeric matrix protein
D16554		polyubiquitin	stress response ,
D79215		Fibroblast growth factor 10	Growth factors
M84221		Benzodiazepin receptor (peripheral)	Signalling
	U03470	Fas antigen ligand	Signalling (death)
	U12425	cyclic nucleotide-gated channel,	channels
X14221		surfactant protein C	surfactant protein C
	Y10054	3-hydroxy-3-methylglutaryl CoA lyase	Energy metabolism

Downregulated

A simple quantitative analysis	K means clustering method	Gene/protein name	Gene/protein classification
AF136943	AF136943	transcriptional intermediary factor 2 (TIF2)	metabolism
L24804	L24804	unactive progesterone receptor, 23 kD	transcription/translation
X57018	X57018	fgr proto-oncogene	oncogens and tumour suppressors,
	AF095740	ubiquitin-like protein NEDD8	transcription/translation
	M24393	Adenosine receptor A3	transcription/translation
	Z17223	mesenchyme homeobox 2	transcription/translation
	L08831	Glucose-dependent insulinotropic peptide	signalling
	X55288	CD28 antigen	
	X57405	notch homolog 1	
	X57986	Protein kinase, cAMP-dependent, catalytic, alpha	signalling
	U06436	RANTES	immune system
	U02534	nitric oxide synthase 3 (NOS3)	metabolism
	Y17295	anti-oxidant protein 2	metabolism
	U12187	ras associated with diabetes protein	intracellular transducer effectors and modulators
	S77858	Sodium channel beta 2	channels
	U37026	nonmuscle myosin alkali light chain	structural protein
	V01217	cytoplasmic beta-actin	structural protein
U11038		Lysyl oxidase	metabolism

stringency, changes in 24 genes were detected (7 upregulated, 17 downregulated). A comparison of both methods showed that four upregulated genes (57%) were common to both types of analyses and similarly 3 downregulated genes (18%) showed commonality. Changes common to both methods of analysis were found for four upregulated genes (transducin beta 3 subunit, Zinc-finger transcription factor, Ribosomal protein S29, cartilage oligomeric matrix protein) and three downregulated genes (transcriptional intermediary factor 2 (TIF2), inactive progesterone receptor, 23 kD, fgr proto-oncogene). Cluster or simple analysis showed that genes upregulated during the ageing process (Table 6. 1) provided a diverse group of genes with few functional links. Nevertheless, it is of interest that the surfactant protein C gene coding for an important surfactant protein was upregulated as the animals became older. Similarly, increases in fibroblast growth factor may well be important in an ageing process in the lung with greater collagen synthesis/deposition. Analysis of the genes downregulated during the ageing process again showed considerable diversity although transcriptional function is noted with four of them. Of interest to the lung/ collagen metabolism was the downregulation of lysyl oxidase an important enzyme in creating cross-links in collagen during ageing. It was therefore paradoxical that this gene is downregulated rather than upregulated.

6. 3. 2. 2 Inflammation; changes in mRNA expression profile of the lungs from MA (5.0 mg)-exposed animals at 49 weeks

The conventional biochemical and histopathological investigations suggested significant inflammatory responses in the MA-exposed lungs at 49 weeks post-instillation (see Chapter 3 and 4). The gene profiles of the MA-exposed lungs for 49 weeks were compared to those in the sham-treated lungs (49 weeks) in order to find inflammatory gene changes (Figure 6. 3). With a simple analysis, a total of 43 out of 1,185 genes were changed compared to the sham-treated lungs. Thirty-three genes were upregulated and included three genes (polyubiquitin, surfactant protein C, fibroblast growth factor) upregulated during the ageing process. A reduced number (10 genes) were down regulated (Table 6. 2) and included two genes (TIF2, nitric oxide synthase 3 (NOS3)) downregulated during the ageing process. Conversely, three

Table 6. 2 The list of the upregulated or downregulated genes in the MA-exposed lungs for 49 weeks (Key as Table 6. 1, The genes in the grey boxes are also changed during the ageing process, yellow boxes are related to inflammation, red characters are linked to protective mechanisms or pulmonary response related genes, bold characters were recognised as changes from both analyses. The horizontal bars separate different clusters A-E.)

			Upregulated		
A simple Quantitative Analysis		K-means Clustering	Gene/Protein Name	Gene/Protein Classification	
D16554	3	D16554	Polyubiquitin	stress response proteins,	A
L00313	4	L00313	cytochrome P450 IIB1 (CYP2B1)	xenobiotic metabolism	A
L08831	4	L08831	gastric inhibitory polypeptide (GIP)	Signalling	A
U82591	3	U82591	growth-related c-myc-responsive protein RCL	cell-cycle	A
X14221	2	X14221	surfactant protein C	surfactant protein C	A
X16956	5	X16956	prostaglandin receptor F2a	inflammation	A
M17698	2	M17698	thymosin beta 10	inflammation	B
S45392	6	S45392	heat shock 90-kDa protein beta	inflammation	B
M61177	8	M61177	mitogen-activated protein kinase 3	signalling	B
Y13714	5	Y13714	osteonectin	signalling	B
M89791	4	M89791	insulin-like growth factor-binding protein 1	signalling	B
M95738	5	M95738	solute carrier family 6 member 11	channel	B
X82551	3	X82551	60S ribosomal protein L39	metabolism	B
L31884	4	L31884	tissue inhibitor of metalloproteinase 2	metabolism	B
U56853	4	U56853	cytochrome P450; 21-hydroxylase	xenobiotic metabolism,	B
X14209	5	X14209	cytochrome c oxidase subunit IV (COX4)	Transcription/translation	B
X63369		X63369	GOS24 (zinc finger transcriptional	Transcription/translation	B
	2		regulator)		B
X68282	3	X68282	ribosomal protein L13A	ribosomal proteins	B
	4	AB010428	acyl-CoA hydrolase	metabolism	B
	2	D79215	fibroblast growth factor 10 (FGF10)	growth factors	B
	3	M19007	protein kinase C beta I	signalling	B
	2	M33201	surfactant protein A (SP-A)	surfactant protein	B
	3	M85299	sodium/hydrogen exchange protein 1	channel	B
	5	M85300	sodium/hydrogen exchange protein 3	channel	B
	1	X59051	40S ribosomal protein S29	ribosomal proteins	B
AB012234	3		nuclear factor I-X1	Transcription/translation	B
AF097593	12		N-cadherin	Structural protein	B
X78167	3		(Sprague Dawley) ribosomal protein L15	Ribosomal protein	B
Y00404	4		Superoxide dimutase 1, soluble	metabolism	B
					B

D10863	7	D10863	inhibitor of DNA binding 2	Transcription/translation	C
D14014	7	D14014	G1/S-specific cyclin D1	cell cycle	C
D17615	3	D17615	tyrosine 3-monooxygenase	metabolism	C
D17711	4	D17711	heterogeneous nuclear ribonucleoprotein K	RNA metabolism	C
L04535	39	L04535	somatostatin receptor 5	signalling	C
M18668	3	M18668	creatine kinase b	Energy metabolism	C
M21730	3	M21730	annexin V	Channels/inflammation	C
U17013	4	U17013	octamer binding protein	transcription	C
U22893	5	U22893	DNA binding protein A (DBPA)	DNA binding protein	C
U37462	5	U37462	mitogen activated protein kinase kinase 5	stress response	C
X14878	4	X14878	Thioredoxin	link to inflammation	C
	10	D00036	phospholipase A2 group IB	↑	C
	7	X71429	heat shock 10-kDa protein	↕	C
	2	M64723	prostaglandin transporter (PGT)	link to inflammation	C
	13	J03752	microsomal glutathione S-transferase 1	xenobiotic metabolism	C
	3	M29853	cytochrome P450 4B1	xenobiotic metabolism	C
	4	AB010428	acyl-CoA hydrolase	metabolism,	C
	3	D86373	acyl-CoA:cholesterol acyltransferase	↑	C
	3	M67465	3-beta hydroxy-5-ene steroid dehydrogenase	↕	C
	4	X56060	deoxyribonuclease I	metabolism	C
	2	X02918	prolyl 4-hydroxylase	surfactant metabolism	C
	3	Y00697	cathepsin L	surfactant secretion	C
	2	AF115380	vimentin (VIM)	stress response proteins	C
	2	X62952	growth arrest & DNA damage-inducible protein	stress response proteins	C
	10	L32591	clusterin	stress response proteins	C
	4	M64862	myeloid cell differentiation protein 1	bcl family proteins	C
	10	D16237	M-phase inducer phosphatase 2	cell cycle	C
	4	D16309	G1/S-specific cyclin D3	cell cycle	C
	3	D37880	Sky proto oncogen	structural protein	C
	2	D63378	ER-60 protease	transcription/translation	C
		K03502	elongation factor 2	↑	C
	3	M27466	cytochrome c oxidase polypeptide VIc2	↕	C
	7	M86870	endoplasmic reticulum stress protein 72	↓	C
	3	X63594	RL/IF-1	transcription/translation	C
	4	M99418	gastrin/cholecystokinin type B receptor	signalling	C
	3	D86345	leukemia inhibitor factor receptor alpha	↑	C
	6	M62781	insulin-like growth factor binding protein 5	↕	C
	3	U16253	corticotropin-releasing factor receptor 2	↓	C
	3	U63315	25-Dx	signalling	C
	3	J03026	matrix Gla protein	structural proteins	C
	4	L11004	Solute carrier family 9	channel	C
	7	M35862	male germ cell-associated kinase	intracellular kinase network	C
	5	M64300	mitogen-activated protein kinase 2	intracellular kinase network	C
	2	S80439	OB-cadherin 1	structural proteins	C
	5	U03734	angiotensin-converting enzyme (ACE)	granulomatous diseases	C
	7	U13253	fatty acid-binding protein 5 (FABP5)	transport	C
	6	M74535	membrane guanylyl cyclase	adenylate/guanylate cyclases	C
	2	U21101	cyclic GMP stimulated phosphodiesterase	adenylate/guanylate cyclases	C
	4	U31867	Tclone15	functionally unclassified proteins	C
	6	U95113	histone 2A (H2A)	histones	C

177

A simple quantitative analysis	K-means clustering		Gene/Protein Name	Gene/Protein Classification	
			Downregulated		
L29090	6	L29090	guanine nucleotide-binding protein	G proteins	D
U03470	7	U03470	Tumor necrosis factor (ligand)	death receptor ligand	D
	2	AF077354	ischemia-responsive 94-kDa protein	stress response	D
	3	U12425	cyclic nucleotide-gated channel	channels	D
AF136943	3	AF136943	transcriptional intermediary factor 2	transcription	E
M65008	3	M65008	Zinc-finger transcription factor NGFI-C (early response gene)	transcription	E
U02534	3	U02534	nitric oxide synthase 3 (NOS3)	metabolism	E
X72914	4	X72914	cartilage oligomeric matrix protein	structural protein	E
Y10054	4	Y10054	mitochondrial hydroxymethylglutaryl-CoA lyase	Energy metabolism	E
AF120100	3		thiopurine methyltransferase	Xenobiotic metabolism	E
AH005431	2		follistatin	signalling	E
Z11558	3		glia maturation factor beta	Growth factor	E

178

genes (guanine nucleotide-binding protein, Zinc-finger transcription factor, cartilage oligomeric matrix protein) upregulated during the ageing process were down regulated following treatment with MA. The genes recognised as upregulated from the simple analysis could be classified as genes, which were related to metabolism (7), inflammation (5; prostaglandin receptor F2a, thymosin beta 10, heat shock 90-kDa protein beta, annexin V, Thioredoxin) and transcription (5). K-means clustering produced 20 different gene clusters in primary analysis but only five clusters (A-E, Table 6. 2) were considered further as these clusters contained gene changes already detected from simple analysis.

With K-means clustering, cluster A was composed of six genes (Polyubiquitin, cytochrome P450 IIBI, gastric inhibitory polypeptide, growth-related c-myc-responsive protein RCL, surfactant protein C and prostaglandin receptor F2a) all of which were recognised as upregulated from the simple quantitative analysis using AtlasImage 2.01. However, two of these genes (Polyubiquitin and surfactant protein C) were also recognised as upregulated during the ageing process.

Cluster B contains 16 genes and 12 of these (tissue inhibitor of metalloproteinase 2, thymosin beta 10, mitogen-activated protein kinase 3, insulin-like growth factor-binding protein 1, solute carrier family 6 member 11, heat shock 90-kDa protein beta, cytochrome P450; 21-hydroxylase, cytochrome c oxidase subunit IV (COX4), GOS24 (zinc finger transcriptional regulator), ribosomal protein L13A, 60S ribosomal protein L39, osteonectin) were noticed to be upregulated from the quantitative analysis. The genes in this group were mainly classified as metabolism (4), transcription (2), inflammation (2) and surfactant protein (1) related.

Cluster C was mainly composed of metabolism (11), transcription (5), translation (5), stress (4) and surfactant (2) related genes. Eleven of 50 genes in this cluster (inhibitor of DNA binding 2, G1/S-specific cyclin D1, tyrosine 3-monooxygenase, heterogeneous nuclear ribonucleoprotein K, somatostatin receptor 5, creatine kinase b, annexin V, cytochrome c oxidase, octamer binding protein 1, DNA-binding protein A;

cold shock domain protein A and Thioredoxin) were also recognised as upregulated from a simple quantitative analysis. Thioredoxin (4 fold) is known to be related to protecting cells against TNF (Tumour necrosis factor)-α induced cytotoxicity (http://www.biosci.ki.se). Moreover, there are two pairs of genes showing functional correlation. The first pair of genes is prolyl 4-hydroxylase (2 fold) related to hydroxyproline (surfactant or collagen moiety) synthesis via hydroxylation of proline (http://www. Cryst.bbk.ac.uk) and cathepsin L (3 fold) which has a role in surfactant C secretion. Both surfactant-related genes were recognised as upregulated in the same cluster. The second pair of genes was phospholipase A2 group 1B (10 fold) related to inflammation and translocation of γGT (Evans *et. al.*, 2001; Touqui and Alaoui-El-Azher, 2001; http://www.bioportfolio.com) and microsomal glutathione S-transferase 1 (13 fold) related to glutathione and the glutamyl cycle. Both genes are related to protecting cells against oxidative stress.

K-means clustering showed that two of the 20 clusters of genes were down regulated. Cluster D (Table 6. 2) was composed of four genes having different functions but two genes (guanine nucleotide-binding protein, TNF (ligand)) were recognised as downregulated from a simple quantitative analysis. The second group (Cluster E) contains five genes (TIF2, Zinc-finger transcription factor, NOS3, cartilage oligomeric matrix protein, mitochondrial hydroxymethylglutaryl-CoA lyase), which were perceived as downregulated and these genes are mainly related to cancer or early response genes.

6. 3. 2. 3 Inflammation and lipoproteinosis; changes in mRNA expression profile of the lungs from CRS (5.0 mg)-exposed animals for 13 weeks

The conventional quantitative biochemical and histochemical analyses detected inflammation and lipoproteinosis related changes in the CRS-exposed lungs for 13 weeks. A simple quantitative analysis showed changes in 28 genes of which 12 were upregulated and 16 downregulated (Table 6. 3). The upregulated genes are involved in metabolism (3) inflammation (2) and ribosomal proteins (3). The downregulated ones are related to metabolism (6), transcription (4), and cell signalling (3). Of particular

Table 6. 3 The list of the up/downregulated genes in the CRS exposed lungs for 13 weeks. (Key as Table 6. 1 and 2)

Upregulated					
A simple Quantitative analysis		K-means clustering	Gene/Protein Name	Gene/Protein Classification	
U82591	56	U82591	growth-related c-myc-responsive protein RCL	cell-cycle	A
L00313	9	L00313	cytochrome P450 IIB1	xenobiotic metabolism	B
L08831	267	L08831	Glucose-dependent insulinotropic peptide	cellular communication	B
L40030	26	L40030	placenta growth factor	inflammation	B
X16956	16	X16956	prostaglandin receptor F2a	inflammation	B
M94043	55	M94043	RAB-related GTP-binding protein	intracellular transducer	B
X59051	2	X59051	Ribosomal protein S29	ribosomal proteins	B
X78167	3	X78167	ribosomal protein L15	ribosomal proteins	B
	2	V01217	cytoplasmic beta-actin	cytoskeleton and motility protein	B
	2	X14221	surfactant protein C	surfactant protein	B
M36589	38	M36589	nerve growth factor beta	growth factors	C
X82551	7	X82551	Ribosomal protein L39	metabolism	C
D17615	16	D17615	Tyrosine 3-monooxygenase/	metabolism	
J03752	57	J03752	microsomal glutathione S-transferase 1	link to inflammation	C
	48	D30035	thioredoxin peroxidase 2		C
	4	M17698	thymosin beta-10		C
	15	S45392	heat shock 90-kDa protein beta		C
	7	X14878	thioredoxin		C
	8	M21730	Annexin V	Channel/ link to inflammation	C
	4	D10728	Lymphocyte antigen CD5	immune system	C
	2	D16554	Polyubiquitin	stress response	C
	3	X62952	vimentin	stress response	C
	12	J03026	Adrenergic, beta 2-, receptor, surface	structural protein	
	23	L11004	Solute carrier family 9	channels	C
	3	Y13714	osteonectin	channels	C
	5	M17528	tissue inhibitor of metalloproteinase 2	metabolism	C
	6	M18668	Creatine kinase, brain	Energy metabolism	C
	4	X14209	cytochrome c oxidase, subunit IV	Energy metabolism	C
	30	U56853	cytochrome P450; 21-hydroxylase	xenobiotic metabolism,	C
	6	M93661	notch homolog 2	oncogens and tumour suppressors,	C
	2	V01218	calcitonin	microfilament proteins	C
	8	X63369	GOS24 (zinc finger transcriptional regulator)	transcription/translation	C C
	2	L31884	guanine nucleotide-binding protein	G proteins	C

Downregulated

A simple Quantitative Analysis		K-means Clustering	Gene/Protein Name	Gene/Protein Classification	
AB003400	8	AB003400	D-amino acid oxidase	metabolism	D
AF120100	25	AF120100	thiopurine methyltransferase	xenobiotic metabolism	D
Y10054	28	Y10054	mitochondrial hydroxymethylglutaryl-CoA lyase	Energy metabolism	D
AH005431	*	AH005431	follistatin	signalling	D
X57018	28	X57018	fgr proto-oncogene	signalling	D
	39	L29090	guanine nucleotide-binding protein	G proteins	D
AF136943	83	AF136943	transcriptional intermediary factor 2	Transcription/translation	E
L24804	8	L24804	23-kDa progesterone receptor-associated protein	↕	E
					E
M65008	250	M65008	zinc finger transcriptional activator	Transcription/translation	E
U02534	8	U02534	nitric oxide synthase 3 (NOS3)	metabolism	E
	59	X72914	cartilage oligomeric matrix protein	structural protein	E
AF072439	35	AF072439	zinc finger protein 37	Transcription/translation	F
L12407	7	L12407	carbonic anhydrase III	metabolism	F
Y17295	4	Y17295	thiol-specific antioxidant protein	metabolism	F
M94152	7	M94152	adenosine A3 receptor	signalling	F
X12752	*	X12752	CCAAT/enhancer-binding protein alpha	stress response protein	F
X55288	*	X55288	CD28 T-cell surface antigen	cell surface antigen	F
	11	M20623	Dopamine beta hydroxylase	metabolism	F
	7	S68245	carbonic anhydrase 4	↕	F
	7	X94371	copper-zinc-containing superoxide dismutase 3 (Cu-Zn SOD3)	metabolism	F
	10	M22413	testis-specific cytochrome c	Energy metabolism	F
	4	U02074	dentin sialophosphoprotein	functionally unclassified proteins	F
	6	U06436	RANTES	immune system proteins	F
	12	U12187	ras associated with diabetes protein	intracellular transducers	F
	4	U94340	poly(ADP-ribose) polymerase	DNA metabolism	F
	20	X57405	notch homolog 1	oncogens and tumour suppressors	F
	7	L11667	cyclophilin 40	Transcription/translation	F
	26	Z17223	Gax, growth-arrest-specific protein	Transcription/translation	F
M24393	*		Myogenin	Transcription/translation	F

interest to this study is the upregulation of placenta growth factor (26-fold), a known marker of acute chest pain (www.hprd.org) and prostaglandin receptor F2a (16-fold) which has a role in platelet stimulation and aggregation (MacIntyre et. al., 1978). Furthermore, substantial upregulation (57 fold) was seen with microsomal glutathione S-transferase 1 which is important for detoxification and protection against oxidative stress. In addition, RAB-related GTP binding protein (absolute function unknown) was upregulated (55 fold) and immunolocalisation of this gene product is thought to be specific to lung epithelial type 2 (and Clara) cells (Osanai et. al., 2001).

K-means clustering recognised six gene groups (A-F) (Table 6. 3) where commonality was apparent with respect to simple analysis. In respect of inflammation, five additional candidate genes (four already detected in MA-exposed lungs at 49 weeks, Table 6. 2, cluster C) were recognised in cluster C (Table 6. 3). Thioredoxin (5-fold) and its peroxidase 2 (48-fold) are important to protect cells against oxidative stress (Koike et. al., 2002). Annexin V functions as a vascular anticoagulant and thymosin beta 10 is proinflammatory and detected in proliferating tissue (Johansson et. al., 2003). Heat shock protein 90 kD has a role in IL-6 gene induction/signalling (Moseley, 1998; Sato et. al., 1989)

K-means clustering (particularly clusters D, E and F which were downregulated) identified large number of genes (14 out of 28) which had already been shown to be changed during the ageing process in healthy animals at 49 weeks post-instillation (Table 6. 3). It would therefore seem that these sensitive marker candidates for the ageing process were downregulated prematurely (at 13 weeks post-instillation) in the CRS-treated lungs.

6. 3. 2. 4 Inflammation, lipoproteinosis and fibrosis; changes in mRNA expression profile of the lungs from CRS (5.0 mg)-exposed animals for 49 weeks

The fibrosis related changes were recognised in the CRS (5.0 mg)-exposed lungs for 49 weeks from the conventional quantitative biochemical and histopathological approaches. A simple quantitative analysis showed 36 gene-changes of which 13 were upregulated and 23 downregulated (Table 6. 4). From simple and K-means clustering

183

Table 6. 4 The list of the up/downregulated genes in the CRS-exposed lungs for 49 weeks. (Key as Table 6. 1 and 2)

Upregulated				
A simple quantitative analysis	K-means clustering	Gene/Protein name	Gene/Protein Classification	
D16554	4	D16554	Polyubiquitin	stress response proteins	A
L08831	4	L08831	Glucose-dependent	extra cellular communication proteins	A
U82591	4	U82591	insulinotropic peptide	cell-cycle related proteins	A
X16956	4	X16956	prostaglandin receptor F2a	inflammation	A
L00313	4	L00313	cytochrome P450 IIB1	xenobiotic metabolism	B
U56853	4	U56853	cytochrome P450; 21-hydroxylase	xenobiotic metabolism,	B
X14221	3	X14221	surfactant protein C	surfactant protien	B
X70871	7	X70871	Cyclin G1	cyclins	B
M15427	4		Murine leukemia viral oncogene homolog 1	oncogens and tumour suppressors	B
M94043	3		RAB-related GTP-binding protein	Intracellular transducers,	B
U06436	5		RANTES	immune system proteins	B
U37026	4		Sodium channel beta 2	channels	B
X59051	3		Ribosomal protein S29	Ribosomal protein	B
	2	D10728	Lymphocyte antigen CD5	immune system proteins	B
	2	M21730	Annexin V	channels, inflammation	B
	3	S45392	heat shock 90-kDa protein beta	inflammation	B
	14	U77697	platelet/endothelial cell adhesion molecule-1	signalling	B
	2	X82551	Ribosomal protein L39	mRNA processing	B

Downregulation

A simple quantitative analysis	K-means clustering		Gene/Protein Name	Gene/Protein Classification	
L29090	6	L29090	guanine nucleotide-binding protein	G proteins	C
U03470	5	U03470	Tumor necrosis factor (ligand)	signalling	C
U12425	5	U12425	cyclic nucleotide-gated channel	channels	C
	4	X72914	cartilage oligomeric matrix protein	structural protein	C
AH005431	3	AH005431	follistatin	signalling	D
M65008	3	M65008	Zinc-finger transcription factor NGFI-C (early response gene)	transcription/translation	D
					D
Y10054	3	Y10054	mitochondrial hydroxymethylglutaryl-CoA lyase	metabolism	D
					D
Y17295	2	Y17295	anti-oxidant protein 2	immune system proteins	D
	4	U06436	RANTES	immune system proteins	D
	2	AF136943	transcriptional intermediary factor 2	transcription/translation	D
	2	Z17223	mesenchyme homeobox	transcription/translation,	D
	2	U02534	2nitric oxide synthase 3 (NOS3)	lipid metabolism	D
	2	V01217	cytoplasmic beta-actin	Energy metabolism	D
	2	X57018	fgr proto-oncogene	metabolism	D
	2	X59051	Ribosomal protein S29	ribosomal proteins	D
AB011365	3	AB011365	Peroxisome proliferator activator receptor, gamma	inflammAtion	E
U02074	3	U02074	Dentine sialoprotein	Dentine sialoprotein	E
X06745	3	X06745	polymerase (DNA directed), alpha	DNA metabolism,	E
AJ222691	5		DNA polymerase delta catalytic subunit	DNA polymerase	E
X98490	5		replication protein A 32-kDa subunit		E
L24804	3		unactive progesterone receptor, 23 kD		E
AF120100	3		thymine-DNA glycosylase		E
X56420	11		N-methylpurine-DNA glycocylase		E
U51166	7		dynein light chain 1	DNA damage repair	E
U66461	7		thiopurine methyltransferase	Xenobiotic metabolism	E
J04810	8		mutS (E. coli) homolog 3	Xenobiotic metabolism	E
X94371	3		Superoxide dimutase 3	metabolism	E
D00753	8		contrapsin-like protease inhibitor related protein	Protease inhibitors	E
J00750	8		metallothionein 1	Functionally unclassified gene	E
J02744	8		glutathione S-transferase mu 3	stress response	E
M65217	8		heat shock transcription factor 2	translation	E
	3	AF072439	zinc finger protein 37	transcription	E
	2	AF095740	ubiquitin-like protein NEDD8		E
	3	D83598	Sulfonylurea receptor 2		E
	3	M24393	Myogenin	transcription	E
	3	M94152	Adenosine receptor A3	G-protein coupled receptors	E
	3	S77858	nonmuscle myosin alkali light chain	cytoskeleton and motility proteins	E
	2	U12187	ras associated with diabetes protein	intracellular transducers	E
	2	X55288	CD28 antigen	signalling	E
	2	X57405	notch homolog 1	signalling	E

185

analyses, three genes (prostaglandin receptor F2a, Annexin V and heat shock protein) were upregulated. Upregulation of these genes was common to lungs treated with MA (49 weeks) and CRS (13 weeks). It would seem therefore that these three genes provide the best markers for the inflammatory processes occurring in the lungs. The macroarray does provide for hybridisation for collagen related moieties (collagen, alpha 1, type 3, collagen IV alpha 3 subunit, fibronectin, Fibroblast growth factor receptor 4, connective tissue growth factor, Fibroblast growth factor 10, fibroblast growth factor 17, TGF-beta 2 short form, transforming growth factor beta 1, Transforming growth factor, beta 3, Fibroblast growth factor 2, fibroblast growth factor 5, fibroblast growth factor receptor 3, transforming growth factor, beta receptor III) but no upregulation was detected in expression of any of these genes for collagen metabolism despite the histopathological results with Masson's trichrome.

In the downregulated clusters (Table 6. 4, groups C-E) once again the changes in genes associated with the ageing process were all detected. Of some importance may be the downregulation of seven genes (simple analysis, Table 6. 4) concerned with DNA metabolism and repair.

6. 4 A comparison of MA/CRS-specific genes using a K-means clustering

The average log value for each MA (5.0 mg)-exposed lungs for 49 weeks (inflammation), CRS (5.0 mg) for 13 (inflammation/lipoproteinosis) and 49 weeks (inflammation/lipoproteinosis/fibrosis) were employed to classify disease-specific genes using the K-means clustering method. These average values have been standardised before the clustering method was applied. There were 20 clusters classified and 8 clusters contained the genes recognised as up/downregulated in one of the MA/CRS-treated lungs (Table 6. 5).

A full comparison of upregulated or downregulated lung genes following MA or CRS exposure is shown in Table 6. 5. The lists were generated in relation to specific clusters (A-F). Both clusters A and C contain all of the genes related to the ageing process (13 to 49 weeks) in healthy sham-treated rats. The large cluster B showed

186

6. 5 The list of the genes in the clusters, which were classified using K-means clustering and contains the genes recognised as up/downregulated. The genes in red characters were upregulated genes and blue were down regulated in each treated group of lung (Key: w=weeks, the genes in grey shade are common in all treated groups, pink are specific to MA, green are specific to CRS, violet are specific to CRS (49 w), yellow are found in both MA (49 w) and CRS (13 w) and in bold characters are lung or inflammation related).

MA (49 w)		CRS (13 w)		CRS (49 w)		Gene/Protein name	Gene/Protein Classification	
D16554	3	D16554	2	D16554	4	polyubiquitin	other stress response proteins	A
U82591	3	U82591	56	U82591	4	growth-related c-myc-responsive protein RCL	cell-cycle	A
V01217	2	V01217	4	V01217	3	cytoplasmic beta-actin	ribosomal proteins	A
X14221	2	X14221	2	X14221	3	surfactant protein C	surfactant protein C	A
X59051	2	X59051	2	X59051	3	40S ribosomal protein S29	ribosomal proteins	A
M20623	1	M20623	11	M20623	1	testis-specific cytochrome c	Enregy metabolism	B
S68245	2	S68245	7	S68245	1	carbonic anhydrase 4	metabolism	B
X17611	1	X17611	4	X17611	1	membrane-associated intestinal alkaline phosphatase		B
M22413	1	M22413	10	M22413	1	carbonic anhydrase III		B
J03572	1	J03572	2	J03572	1	alkaline phosphatase		B
AB003400	1	AB003400	8	AB003400	1	D-amino acid oxidase		B
L12407	1	L12407	7	L12407	2	dopamine beta-hydroxylase		B
X94371	1	X94371	7	X94371	3	copper-zinc-containing superoxide dismutase 3		B
AF095740	1	AF095740	2	AF095740	3	ubiquitin-like protein NEDD8	metabolism	B
AB011365	1	AB011365	7	AB011365	3	peroxisome proliferator-activated receptor gamma	inflammation	B
D00036	3	D00036	5	D00036	2	phospholipase A2 group IB	inflammation	B
D43950	2	D43950	2	D43950	1	T-complex protein 1 epsilon subunit	inflammation	B
AH005431	3	AH005431	*	AH005431	4	follistatin	signalling	B
M27156	2	M27156	48	M27156	1	prostatic secretory protein probasin	signalling	B
X55288	2	X55288	*	X55288	3	CD28 T-cell surface antigen	signalling	B
M94152	1	M94152	7	M94152	3	adenosine A3 receptor	signalling	B
M24393	1	M24393	*	M24393	3	myogenin	transcription	B

X12752	3	X12752	*	2	CCAAT/enhancer-binding protein alpha	transcription	B
X67859	3	X67859	1	2	autoantigen	transcription	B
L36388	3	L36388	7	2	HFH-4	transcription	B
D10864	1	D10864	4	1	inhibitor of DNA-binding protein 3	transcription	B
D13062	2	D13062	2	1	adenylate kinase 3	transcription	B
D55627	2	D55627	50	2	retinoblastoma gene product-related protein	Oncogens and tumour suppressors	B
X57405	2	X57405	20	3	notch homolog 1	oncogens and tumour suppressors	B
M15427	2	M15427	2	3	c-raf proto-oncogene; raf-1	Oncogen and tumour suppressors	B
L11667	1	L11667	7	1	cyclophilin 40	translation	B
L29428	3	L29428	24	2	K-kininogen	immune system proteins	B
L41275	2	L41275	33	3	CDK-interacting protein 1	CDK inhibitors	B
M11670	1	M11670	3	1	liver catalase	stress reponse proteins	B
M23697	1	M23697	3	1	tissue-type plasminogen activator	Serine protease	B
S80439	2	S80439	1	1	OB-cadherin 1	Structural protein	B
U02074	1	U02074	4	3	dentin sialophosphoprotein	functionally unclassified proteins	B
U12187	2	U12187	3	5	ras associated with diabetes protein	intracellular transducers	B
U17837	2	U17837	9	1	retinoblastoma protein-interacting zinc finger protein	cell cycle	B
U37026	2	U37026	7	4	sodium channel, beta 2 subunit, brain	channels	B
U94340	1	U94340	4	1	poly(ADP-ribose) polymerase	DNA damage repair	B
X06745	1	X06745	3	3	DNA polymerase alpha catalytic subunit	DNA polymerase	B
X56600	1	X56600	3	1	mitochondrial superoxide dismutase 2	stress reponse proteins	B
X57986	2	X57986	6	2	cAMP-dependent protein kinase catalytic subunit	intracellular kinease network members	B
AF136943	3	AF136943	83	3	transcriptional intermediary factor 2	Transcription/translation	C
Z17223	1	Z17223	27	3	growth-arrest-specific protein	↔	C
L24804	1	L24804	8	3	23-kDa progesterone receptor-associated protein		C
M65008	3	M65008	250	3	zinc finger transcriptional activator	Transcription/translation	C
U02534	3	U02534	8	3	nitric oxide synthase 3	metabolism	C
Y10054	3	Y10054	28	3	mitochondrial hydroxymethylglutaryl-CoA lyase	Energy metabolism	C

Y17295	1	Y17295	4	Y17295	3	thiol-specific antioxidant protein	metabolism	C
U06436	2	U06436	6	U06436	4	RANTES	immune system protein	C
X57018	2	X57018	28	X57018	1	fgr proto-oncogene	oncogens and tumour suppressors	C
X72914	1	X72914	59	X72914	4	cartilage oligomeric matrix protein	Matirx adhesion receptors	C
D10863	7	D10863	4	D10863	2	inhibitor of DNA binding 2	transcription	D
X63369	5	X63369	8	X63369	1	GOS24 (zinc finger transcriptional regulator)	transcription	D
D10952	2	D10952	2	D10952	1	cytochrome c oxidase polypeptide Vb	Energy metabolism	D
M18668	3	M18668	6	M18668	1	creatine kinase b	Energy metabolism	D
X14209	4	X14209	4	X14209	1	cytochrome c oxidase subunit IV	Energy metabolism	D
U56853	4	U56853	30	U56853	4	cytochrome P450; 21-hydroxylase	xenobiotic metabolism	D
K03502	3	K03502	1	K03502	1	elongation factor 2	xenobiotic metabolism	D
J00801	2	J00801	2	J00801	1	whey acidic protein	metabolism	D
L31884	3	L31884	4	L31884	1	tissue inhibitor of metalloproteinase 2	metabolism	D
X56060	2	X56060	2	X56060	1	deoxyribonuclease I	metabolism	D
D63378	3	D63378	2	D63378	1	probable protein disulfide isomerase ER60	cell adhesion receptors and proteins	D
D86373	3	D86373	4	D86373	1	acyl-CoA:cholesterol acyltransferase	signalling	D
J00717	2	J00717	1	J00717	1	gamma crystallin C	Functionaaly unclassified proteins	D
M36589	1	M36589	40	M36589	1	nerve growth factor beta	Growth factors	D
M85299	3	M85299	3	M85299	1	sodium/hydrogen exchange protein 1	channel	D
M86870	2	M86870	1	M86870	2	endoplasmic reticulum stress protein 72	translation	D
U31867	2	U31867	1	U31867	1	Tclone15	functionally unclassified proteins	D
X02918	2	X02918	1	X02918	1	prolyl 4-hydroxylase	Hydroxylation of proline	D
Y00697	3	Y00697	2	Y00697	1	cathepsin L	Surfacthat secretion	D
X14878	4	X14878	5	X14878	2	thioredoxin	inflammation	D
Y13714	5	Y13714	8	Y13714	1	osteonectin	Structural protein	D
X68282	2	X68282	1	X68282	1	ribosomal protein L13A	Ribosomal proteins	D
X51707	2	X51707	1	X51707	2	40S ribosomal protein S19	Ribosomal proteins	D
D10728	2	D10728	4	D10728	3	T-cell surface glycoprotein CD5	immune system proteins	E

Accession		Accession			Protein	Functional category	
L00313	4	L00313	9	4	cytochrome P450 IIB1	xenobiotic metabolism	E
L08831	4	L08831	269	4	gastric inhibitory polypeptide	extra cellular communication proteins	E
X62952	3	X62952	3	2	vimentin	stress response proteins	E
L40030	2	L40030	26	1	placenta growth factor	inflammation	E
M17698	2	M17698	2	1	thymosin beta 10	inflammation	E
M21730	3	M21730	3	3	annexin V	inflammation	E
X16956	5	X16956	16	4	prostaglandin receptor F2a	inflammation	E
S45392	6	S45392	7	3	heat shock 90-kDa protein beta	Lung epthelial type 2 cell	E
M94043	2	M94043	55	2	RAB-related GTP-binding protein	inflammation	E
S77858	1	S77858	2	3	nonmuscle myosin alkali light chain	cytoskeleton and motility proteins	E
X82551	3	X82551	7	3	60S ribosomal protein L39	ribosomal proteins	E
X78167	3	X78167	3	2	ribosomal protein L15	mRNA metabolism	E
D17615	3	D17615	16	1	tyrosine 3-monooxygenase	metabolism	F
J03026	5	J03026	12	2	matrix Gla protein	lipid metabolism	F
M21208	2	M21208	3	1	cytochrome P450 17	lipid metabolism	F
M20622	2	M20622	2	1	cytochrome c expressed in somatic tissues	lipid metabolism	F
J03752	13	J03752	57	6	microsomal glutathione S-transferase 1	Energy metabolism	F
D30035	4	D30035	48	1	thioredoxin peroxidase 2	inflammation	F
J02701	2	J02701	3	2	sodium/potassium-transporting ATPase beta 1 subunit	inflammation	F
L11004	4	L11004	23	1	sodium-hydrogen exchange protein-isoform 2	ATPase transporters	F
M17528	2	M17528	15	1	guanine nucleotide-binding protein G(I) alpha 2 subunit	translational	F
M81687	1	M81687	1	3	ryudocan/syndecan 2	G proteins	F
M93661	2	M93661	6	2	notch homolog 2	Cytoskeleton and motility proteins	F
U65656	1	U65656	2	5	gelatinase A	signalling	F
V01218	2	V01218	2	5	skeletal muscle alpha-actin; alpha-actin 1	Structural protein	F
X98517	1	X98517	3	1	macrophage metalloelastase	microfilament proteins	F

very few changes in the lungs exposed to MA but in contrast has seven common downregulated genes (of diverse function) in CRS treated lungs. With the possible exception of copper zinc containing superoxide dismutase 3, none of these genes have any clear link to the inflammatory process.

Collective consideration of cluster D, E, and F showed that 12 genes were upregulated in MA (49 weeks) and CRS (13 weeks) but not in CRS (49 weeks) where the inflammatory process may well have subsided and focal fibrosis is in place. Thus, it would seem that these 12 genes may represent the best candidate markers of inflammation.

The cluster F included 14 but none of these genes was changed in the CRS (49 weeks. Focal fibrosis)-exposed lungs. Four genes (tyrosine 3-monooxygenase, matrix Gla protein, microsomal glutathione S-transferase 1, sodium-hydrogen exchange protein-isoform 2) were upregulated in both the MA (49 weeks) and CRS (13 weeks)-exposed lungs which showed inflammatory responses. Four genes (thioredoxin peroxidase 2, guanine nucleotide-binding protein, notch homolog 2, skeletal muscle alpha-actin) in this cluster were upregulated only in the CRS-exposed lungs for 13 weeks. These characteristics suggested that this cluster could be closely related to inflammation in the lungs.

6. 5 Discussion

A commercial gene expression system (macroarray) was employed to investigate inflammatory, lipoproteinosis and fibrotic responses to treatment with volcanic ash (MA) and its major bioreactive component (CRS).

There are a number of characteristics of the array procedure, which need close attention. These include knowledge of animal intervariability, the quantity or quality of the mRNA extracted from the lungs, non-specific hybridisation of probes and commercial nylon membrane quality for the array. Other factors include establishing the correct specificity of $[\alpha\text{-}^{32}P]$ ATP, the activity of reverse transcriptase and

exposure procedure. All of these issues are critical in the production of suitable array data. Once these and reproducibility were established, decisions had been taken on the analysis of these data.

The approach adopted was a simple quantification of intensity of cDNA hybridised with mRNA extracted from the lungs based on a five-fold change relative to tissue from an age-matched sham-treated animal. This stringent analysis was relaxed using K-means clustering (Alon *et. al.,* 1999; Eisen *et. al.,* 1998; Tamayo and Ramaswamy, 2002) to include the identification of genes changing in a similar manner but not necessarily 5-fold from that detected in sham-treated lungs.

Studies of healthy animal lungs at 13 and 49 weeks post-sham instillation established that 12/24 (a simple quantitative analysis/K-means clustering) genes were affected during the ageing process. The majority of these genes were changed and appeared with regularity in gene expression lists derived from the rat lungs treated with the MA or the CRS. Thus, it is unlikely that these genes have any direct specificity to the inflammatory process induced by MA or CRS.

However, a number of other candidate gene inflammatory markers were identified. Primary candidates would include microsomal glutathione S-transferase 1 (57 fold increase), placenta growth factor (26 fold increase) and thioredoxin peroxidase (48 fold) although more minor changes were detected with a further 15 genes.

Inflammation apart, the gene expression study suggested that epithelial cell changes were also taking place in the lung. Notable was the upregulation of SP-C but this seemed to be related to the ageing process. Lungs treated with MA (49 weeks) showed upregulation of another type 2 epithelial cell specific marker (SP-A). In addition, CRS treated lungs (13 weeks) where lipoproteinosis is considered likely showed an upregulation in RAB-related GTP binding protein, a specific marker of lung epithelial type 2 (or Clara) cells.

No candidate gene markers could be identified for fibrosis. It is possible that the chosen Atlas array had insignificant markers to detect fibrosis and this could be overcome by using a more specific array system. Alternatively, the stringent analysis employed was too insensitive to detect any fibrotic changes which histopathology has established to be very focal in localisation. Thus, insufficient mRNA related to fibrotic changes may not have been present in the lung isolate.

In conclusion, the macroarray technology has provided additional information on MA and CRS induced inflammation. The candidate genes identified now need further confirmation and quantification using alternative techniques such as qunatitative PCR (Q PCR), northern blotting or *in situ* hibridisation studies.

7 General discussion

7. General discussion

Following the eruption of ash with a high content of toxic crystalline silica from the volcano on the Soufriere hills on Montserrat, concern was expressed for the health of the island's residents. In response, the present project was undertaken to explore the bioreactivity of ash and the effects of different levels of exposure to it. A multidisciplinary *in vivo* study using rats was designed based on the worst-case scenario using a high dose (up to 5.0 mg of single instillation) of ash itself, ANR (known to be minimally bioreactive) and CRS (known to be toxic), which are two major components of the MA.

The rats were exposed to three different doses (1.0, 2.5 and 5.0 mg) of the particles by a single instillation and then sacrificed at four different time points (6, 13, 25 and 49 weeks). The standard dose for a single instillation is 1.0 mg whereby bioreactive minerals such as crystalline silica produce inflammation within 12 weeks. This dose and period were extended to 5.0 mg and 49 weeks in order to find whether long-term exposure resulted in progressive inflammation or fibrosis in the lung. It was possible that the instillation of such a high dose of even inert mineral as a one off aggressive dose could cause lung "overload" and set up inflammatory reactions. However, this did not prove to be the case and indeed animals exposed to 5.0 mg of ANR for period of up to 49 weeks showed very few, if any, changes from those seen in sham-treated rats. Thus, ANR, which is minimally bioreactive, was well tolerated when instilled into the lungs at such a high dose (5.0 mg).

The changes induced by the particles instilled into the lung were examined using quantitative biochemical and cellular, and semi quantitative histopathological methods. Epithelial lining fluid alkaline phosphatase and γGT activities were employed to examine the changes in epithelial type 2 cells but no significant differences were found among sham, ANR, MA or CRS—exposed groups. It may well be that a 6-week exposure period was too late to detect such enzymatic changes at the lung surface. These enzyme markers could prove more suitable for a short-term exposure study such as 1 or 3 days following instillation or may be better markers for *in vitro* assays.

In contrast, the number of PMNs recovered from the lung lavage was a very sensitive marker to detect persistent inflammatory changes in the lungs. However, it was noted that once CRS had been in the lung for a long time (49 weeks) few PMN's could be detected in lavage fluid and this was coincidental with elevated hydroxyproline levels in lung parenchyma. Histopathological examination of such CRS-treated lungs confirmed fibrosis and that it was accompanied by interstitial thickening and cell debris. Therefore, it was surmised that the efficiency of the lavage process decreases with progressive disease development and thus once this occurs accurate quantification of PMN's (or other cells) in lavage may not be possible. Such a finding clearly showed the importance of running histopathological assessment alongside the quantitative conventional cellular approaches.

The importance of running biochemical/cellular investigations parallel with histopathological approaches was suggested again as the research progressed. Both hydroxyproline (found in collagen and surfactant protein-A and D moieties) levels in the lung (quantitative biochemical approaches) and Masson's trichrome staining (semi quantitative histopathological method) were employed in order to detect changes related to fibrosis in the lung. Both the hydroxyproline level and the area stained green by Masson's trichrome in the lung were increased significantly by CRS (5.0 mg) at 13 and 49 weeks post-exposure. However, histopathology successfully visualised the differences in these increases at 13 weeks post-instillation. Most of the regions stained green were the MACs or alveolar septa without alveolar wall thickening. In contrast, most of the regions stained green at 49 weeks post-instillation were interstitial regions associated with alveolar wall thickening. These differences suggested that the increases in the hydroxyproline level and the area stained green by Masson's trichrome were caused by lipoproteinosis (increase in surfactant protein) at 13 weeks post-exposure but those increases were attributable to fibrosis at 49 weeks. This raised the point that future work could investigate lipoproteinosis in the lung using immunostaining with specific antigens such as surfactant protein-A (SP-A) or surfactant protein-D (SP-D) in order to compare the regions stained with these antigens or Masson's trichrome. Equally, antigens to specific types of collagen (e.g. type 1 or 3) might be employed to monitor the onset of fibrosis.

Histopathology revealed earlier changes (at 13 weeks post-instillation) in thoracic lymph nodes (Size augmentation, granulomas) caused by instilled MA before inflammation was noted in the lung tissue (at 49 weeks). Particle depositions were recognisable in the granulomatous area in thoracic lymph nodes by light microscopy of sections. Moreover, BSE images using E-SEM suggested that most of the particles drained from the lung were deposited in the granulomatous area in the lymph nodes and those remaining in the lung were in the alveolar MACs. Furthermore, compositional analysis using EDX associated with E-SEM suggested a higher content of crystalline silica in the MA deposited in thoracic lymph nodes than those in the MA remaining in the lung or the original instilled MA. These phenomena support the hypothesis that the granulomatous symptoms in thoracic lymph nodes were caused by the crystalline silica component of the MA drained by MACs from the lung. Furthermore, the higher crystalline silica contents of the MA deposited in the nodes explain why the granulomatous symptoms in the lymph nodes were caused 36 weeks earlier than inflammation in the lung. Therefore, the size augmentation and the granuloma in thoracic lymph nodes are very sensitive early markers for assessment of the bioreactivity of silica containing mineral dusts instilled into the lung.

When the results gained from these investigations into the changes in lung and lymph nodes caused by a single instillation of mineral dust were integrated, links could be made between different biological endpoints in the lung from the average size of thoracic lymph nodes (Figure 7. 1). By deduction lung inflammation developed when the average size of the lymph nodes increased from two to four times their normal size. Furthermore, fibrosis was triggered during the period that the size of the lymph nodes had already reached near the maximum size (>4 times). It is possible that these observations may be useful in clinical diagnosis of mineral-induced damage in human subjects exposed to MA. Size augmentation of thoracic lymph nodes detected from patient radiographs could be used to determine the risk potential for inflammatory/ fibrotic effects in the lungs.
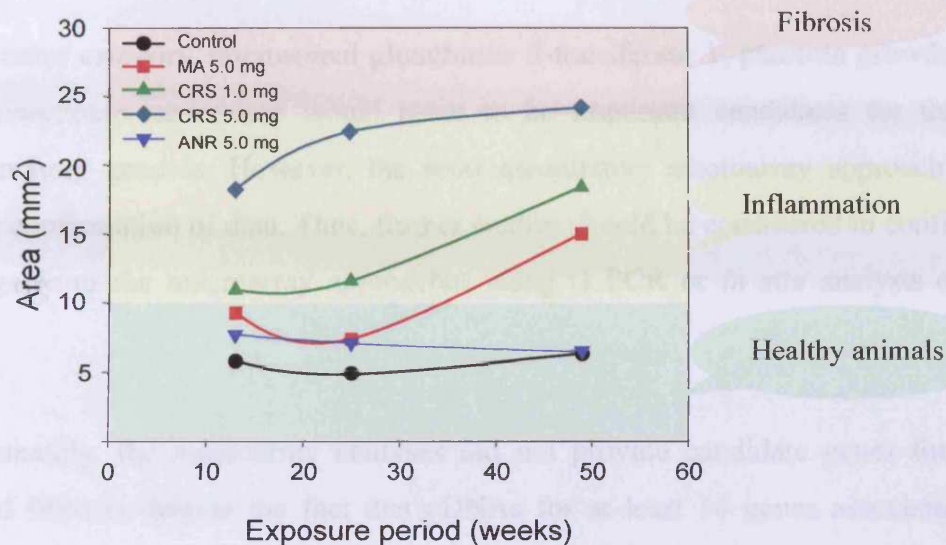
Figure 7. 1 The diagram shows the changes in the average size of the lymph nodes from sham, MA (5.0 mg), CRS (1.0 or 5.0 mg) or ANR (5.0 mg)-exposed animals for 13, 25 or 49 weeks linked to different biological endpoints in the lung.

The degree of size changes in nodes and lung effects in rats were closely related to crystalline silica content in that ANR produced very similar profiles to those noted in sham-treated animals (Figure 7. 1). In support of this, the MA (5.0 mg) containing approximately 1.0 mg of crystalline silica demonstrated similar trends in the size augmentation in thoracic lymph nodes with exposure-time when compared to the trends in the changes in the sizes of the lymph nodes from the pure CRS (1.0 mg)-exposed animals. These phenomena suggested that the crystalline silica content in the MA would be the key factor to explain the bioreactivity of the MA.

The effect on gene expression in the MA or CRS-treated lungs was further investigated using a macroarray. This commercial system is relatively inexpensive and available to all laboratories thus providing the opportunity for production of comparable data. Bioinformatic analyses are still evolving and often laboratory specific. K-means clustering utilised in these studies, whilst producing some substantial gene lists, were considered useful in grouping genes with linked function.

198

From the data obtained this was evident in grouping genes associated with the ageing process in healthy animals and genes associated with inflammation.

In the latter category, microsomal glutathione S-transferase 1, placenta growth factor and thioredoxin peroxidase would seem to be important candidates for the lung inflammatory process. However, the semi quantitative macroarray approach needs further confirmation of data. Thus, further studies should be considered to confirm the findings from the macroarray approaches using Q PCR or *in situ* analysis of lung tissue.

Unfortunately, the macroarray analyses did not provide candidate genes for CRS-induced fibrosis despite the fact that cDNAs for at least 14 genes associated with collagen metabolism were present on the array.

The reasons for this discrepancy are unknown but the most likely explanation is that CRS causes very focal fibrosis and thus most of the mRNA derived from the lung was from non-fibrotic tissue. Thus, there may be a sensitivity issue to overcome in further studies. Micro-dissection, using laser ablation, might overcome this problem.

Overall the outcomes from the macroarray work certainly suggest helpful approaches for the further study of dust-induced mechanisms of lung change. In addition, it would be interesting to monitor the primary effects on gene expression of CRS on granuloma formation in thoracic lymph nodes using the macroarray technology.

References

References

Adamson, I. Y. R. and Hedgecock, C. (1995) Patterns of particle deposition and retention after instillation to mouse lung during acute injury and fibrotic repair. *Exp. Lung. Res.* 21:695-709.

Adamson, I. Y. and Prieditis, H. (1998) Silica deposition in the lung during epithelial injury potentiates fibrosis and increases particle translocation to lymph nodes *Exp. Lung Res.* 24: 293-306

Alon, U., Barkai, N., Notterman, D. A., Gish, K., Ybarra, S., Mack, D. and Levine, A. J. (1999) Broad patterns of gene expression revealed by clustering analysis of tumor and normal colon tissue probed by oligonucleotide arrays. *Proc. Natl. Acad. Sci. USA* 96: 6745-6750

American Thoracic Society. (1997) Adverse effects of crystalline silica exposure. *Am. J. Respir. Crit. Care.* Med. 155:761-765.

Baxter, P. J., Bonadonna, C., Dupree, R., Hards, V. L., Kohn, S. C., Murphy, M. D., Nichols, A., Nicholson, R. A., Norton, G., Searl, A., Sparks, R. S., and Vickers, B. P. (1999) Cristobalite in volcanic ash of the Soufriere Hills volcano, Montserrat, British West Indies. *Science* 283:1142-1145.

Beck, B. D., Brain, J. D. and Bohannon, D. E. (1981) the pulmonary toxicity of an ash sample from the Mt. St. Helens volcano. *Exp. Lung Res.* 2: 289-301.

Blum, A. E. and Stillings, L. L (1995) Feldspar dissolution kinetics In: Reviews in Mineralogy : Chemical weathering rates of silicate minerals (eds White A. F and Brantley S. L). Mineralogical society of America, USA, pp 291-304

Bradford, M. M. (1976) A rapid and sensitive method for the quantification of microgram quantities of protein utilising the principle of protein-dye binding. *Anal. Biochem.* 72:248-254.

Brent, R. (1999) Functional genomics: Learning to think about gene expression data *Curr. Biol.* 9: R338-341

Buist, A. S, Vollmer, W. M, Johnson, L. R, Bernstein, R. S and McCamant (1986). A four-year prospective study of the respiratory effects of volcanic ash from Mt. St. Helens *Am Rev. Respir. Dis.* 133: 526-534

Castranova, V, Bowman, L, Shreve, JM, Jones, GS and Miles, PR (1982). Volcanic ash: Toxicity to isolated lung cells. *J Toxicol. Environ Hlth.* 9: 317-325

Craighead, J. E., Adler, K. B., Butler, G. B., Emerson, R. J., Mossman, B. T., and Woodworth, C. D. (1983) Biology of disease: Health effects of Mount St. Helens volcanic dust. *Lab. Invest.* 48:5-12.

Crouch, E., Persson, A., Chang, D., and Parghi, D. (1991) Increased accumulation in silica-induced pulmonary lipoproteinosis *Am. J. Pathol.* 139: 765-776

Dai, J., Gilks, B., Price, K., and Churg, A. (1998) Mineral dust directly induce epithelial and interstitial fibrogenic mediators andmatrix components in the airway wall *Am. J. Respir. Crit. Care. Med.* 158:1907-1913

Davis, G. S., Holmes, C. E., Pfeiffer, L. M., and Hemenway, D. R. (2001) Lymphocytes, lymphokines and silicosis. *JEPTO* 20:53-65.

Devlin T. M. (1993) 'Textbook of biochemistry with clinical correlation' (3rd. edn), PP 230-231, 437-438, 465-466, 523-525

Driscoll, K. E., Costa, D. L., Hatch, G., Henderson, R., Oberdorster, G., Salem, H., and Schlesinger, R. B. (2000) Intratracheal instillation as an exposure technique for the evaluation of respiratory tract toxicity: Uses and limitations *Toxicol. Sci.* 55: 24-35

Driscoll K. E., Maurer J. K., Lindenschmidt R. E., Romberger D., Rennard S. I., and Crosby L. (1990) Reparatory tract responses to dust: relationships between dust burden, lung injury, alveolar macrophage fibronectin release, and the development of pulmonary fibrosis *Toxic. Appl. Pharm* 106: 88-101

Eisen, M. B., Spellman, P., T., Brown, P. O. and Botstein, D. (1998) Cluster analysis and display of genome-wide expression patterns Proc. *Natl. Acd. Sci. USA* 95:14863-14868

Evans, J. H., Spencer D. M., Zweifach, A. and Leslie C. C. (2001) Inracellular calcium signals regulating cytosolic phospholipase A2 translocation to internal membranes. *J. Biol. Chem.* 276:30150-30160

Farrell, P. M. (1982) Morphologic aspects of lung maturation In: Lung development: Biological and clinical prospective (eds Farrell P. M.), vol. 1 Acadmic press, New York pp 13-26

Friedetzky, A., Garn, H., Kirchner, A., and Gemsa, D. (1998) Histopathological changes in enlarged thoracic lymph nodes during the development of silicosis in rats. *Immunobiology* 199:119-132.

Fubini, B. and Arean, C. O., (1999) *Chemical aspects of the toxicity of inhaled mineral dusts. Chem. Soc. Rev.* 28:373-381

Fubini, B., Bolis, V., Cavenago, A., and Volante, M. (1995) Physicochemical properties of crystalline silica dusts and their possible implication in various biological responses. *Scan. J. Work Environ. Health* 21:9-14

Fubini, B., Zanetti, G., Altilia, S., Tiozzo, R., Lison, D., and Saffiotti, U. (1999) Relationship between surface properties and cellular responses to crystalline silica: Studies with heat-treated cristobalite. *Chem. Res. Toxicol.* 12: 737-745.

Fulmer, J. D. and Crystal, R. G. (1976) The biological basis of pulmonary function In: The biological basis of pulmonary function (eds Crystal, R. G.) Marcel Dekker, INC. New York pp 419-466

Garn, H., Friedetzky, A., Davis, G. S., Hemenway, D. R. and Gemsa, D. (1997) T-lymphocyte activation in the enlarged thoracic lymph nodes of rats with silicosis *Am. J. Respir. Cell Mol. Biol.* 16:309-316

Gordon, T. and Amdur, M. O. (1991) Responses of the respiratory system to the toxic agents In: Toxicology (4th edn), (eds Casarett and Dowlls) Pergamon press, pp 383-406

Governa M., Valentino M., Tosi P., Luzi P., Miracco C., Sartorelli E., Loi F., Franzinelli A., and Gori R. (1986) Pulmonary alveolar lipoproteinosis in rats following intratracheal injection of pyrite particles *J of Toxicol and Envrion Health.* 19: 403-412

Green, F. H., Vallyathan, V., Mentnech, M. S., Tucker, J. H., Merchant, J. A., Kiessling, P. J., Antonius, J. A, and Parshley, P. (1981) Is volcanic ash a pneumoconiosis risk? *Nature* 293: 216-217.

Hemenway, D. R., Absher, M. P., Fubini, B., and Bolis, V. (1993) What is the relationship between haemolytic potential and fibrogenicity of mineral dust? *Arch. Environ. Health* 48: 343-347.

Henderson, R. F., Driscoll, K. E., Harkema, J. R., Lindenschmidt, R. C., Chang, I-Y., Maples, K. R., and Barr, E. B. (1995) A comparision of the inflammatory responses of the lung to inhaled versus instilled particles in F344 rats. *Fund. Appl. Toxic.* 24: 183-197

Housley, D. G., Berube, K. A., Jones, T. P., Anderson, S., Pooley, F. D., and Richards, R. J. (2002) Pulmonary epithelial response in the rat lung to instilled Montserrat respirable dusts and their major mineral components. *Occup. Environ. Med.* 59: 466-472.

Hughes, J. M., Weill, H., Checkoway, H., Jones, R. N., Henry, M. M., Heyer, N. J., Seixas, N. S., and Demers, P. A. (1998) Radiographic evidence of silicosis risk in the diatomaceous earth industry. *Am. J. Respir. Crit. Care. Med.* 158: 807-814.

Huszar, G., Maiocco, J., and Naftolin, F. (1980) Monitoring of collagen and collagen fragments in chromatography of protein mixtures. *Anal. Biochem.* 105: 424-429.

Johansson, U., Olsson, A., Gabrielsson, S., Nilsson, B., and Korsgren, O. (2003) Inflammatory mediators expressed in human islets of Langerhans: implications for islet transplantation *Biochem. Biophys. Res. Commun.* 308: 474-479

Johnson, K. G., Loftsgaarden, D. O., and Gideon, R. A. (1982) The effects of Mount St. Helens volcanic ash on the pulmonary function of 120 elementary school children. *Am. Rev. Repir. Dis.* 126: 1066-1069.

Jones, T. P. (2000) Earth Science Dep. Cardiff University pers comm

Khubchandani, K. R. and Snyder, J. M. (2001) Surfactant protein A (SP-A): the alveolus and beyond. *FASEB* 15: 59-69.

Kinsley, D. H., Rye, K., Boggs, S., Tovey, N. K (1998) 'Backscattered scanning electron microscopy and image analysis of sediments and sedimentary rocks' Cambridge university press, UK, pp 4-35

Koike, E., Hirano, S., Shimojo, N. and Kobayashi, T. (2002) cDNA microarray analysis of gene expression in rat alveolar macrophages in response to organic extract of diesel exhaust particles *Toxicological sciences* 67:241-246

Kuhn, III C. (1976) The cells of the lung and their organelles In: The biological basis of pulmonary function (ed Crystal, R. G.) Marcel Dekker INC. New York pp 3-48

Kuempel, E. D., O'Flaherty, E. J., Stayner, L. T., Smith, R. J., Green, F. H. Y., and Vallyathan, V. (2001) A biomathmatical model of particle clearance and retention in the lung of coal miners *Regulatory Toxicology and Pharmacology* 34: 69-87

Kwok-wai Lam, Chin-Yang Li, Lung T. Yam, Smith R. S., and Hacker B. (1982) Composition of prostatic and non prostatic acid phosphatse In: Prostatic acid phosphatase measurement: its role in detection and management of prostatic cancer. (eds Shaw L. M., Romas N. A., Cohens H.) Annals of New York Academy of sciences, New York Academy of sciences, 390: 1-15

Le Bouffant, L., Daniel, H., Martin, J. C., and Bruyere, S. (1982) Effect of impurities and associated minerals on quartz toxicity. *Am. Occup. Hyg.* 26: 625-634.

Martin, T. R., Chi, E. Y., Covert, D. S., Hodson, W. A., Kessler, D. E., Moore, W. E., Altman, L. C., and Butler, J. (1983) Comparative effects of inhaled volcanic ash and quartz in rats. *Am. Rev. Respir. Dis.* 128: 144-152

Martin, T. R., Ayars, G., Butler, J., and Altman, L. C. (1984) The comparative toxicity of volcanic ash and quartz. Effects on cells derived from the human lung. *Am. Rev. Respir. Dis.* 130: 778-782.

Mason, R. J., Greene, K., and Voelker, D. R. (1998). "Surfactant protein A and surfactant protein D in health and disease." *Am. J. Physiol.* 275:L1-L13

Morrow, P. E., Haseman, J. K., Hobbs, C. H., Driscoll, K. E., Vu, V., and Oberdorster, G. (1996) The maximum tolerated dose for inhalation bioassays: toxicity vs overload. *Fund. Appl. Toxic.* 25:155-167

Moseley, P. L. (1998) Heat shock proteins and the inflammatory response. *Ann. N Y Acad. Sci.* 856: 206-213

Mossman B. T., and Churg A. (1998) Mechanisms in the pathogenesis of asbestosis and silicosis *Am. J. Repir. Cirt. Care. Med.* 157: 1666-1680

Muhle, H., Kittel, B., Ernst, M., Mohr, U., and Mermelstein, R. (1995) Neoplastic lung lesions in rat after chronic exposure to crystalline silica *Scan J. Work Environ. Health* 21: 27-29

Murphy, S. A., BeruBe, K. A., Pooley, F. D., and Richards, R. J. (1998) The response of lung epithelium to well characterised particles. *Life Sci.* 62: 1789-1799.

Nash, T., Allison, A. C., and Harington, J. S. (1966) Physicochemical properties of silica in relation to its toxicity. *Nature* 210: 259-261

Olenchock, SA, Mull, JC, Mentnech, MS, Lewis, DM and Bernstein, RS (1983) Changes in humoral immunologic parameters after exposure to volcanic ash, *J. Toxicol. Environ. Hlth.* 11: 395-404.

Osanai, K., Iguchi, M., Takahashi, K., Nambu, Y., Sakuma, T., Toga, H., Ohya, N., Shimizu, H., Fisher, J. H. and Voelker, D. R. (2001) Expression and localization of a novel Rab small G protein (Rab38) in the rat lung, *Am J Pathol.* 158:1665-1675

Piguet, P. F., Van, G. Y. and Guo, J. (1996) Heparin attenuates bleomycin but not silica-induced pulmonary fibrosis in mice: possible relationship with involvement of myofibroblasts in bleomycin and fibroblasts in silica-induced fibrosis, *Int. J. Exp. Path.* 77: 155-161

Prescott, D. M. (1998) 'Cells: Principles of molecular structure and function' Jones and Burtlett publishers, Boston, PP 169-170,

Quinn, G. P. and Keough, M. J. (2002) Experimental design and data analysis for biologists. Cambridge university press. Cambridge

Raub, J. A., Hatch, G. E., Mercer, R. R., Grady, M., and Hu, P. C. (1985) Inhalation studies of Mt. St. Helens volcanic ash in animals. II. Lung function, biochemistry and histology. *Environ. Res*. 37: 72-83.

Reiser, K. M., Hascheck, W. M., Hesterberg, T. W., and Last, J. A. (1983) Experimental silicosis: Long term effects of intratracheally instilled quartz on collagen metabolism and morphologic characteristics of rat lungs *Am. J. Pathol.* 110:30-41

Reynolds, L. J and Richards, R. J (2001) Can toxicogenomics provide information on the bioreactivity of diesel exhaust particles? *Toxicology* 165: 145-152

Richards, R. J, BeruBe, K. A, Masaek, L, Symons, D and Murphy, S. A. (1999) The biological effects on lung epithelium of well-characterised fine particles In: Particulate matter (eds Maynard R. L. and Howard C. V.). BIOSI Scientific Publishers, Oxford, pp 97-113

Richards, R. J. and Curtis, C. G. (1984) Biochemical and cellular mechanisms of dust-induced lung fibrosis. *Environ. Health Perspec*. 55: 393-416.

Richards, R. J., Masek, L. C., and Brown, R. F. (1991) Biochemical and cellular mechanisms of pulmonary fibrosis. *Toxicol. Pathol*. 19: 526-539.

Robinson, AV and Schneider, RP (1982). In vitro toxicity of Mount St. Helens volcanic ash: Final report to NIEHS on Task 3, Health effects of Mount St. Helens volcano. Richland WA, Batelle Pacific Northwest Laboratories.

Rochow, T. G. and Tucker, P. A. (1999) 'Introduction to microscopy by means of light, electron, X-rays or acoustics' (2nd edn) Plenum press, NY, pp 297-327

Ross, M. H., and Reith E. J. (1985) 'Histology' Harper and Row publisher, J. B. Lippincott company pp 504-527

Sato, N., Yamamoto, T., Sekine, Y., Yumioka, T., Junicho, A., Fuse, H. and Matsuda, T. (2993) Involvement of heat-shock protein 90 in the interleukin-6-mediated signalling pathway through STAT3 *Biochem. Biophys. Res. Commun*. 300: 847-852

Searl, A., Nicholl, A., and Baxter, P. J. (2002) Assessment of the exposure of islanders to ash from the Soufriere Hills volcano, Montserrat, British West Indies. *Occup. Environ. Med.* 59: 523-531.

Seaton, A., and Cherrie, J. W. (1998) Quartz exposures and severe silicosis: a role for the hilar nodes. *Occup. Environ. Med.* 55: 383-6.

Tamayo, P. and Ramaswamy, S. (2002) Cancer genomics and molecular pattern recognition In: Expression profiling of human tumors: diagnostic and research applications (eds. Ladanyi M and Gerald W.) Humana press pp1-29

Touqui, L. and Alaoui-El-Azher, M. (2001) Mammalian secreted phospholipases A2 and their pathophysiological significance in inflammatory diseases. *Curr Mol Med* 1:739-754

Vallyathan, V and Green, F. H. (1985) The role of analytical technique in the diagnosis of asbestos-associated disease *Crit. Rev. Clin. Lab. Sci.* 22:1-42

Vallyathan, V, Mentnech, M. S, Stettler, L. E, Dollberg, D. D and Green, H. Y (1983). Mount St Helens' volcanic ash: Hemolytic activity. *Environ. Res.* 30: 349-360.

Vallyathan, V, Robinson, V, Reasor, M, Stettler, L and Bernstein, R (1984). Comparative in vitro cytotoxcity of volcanic ashes from Mount St. Helens, El Chichon and Galunggung. *J. Toxicol. Environ. Hlth.* 14: 641-654.

Wehner, A. P, Dagle, G. E, and Clark, M. L. (1983) Lung changes in rats inhaling volcanic ash for one year. *Am. Rev. Respir. Dis.* 128: 926-932.

White, A. F. (1995) Chemical weathering rates of silicate mineral in soils In: Reviews in Mineralogy : Chemical weathering rates of silicate minerals (eds White A. F and Brantley S. L). Mineralogical society of America, USA, pp 440-455

White, A. F. and Brantley, S. L (1995) Chemical weathering rates of silicate minerals: An overview In: Reviews in Mineralogy : Chemical weathering rates of silicate minerals (eds White A. F and Brantley S. L). Mineralogical society of America, USA, pp 2-20

Williamson, B. (2000) Min. Dept. NHM. Personal communication

Wilson, M. R., Stone, V., Cullen, R. T., Searl, A., Maynard, R. L., and Donaldson, K. (2000) *In vitro* toxicology of respirable Montserrat volcanic ash. *Occup. Environ. Med.* 57: 727-733.

Yano, E., Takeuchi, A., Nishii, S., Koizumi, A., Poole, A., Brown, R. C., Johnson, N. F., Evans, P. H., and Yukiyama, Y. (1985) *In vitro* biological effects of volcanic ash from Mount Sakurajima. *J. Toxicol. Environ. Health* 16: 127-135.

Yano, E., Yokoyama, Y., and Nishii, S. (1986) Chronic pulmonary effects of volcanic ash: an epidemiologic study. *Arch. Environ. Health* 41: 94 – 99.

Young, B. and Heath, J. W. (2000) 'Wheater's Functional Histology' (4th edn), Churchill Livingstone pp 222-236

Young, S., Sparks, S., Robertson, S., Lynch, L., and Aspicall, W. (1997) Eruption of Soufriere Hills volcano in Montserrat continues. *EOS Transactions* 78:401-409.

http://volcano. und. nodak. Edu

http://www.bioportfolio.com

http://www.biosci.ki.se

http://www. Cryst.bbk.ac.uk

http://www.hprd.org

http://www.medterms.com

http://www.volcano.si.edu

http://www.volcanoworld.com

http://www.discovery.com

http://www.whfreeman.com